Alaska University Transportation Center

Smart FRP Composite Sandwich Bridge Decks in Cold Regions

Final Report

J. Leroy Hulsey
Pizhong Qiao
Wei Fan
David McLean

July 2011

Prepared For:

Alaska University Transportation Center
Duckering Building Room 245
P.O. Box 755900
Fairbanks, AK 99775-5900

Washington State University
Pullman, WA 99164-2910

INE/ AUTC # 12.09

REPORT DOCUMENTATION PAGE

Form approved OMB No.

1. AGENCY USE ONLY (LEAVE BLANK)	2. REPORT DATE	3. REPORT TYPE AND DATES COVERED
	July 2011	Final (8/3/2007-4/30/2011)

4. TITLE AND SUBTITLE
Smart FRP Composite Sandwich Bridge Decks in Cold Regions

5. FUNDING NUMBERS
AUTC # 107018

DTRT06-G-0011

6. AUTHOR(S)

J. Leroy Hulsey
Pizhong Qiao
Wei Fan
David McLean

7. PERFORMING ORGANIZATION NAME(S) AND ADDRESS(ES)
Alaska University Transportation Center
P.O. Box 755900
Fairbanks, AK 99775-5900

8. PERFORMING ORGANIZATION REPORT NUMBER
INE/AUTC # 12.09

9. SPONSORING/MONITORING AGENCY NAME(S) AND ADDRESS(ES)
Washington State University
Pullman, WA 99164-2910

10. SPONSORING/MONITORING AGENCY REPORT NUMBER

11. SUPPLENMENTARY NOTES

12a. DISTRIBUTION / AVAILABILITY STATEMENT
No restrictions

12b. DISTRIBUTION CODE

13. ABSTRACT (Maximum 200 words)

What if every time a bridge on a lonely road got icy, it automatically notified the local DOT to begin ice-control safety measures? What if a bridge could tell someone every time an overloaded truck hit the decking, or when the trusses under it began to weaken? This project, a partnership of Washington State University, the University of Alaska Fairbanks, and Kansas Structural Composites, Inc. takes the first steps to develop, manufacture, test, and implement Smart Honeycomb Fiber-Reinforced Polymer (S-FRP) sandwich materials for transportation projects. This material integrates advanced composite materials with sensors and actuators. So far, researchers have tested an S-FRP sandwich deck panel, evaluated several S-FRP sandwich beams in cold temperatures, and developed effective structural-health monitoring strategies. Dynamic tests of the S-FRP sandwich deck panel with and without damage continue, and structural-health monitoring strategies for cold temperature exposures will be developed. A combined experimental, theoretical, and numerical approach will result in new techniques for structural-health monitoring and damage identification of thick sandwich deck panels. It is anticipated that, with wireless communication technologies, the developed structural-health monitoring strategies will be capable of remotely monitoring and assessing the structural integrity of sandwich bridge decks in cold regions.

14- KEYWORDS: Bridge decks; Bridge design; Bridges; Cold weather construction; Fiber reinforced materials; Frigid regions; Highway bridges; Piezoelectric sensors; Rapid construction; Research projects; Sandwich construction; Snow and ice control; Wireless communication systems

15. NUMBER OF PAGES
250

16. PRICE CODE
N/A

17. SECURITY CLASSIFICATION OF REPORT	18. SECURITY CLASSIFICATION OF THIS PAGE	19. SECURITY CLASSIFICATION OF ABSTRACT	20. LIMITATION OF ABSTRACT
Unclassified	Unclassified	Unclassified	N/A

ACKNOWLEDGMENTS

This research was supported by the Alaska University Transportation Center (AUTC), State of Alaska Department of Transportation & Public Facilities, and US Department of Transportation (Contract/Grant Number: DTRT06-G-0011). The composite honeycomb sandwich materials (beams and decks) used in this study were fabricated by Kansas Structural Composites, Inc. (KSCI), and the technical support and match provided to this project by Dr. Jerry Plunkett, President of KSCI are gratefully acknowledged.

The technical assistance and help in experimental preparation and testing provided by Bill Elliott in the WSU-CEE department, Norman Martel in the WSU-ME shop, and Bob Duncan and Scott Lewis in WSU-CMEC are also acknowledged. The assistance and help from Kathy Petersen and Jill Dewey-Davidson of AUTC and Vicki Ruddick, Lola Gillespie and Susan Lewis of WSU-CEE are acknowledged. The involvement and assistance in the experimental portion of this research by the graduate students Hussam Saleem, Nicolas Lopez, Fangliang Chen, Xuping Huo, and Jianmin Zhuang at the WSU-Smart Structures Lab are very much appreciated.

SUMMARY

In this study, new and integrated Smart honeycomb Fiber-Reinforced Polymer (S-FRP) sandwich materials for various transportation construction applications, with particular emphasis on highway bridge decks in cold regions, were developed and tested. The novelty integrates advanced polymer composite materials with smart piezoelectric sensors and actuators to form smart structures, and along with advanced material technologies and proposed damage identification algorithms, it is capable of improving construction speed in cold climates and self-monitoring structural conditions in remote sites. A combined experimental and analytical study to develop, evaluate and test the S-FRP sandwich materials was conducted, and related studies on dynamic response, temperature effect and scale-up of test results, development of viable and effective damage identification algorithms and techniques more suitable for 2-D plate-type structures, and experimental characterization were investigated.

Structural health monitoring and damage identification methods for composite beams and plate-type structures were studied, especially for FRP sandwich beams and deck panels. A literature review showed that research on 2-D damage identification method for plate-type structures is relatively limited. The dynamic response of FRP sandwich beams with sinusoidal core configuration along either the longitudinal or transverse direction was investigated based on a high-order sandwich beam theory. The results were compared with Timoshenko's beam theory, numerical simulation and experimental test results to illustrate the improvement of the high-order approach. The temperature effect on dynamic response of FRP sandwich beams/panels was also studied for condition assessment. A series of FRP sandwich beams and an as-manufactured FRP sandwich panel were investigated for dynamic response change under temperature effect based on the material data obtained from dynamic mechanical analysis.

To make the integrated S-FRP sandwich system viable of structural health monitoring, two dynamic response-based methods were developed for defect or damage identification of plate-type of structures, like the bridge decks. First, the 2-D continuous wavelet transform (CWT)-based method was proposed for damage localization. Then, a strain energy-based Damage Severity Correction Factor (DSCF) method was proposed for damage localization and quantification. In this method, a damage location factor matrix and a damage severity correction factor matrix were generated from the curvature mode shape of a plate and then used for damage localization and quantification. A structural health monitoring strategy was then proposed for FRP sandwich panels using the combination of experimental modal testing technique and damage identification method. Using this strategy, the two proposed methods were applied to the modal testing data of an as-manufactured FRP sandwich deck panel for damage identification. The 2-D CWT-based strategy used an accelerometer and an impact hammer modal testing system, while the DSCF-based strategy adopted a polyvinylidence fluoride (PVDF) sensor network and an impact hammer system which both simulates the proposed S-FRP deck panel system and may eventually lead to development of integrated S-FRP sandwich materials. The application of 2-D CWT method on mode shape data from experimental modal analysis showed that it could effectively indicate the location and area of damage in the FRP sandwich deck panel. The application of DSCF-based damage identification method on curvature mode shape data from the FE/experimental modal analysis showed that it could not only effectively indicate the location of damage but also approximate the damage severity in a FRP sandwich plate-type structure. The potential integration of the proposed S-FRP sandwich materials system with wireless communication technology and obstacles facing the implementation of wireless sensor networks (WSNs) were discussed as well. Outcomes of this study deliver a viable technology

using integrated advanced polymer sandwich materials and smart piezoelectric sensors/actuators to address transportation safety, security, and innovation in cold regions.

TABLE OF CONTENTS

LIST OF FIGURES

LIST OF TABLES

CHAPTER 1

INTRODUCTION

1.1 Overview

Commercial development and implementation of new, advanced and low-cost engineered materials can alleviate major adverse effects to infrastructure deterioration worldwide. For example, new nonferrous materials do not corrode, and the costs of labor for installation of these lightweight products may be less. Other advantages may include reduced energy consumption, less environmental pollution, and better response to the devastating effects of earthquakes. Motivated by the need to improve and rehabilitate transportation infrastructure, advanced polymer or fiber-reinforced polymer (FRP) composites have been increasingly used in civil infrastructure applications and are being considered to partially replace and/or complement conventional materials. This is mainly due to the advantageous properties of these materials. The advantages include high strength, lightweight, improved resistance to corrosion and fatigue, superior damage tolerance and the ability to be tailored to meet specific applications, compared to traditional steel and reinforced concrete structures.

In the past few years, FRP composite decks have received significant attention for use in rehabilitation and new construction. This is because of their inherent advantages in high stiffness and strength to weight ratios, improved fatigue resistance, and superior damage tolerance capability as compared to traditional steel reinforced concrete decks. FRP bridge decks are commonly placed transverse to the supporting structure such as longitudinal girders, cross beams, and stringers. FRP decks are typically connected to the underlying supports by using shear studs or bolted connections. These connections often act simply supported and therefore do not necessarily provide for composite action. The modular FRP bridge deck systems can

either serve as bridge panels for 20- to 30-foot spans or be installed over supporting stringers for longer spans.

The existing application of FRP composites in bridge decks is not fully developed. The dynamic response of FRP decks which is useful for developing damage detection and health monitoring strategies is encouraging but not fully utilized. On the other hand, effective and reliable structural health monitoring (SHM) techniques for damage detection in composite structures are highly in demand. Damages or defects, such as (1) manufacturing imperfection, (2) delamination, fiber breaking and matrix cracking in composites, (3) debonding of face sheets from core, face sheet crimping and dimpling, core crushing caused by excessive core buckling in sandwich, and (4) debonding of adhesively bonded shapes, can be introduced in the FRP decks during manufacturing process or during installation process and service life (i.e., impact and service loading). Coupled with temperature, moisture, and environmentally-related aging effects, structural defects are present and affect serviceability of the FRP bridge decks. Effective SHM strategy is able to probe these long-standing undetected damages in FRP bridge decks and recommend proper recommendations for repair or disuse, thus preventing rapid catastrophic failures.

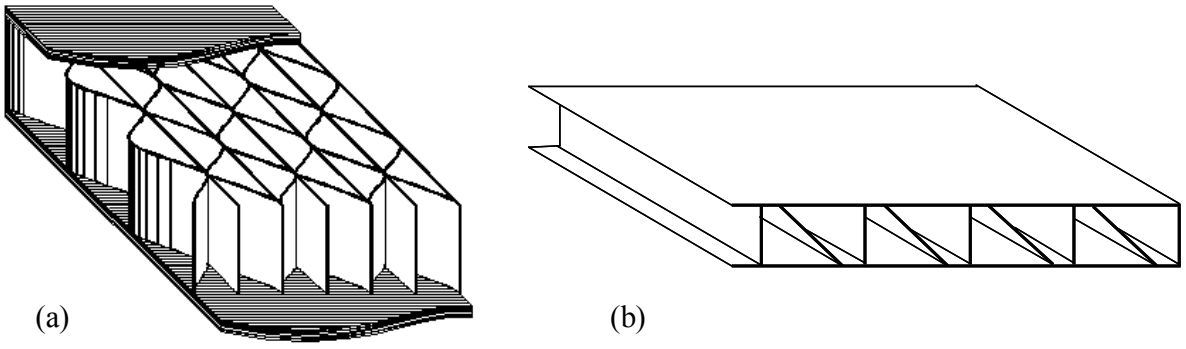

Figure 1.1 Typical FRP deck configurations

(a) Sandwich material panel, and (b) Adhesively bonded pultruded shapes

Unlike standard materials, FRP composites are typically orthotropic or anisotropic, and their analyses are much more difficult than traditional materials. For example, while changes in the geometry of FRP shapes can be easily related to changes in stiffness, changes in the material constituents do not lead to such obvious results. Structural geometric shapes of FRP decks are also relatively complicated (e.g., a honeycomb sandwich deck with a sinusoidal core, see Figure 1.1(a)). Subsequently, conventional analytical approaches cannot be directly applied to these uncommon geometries. Shear deformations for FRP composite materials (e.g., the transverse shear in sandwich materials is primarily carried by the honeycomb cores) are usually significant, and therefore, the modeling of FRP structural components should account for shear effects.

There are at least four major FRP bridge decks currently available for field applications: (1) SuperDeck™, a cross-section of full-depth hexagons and half-depth trapezoids, forming an "H-Deck", which was developed by West Virginia University researchers and Creative Pultrusions, Inc. (CP); (2) Honeycomb FRP sandwich deck, a polymer bridge deck based on sandwich construction with a sinusoidal core element and top and bottom face sheets, which is produced by the contact-molding process and manufactured by Kansas Structural Composites Inc. (KSCI); (3) an FRP bridge deck, produced by SCRIMP - a resin infusion technology which was patented by DuPont Composites; and (4) DuraSpan^{TM}, pultruded FRP bridge deck by Martin Marietta Composites, consisting of "truss-type" tubes bonded with adhesive. These decks were designed for minimum material weight to provide sufficient structural performance to withstand highway bridge loads for both old and new bridges.

A honeycomb structure is the most efficient configuration to provide optimum mechanical performance per unit weight. For this reason, honeycomb materials are widely used in the aerospace and automotive industries. In civil infrastructure, a lightweight and heavy-duty

honeycomb FRP panel for highway bridge decks was developed by the Kansas Structural Composites Inc. (KSCI) (Plunkett 1997). This sandwich deck has a vertically-oriented sinusoidal core configuration. An analytical model verified by Finite Element analyses and experimental testing was developed by Davalos and Qiao et al. (2001). The use of honeycomb materials is not new, and it is widely found in applications ranging from cardboard boxes to aircraft structures and control surfaces. The honeycomb FRP sandwich panels with sinusoidal core configuration proposed by KSCI were adopted in this study, and they were integrated with smart piezoelectric sensors to form the so-called S-FRP sandwich materials.

FRP deck structures are susceptible to defects, which can be originated from imperfections in the manufacturing process or developed during service life. Defects in composites like fiber breakage, matrix crazing/cracking, debonding between core and face sheets or among bonded pultruded FRP shapes, core crushing, and delamination in laminated panels are typical damages in composite structures. Damage resulting in system defects can occur during service life from impact of wheel loads to the structures (heavy service loads or fatigue), or due to environment-induced effects in the FRP decks. These defects can significantly reduce structural strength and may grow to failure. Accordingly, reliable and accurate SHM techniques are an important proactive and cost effective way to prevent a catastrophic failure, which often leads to tragic consequences. Further, SHM is a naturopathic approach to maintenance and repair of our infrastructures. In other words, the SHM information can be used to ensure safety and enhance structural life.

Structural health monitoring, especially structural damage identification technique, has gained increasing attention from the scientific and engineering communities because the unpredicted structural failure may cause catastrophic economic and human life loss. A reliable

and effective non-destructive structural damage identification technique is crucial to maintain safety and integrity of structures.

Damage identification algorithm is the core to SHM technique. The changes of physical properties in the structure due to damage will alter the dynamic response, such as natural frequencies, damping and mode shapes. Vibration-based damage identification algorithms try to detect the damage by monitoring these dynamic responses. While wave-based damage identification algorithms try to detect the damage by monitoring the reflection or scattering of ultrasonic wave. The response information needed to evaluate structural condition immensely depends on experimental data measurement, type and extent. Hence, the method of acquiring data must be reliable and robust. Due to the unique sensing and actuating capabilities, smart materials-based sensors are increasingly being integrated with base materials to form smart structures, and they are used in structural control, vibration suppression and damping. Before such materials can be applied to health and usage monitoring systems, appropriate analytical and experimental techniques should be established, and the feasibility of applications should be conducted.

As the current state of the art in SHM, the 1-D damage identification algorithms for damage detection of beam-type structures have been extensively investigated and developed (Fan and Qiao 2011). However, research on 2-D damage identification algorithms for damage detection of plate-type structures, especially for plate-type sandwich structures, is still relatively limited.

1.2 Objectives

With the aim to develop the S-FRP sandwich materials for bridge deck application with integrated function of health and usage monitoring, the objectives of this project are three-fold:

(1) To evaluate dynamic response analysis of FRP sandwich structures with smart piezoelectric sensors and assess temperature effect (particularly the cold temperature) on dynamic response of FRP sandwich structures;

(2) To develop viable and effective 2-D damage identification algorithms for plate-type composite structures;

(3) To develop structural monitoring strategy and perform lab testing of the full size FRP sandwich deck panel using dynamic response-based structural health monitoring (SHM) techniques.

The overall goal of the project is to develop and test the proposed S-FRP sandwich materials suitable for highway bridge application, particularly in cold climate. To make the S-FRP sandwich materials as a viable technology for highway bridges, development and evaluation of effective and reliable structural health monitoring strategy and damage identification algorithms for composite structures are essential. The proposed damage identification should be able to detect the existence of damage and approximate the location/magnitude of the damage. The proposed structural health monitoring strategy should have the potential to be developed for on-site, automatic, real-time, global health monitoring of structure.

1.3 Outline of report

This report consists of a total of ten chapters. A brief outline of the coming chapters and their content is listed as follows:

Chapter 2 provides a comprehensive literature review on structural health monitoring techniques and damage identification algorithms for beam-type or plate-type structures. Both the vibration-based and wave-based damage identification algorithms were discussed in this chapter.

Chapter 3 presents a detailed study on dynamic response of the proposed S-FRP sandwich materials. The analytical analysis on dynamic response of FRP sandwich beams is based on a high-order sandwich beam theory, and the modal testing of cantilevered FRP sandwich beams was performed using the surface-bonded piezoelectric sensors. The results were compared with Timoshenko's beam theory, numerical simulation and experimental test results to illustrate the effectiveness of the high-order approach.

Chapter 4 presents a study of temperature effect on dynamic response of FRP sandwich beams/panels. In particular, the effect of low temperature on the dynamic response of FRP sandwich structures was investigated. A series of FRP sandwich beams with either the longitudinal or transverse sinusoidal core as well as an as-manufactured FRP sandwich panel were investigated for dynamic response change under temperature effect. The dynamic mechanical analysis (DMA) test was conducted as well, and the scale-up of test results to predict the dynamic response of FRP sandwich materials at structural level was performed.

Chapter 5 proposes a 2-D CWT-based damage detection algorithm using "Dergauss2d" wavelet for plate-type structures. The viability of this method was demonstrated by the analysis of numerical and experimental mode shapes of a cantilevered plate.

Chapter 6 presents a comparative study based on the finite element model to evaluate five extensively-used damage detection algorithms for beam-type structures and three damage detection algorithms for plate-type structures.

Chapter 7 proposed a damage severity correction factor (DSCF)-based damage identification method for plate-type structures. A damage location factor (DLF) matrix and a DSCF matrix could be generated from the curvature mode shape of a plate. The damage

identification method using DSCF and DLF were proposed for damage localization and quantification. The viability of this method was demonstrated by the numerical investigation.

In Chapter 8, the damage identification methods proposed in Chapters 5 and 7 was applied for damage identification of an as-manufactured FRP sandwich deck panel. Both data from Finite Element (FE) simulation and experimental modal analysis were examined using the proposed 2-D CWT-base method (Chapter 5) and DSCF-based method (Chapter 7).

Chapter 9 discusses the potential integration of the proposed S-FRP sandwich materials system with wireless communication technology as well as the obstacles facing implementation of wireless sensor networks (WSNs).

Finally, the conclusions and outcomes from this study are presented in Chapter 10.

CHAPTER 2

LITERATURE REVIEW

2.1 Introduction

To develop the integrated S-FRP sandwich materials capable of assessing structural condition and identifying potential damage, structural health monitoring techniques are essential. Structural health monitoring, especially in the form of structural damage identification techniques, has gained increasing attention from the scientific and engineering communities because the unpredicted structural failure may cause catastrophic economic and human life loss. A reliable and effective non-destructive structural damage identification technique is crucial to maintain safety and integrity of structures.

Most non-destructive damage identification methods can be categorized as either local or global damage identification techniques (Doebling et al. 1996). Local damage identification techniques, such as ultrasonic methods and X-ray methods, require that the vicinity of damage is known a priori and readily accessible for testing, which cannot be guaranteed for most cases in civil or aerospace engineering. Hence, the global damage identification technique, such as vibration-based damage identification method, is developed to overcome these difficulties.

Damage identification methods can also be classified as 'model-based method' or 'response-based method'. The model-based method assumes that a detailed numerical model of the structure is available for damage identification; while the response-based method depends only on experimental response data from structures.

The objective of this chapter is to provide a review on damage identification algorithm for beam-type or plate-type structures. There are two main reasons for the focus on simple structures, such as beams or plates: (1) most structures or their major components in civil and

mechanical engineering can be simplified as a beam or plate, and (2) the problem of identifying a specific damage in a beam/plate provides an important benchmark for effectiveness and accuracy of identification techniques. This chapter is intended to identify starting points for research in damage identification and structural health monitoring and in choosing and implementing the available damage identification algorithms and signal processing methods in damage identification of simple structures.

The fundamental idea for the vibration-based damage identification is that the damage-induced changes in the physical properties (e.g., mass, damping, and stiffness) will cause detectable changes in modal properties (e.g., natural frequencies, modal damping and mode shapes). For instance, reductions in stiffness result from the onset of cracks. Therefore, it is intuitive that damage can be identified by analyzing the changes in vibration features of the structure.

Although in vibration test, the excitation and response are always measured and recorded in the form of time history, it is usually difficult to examine the time domain data for damage identification. A more popular method is to examine the modal domain data through modal analysis technique, in which the time domain data is transformed into the frequency domain, and then the modal domain data can be farther extracted from the frequency domain data. During the past three decades, great effort has been made in the researches within all three domains (i.e., time, frequency, and modal domains). It seems that this effort will continue since no single existing method can solve all the damage identification problems from various types of damages and structures. However, the modal domain methods attract more attention and play a dominant role in the state-of-the-art of structural damage identification. The modal domain methods evolve along with the rapid development of experimental modal analysis technique, and they

gain their popularity because the modal properties (i.e., natural frequencies, modal damping, modal shapes, etc.) have their physical meanings and are thus easier to be interpreted or interrogated than those abstract mathematical features extracted from the time or frequency domain.

During the last three decades, extensive research has been conducted in vibration-based damage identification, and significant progress has been achieved in this highlight area. A broad range of techniques, algorithms and methods are developed to solve various problems encountered in different structures, from the basic structural components (e.g., beams and plates) to complex structural systems (e.g., bridges and buildings). Doebling et al. (1996) presented an extensive review of vibration-based damage detection methods up to 1996. Sohn et al. (2003) then presented an updated version of this review on the literature up to 2001. In both the articles, the features extracted for identification were considered to classify the damage identification methods. Following closely this classification, Carden and Fanning (2004) presented a literature survey with particular emphasis on the papers and articles published from 1996 to 2003.

The literature review on vibration-based damage identification is organized by the classification using the features extracted for damage identification, and these damage identification methods are categorized as follows:

- Natural frequency-based methods;
- Mode shape-based methods;
- Curvature/strain mode shape-based methods;
- Other methods based on modal parameters.

2.2 Natural frequency-based methods

Natural frequency-based methods use the natural frequency change as the basic feature for damage identification. The choice of the natural frequency change is attractive because the natural frequencies can be conveniently measured from just a few accessible points on the structure and are usually less contaminated by experimental noise.

2.2.1 The forward problem

The forward problem of this issue is to determine the natural frequency changes of a given structure based on damage location and severity, and it serves as a theoretical foundation for the natural frequency-based methods. Gudmundson (1982) used an energy-based perturbation approach and derived an explicit expression for the resonance frequencies of a wide range of damaged structure. This method can account for a loss of mass in addition to a loss of stiffness. Liang et al. (1992) addressed the issue of determining frequency sensitivity for simply supported or cantilevered beam with one crack and developed analytical relationships between the first-order changes in the eigenfrequencies and the location and severity of the damage. This method requires symbolic computation of the characteristic equation. Morassi (1993) showed that the frequency sensitivity of a cracked beam-type structure can be explicitly evaluated by using a general perturbation approach. Frequency sensitivity turns to be proportional to the potential energy stored at the cracked cross section of the undamaged beam. Moreover, the ratio of the frequency changes of two different modes turns to be a function of damage location only. Both Liang and Morassi's methods were based on Euler-Bernoulli beam theory and modeled crack as a massless, infinitesimal rotational spring. All of the above-mentioned three explicit expressions are valid only for small defects. Kasper et al. (2008) derived the explicit expressions of wavenumber shift and frequency shift for a cracked symmetric uniform beam. These

expressions apply to beams with both shallow and deeper cracks. But the explicit expressions are based on high frequency approximation, and therefore, they are generally inaccurate for the fundamental beam mode and for a crack located in a boundary near field.

2.2.2 The inverse problem

The inverse problem of this issue is to determine damage location and size of a given structure based on natural frequency measurement. The study on this inverse problem dates back to 1978, when Adams et al. (1978) presented a method for detection of damage in a one-dimensional component utilizing the natural frequencies of longitudinal vibrations. In 1997, Salawu (1997) presented an extensive review of publications before 1997 dealing with the detection of structural damage through frequency changes. In the conclusion of this review paper, Salawu suggested that the natural frequency changes alone may not be sufficient for a unique identification of the location of structural damage because cracks associated with similar crack lengths but at two different locations may cause the same amount of frequency change.

Messina et al. (1998) proposed a correlation coefficient termed the Multiple Damage Location Assurance Criterion (MDLAC) by introducing two methods of estimating the size of defects in a structure. The method is based on the sensitivity of the frequency of each mode to damage in each location. "MDLAC" is defined as a statistical correlation between the analytical predictions of the frequency changes δf and the measured frequency changes Δf. The analytical frequency change δf can be written as a function of the damage extent vector δD. The required damage state is obtained by searching for the damage extent vector δD which maximizes the MDLAC value:

$$\text{MDLAC}(\{\delta \text{D}\}) = \frac{\left|\{\Delta f\}^T \cdot \{\delta f(\{\delta D\})\}\right|^2}{\left(\{\Delta f\}^T \cdot \{\Delta f\}\right) \cdot \left(\{\delta f(\{\delta D\})\}^T \cdot \{\delta f(\{\delta D\})\}\right)} \tag{2-1}$$

Two algorithms (i.e., the first and second order methods) were developed to estimate the absolute damage extent. Both the numerical and experimental test results were presented to show that the MDLAC approach offers the practical attraction of only requiring measurements of the changes in a few of natural frequencies of the structure between the undamaged and damaged states and provides good predictions of both the location and absolute size of damage at one or more sites.

Liang et al. (1991) developed a method based on three bending natural frequencies for the detection of crack location and quantification of damage magnitude in a uniform beam under simply supported or cantilever boundary conditions. The method involves representing the crack as a rotational spring and obtaining plots of its stiffness with crack location for any three natural modes through the characteristic equation. The point of intersection of the three curves gives the crack location and stiffness. The crack size is then computed using the standard relation between stiffness and crack size based on fracture mechanics. This method had been extended to stepped beams (1997) by Nandwana and Maiti and to segmented beams (2000) by Chaudhari and Maiti using the Frobenius method to solve Euler-Bernoulli type differential equations. Chinchalkar (2001) used a finite element-based numerical approach to mimic the semi-analytical approach using the Frobenius method. This approach does not require quadruple precision computation, and it is relatively easy to apply to different boundary conditions. Lele and Maiti (2002) extended Nandwana and Maiti's method to short beam, taking into account the effects of shear deformation and rotational inertia through the Timoshenko beam theory. Patil and Maiti (2003) proposed a frequency shift-based method for detection of multiple open cracks in an Euler-

Bernoulli beam with varying boundary conditions. This method is based on the transfer matrix method, and it extends the scope of the approximate method given by Liang et al. (1991) for a single segment beam to multi-segment beams. Murigendrappa et al. (2004a; 2004b) later applied Patil and Maiti's approach to single/multiple crack detection in pipes filled with fluid.

Morassi (2001) presented a single crack identification in a vibrating rod based on the knowledge of the damage-induced shifts in a pair of natural frequencies. The analysis is based on an explicit expression of the frequency sensitivity to damage and enables non-uniform bars under general boundary conditions to be considered. Some of the results are also valid for cracked beams in bending. Morassi and Rollo (2001) later extended the method to the identification of two cracks of equal severity in a simply supported beam under flexural vibrations. However, the inverse problem is ill-posed, just as many other frequency-based methods; namely, even by leaving symmetrical positions aside, cracks with different severity in two sets of different locations can produce identical changes in the first three natural frequencies.

Kim and Stubbs (2003) proposed a single damage indicator (SDI) method to locate and quantify a crack in beam-type structures by using changes in a few natural frequencies. A crack location model and a crack size model were formulated by relating fractional changes in modal energy to changes in natural frequencies due to damage. In the crack location model, the measured fractional change in the *i*th eigenvalue Z_i and the theoretical (FEM-based) modal sensitivity of the *i*th modal stiffness with respect to the *j*th element F_{ij} is defined, respectively. The theoretical modal curvature is obtained from a third order interpolation function of theoretical displacement mode shape, and they are expressed as

$$Z_i = \delta\omega_i^2 / \omega_i^2 \tag{2-2}$$

$$F_{ij} = K_{ij}/K_i = \frac{\int_{x_j}^{x_{j+1}} \{\phi''\}^2 dx}{\int_0^L \{\phi''\}^2 dx} \tag{2-3}$$

Then, an error index e_{ij} is introduced to represent the localization error for the ith mode and the jth location

$$e_{ij} = \frac{Z_i}{\sum_{k=1}^{NM} Z_k} - \frac{F_{ij}}{\sum_{k=1}^{NM} F_{kj}} \tag{2-4}$$

where NM denotes the number of measured vibration modes. To account for all available modes, a single damage indicator (SDI) is defined to indicate the damage location

$$SDI_j = \left[\sum_{i=1}^{NM} e_{ij}^2 \right]^{-1/2} \tag{2-5}$$

While in the crack size model, the damage inflicted a_j at predefined locations can be predicted using the sensitivity equation. The crack depth can be computed from a_j and the crack size model based on fracture mechanics. The feasibility and practicality of the crack detection scheme were evaluated by applying the approach to the 16 test beams.

Zhong et al. (2008) recently proposed a new approach based on the auxiliary mass spatial probing using the spectral centre correction method (SCCM), to provide a simple solution for damage detection by just using the output-only time history of beam-like structures. An SCCM corrected high accurate natural frequency vs. auxiliary mass location curve is plotted along with the curves of its derivatives (up to 3rd order) to detect the crack. However, only the FE verification was provided to illustrate the method. Since it is not so easy to get a high resolution natural frequency vs. auxiliary mass location curve in the experiment as in the numerical

simulation, the method's applicability and practicality in *in-situ* testing or even laboratory testing are still in question.

There are also several frequency change-based methods using soft optimization process for damage detection. Maity and Tripathy (2005) used the so-called Genetic Algorithm (GA) to detect and assess the structural damage from changes in natural frequencies. Pawar and Ganguli (2005) applied the genetic fuzzy system to detect the matrix crack in thin-walled composite structures based on changes in natural frequencies.

2.2.3 Limitations of frequency-based methods

Although the use of natural frequency changes for crack detection has been extensively studied in the past three decades, the aforementioned traditional damage detection methods based on frequency change still have several common limitations.

One fundamental limitation lies in the modeling of structure and damage. Except the approach in Zhong et al. (2008), all of the frequencies-based methods are model-based. Most methods for damage identification in beam-type structures rely on Euler-Bernoulli beam theory (except the shear deformable model in Lele and Maiti (2002)), and they model crack as a rotational spring. It is well known that Euler-Bernoulli beam theory over-predicts natural frequencies in short beams and high frequency bending modes. It is also known that modeling of crack as a rotational spring based on fracture mechanics will lose its credibility in high frequency modes or deep crack cases. Therefore, these methods are only applicable to a slender beam-type structure with small cracks. Moreover, the range of vibration modes which are suited for damage detection is narrowed to the first few modes due to the basic assumptions of these methods.

Another critical limitation is that the frequency changes due to damage are usually very small and may be buried in the changes due to environmental and operational conditions. For this reason, most successful damage identification methods using frequency are verified only in controlled laboratory scale rather than testing of real structures in their operating environment. Given that it is acknowledged that the *in-situ* measured frequency variation due to ambient vibration and environmental effects can be as high as 5–10%, generally, it would be necessary for a natural frequency to change by about 5% for damage to be detected with confidence (Salawu 1997). To account for this effect, a statistical damage detection model using the pattern recognition technique is needed to distinguish between damage-induced changes from environment-induced changes. Ni et al. (2005) addresses the modeling of temperature effects on modal frequencies based on a long-term structural health monitoring system of Ting Kau Bridge. The support vector machine (SVM) technique is applied to formulate the regression models which quantify the effect of temperature on modal frequencies. It shows that the SVM models exhibit good capabilities of mapping between the temperature and modal frequencies. Kim et al. (2007) presented a vibration-based damage monitoring scheme to give warning of the occurrence, location, and severity of damage under the temperature-induced uncertainty conditions. A damage warning model is selected to statistically identify the occurrence of damage by recognizing the patterns of damage-driven changes in natural frequencies of the test structure and by distinguishing temperature-induced off-limits.

Another limitation is that the damage identification problem is often ill-posed even without noise pollution, which leads to non-uniqueness of the solutions of damage location and severity. First, it is obvious that damage with same severity in symmetric locations of a symmetric structure will cause identical frequency changes. Furthermore, damage with different severity in

different locations can also produce identical changes in a few measured natural frequencies. This problem is even more severe for detection of multiple cracks. To avoid non-uniqueness, several damage detection methods require that the number of measurable modal frequencies should be close to the number of system parameters required to characterize the damage. However, the number of accessible vibration modes which is suited for damage detection is very limited (typically the first few modes), usually much less than the number of system parameters required. To overcome this difficulty, Dilena and Morassi (2004) suggested that an appropriate use of frequencies and anti-resonances may avoid the non-uniqueness of the damage location problem which occurs when only frequency measurements data is used in single crack identification. Jiang et al. (2006) incorporated a tunable piezoelectric transducer circuitry into the structure to enrich the modal frequency measurements, meanwhile implementing a high-order identification algorithm to sufficiently utilize the enriched information. It is shown that the modal frequencies can be greatly enriched by the inductance tuning, which, together with the high-order identification algorithm, leads to a fundamentally-improved performance on the identification of single and multiple damages with the usage of only lower-order frequency measurements.

In summary, the frequency change-based damage identification method can be successfully applied to simple structures with small crack (typically, a slender beam-type structure with artificially induced cracks) in a controlled laboratory condition. However, due to its inherent drawbacks, its applications for real complex structures or multiple/severe damage detection is limited.

2.3 Mode shape-based methods

Compared to using natural frequencies, the advantage of using mode shapes and their derivatives as a basic feature for damage detection is quite obvious. First, mode shapes contain local information, which makes them more sensitive to local damages and enables them to be used directly in multiple damage detection. Second, the mode shapes are less sensitive to environmental effects, such as temperature, than natural frequencies (Farrar and James 1997). The disadvantage is also apparent. First, measurement of the mode shapes requires a series of sensors; second, the measured mode shapes are more prone to noise contamination than natural frequencies.

In the past three decades, many damage identification methods have been developed based on direct or indirect use of measured mode shapes. These methods are roughly categorized into two types. The traditional 'mode shape change methods' try to establish a relationship between damage location/severity and mode shape change through a theoretical or finite element model. Hence, they depend on mode shape data from both intact and damaged structure. With the development of modern signal processing technique and its application in damage identification, a series of relatively new damage identification methods have been developed. The modern 'signal processing methods' can be applied either to mode shape change or to mode shape data from damaged structures alone. These methods take mode shape change or mode shape data as a spatial-domain signal and use signal processing technique to locate damage by detecting the local discontinuity of mode shape curve caused by damage.

2.3.1 Traditional mode shape change method

The traditional mode shape change method uses the mode shape change from intact and damaged structures as a basic feature for damage identification. The baseline data from intact

structure can be obtained from either an experimental test on the intact structure or an accurate numerical model of the intact structure. When experimental data on the intact structure is not available, a finite element model is usually adopted to generate the baseline data.

Shi et al. (2000a) extended the damage localization method based on multiple damage location assurance criterion (MDLAC) (Messina et al. 1998) by using incomplete mode shape instead of modal frequency. The two-step damage detection procedure is to preliminarily localize the damage sites by using incomplete measured mode shapes and then to detect the damage site and its extent again by using measured natural frequencies. No expansion of the incomplete measured mode shapes or reduction of finite element model is required to match the finite-element model, and the measured information can be used directly to localize damage sites. The method was demonstrated in a simulated 2-D planar truss model. Comparison showed that the new method is more accurate and robust in damage localization with or without noise effect than the original MDLAC method. In this method, the use of mode shape is only for preliminary damage localization, and the accurate localization and quantification of damage still rely on measured frequency changes.

Lee et al. (2005) presented a neural networks-based technique for element-level damage assessments of structures using the mode shape differences or ratios of intact and damaged structures. The effectiveness and applicability of the proposed method using the mode shape differences or ratios were demonstrated by two numerical example analyses on a simple beam and a multi-girder bridge. Hu and Afzal (2006) proposed a statistical algorithm for damage detection in timbers using difference of the mode shapes before and after damage. The different severities of damage, damage locations, and damage counts were simulated by removing mass from intact beams to verify the algorithm. The results showed that the algorithm is reliable for

the detection of local damage under different severities, locations, and counts. Pawar et al. (2007) investigated the effect of damage on beams with the clamped boundary conditions using Fourier analysis of mode shapes in the spatial domain. The damaged mode shapes are expanded using a spatial Fourier series, and a damage index in the form of a vector of Fourier coefficients is formulated. A neural network is trained to detect the damage location and size using Fourier coefficients as input. Numerical studies showed that the damage detection using Fourier coefficients and neural networks has the capability to detect the location and damage size accurately. However, the use of this method is limited to beams with the clamped-clamped boundary condition. Abdo and Hori (2002) suggested that the rotation of mode shape is a sensitive indicator of damage. Based on a finite element analysis of a damaged cantilevered plate and a damaged simply-supported plate, the rotation of mode shape is shown to have better performance of multiple damage localization than the displacement mode shape itself.

In general, the traditional mode shape change methods are not very sensitive to damages and commonly subjected to several limitations. For example, they are only sensitive to damage in certain area of the structures (e.g., around mid-span of a clamped-clamped beam); without further signal processing or pattern recognition technique, they can only be adopted for preliminary damage localization rather than accurate localization and quantification of damage; their applications in in-situ structures are also very limited.

2.3.2 Modern signal processing methods using mode shape

In most *in-situ* cases, experiment on intact structures is not feasible. For the model-based methods, the credibility of a numerical model must be established through careful model verification and validation (Hemez 2004). The lacks of experimental data from intact structures also increase the difficulty in establishing an accurate numerical model. Furthermore, numerical

analysis requires considerable computational cost, especially when integrated in an iterative optimization process. This limitation makes the model-based methods not suitable for real-time structure damage detection.

In order to solve these problems, developing a response-based method that depends on experimental data only from damaged structures has recently become a focused research topic in damage identification. These methods do not require a theoretical or numerical model. Their basic assumption is that the mode shape data from a healthy structure contains only low-frequency signal in spatial domain compared to the damage-induced high-frequency signal change. Several signal processing technique-based damage detection algorithms, such as fractal dimension method and wavelet transform method, have been investigated. It should be noted that the 'signal processing method' can be applied to both the mode shape change and damaged mode shape data alone. When only the damaged mode shape data are used, these methods cannot be used for damage quantification due to its inherent limitation.

Fractal dimension method

Hadjileontiadis et al. (2005; 2007) proposed a response-based damage detection algorithm for beam and plate using fractal dimension (FD). For beam-type structures, the FD of a curve is estimated by

$$FD = \frac{\log_{10}(n)}{\log_{10}(\frac{d}{L}) + \log_{10}(n)}, \tag{2-6}$$

where n is the number of steps in the curve; d is the diameter estimated as the distance between the first point of the sequence P_1 and the ith point P_i of the sequence that provides the farthest distance; and L is the total length of the curve or the sum of distances between successive points.

$$d = \max dist(P_1, P_i)$$
$$L = \sum_{i}^{n-1} dist(P_i, P_{i+1}) \tag{2-7}$$

This method calculates the localized fractal dimension of the fundamental mode shape directly. The damage features are established by employing a sliding window of length *M* across the mode shape and estimating the *FD* at each position for the regional mode shape inside the window. Damage location and size are determined by a peak on the FD curve indicating the local irregularity of the fundamental mode shape introduced by the damage.

If the higher mode shapes were considered, this method might give misleading information as demonstrated in their study. To overcome this shortcoming, Wang and Qiao (2007) proposed a modified fractal dimension method termed 'generalized fractal dimension' (GFD) method by introducing a scale factor *S* in the FD algorithm

$$GFD = \frac{\log_{10}(n)}{\log_{10}(\frac{d_s}{L_s}) + \log_{10}(n)},$$
$$d_s = \max_{1<j\le M} \sqrt{\left(y_{i+j} - y_i\right)^2 + S^2\left(x_{i+j} - x_i\right)^2}, \tag{2-8}$$
$$L_s = \sum_{j=1}^{M} \sqrt{\left(y_{i+j} - y_{i+j-1}\right)^2 + S^2\left(x_{i+j} - x_{i+j-1}\right)^2}$$

Instead of directly applying the algorithm to the fundamental mode shape, *GFD* is applied to the 'uniform load surface' (ULS) (Zhang and Aktan 1998) to detect the damage in the paper. Three different types of damage in laminated composite beams have been successfully detected by the *GFD* (Qiao et al. 2007b; Wang and Qiao 2007) . It should be pointed out that the *GFD* bears no conventional physical meaning as compared to the *FD*, and it only serves as an indicator of damage. A scale factor *S* has to be carefully chosen in order to detect damage successfully.

Recently, Qiao and Cao (2008) proposed a novel waveform fractal dimension-based damage identification algorithm. An approximate waveform capacity dimension (AWCD) is formulated first, from which an AWCD-based modal irregularity algorithm (AWCD-MAA) is systematically established. Then, the basic characteristics of AWCD-MAA on irregularity detection of mode shapes, e.g., crack localization, crack quantification, noise immunity, etc., are investigated based on an analytical crack model of cantilever beams using the linear elastic fracture mechanics. In particular, from the perspective of isomorphism, a mathematical solution on the use of applying the waveform fractal dimension to higher mode shapes for crack identification is originally proposed, from which the inherent deficiency of waveform fractal dimension to identify crack when implemented to higher mode shapes is overcome. The applicability and effectiveness of the AWCD-MAA is validated by an experimental program on damage identification of a cracked composite cantilever beam using directly measured strain mode shape from smart piezoelectric sensors.

Wavelet transform method

Wavelet analysis has shown its inherent merits in damage detection over traditional methods due to its ability to closely examine the signal with multiple scales to provide various levels of detail and approximations. The use of wavelet transform to identify damage from mode shape has been one of the most popular techniques. These methods treat mode shape data as a signal in spatial domain, and they use spatial wavelet transform technique to detect the signal irregularity caused by damage.

Liew and Wang (1998) first used spatial wavelet coefficients for crack detection based on the numerical solution for the deflection of a beam under oscillating excitation. Wang and Deng (1999) considered Haar wavelet transforms to analyze spatially distributed signals (displacement

and strain measurements) for damage detection of a cracked beam and plate. Quek et al. (2001) examined the sensitivity of wavelet technique in the detection of cracks in beam structures. Although their works focused on deflection under the static or impact loading other than the mode shape, they demonstrated the potential of using wavelet transform on the mode shape for damage detection.

Hong et al. (2002) showed that the continuous wavelet transform (CWT) of mode shape using a Mexican hat wavelet is effective to estimate the Lipschitz exponent for damage detection of a damaged beam. The magnitude of the Lipschitz exponent can be used as a useful indicator of the damage extent. It is also proved in their work that the number of the vanishing moments of wavelet should be at least 2 for crack detection in beams. Douka et al. (2003; 2004) applied one-dimensional symmetrical 4 wavelet transform on the mode shape for crack identification in beam and plate structures. The position of the crack is determined by the sudden change in the wavelet coefficients. An intensity factor is also defined to estimate the depth of the crack from the coefficients of the wavelet transform.

Gentile and Messina (2003) presented a comprehensive investigation on the application of CWT on mode shape for damage detection of a cracked beam. It is shown that when the scale s is small, CWT with m vanishing moment can be a good approximation of the mth derivatives of the spatial domain signal except for the discrepancies at the boundaries. The Gaussian derivative wavelet family (Gaus1~4) was suggested due to its particular advantage in damage detection because it will not cause an interruption of the singularity in the signal towards the finest scales. The wavelets are shown to be able to de-noise the mode shape data and preserve the peaks indicating damage location by adopting a tradeoff between the finest and larger scales. It is also shown that weighting the mode shape through a window can effectively reduce the boundary

effect caused by signal discontinuity. For application of classical Gaussian wavelets, a relatively high density of sensors is required due to their natural difficulty to process a low number sampling points.

Zhong and Oyadiji (2007) proposed a crack detection algorithm in symmetric beam-like structures based on stationary wavelet transform (SWT) of mode shape data. Two sets of mode shape data, which constitute two new signal series, are, respectively, obtained from the left half and reconstructed right half of modal displacement data of a simply supported damaged beam. The difference of the detail coefficients of the two new signal series is used for damage detection. The method is verified using the modal shape data generated by a finite element analysis of 36 damage cases of a simply supported beam with an artificial random noise of 5% SNR. The effects of crack size, depth and location as well as the effects of sampling interval were examined. The results show that all the cases can provide evidence of crack existence at the correct location of the beam and that the proposed method can be recommended for identification of small cracks as small as 4% crack ratio in real applications with measurement noise being present. However, there are two main disadvantages of this method. First, the use of this method based on SWT requires fairly accurate estimates of the mode shapes. Second, the method cannot tell the crack location from its mirror image location due to its inherent limitation. Therefore, in applying the method, both the crack location predicted and its mirror image location should be checked for the presence of a crack.

Chang and Chen (2005) presented a spatial Gabor wavelet-based technique for damage detection of a multiple cracked beam. Given natural frequencies and crack positions, the depths of the cracks are then solved by an optimization process based on traditional characteristic equation. Analysis and comparison show that it can detect the positions of cracks and their

depths and also has high sensitivity to the crack depth and the accuracy of this method is good. The limitation of this method is very common in wavelet transform methods, i.e., there are peaks near the boundaries in the wavelet plot caused by discontinuity and the crack cannot be detected when the crack is near the boundaries. Chang and Chen (2004) also applied this technique to detect damage in a rectangular plate.

Poudel et al. (2007) proposed a damage detection method for the beam-type structures based on complex Gaussian wavelet transform of mode shape difference. The uses of three different wavelet transforms (i.e., Gaussian wavelet, complex Gaussian wavelet, Morlet wavelet) are compared. The determination of maximum and minimum scale to avoid edge effect and noise effect was also discussed. The laboratory experiment on a simply supported beam using the high-speed digital video camera was conducted to verify the method. Results show that the wavelet transformation of the mode shape difference function provides an inspection-friendly display of local changes due to structural damage. The maximum modulus and sign change of phase angle in the wavelet coefficients indicate the damage locations.

Rucka and Wilde (2006) applied the respective Gaussian wavelet and reverse biorthogonal wavelet transform on the fundamental mode shapes of beam and plate structures for damage detection.

Recently, Cao and Qiao (2008) proposed a novel wavelet transform technique (so called 'integrated wavelet transform'), which takes synergistic advantage of the stationary wavelet transform (SWT) and the continuous wavelet transform (CWT), to improve the robustness of irregularity analysis of mode shapes in damage detection. Two progressive wavelet analysis steps are considered, in which the SWT-based multiresolution analysis (MRA) is first employed to refine the retrieved mode shapes, followed by the CWT-based multiscale analysis (MSA) to

magnify the effect of slight irregularity. The SWT-MRA is utilized to separate the multi-component modal signal, eliminate random noise and regular interferences, and thus extract purer damage information; while the CWT-MSA is employed to smoothen, differentiate or suppress polynomials of mode shapes to magnify the effect of irregularity. The choice of the optimal mother wavelet in damage detection was also elaborately discussed. The proposed methodology was evaluated using the mode shape data from the numerical finite element analysis and experimental testing of a cantilever beam with a through-width crack. The methodology presented provides a robust and viable technique to identify minor damage in a relatively lower signal-to-noise ratio environment.

2.4 Mode shape curvature/strain mode shape-based methods

It has been shown by many researchers that the displacement mode shape itself is not very sensitive to small damage, even with the high density mode shape measurement (Huth et al. 2005; Khan et al. 1999; Salawu and Williams 1994). As an effort to enhance the sensitivity of mode shape data to the damage, the mode shape curvature is investigated as a promising feature for damage identification. Once again, the modal curvature-based methods can be commonly categorized into two types: (1) the traditional 'modal curvature change methods', and (2) the modern 'signal processing methods'. The curvature mode shapes also closely involve in the modal strain energy-based method (Kim et al. 2003; Shi and Law 1998; Shi et al. 2000a; Stubbs and Kim 1996; Stubbs et al. 1995) (see Section 2.4.3).

2.4.1 Traditional modal curvature change method

Pandey et al. (1991) suggested for the first time that the mode shape curvature (MSC), i.e., the 2nd derivatives of mode shape, is highly sensitive to damage and can be used to localize it. The curvature mode shapes are derived using a central difference approximation as follows

$$\kappa_i = (w_{i+1} + w_{i-1} - 2w_i) / h^2 \tag{2-9}$$

where h is the sensor spacing.

Results showed that the difference of curvature mode shapes from intact and damaged structure can be a good indicator of damage location. It was also pointed out (Abdel Wahab and De Roeck 1999) that for the higher modes, the difference in modal curvature shows several peaks not only at the damage location but also at other positions, which may lead to a false indication of damage. Hence, in order to reduce the possibility of a false alarm, only the first few low curvature mode shapes can be used for damage identification.

Salawu and Williams (1994) compared the performance of both the curvature and displacement mode shapes for locating damage and confirmed the mode shape curvature as a sensitive indicator of damage. However, the sensitivity and effectiveness of mode shape curvature method were also questioned by several researchers with experimental evidence showing that the modal curvature by itself cannot locate small damages (Ratcliffe 2000). Abdel Wahab and De Roeck (1999) investigated the accuracy of using the central difference approximation to compute the mode shape curvature based on finite element analysis. The authors suggested that a fine mesh is required to derive the modal curvature correctly for the higher modes and the 1st mode will provide the most reliable curvature in practical application due to the limited number of sensors needed. Then, a damage indicator called “curvature damage factor”, which is the average absolute difference in the intact and damaged curvature

mode shapes of all modes, is introduced. The technique was further applied to a real structure, namely bridge Z24, to show its effectiveness in multiple damage location. Just-Agosto et al. (2007) used the mode shape curvature data and a properly trained neural network (NN) scheme to implement a successful damage detection for composite sandwich beam.

Deriving the mode shape curvature from curve fitting or finite difference approximation may introduce some considerable error. According to Euler-Bernoulli beam theory, the strain at top surface of a beam under bending is proportional to the curvature of the beam. Therefore, the curvature mode shape of a slender beam can be directly measured by measuring the strain mode shape.

Swamidas and Chen (1995) performed a finite element-based modal analysis on a cantilever plate with a small crack. It was found that the surface crack in the structure will affect most of the modal parameters, such as the natural frequencies of the structure, amplitudes of the response and mode shapes. Some of the most sensitive parameters are the difference of the strain mode shapes and the local strain frequency response functions. By monitoring the changes in the local strain frequency response functions and the difference between the strain mode shapes, the location and severity of the crack that occurs in the structure can be determined. Laboratory experiment by Zhou et al. (2007) showed that the direct measurement of curvature using appropriately placed strain gauges was found to improve the localization resolution, a fact attributed to the elimination of several data processing steps required when the acceleration data are used. Li et al. (2005) presented a crack damage detection using a combination of natural frequencies and strain mode shapes as input in artificial neural networks (ANN) for location and severity prediction of crack damage in beam-like structures. In the experiment, several steel

beams with six distributed surface-bonded strain gauges and an accelerometer mounted at the tip were used to obtain modal parameters such as resonant frequencies and strain mode shapes.

Recently, Qiao and his coworkers (Hamey et al. 2004; Lestari and Qiao 2005; Lestari et al. 2007; Qiao et al. 2007a; Qiao et al. 2007b) conducted a series of studies on using the strain mode shapes measured from the surface-bonded piezoelectric sensors to identify various damage in composite beam or plate structures. Hamey et al. (2004) evaluated several damage detection algorithms in carbon/epoxy composite beams with several possible damage configurations using the directly measured curvature mode shape (strain mode shape). The results showed that all the methods of the curvature modes measured by the piezoelectric strain sensors (PVDF) could be used as a potential tool in damage detection techniques, and the damage index method (DIM) (Stubbs et al. 1995) detected and isolated the damage better than other ones studied. Lestari and Qiao (2005) adopted a similar approach of using the directly measured curvature mode shapes from the PVDF sensor to detect debonding and core crushing in composite honeycomb sandwich beams, and both the location and relative size of damage were evaluated.

2.4.2 Modern signal processing methods using modal curvature

Ratcliffe (1997) developed a response-based gapped smoothing method (GSM) to locate the damage by fitting a localized cubic polynomial curve to the mode shape curvature and calculating a difference between the cubic and Laplacian as

$$\delta_i = (a_0 + a_1 x + a_2 x^2 + a_3 x^3) - \kappa_i \tag{2-10}$$

where a_0, a_1, a_2, a_3 are coefficients to be determined by fitting the mode shape curvature $\kappa_{i-2}, \kappa_{i-1}, \kappa_{i+1}, \kappa_{i+2}$ of damaged structure. The mode shape curvature can be obtained by a finite difference approximation using equation (2-9) or by directly measuring the strain mode shape. This method was verified by a laboratory experiment on a slotted steel beam under free-free

boundary condition. The GSM is similar to Pandey et al.'s curvature mode shape difference method in both using the mode shape curvature, but it does not require the baseline mode shape. Ratcliffe also suggested that the mode shape data from the fundamental mode are most suited to this technique. Ratcliffe and Bagaria (1998) successfully applied the GSM to locate a delamination in a composite beam. A damage index defined as the square of the difference between the curvature and the gapped cubic was used to determine the location and size of the damage. Ratcliffe (2000) later extended the GSM to broadband the operating shape curvature. The separate gapped cubic polynomials are calculated for each of the real and imaginary parts of the complex curvature functions. The damage index at each point is determined as the squared magnitude of the difference between the two cubic polynomials and the experimental curvatures. It is shown in experiment that using the broadband data can offer a better damage detection sensitivity than using the resonant data due to higher data accuracy. Yoon et al. (2001) expands the GSM by introducing a 'globally optimized smooth shape' from the analytic mode shape function. Yoon et al. (2005) generalized the one-dimensional GSM to two dimensional plate-like structural applications. Local features in the vibration curvature shapes are extracted using a two-dimensional localized surface fit. A structural irregularity index is defined to represent the structural stiffness variability for each test point on the structure. A statistical-based outlier detection method is applied to the indices to detect damaged areas. The procedure can either use the mode shape data, or broadband the operating shape data. The results confirm Ratcliffe's conclusion that using the broadband data can offer a better damage detection sensitivity than using the resonant data.

Amaravadi et al. (2001) proposed a orthogonal wavelet transform technique that operates on the curvature mode shape for enhancing the sensitivity and accuracy in damage location.

First, the curvature mode shape is calculated by the central difference approximation from the mode shapes experimentally obtained from the scanning laser vibrometer (SLV). Then, a threshold wavelet map is constructed for the curvature mode shape to detect the damage. The experimental results are reasonably accurate.

Kim et al. (2006b) proposed a curvature mode shape-based damage identification method for beam-like structures using wavelet transform. Using a small damage assumption and the Haar wavelet transformation, a set of linear algebraic equations is given by damage mechanics. With the aid of singular value decomposition, the singularities in the damage mechanism were discarded. Finally, the desired damage index was reconstructed using the pseudo-inverse solution. The performance of the proposed method was compared with two existing NDE methods (i.e., the mode shape curvature (MSC) method by Pandey et al. (1991) and the damage index (DI) method by Stubbs et al. (1996; 1995)) for an axially loaded beam without any special knowledge about the mass density and applied axial force. The effect of random noise on the performance was examined. The proposed method was verified by a finite element model of a clamped-pinned pre-stressed concrete beam and by field test data on the I-40 Bridge over the RioGrande. The proposed method resolves some existing deficiencies of the MSC method and the DI method, including the mode selection problem, the singularity problem, the axial force consideration, and the estimation of the absolute severity of damage. Despite its strong features, the proposed method still has at least the following two weaknesses. First, a dense measurement of grid is needed for good accuracy. Second, the accurate extraction of the mode shapes is considered to be a prerequisite.

2.4.3 Modal strain energy-based methods

Another category of widely used damage identification methods is modal strain energy method. These methods use the fractional modal strain energy change for damage detection. For beam-type or plate-type structures, the modal strain energy can be directly related to (and are usually derived from) the mode shape curvatures. Hence, the modal strain energy-based method can also be considered as a special case of mode shape curvature-based method in the context of beam-type or plate-type structures.

Stubbs et al. (1996; 1995) developed a damage index (DI) method based on the change in the modal strain energy. This method assumes that if the damage is primarily located at a single sub-region, then the fractional strain energy will remain relatively constant in sub-regions. For beam-type structures, the bending stiffness *EI* is assumed to be essentially constant over the length of the beam for both the undamaged and damaged modes. The damage index β at sub-region *j* can be obtained by

$$\beta_j = \frac{\sum_{i=1}^{m}(F_{ij}^* + 1)}{\sum_{i=1}^{m}(F_{ij} + 1)} = \frac{\sum_{i=1}^{m}\left[\left(\int_j (\kappa_i^*)^2 dx + \int_0^L (\kappa_i^*)^2 dx\right)\int_0^L (\kappa_i)^2 dx\right]}{\sum_{i=1}^{m}\left[\left(\int_j (\kappa_i)^2 dx + \int_0^L (\kappa_i)^2 dx\right)\int_0^L (\kappa_i^*)^2 dx\right]} \tag{2-11}$$

where F_{ij} and F_{ij}^* are the fractional strain energy of undamaged and damaged beam for *i*th mode at sub-region *j*; κ_i and κ_i^* are the curvature mode shapes of undamaged and damaged beam for *i*th mode, respectively; and *m* is the number of measured bending modes. The curvature mode shape can be obtained from a third order interpolation function of displacement mode shape.

Then, assuming that the damage indices β at different sub-regions is a normally distributed random variable, a normalized damage index Z at sub-region *j* can be obtained using

$$Z_j = \frac{\beta_j - \overline{\beta}}{\sigma_\beta} \tag{2-12}$$

where $\overline{\beta}$ and σ_β represent the mean and standard deviation of the damage indices β_j, respectively. Usually, a damage detection criterion can be set as the normalized damage index Z_j larger than 2.

Cornwell et al. (1999) generalized the DI method for one-dimensional beam-type structure into plate-type structures. Shi and Law (1998; 2000b) presented a damage localization method for beam, truss or frame type structures based on the modal strain energy change. The Modal Strain Energy Change (MSEC) at the element level is suggested as an indicator for damage localization. Law et al. (1998) applied this strain energy method to detect the damage location in a structure with incomplete and noisy measured modal data. The method consists of three stages: expansion of the measured mode shapes, localization of the damage domain using the elemental energy quotient difference, and damage quantification based on sensitivity of the modal frequency. The complete procedure of analysis is evaluated by several damage case studies of a finite element model of European Space Agency structure and verified by a laboratory experiment on a two-story steel plane frame structure. Results indicate that this method is effective and practical in detecting and quantifying single or multiple damages in the structure. Au et al. (2003) followed a similar approach as proposed by Law et al. (1998) in damage detection using the incomplete and noisy modal test data, but adopted a micro-genetic algorithm in damage quantification stage instead of the traditional iterative algorithm based on minimum rank update.

2.5 Other methods based on modal parameters

Topole and Stubbs (1995) presented for the first time a damage detection method to locate and size structural damage from the measured natural frequencies and mode shapes of damaged structure without a priori knowledge of the modal characteristics of a baseline structure. However, its application is limited by several requirements which are difficult to meet in real experiment, such as the knowledge of baseline mass and stiffness, measurement of mode shapes from all DOFs and many modes. Since then, in order to find an effective and accurate damage identification method, extensive research effort has also been put into damage identification methods utilizing both the mode shapes and frequencies or modal parameters derived from mode shapes and frequencies, such as the modal flexibility and uniform load surface.

2.5.1 Modal flexibility-based methods

Pandey and Biswas (1994) suggested using changes in modal flexibility for damage detection. Zhang and Aktan (1998) studied the modal flexibility and its derivative 'uniform load surface' (ULS). It is easy to note that the ULS is essentially a weighted average of mode shapes. Consequently, it is less sensitive to noise compared to the mode shapes. Wu and Law (2004; 2005) applied the ULS curvature to plate structures for damage localization and quantification. It is found that the ULS curvature is sensitive to the presence of local damages, even with the truncated, incomplete, and noisy measurements. Wang and Qiao (2007) modified the gapped smoothing method proposed by Ratcliff (1997) to locate delamination in a composite beam. A simplified gapped-smoothing (SGS) method using a fourth order polynomial is considered to fit the ULS curve of a damaged beam, and the difference between the polynomial and ULS curves is squared to obtain the damage index.

2.5.2 Optimization algorithm based methods

There are also several methods that formulate the damage identification method as an optimization problem and use multiple modal parameters as objective function.

Ren and De Roeck (2002a; 2002b) proposed a damage identification technique based on finite element model using the frequencies and mode shape change. The element damage equations have been established through the eigenvalue equations that characterize the dynamic behavior. Several solution techniques were discussed and compared. The results showed that The SVD-R method based on the singular value decomposition (SVD) is most effective. The method has been verified by a simple beam and a continuous beam numerical model with numbers of simulated damage scenarios. The method is further verified by a laboratory experiment of a reinforced concrete beam.

Rahai et al. (2007) presents a finite element-based approach for damage detection in structures utilizing the incomplete measured mode shapes and natural frequencies. Mode shapes of a structure are characterized as a function of structural stiffness parameters. More equations were obtained using the elemental damage equation which requires the complete mode shapes. This drawback is resolved by presenting the mode shape equations and dividing the structural degrees of freedom to measured and unmeasured parts. The non-linear optimization problem is then solved by the sequential quadratic programming (SQP) algorithm. Monte Carlo simulation is applied to study the sensitivity of this method to noise in the measured modal displacements.

Since the ill-posed nature of this type of optimization problems, the soft optimization algorithms, such as the genetic algorithm, simulation annealing or neural network algorithm, are considered useful tools for solving these problems. Ruotolo and Surace (1997) utilized the genetic algorithm to solve the optimization problem. The objective function is formulated by

introducing terms related to global damage and the dynamic behavior of the structure, i.e., the natural frequencies, mode shapes and modal curvature. The damage assessment technique has been applied both to the simulated and experimental data related to cantilevered steel beams, each one with a different damage scenario. It was demonstrated that this method can detect the presence of damage and estimate both the crack positions and sizes with satisfactory precision. The problems related to the tuning of the genetic search and to the virgin state calibration of the model are also discussed. Hao and Xiao (2002) applied a genetic algorithm with real number encoding to minimize the objective function, in which three criteria were considered: the frequency changes, the mode shape changes, and a combination of the two. A laboratory tested cantilever beam and a frame structure were used to verify the proposed technique. The algorithm does not require an accurate analytical model and provides better damage detection results for the beam than the conventional optimization method.

2.6 Literature on comparative study of damage identification method

Farrar and Jaurequi (1998a; 1998b) conducted a comprehensive experimental and numerical study of different methods of damage detection (i.e., damage index, curvature mode shape, change in flexibility, change in uniform load surface curvature, and change in stiffness) on the interstate 40 bridge.

Ndambi et al. (2002) presented a comparative study of damage detection methods based on laboratory test of two cracked RC beam. The damage detection methods based on eigenfrequencies, MAC, COMAC, flexibility matrices and strain energy are evaluated. The results showed that (1) the eigenfrequency evolutions can follow the damage severity but are not influenced by the crack damage locations; (2) the MAC factors are, in contrast, less sensitive to crack damage compared with eigenfrequencies; (3) With the COMAC factor evolution, it is

possible to detect and locate damage in the tested RC beams but difficult to follow severity and spreading; (4) The change in flexibility matrices allows also detection of the crack damage in RC beams, but the damage localization is difficult; and (5) Damage index method based on the strain energy appears to be more precise than the others in damage localization, but the difficulty remains when the damage is spread out over a certain length of the RC beam.

Huth et al. (2005) compared several response-based identification techniques based on test data on a progressive damaged prestressed concrete bridge. Although the bridge was severely cracked, natural frequencies as well as mode shapes display only minor changes. However, the relative changes of mode shapes are larger than those observed for the natural frequencies. A novel damage indicator, called the mode shape area index, based on changes of mode shapes, was developed and found as a sensitive damage detection approach. Damage detection or localization via changes of the flexibility matrix performed better than the natural frequencies or mode shapes alone.

Zhou et al. (2007) conducted a laboratory experiment and finite element analysis study to evaluate five different vibration-based damage detection methods in detection and localization of small-scale damage on the deck slab of a simply supported bridge. The five methods include three curvature-based (i.e., mode shape curvature method, strain energy method and flexibility curvature method) and two other methods (i.e., mode shape method and flexibility method). The mode shape curvatures are obtained from a natural cubic spline interpolation of mode shape. The comparative study showed that the three curvature-based methods tend to predict damage location at the measurement point due to its piecewise linear distribution caused by cubic spline interpolation. They produced virtually identical results, displaying a maximum error in damage localization of approximately half of the sensor spacing. The other two methods performed

better when the finite element data were used, but were similar to the curvature methods when the experimental data were used. The performance of all five methods investigated declined when damage was located in a near-support region. An increase in the number of measurement points led to a proportional improvement in localization resolution for the three curvature-based methods, but increasing the number of modes considered from one to three did not significantly improve the performance of the techniques.

Qiao et al. (2007b) evaluate three response-based damage detection algorithms (i.e., simplified gapped smoothing method (GSM), generalized fractal dimension (GFD), and strain energy method (SEM)) for composite laminated plates using the data acquired from these two measurement systems (i.e., a surface-bonded piezoelectric sensor PVDF system and a scanning laser vibrometer SLV system). From the damage detection outcomes, it is observed that the SLV system proves to be more convenient and effective, and it is capable of scanning high-density mode shape data over the entire plate specimens; while the PVDF system, in which the curvature mode shapes are directly acquired, exhibits good sensitivity to damage. The damage detection algorithms like GSM, GFD and SEM based on the utilization of three consecutive mode curvatures (modes 3-5) and resulting ULS curvature successfully identify the presence, location, and relative size of delamination in the composite plate.

2.7 Temperature effect on composite sandwich structures

The review in this Section focuses on temperature effect on composite sandwich structures. The temperature effect may substantially change the dynamic behavior of the GFRP materials and in turn cause potential failure of the GFRP sandwich beams/panels under working load, particularly in low temperature.

Literature on the effect of low temperature (around -60°C) on dynamic response of composites materials is relatively limited. It is interesting to note that the low temperature record in U.S. is -62.11°C in northern Alaska in the Endicott Mountains on January 23, 1971. Some related studies on the effect of temperature on the behavior of composite materials are summarized as follows.

Icten et al. (2009) investigated the low temperature effects on impact response of E-glass/epoxy laminated plates with stacking sequence $[0/90/45\text{-}45]_s$ at 20°C, -20°C, and -60°C, respectively. The impact energy was ranged from 5J to 70J. They found that the perforation threshold increase with decrease of test temperature. They also noticed that up to the impact energy of 20J the impact response and the damage tolerance of the composite is practically the same for all temperatures and beyond 20J the temperature affects significantly variation of impact characteristics.

Ibekwe et al. (2007) studied on glass fiber reinforced unidirectional and cross-ply laminated composite beams subjected to low velocity impact and compression after impact testing at low temperatures ranging from 20°C to -20°C. They concluded that the temperature has a significant effect on impact responses of laminated composites and more impact damage was induced in specimens with decreasing temperature.

Wu et al. (2006) examined the durability of FRP composite Bridge Deck materials to freeze-thaw cycling between 4.4°C and -17.8°C in different type of air (dry, distilled water, saltwater) and constant freeze at -17.8°C. Experimental results showed that the freeze-thaw cycling caused very insignificant or no change and the constant freeze at -17.8°C results in a minor increase in the flexural strength and storage modulus.

2.8 Concluding remarks on literature review

This Chapter provides a summary review on modal parameters-based damage identification algorithms for beam-type or plate-type structures as well as the effect of temperature on sandwich structures. The modal parameters-based damage identification methods are categorized as the natural frequency-based methods, mode shape-based methods, curvature mode shape-based methods and methods using both the mode shape and frequencies.

The frequency change-based damage identification method can be successfully applied to locate and quantify damage in simple structures with small damage (typically, a slender beam-type structure with artificially induced cracks) in a controlled laboratory condition. However, due to its inherent limitations, in general it is not reliable for damage detection in real complex structures or multiple/severe damage cases. Most mode shape-based and curvature-based methods only focus on damage localization. The direct use of mode shape change can only roughly locate the damage. In order to precisely locate the damage, the mode shape-based methods have to rely on optimization algorithms or signal processing techniques. The curvature-based methods are in general a very effective type of damage localization algorithms. A curvature-based algorithm, either using direct change in curvature or applying signal processing techniques on curvature, usually can successfully locate the damage.

There are still many questions to be addressed in this area. In particular, the following research topics of interest need immediate attention:

(1) Development of robust multiple damage identification methods under environmental noise. Among all available techniques, the pattern recognition technique has shown its great potential in building a robust statistical model to distinguish multiple damages in different locations and/or different types under environmental noise.

(2) Development of quantification techniques for damage magnitude. The localization of the damage is primarily studied in the literature; while the quantification of the damage, as the follow-up step in damage identification, is still in a relatively immature stage, worth immediate attention and investigation.

(3) Development of viable damage identification methods for 2-D plates. There are only limited studies available for plates, with most of them being generalized from the 1-D algorithms. It should be mentioned that the methods using the novel signal processing techniques, such as the 2-D wavelet transform, show their potential to be a powerful tool in damage identification of plates and thus demand further research.

CHAPTER 3

DYNAMIC RESPONSE OF HONEYCOMB FRP SANDWICH STRUCTURES

3.1 Introduction

In the past few years, FRP composite decks have received considerable attention for use in rehabilitation and new construction of highway bridges. This is because of their inherent advantages in high stiffness and strength to weight ratios, improved fatigue resistance, and superior damage tolerance capability as compared to traditional steel reinforced concrete decks. Due to lightweight constituent materials and thin-walled/cellular configuration, FRP bridge decks promote rapid new constructions and replacements of existing deteriorated concrete decks. FRP bridge decks are commonly honeycomb FRP sandwich structures placed transversely to the supporting structures.

Before developing any damage identification method for sandwich beams or plates, it is crucial to examine the static/dynamic mechanical properties of FRP sandwich structures. Sandwich structures, which are typically constructed by two thin face sheets and a soft and thick core, have been widely used in civil, mechanical and aerospace engineering. The core is usually made of soft materials and/or in the form of foams or honeycombs for weight reduction and energy absorption purpose. In such a configuration, the stiffness of the core is usually very low and its compressible deformation cannot simply be neglected in accurate dynamic analysis of the whole sandwich systems.

For the analysis of sandwich beams, there are mainly two types of theories: (1) equivalent single layer theory, and (2) layer-wise lamination theory. In the equivalent single layer displacement-based theories, one single expansion of each displacement component is used through the thickness of the laminates. The classical beam theory (Tauchert 1975) of this type is

based on the Euler-Bernoulli assumption that the planes initially normal to the mid-plane remain plane and normal to the mid-plane after bending. This method leads to high level of error due to completely neglecting of the transverse shear deformation. An improved one of this type is Timoshenko beam theory, also known as the first-order shear deformable theory, which assumes the transverse shear stress/strain distribution is constant through the beam thickness. Gordaninejad and Bert (1989) adopted this theory for the analysis of laminated beams. While in the layer-wise theories, each layer is treated as a separate beam, and the transverse shear effects in discrete layers are introduced into the assumed displacement field. There are many theories of this type, e.g., the layer-wise Euler-Bernoulli laminated beam theory (Murty 1985; Ojalvo 1977), first-order shear deformable laminate beam theory (Davalos et al. 1994), and higher-order laminate beam theory (Lu and Liu 1992; Reddy 1987). Lately, Frostig et al. (Frostig et al. 1992; Frostig and Thomsen 2004) presented a high-order sandwich panel theory approach for the free vibration analysis of sandwich panels with a flexible core. The formulation uses the classical thin plate theory for the face sheets and a three-dimensional elasticity theory for the core. The full dynamic effects, including both the horizontal vibration and rotary inertia of the core, are taken into consideration. Yang and Qiao (2005) used a similar approach to solve the impact problems of the sandwich beam. Only the cases with simply supported boundary conditions were presented in Frostig and Thomsen (2004) and Yang and Qiao (2005).

In this chapter, the dynamic response of an as-manufactured FRP honeycomb sandwich beam is analytically and experimentally evaluated. The analytical study follows the similar sandwich beam formulation as in Frostig and Thomsen (2004) and Yang and Qiao (2005). However, without the derivation of the details of the equations of motions in the form of differential equations, the problem is formulated by Hamilton's variational principle and solved

directly by the Ritz method. Then, the solutions are compared with the Timoshenko beam theory, numerical finite element simulation and experimental modal testing results. The rest of the chapter is organized as follows. The derivation of the equivalent elastic properties for face laminate and honeycomb core is introduced in Section 3.2. The formulation of the high-order sandwich beam theory and the solutions for cantilevered beams by the Ritz method are given in Section 3.3. The finite element analysis and the experimental program are described in Section 3.4. The results of analytical/numerical solutions and experimental tests are discussed in Section 3.5, and a parametric study is also presented to show the effects of soft core materials and beam length in Section 3.5.

3.2 Modeling of FRP honeycomb sandwich beams

Using a micro/macro mechanics approach for the face laminates and a mechanics of material approach for honeycomb core, the modeling of equivalent elastic properties for the face laminate and honeycomb core is presented in this section.

3.2.1 Geometry of FRP sandwich materials

The FRP sandwich materials used in this study were manufactured by Kansas Structural Composites, Inc. (KSCI) (Davalos and Qiao et al. 2001). Originated from the basic concept of sandwich structures, the geometry of the FRP structure is designed as an FRP honeycomb core sandwiched by two FRP face laminates (see Fig. 3.1). It should be noted that the thermosetting property of the polyester resins used in the FRP panel distinguishes the honeycomb cores from their metal counterparts in both manufacturing and consequent corrugated shapes. Unlike the traditional metal honeycomb cores with hexagonal or circular shape configuration, the shape of the FRP corrugated cell wall follows a sinusoidal function in the panel (see Fig. 3.2). The curved

walls are produced by forming FRP sheets to a corrugated mold with a sinusoidal configuration. Then, the flat FRP sheets and corrugated sheets are sequentially bonded together to produce the combined flat and curved core wall. The assembled honeycomb core is then co-cured with the top and bottom face laminates to build a sandwich beam.

The wave function of corrugated core wall can be defined as

$$y = \frac{b}{2}(1 - \cos\frac{\pi x}{a}) \tag{3-1}$$

The dimensions of the sinusoidal core are a = 50.8 mm, b = 50.8 mm, $t_1 = t_2$ = 2.28 mm, as shown in Fig. 3.2.

Two types of sandwich beams are investigated in this study: one with the longitudinal core, the other with transverse core. The only difference is that the length direction of the longitudinal core beam is in the x direction; while the length direction of the transverse core beam is in the y direction, as shown in Fig. 3.1.

The FRP sandwich beams in this study are 0.203 m in width. The beams have two unit cells in width. The unit cell is shown in Fig. 3.2. The thickness of face laminates and honeycomb core are 11 mm and 83 mm, respectively, so the total thickness of the FRP panel is 105 mm. The constituent materials used for the honey-comb sandwich panel (both face laminates and core) are E-glass fiber and polyester resins.

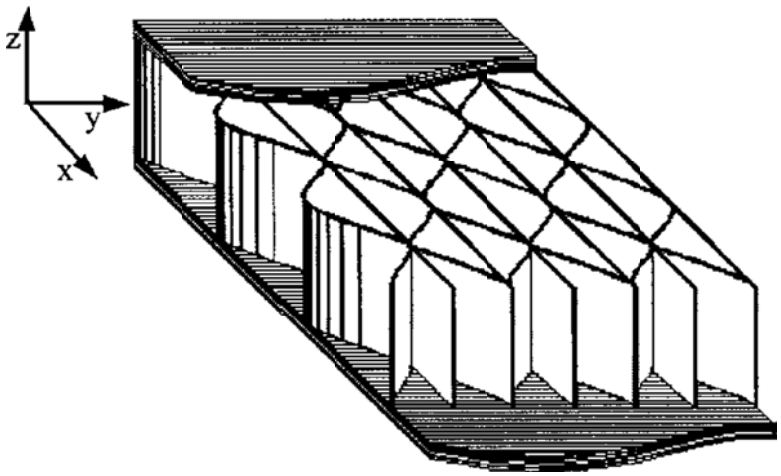

(a)

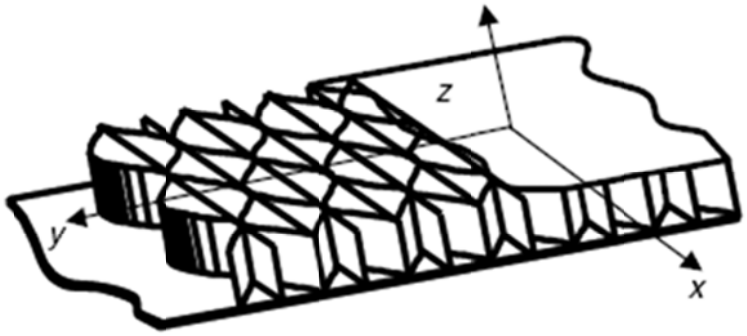

(b)

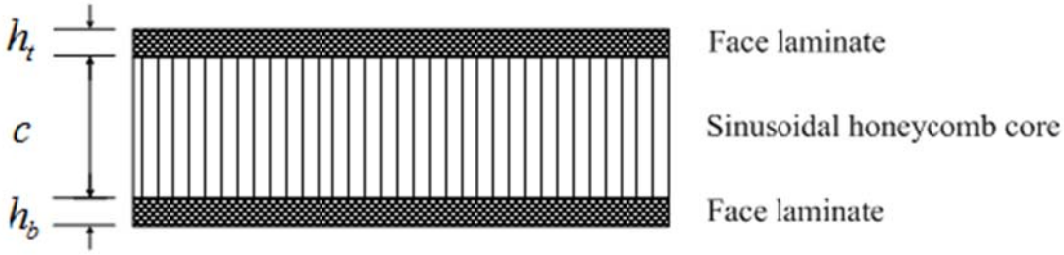

(c)

Figure 3.1 Configuration of FRP sandwich beam

(a) longitudinal core; (b) transverse core; (c) cross-section of core

($h_t = h_b = 11$ mm, c = 83 mm).

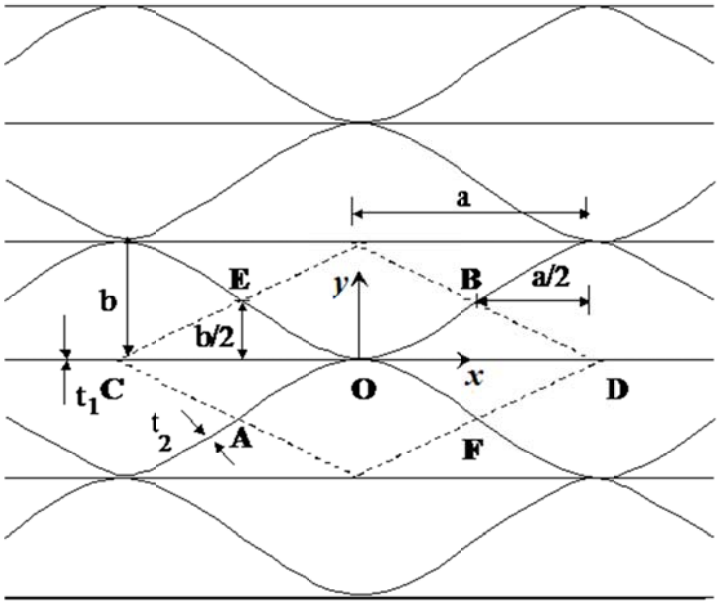

Figure 3.2 Geometry of sinusoidal core in honeycomb structures

(a = 50.8mm, b = 50.8mm, $t_1 = t_2 = 2.08$ mm).

3.2.2 Modeling of face laminates

The lay-up of the face laminates and the properties of each ply are given in (Davalos et al. 2001) and shown here in Fig. 3.3 and Table 3.1. The apparent engineering properties of the face sheets of the FRP sandwich beams were predicted by Davalos, Qiao et al. (2001) using a combined micro- and macro-mechanics approach. A set of equivalent laminate stiffness properties can be defined for approximately balanced symmetric face laminates, and they are given in Table 3.2. These elastic constants for face laminates represent the stiffness of an equivalent, orthotropic plate that behaves like the actual laminates under in-plane loads.

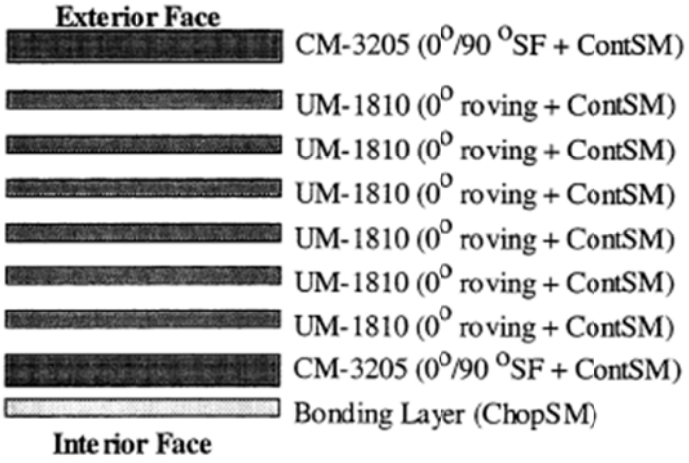

Figure 3.3 Face laminates lay-up.

Table 3.1 Ply stiffness obtained from micromechanics model

Ply name	orientation	E_1 (GPa)	E_2 (GPa)	G_{12} (GPa)	G_{23} (GPa)	ν_{12}	ν_{23}
Bond layer	random	9.72	9.72	3.50	2.12	0.394	0.401
CM 3205	0^o or 90^o	27.72	8.00	3.08	2.88	0.402	0.390
	random	11.79	11.79	4.21	2.36	0.402	0.400
UM 1810	0^o	30.06	8.55	3.30	3.08	0.293	0.386
	random	15.93	15.93	5.65	2.96	0.409	0.388
ChopSM 308	random	11.79	11.79	4.21	2.97	0.402	0.388

Table 3.2 Material properties of face laminates

	ρ_f, g/cm^3	E_x^f, GPa	E_y^f, GPa	G_{xy}^f, GPa	G_{xz}^f, GPa	G_{yz}^f, GPa	ν_{xy}
Face laminates	1.592	19.62	12.76	3.76	3.75	3.68	0.302

3.2.3 Modeling of honeycomb core

The microstructure of core walls, either the flat or the curved walls, consists of two layers of ChopSM (ChopSM308). The ChopSM can be modeled as an isotropic layer, and its stiffness properties are listed in Table 3.1. So the core wall can also be modeled as an isotropic layer with double thickness of the ChopSM and the same stiffness properties as the ChopSM. To predict the equivalent stiffness properties of the sinusoidal core, a mechanics of material approach proposed by Qiao and Wang (2005) is adopted. The solution for the equivalent stiffness can be expressed as follows:

$$\begin{aligned} E_x^c &= \frac{t_1}{b} E_1^w = 0.0449 E_1^w \\ E_y^c &= \frac{2Ph}{b\Delta_y} = 3.81\times10^{-3} E_1^w \\ E_z^c &= \frac{at_1 + t_2 S}{ab} E_1^w = 0.110 E_1^w \\ G_{xy}^c &= \frac{2Fh}{b\Delta_x} = 2.01\times10^{-3} E_1^w \end{aligned} \tag{3-2}$$

where E_1^w is the longitudinal Young's modulus of solid core wall (i.e., ChopSM 308); S is the length of the segment AB in Fig. 3.2.

The solutions for the core effective transverse shear moduli are available in Xu et al. (2001)

$$\begin{aligned} G_{xz}^c &= (\frac{t_1}{b} + \frac{at_2}{bS}) G_{12}^w = 0.0755 G_{12}^w \\ G_{yz}^c &= \frac{bt_2}{aS} G_{12}^w = 0.0307 G_{12}^w \end{aligned} \tag{3-3}$$

where G_{12}^w is the in-plane shear modulus of solid core wall (i.e., ChopSM 308); S is the length of the segment AB in Fig. 3.2.

The Equivalent stiffness properties of sinusoidal honeycomb core are listed in Table 3.3.

Table 3.3 Equivalent stiffness properties of honeycomb core

	ρ_c, kg/m^3	E_x^c, GPa	E_y^c, GPa	E_z^c, GPa	G_{xy}^c, GPa	G_{xz}^c, GPa	G_{yz}^c, GPa	v_{xy}^c
Sinusoidal core	149	0.529	0.0449	1.30	0.0237	0.318	0.129	0.291

3.2.4 One layer model of the sandwich beam

In order to predict the natural frequencies of the sandwich beam using Timoshenko beam theory, the equivalent stiffness properties of the sandwich beam are derived from the properties of face sheets and core given in Sections 3.2.2 and 3.2.3. The derivation of the equivalent material properties of the sandwich beams were given by Lestari and Qiao (2006). The stiffness properties in Table 3.4 represent the stiffness of an equivalent, homogeneous one layer beam that behaves like the actual sandwich beam under bending. The natural frequencies of the equivalent homogeneous beam can be calculated using Timoshenko beam theory. The results are listed in Table 3.6 for comparison with the high order sandwich beam theory.

Table 3.4 The equivalent material properties adopted in Timoshenko beam theory

Core	$\rho A(kg/m)$	$\rho I(kg\cdot m)$	$EI(\times 10^6 N\cdot m^2)$	$\kappa GA(\times 10^6 N)$
Longitudinal	9.6204	0.0172	0.3018	8.15
Transverse	9.6204	0.0172	0.1933	3.34

3.3 High-order sandwich beam theory for cantilevered beams

3.3.1 Mathematical formulation

The High-order sandwich beam theory considered in this study follows the same model of sandwich beams as in Yang and Qiao (2005). The top and bottom face sheets are modeled as

classical Euler-Bernoulli beam, and the core are modeled as a three-dimensional elastic body. The geometry and coordinate system of the sandwich beam are shown in Fig. 3.4(a). The internal resultants and stresses are shown in Fig. 3.4(b). The mathematical formulation is derived by finding the extremum of the integral over the Lagrangian. The Hamilton principle reads:

$$\delta\int_{t_1}^{t_2}(V+U-T)dt=0 \tag{3-4}$$

where T,U,V are the kinetic energy, the strain energy and the potential of the external loads of the whole sandwich beam, respectively; t is the time coordinate between the time t_1 and t_2; δ denotes the variation operator.

The total kinetic energy of the sandwich beam T can be expressed as

$$T=T_t+T_b+T_c=\frac{1}{2}\rho_t\int_{V_t}(\dot{w}_t^{\,2}+\dot{u}_t^{\,2})dV+\frac{1}{2}\rho_b\int_{V_b}(\dot{w}_b^{\,2}+\dot{u}_b^{\,2})dV+\frac{1}{2}\rho_c\int_{V_c}(\dot{w}_c^{\,2}+\dot{u}_c^{\,2})dV \tag{3-5}$$

where ρ_t, ρ_b, ρ_c is the density of the top and bottom face sheets and the core, respectively; $\dot{u}_i$, $\dot{w}_i$ ($i=t,b,c$) are the velocities in the longitudinal direction (x-direction) and transverse direction (z-direction), respectively; V_i ($i=t,b,c$) is the volume of each part of the beam.

The total potential of the external loads V of the sandwich beam under free vibration is 0. The strain energy of the core and the face sheets are

$$U_c=\frac{1}{2}\int_A\int_z(\sigma_{cxx}\varepsilon_{cxx}+\sigma_{czz}\varepsilon_{czz}+\tau_{cxz}\gamma_{cxz})dzdA, \tag{3-6}$$

$$\begin{aligned}U_f&=\frac{1}{2}\int_A\int_z(\sigma_{fxx}\varepsilon_{fxx}+\tau_{fxz}\gamma_{fxz})dzdA\\&=\frac{1}{2}\int_A(N_{fx}\partial u_{0f}/\partial x-M_{fx}\partial^2 w_f/\partial x^2)dA,\end{aligned} \tag{3-7}$$

where U_f ($f=t,b$) and U_c are the strain energy of the top and bottom face sheets and the core, respectively; N_{fx} and M_{fx} ($f=t,b$) are the stress resultants in the face sheets.

For the core, the strain compatibility equations and constitutive equations give

$$\begin{aligned}
&\frac{\partial u_c}{\partial x} = \varepsilon_{cxx} = \frac{\sigma_{cxx}}{E_{cx}} \\
&\frac{\partial w_c}{\partial z} = \varepsilon_{czz} = \frac{\sigma_{czz}}{E_{cz}}, \\
&\frac{\partial u_c}{\partial z} + \frac{\partial w_c}{\partial x} = \gamma_{cxz} = \frac{\tau_{xz}}{G_c},
\end{aligned} \tag{3-8}$$

Substituting equation (3-8) into equation (3-6), we obtain

$$U_c = \frac{1}{2}\int_A \int_z [E_{cx}(\frac{\partial u_c}{\partial x})^2 + E_{cz}(\frac{\partial w_c}{z})^2 + G_c(\frac{\partial u_c}{\partial z} + \frac{\partial w_c}{\partial x})^2]dzdA \tag{3-9}$$

For the face sheets, from the basic assumptions of the Euler-Bernoulli beam theory, u_t and u_b are given as

$$u_t(x,z) = u_{0t}(x) - z\frac{\partial w_t(x)}{\partial x}, u_b(x,z) = u_{0b}(x) - z\frac{\partial w_b(x)}{\partial x} \tag{3-10}$$

where u_{0t} and u_{0b} are the longitudinal displacement of the mid-plane of the top and bottom face sheets, respectively.

The constitutive equations (including the bending-stretching coupling effects) give,

$$N_{fx} = A_{f11}\frac{\partial u_{0f}}{\partial x} - B_{f11}\frac{\partial^2 w_f}{\partial x^2}, M_{fx} = B_{f11}\frac{\partial u_{0f}}{\partial x} - D_{f11}\frac{\partial^2 w_f}{\partial x^2} \tag{3-11}$$

where A_{f11}, B_{f11}, and D_{f11} ($f = t, b$) are the extensional, extensional-bending coupling and bending stiffness of the face sheets, respectively.

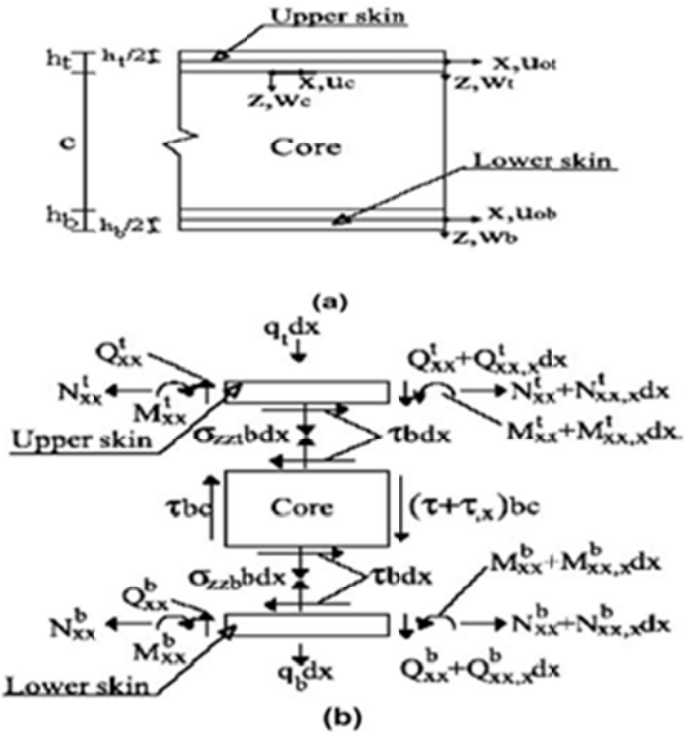

Figure 3.4 The coordinate systems of sandwich beam
(a) geometry and coordinates, and (b) internal resultants and stresses.

Substituting Eq. (3-11) into Eq. (3-8), we obtain

$$U_f = \frac{1}{2}\int_A [A_{f11}(\frac{\partial u_{0f}}{\partial x})^2 - 2B_{f11}\frac{\partial u_{0f}}{\partial x}\frac{\partial^2 w_f}{\partial x^2} + D_{f11}(\frac{\partial^2 w_f}{\partial x^2})^2]dA \tag{3-12}$$

The total strain energy of the sandwich beam is given as

$$U = U_t + U_b + U_c \tag{3-13}$$

From equations (3-4), (3-9) and (3-12), Lagrangian in the Hamilton principle can be expressed as

$$\Pi = U - T = \Pi(w_t, w_b, u_{0t}, u_{0b}, w_c, u_c) \tag{3-14}$$

To further simplify the problem, the following assumptions are made for the core:

(1) The vertical displacement of the core w_c takes a quadratic pattern through the thickness of the core, i.e., w_c is a quadratic function of z:

$$w_c = w_{c2}(x)z^2 + w_{c1}(x)z^1 + w_{c0}(x) \tag{3-15}$$

(2) The longitudinal displacement of the core u_c takes a cubic pattern through the thickness of the core, i.e., u_c is a cubic function of z:

$$u_c = u_{c3}(x)z^3 + u_{c2}(x)z^2 + u_{c1}(x)z^1 + u_{c0}(x) \tag{3-16}$$

Based on the coordinate system showed in Fig. 3.4, the continuity conditions at the two core-face sheet interfaces give

$$w_c(x, z=0) = w_t, w_c(x, z=c) = w_b \tag{3-17}$$

$$u_c(x, z=0) = u_{0t} - \frac{h_t}{2} w_t, u_c(x, z=c) = u_{0b} - \frac{h_b}{2} w_b \tag{3-18}$$

Substituting equation (3-16) into equation (3-18), we obtain

$$w_c = \frac{w_b - w_t - cw_{c1}}{c^2} z^2 + w_{c1} z + w_t \tag{3-19}$$

Substituting equation (3-17) into equation (3-19), we obtain

$$u_c = u_{c3} z(z^2 - c^2) + u_{c2} z(z-c) + \frac{z}{c}(u_{0b} + w_{b,x}\frac{h_b}{2}) + \frac{c-z}{c}(u_{0t} - w_{t,x}\frac{h_t}{2}) \tag{3-20}$$

Using equations (3-20) and (3-21), Lagrangian in the Hamilton principle can be further expressed as a function of seven variables:

$$\Pi = T - U = \Pi(w_t, w_b, u_{0t}, u_{0b}, w_{c1}, u_{c2}, u_{c3}) \tag{3-21}$$

3.3.2 Cantilevered beam solution using Ritz method

For the sandwich beam with one end clamped and the other end free, the Rayleigh-Ritz method is used to solve the problem. In order to satisfy the boundary conditions, the shape functions for the displacements are assumed to be

$$
\begin{aligned}
w_t(x,t) &= e^{i\omega t}\sum_{n=1}^{m} C_{wtn}(\cos\frac{(2n-1)\pi x}{2L}-1+(\frac{2n-1}{2n})^3(\sin\frac{n\pi x}{L}-\frac{n\pi x}{L})),\\
w_b(x,t) &= e^{i\omega t}\sum_{n=1}^{m} C_{wbn}(\cos\frac{(2n-1)\pi x}{2L}-1+(\frac{2n-1}{2n})^3(\sin\frac{n\pi x}{L}-\frac{n\pi x}{L})),\\
u_{0t}(x,t) &= e^{i\omega t}\sum_{n=1}^{m} C_{utn}(\sin\frac{(2n-1)\pi x}{2L}+(\frac{2n-1}{2n})^2(\cos\frac{n\pi x}{L}-1)),\\
u_{0b}(x,t) &= e^{i\omega t}\sum_{n=1}^{m} C_{ubn}(\sin\frac{(2n-1)\pi x}{2L}+(\frac{2n-1}{2n})^2(\cos\frac{n\pi x}{L}-1)),\\
w_{c1}(x,t) &= e^{i\omega t}\sum_{n=1}^{m} C_{wc1n}(\cos\frac{(2n-1)\pi x}{2L}-1+(\frac{2n-1}{2n})^3(\sin\frac{n\pi x}{L}-\frac{n\pi x}{L})),\\
u_{c2}(x,t) &= e^{i\omega t}\sum_{n=1}^{m} C_{uc2n}(\sin\frac{(2n-1)\pi x}{2L}+(\frac{2n-1}{2n})^2(\cos\frac{n\pi x}{L}-1)),\\
u_{c3}(x,t) &= e^{i\omega t}\sum_{n=1}^{m} C_{uc3n}(\sin\frac{(2n-1)\pi x}{2L}+(\frac{2n-1}{2n})^2(\cos\frac{n\pi x}{L}-1))
\end{aligned}
\tag{3-22}
$$

where C_i $(i = wtn, wbn, utn, ubn, wc1n, uc2n, uc3n)$ are the amplitude coefficients of displacements for the *n*th term, and *m* is the total mode of interest.

Based on the principle of extremum energy, the Lagrangian Π is minimized with respect to the unknown coefficients in the shape functions of the displacements

$$\partial\Pi / \partial C_i = 0 \tag{3-23}$$

From equation (3-23), the governing equations in the matrix form are given as

$$
\left\{\begin{bmatrix}
K_{11} & K_{12} & K_{13} & K_{14} & K_{15} & K_{16} & K_{17}\\
 & K_{22} & K_{23} & K_{24} & K_{25} & K_{26} & K_{27}\\
 & & K_{33} & K_{34} & K_{35} & K_{36} & K_{37}\\
 & & & K_{44} & K_{45} & K_{46} & K_{47}\\
 & & & & K_{55} & K_{56} & K_{57}\\
 & & & & & K_{66} & K_{67}\\
 & & & & & & K_{77}
\end{bmatrix} - \omega^2 \begin{bmatrix}
M_{11} & M_{12} & M_{13} & M_{14} & M_{15} & M_{16} & M_{17}\\
 & M_{22} & M_{23} & M_{24} & M_{25} & M_{26} & M_{27}\\
 & & M_{33} & M_{34} & M_{35} & M_{36} & M_{37}\\
 & & & M_{44} & M_{45} & M_{46} & M_{47}\\
 & & & & M_{55} & M_{56} & M_{57}\\
 & & & & & M_{66} & M_{67}\\
 & & & & & & M_{77}
\end{bmatrix}\right\}\begin{bmatrix}
C_{wtn}\\ C_{wbn}\\ C_{utn}\\ C_{ubn}\\ C_{wc1n}\\ C_{uc2n}\\ C_{uc3n}
\end{bmatrix}
$$

$$= 0 \tag{3-24}$$

where $K_{ij} = \frac{\partial^2 U}{\partial C_i \partial C_j}, M_{ij} = \frac{\partial^2 T}{\partial C_i \partial C_j}$.

By solving the eigenvalues of $[K]$ and $[M]$ matrix, the modal frequencies can be obtained. The mode shapes can be subsequently obtained from the eigenvectors.

Substituting the equivalent elastic properties of the sandwich beam obtained in Section 3.2 into equation (3-24), the modal frequencies are extracted as shown in Tables 3.5 and 3.6.

Table 3.5 Comparison of the natural frequencies of the cantilever beams using different methods (Longitudinal core)

Mode	FEA	Test	Timoshenko beam theory	High-order sandwich beam theory
L=0.762				
1	126.5	87.9	149.0	127.9
2	534.3	369.1	606.7	554.6
3	1125.5	1004.0	1268.2	1069.1
4	1702.3	1412.0	1901.0	1801.1
5	>2000	>2000	>2000	>2000
L=1.016				
1	74.6	56.6	88.6	75.3
2	352.6	267.6	405.0	363.4
3	774.9	748.0	879.5	802.1
4	1210.0	1148.0	1361.3	1276.4
5	1648.0	1563.0	1846.5	1750.7
L=1.270m				
1	48.9	50.8	58.3	53.5
2	249.2	218.8	288.8	273.6
3	568.8	572.3	649.9	627.9
4	913.1	882.8	1033.4	1014.9
5	1265.0	1174.0	1423.9	1412.6
L=1.524m				
1	34.4	37.1	41.1	34.7
2	184.5	162.1	215.4	188.3
3	435.3	449.2	500.5	449.9
4	716.0	705.1	814.7	750.1
5	1008.0	974.6	1139.7	1067.2
L=1.778m				
1	25.5	21.5	30.5	25.7
2	141.5	127.0	166.1	144.0
3	343.3	349.6	397.0	353.6
4	576.9	544.9	659.9	602.4
5	824.6	773.4	936.2	871.7
L=2.032m				
1	19.6	13.7	23.5	19.8
2	111.7	99.6	131.7	113.4
3	277.2	257.8	322.1	284.6
4	474.6	490.2	545.4	494.1
5	687.6	658.2	784.0	726.1

Table 3.6 Comparison of the natural frequencies of the cantilever beams using different methods (Transverse core)

Mode	FEA	Test	Timoshenko beam theory	High order sandwich beam theory
L=0.508				
1	169.2	-	212.2	188.6
2	561.2	-	698.6	659.3
3	1081.9	-	1351.4	1237.9
4	1542.2	-	1925.2	1886.4
5	-	-	--	--
L=1.016				
1	54.1	-	68.2	58.2
2	225.8	-	286.1	260.1
3	474.2	-	602.3	559.4
4	714.9	-	909.8	862.1
5	956.5	-	1218.1	1167.5
L=1.524m				
1	31.34	25.39	32.27	27.2
2	152.17	144.53	158.2	139.9
3	339.10	325.18	353.6	321.5
4	534.70	532.21	559.5	520.4
5	732.53	707.98	768.3	724.6
L=2.032m				
1	18.06	18.56	18.6	15.62
2	95.71	84.96	99.3	86.3
3	224.21	216.81	233.7	208.8
4	366.96	356.46	383.8	310.9
5	514.93	505.88	539.9	503.8

3.4 Finite element analysis and experimental test

3.4.1 Finite element analysis

The commercial Finite Element Analysis package ABAQUS is used to conduct an eigenvalue analysis to extract the natural frequencies and the mode shapes of the cantilevered sandwich beam. The sandwich beam was modeled as two face sheets and a detailed sinusoidal

core. The face sheets and the sinusoidal core walls are modeled as 4-node first-order plate elements S4 and 3-node first-order plate elements S3. The lay-ups and corresponding material properties of face sheets and core walls are the same as shown in Fig. 3.3 and Table 3.1. The sandwich beam is clamped at one end and free at the other end. The beams with different lengths are considered in the modeling. Fig. 3.5 gives the first five mode shapes for the span of the 2.032 *m* long cantilevered beam with transverse core. The natural frequencies obtained by FEM of the cantilever beams with the transverse and longitudinal cores are listed in Table 3.5 and 3.6, respectively, for comparison.

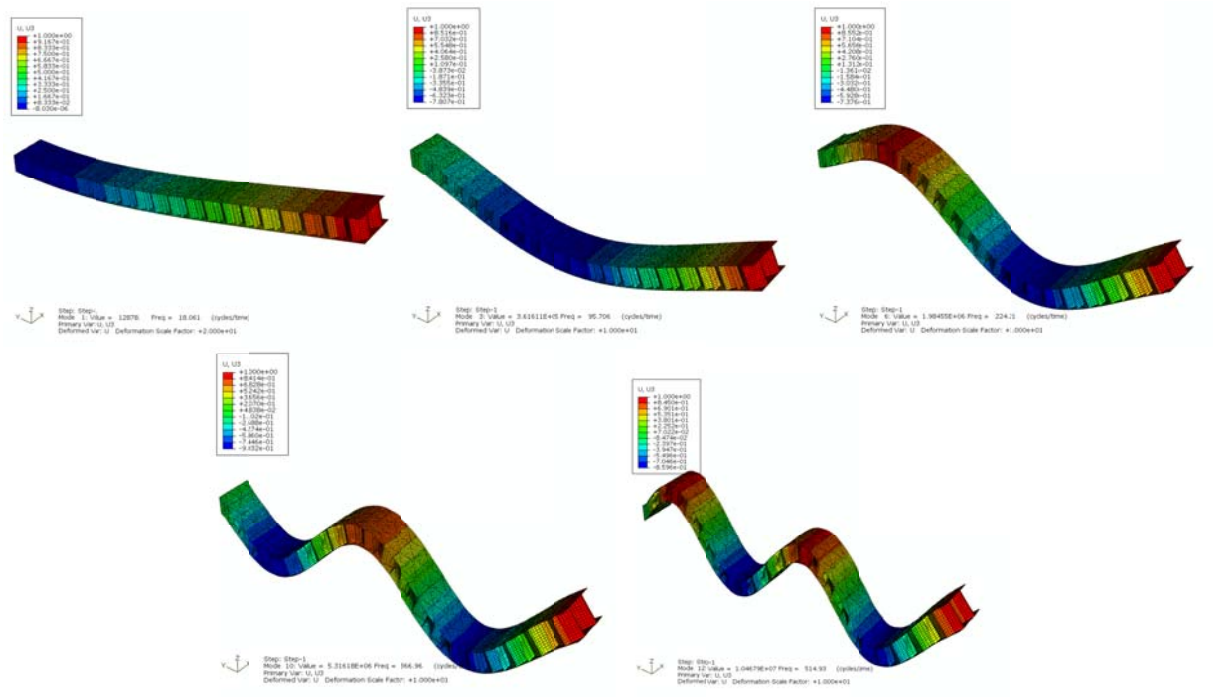

Figure 3.5 First five mode shapes of beam with transverse core by FE.

3.4.2 Experimental test

The FRP sandwich beams tested in this experiment were manufactured by Kansas Structural Composites, Inc. (KSCI). The sandwich beams were clamped and tested at different lengths. To simulate a cantilevered condition, one end of the beam was clamped in a tightened

steel frame such that the beam specimen posed well in place. This condition was considered as the clamped boundary condition for both the face sheet and the core at this particular end.

The modal testing of the beam is conducted with an impact hammer and a piezoelectric sensor. The beams were subjected to a dynamic pulse load applied at the free end using the modally tuned hammer (PCB 652B10). One polyvinylidence fluoride (PVDF) film (a piezoelectric-based material) bonded to the surface of the beam at the free end was used as a sensor to record the response signals. The analog excitation/response signals then passed a low-pass anti-aliasing filter to prevent the aliasing problem. The maximum frequency of interest was 1 kHz, so that at least the first five natural frequencies of the beam could be measured. A Krohn-Hite 3382 8-pole dual channel filter was employed to filter out the high frequency signals above the cut-off frequency of 2 kHz. The filtered signals were then digitized and collected by the data acquisition system dSPACE CP1103 at the sampling frequency of 4 kHz. The measurements at each point were repeated 16 times, and the synchronized time histories from the excitation and response measurements were averaged to enhance the signal-to-noise ratio (SNR). From these synchronized excitation and response time-histories, the frequency-response functions (FRFs) of these tested points are calculated. Then, the natural frequencies of the beam can be identified from the peaks of the FRF curves.

The experimental set-up is shown in Fig. 3.6. Results of natural frequency from modal testing of sandwich beams with different lengths are presented in Tables 3.5 and 3.6 for comparison.

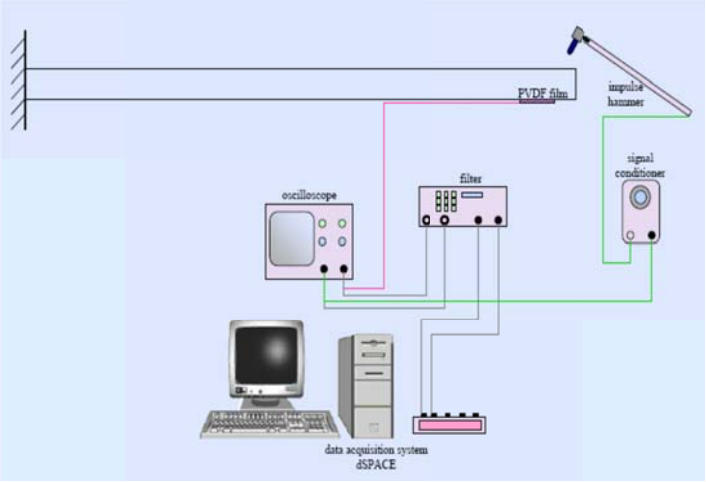

(a) Experimental set-up

(b) Experimental set-up in laboratory

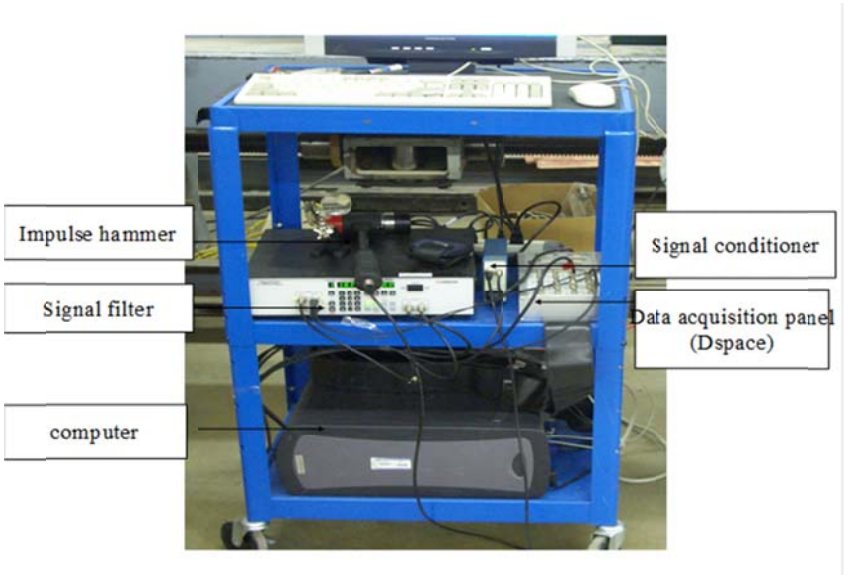

(c) Testing devices

Figure 3.6 Experimental set-up.

3.5 Results and Discussion

The results of natural frequencies from the finite element analysis (FEA), experimental test, Timoshenko's beam theory (TBT) and high-order sandwich beam theory (HSBT) are listed in Tables 3.5 and 3.6 for the transverse and longitudinal cores, respectively. In Tables 3.5 and 3.6, it can be noticed that the experimental test shows good agreement with the FEA results in the beams with the longitudinal core. Since in the experiment the ideal fully-clamped boundary condition could not be achieved, the experimental test generally gives lower natural frequencies than FEA, especially for the 1^{st} and 2^{nd} modes in the short beam cases. Due to the complexity of the sinusoidal core sandwich beam, an exact theoretical solution is very difficult, if not impossible. Therefore, the FEA with a detailed model of sinusoidal core is considered as an exact solution in this study.

3.5.1 Validation of high-order sandwich beam model

Based on Tables 3.5 and 3.6, the high-order sandwich beam theory (HSBT) shows close agreement with the FEA results and gives better prediction of natural frequencies than Timoshenko's beam theory (TBT). In general, using the equivalent material properties given by micro/macro mechanics, the HSBT can accurately predict the natural frequencies of a sinusoidal core sandwich beam.

In the longitudinal core case, the HSBT shows very close agreement with the FEA at all investigated length to depth ratios (L/h) and gives an approximation of natural frequencies between the FEA and the TBT in most cases, as shown in Fig. 3.7(a).

In the transverse core case, although the prediction by HSBT is not as close to the FEA as in the longitudinal core case, the HSBT results still considerably improve the TBT results,

especially at a length to depth ratio (*L/h*) less than 10, as the effect of transverse shear deformation become more significant.

In conclusion, for short sandwich beams, using HSBT instead of TBT to predict the free vibration behavior is necessary to improve the accuracy.

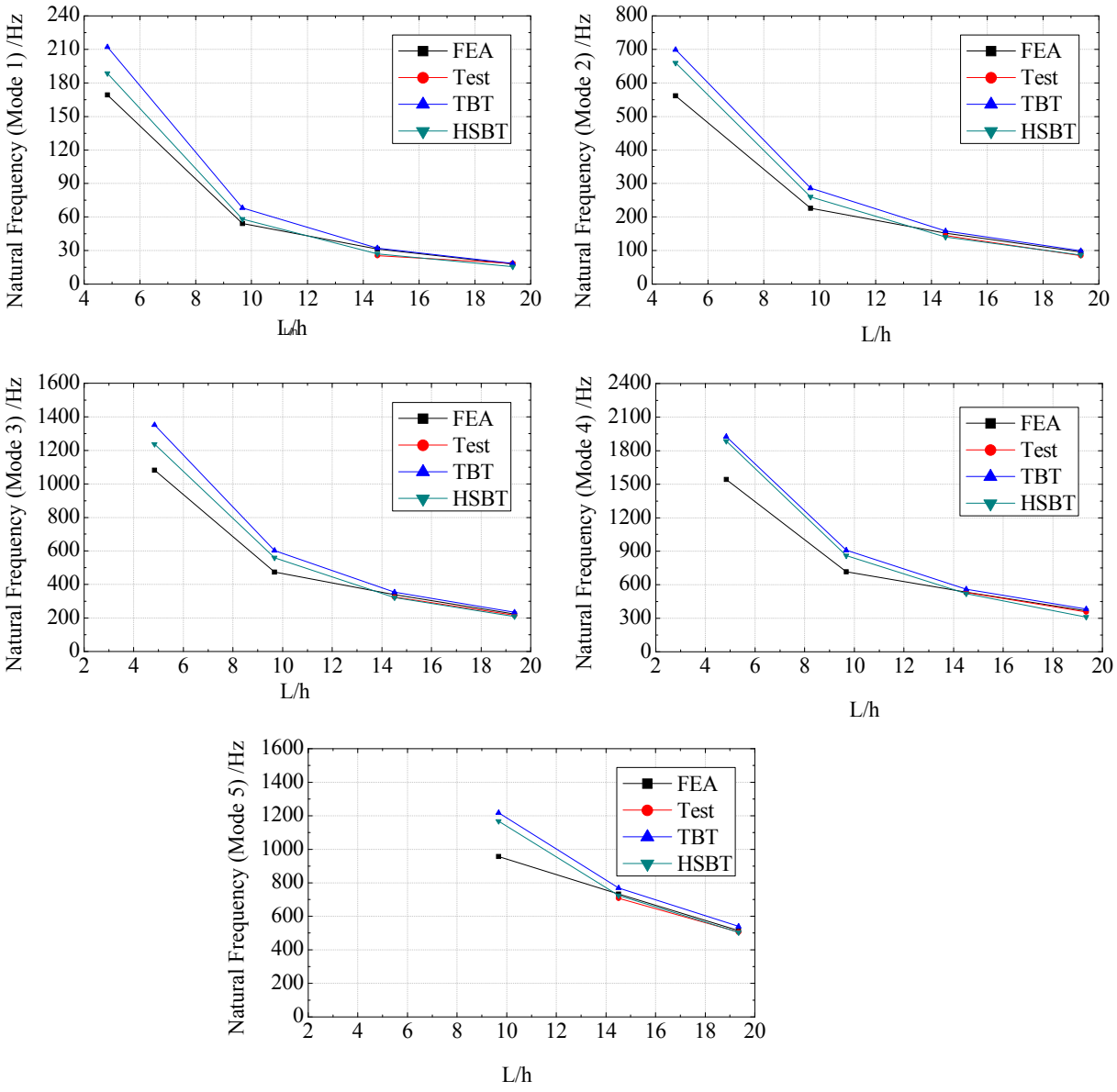

(a) Transverse Core

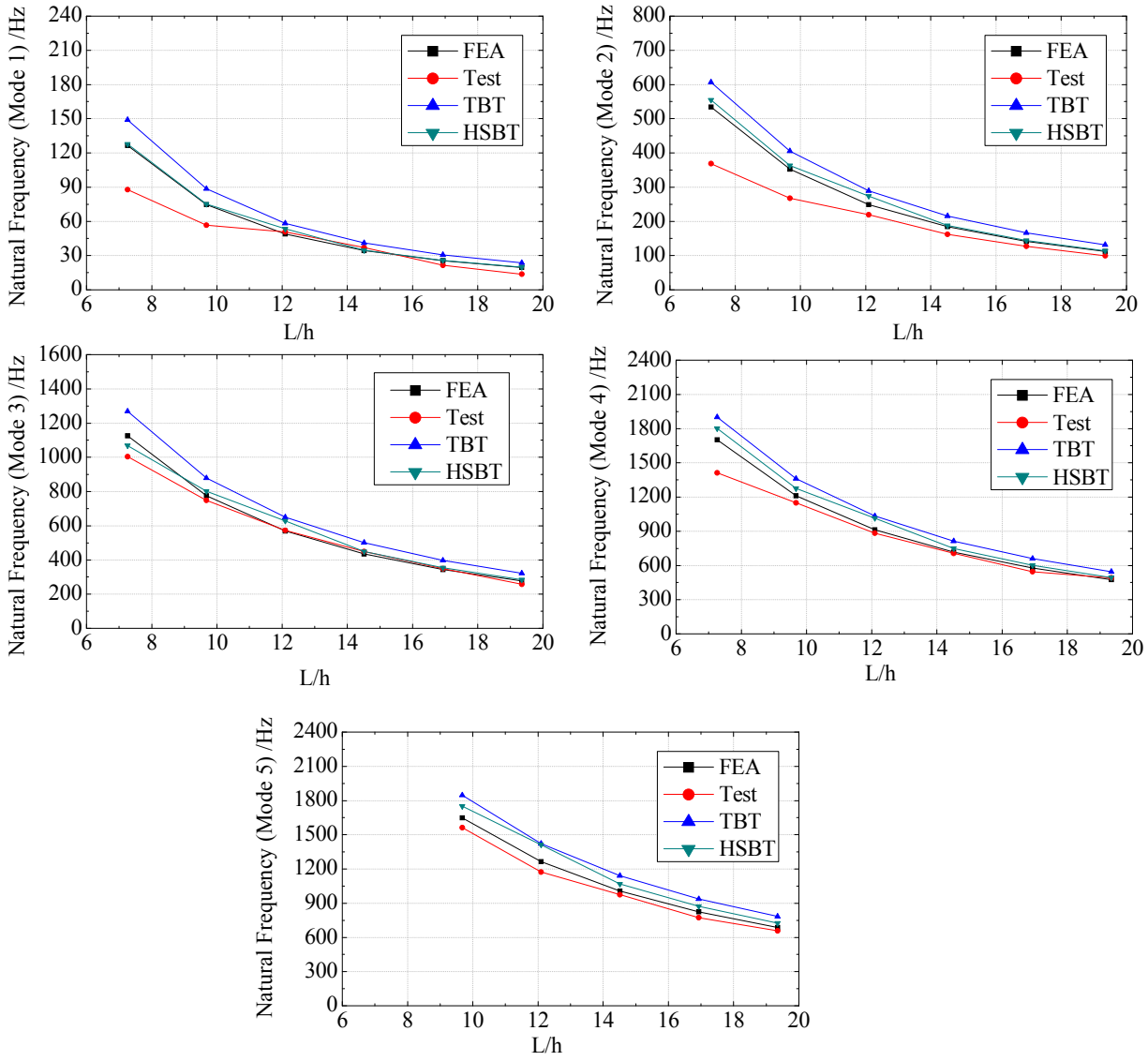

(b) Longitudinal Core

Figure 3.7 Natural frequencies from sandwich beam with different length to depth ratio (*L/h*)

3.5.2 Parametric study

A parametric study of the free vibration of the cantilevered sinusoidal core sandwich beam is conducted to investigate the effect of varying parameters, such as transverse shear modulus of core and compressional/extensional modulus of core in z-direction.

3.5.2.1 Effect of shear modulus of core

From the basic mechanics of sandwich beam, it is well known that the face sheets provide the main bending stiffness while the core provides the major shear resistance. Since the sinusoidal core is hollow and the composite material usually has a lower shear modulus than the conventional metallic materials, the transverse shear deformation may take a considerable portion of the total deformation of the beam, especially in short beam case. Hence, the effect of the variation of the shear modulus G_{yz}^{c} of the transverse core is investigated in this parametric study, with other parameters unchanged.

The variation of natural frequencies of the transverse core beam with different core shear modulus G_{yz}^{c} are shown in Fig. 3.8. For simplicity, the core shear modulus G_{yz}^{c} is non-dimensionlized with face sheet extensional modulus E_{y}^{f} in Fig. 3.8. It should be noted that in the case G_{yz}^{c} in Table 3.3 is used, G_{yz}^{c}/E_{y}^{f} = 0.010. As we can see in Fig. 3.8, using the equivalent material properties derived by micro/macro mechanics, both HSBT and TBT will over-predict the natural frequencies of the sandwich beam, especially for higher modes. Furthermore, due to the discrepancy introduced by the equivalent material properties during homogenization process, the FEA, TBT and HSBT will converge to different values when the core shear modulus reaches infinite large. However, it can be easily noticed that HSBT is in closer agreement with FEA than TBT. It can also be concluded from the figure that the TBT tends to exaggerate the effect of core shear modulus. In general, the effect of variation of core shear modulus on the free vibration behavior of the sandwich beam cannot be neglected, especially for higher modes as well as very short beams. Hence, it should be taken into careful consideration in analysis. HSBT is recommended to be adopted to improve the accuracy of the prediction when compared to TBT.

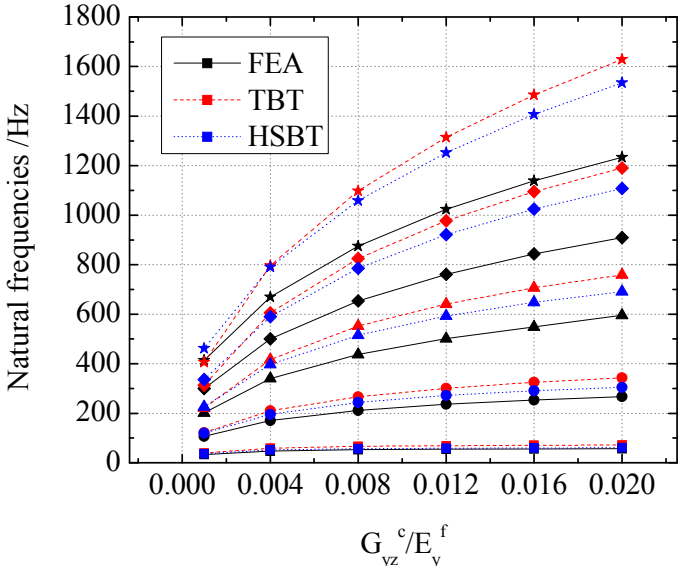

Figure 3.8 Effect of G_{yz}^{c}/E_{y}^{f}

3.5.2.2 Effect of core compressional modulus in z-direction

The variation of natural frequencies of the transverse core beam with different core compressional modulus in the z direction E_z^c based on HSBT are shown in Fig. 3.9. For simplicity, E_z^c is non-dimensionlized with the face sheet extensional modulus E_y^f in Fig. 3.9. Since TBT cannot take E_z^c into consideration, only HSBT results are shown here. It should be noted that in the case E_z^c in Table 3.3 is used, $E_z^c/E_y^f = 0.102$. It can be seen from Fig. 3.9 that the natural frequencies are insensitive to the variation of E_z^c except in the case of mode 5 and extremely low E_z^c value. In all other cases, the results are very close to the case when E_z^c reaches infinity large. Hence, it can be concluded that for the sandwich beams investigated in this study and most of other honeycomb core cases made of similar composite materials, the core can be considered as incompressible.

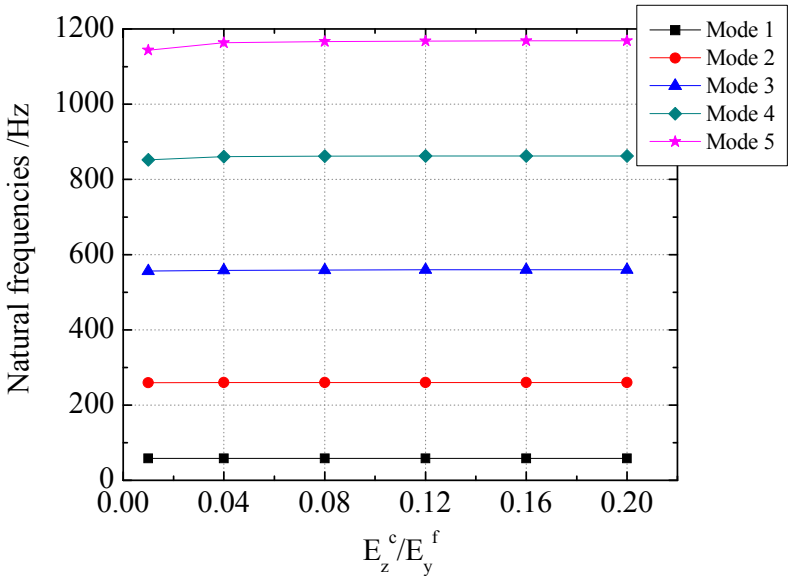

Figure 3.9 Effect of E_z^c/E_y^f from HSBT.

3.6 Summary

In this chapter, a detailed analytical and experimental study on dynamic response of the cantilevered sinusoidal core FRP sandwich beam was conducted. Two types of beams were investigated, one with the transverse sinusoidal core, and the other with the longitudinal sinusoidal core. A micro/macro mechanics and mechanics of material approach were adopted to derive the equivalent mechanical properties of the face sheets and sinusoidal core. The free vibration analysis is based on a high-order sandwich beam theory. The analytical solutions using the high-order sandwich beam theory were compared with Timoshenko's beam theory, numerical simulation and experimental test results to illustrate the effectiveness of the high-order approach. The surface-bonded piezoelectric sensors (PVDF films) were used to measure the dynamic response of FRP sandwich beams, from which the frequencies and mode shapes were obtained. The results show that in combination with micro/macro mechanics, the high-order sandwich beam theory (HSBT) can accurately predict the natural frequencies of a sinusoidal core

sandwich beam. For the short sinusoidal core sandwich beams, especially for transverse core, HSBT greatly improves the accuracy of the prediction of natural frequencies from TBT. The results demonstrated the validity of the high order beam theories, which improve the accuracy of sandwich beam analysis without a high cost of evaluation. HSBT can be used effectively as a versatile tool to analyze, design and optimize the composite sandwich structures for dynamic response, and it also shows its potential in application of structure health monitoring and damage identification of sandwich structures.

Furthermore, a parametric study was conducted to discuss the effect of core transverse shear modulus and core compressional modulus in the z-direction. The study shows that in general the dynamics of sinusoidal core sandwich beam depend more on the shear stiffness but less on the compressional stiffness in the *z* direction. Hence, its dynamic response is sensitive to the variation of core transverse shear modulus but insensitive to the variation of compressional stiffness.

CHAPTER 4

TEMPERATURE EFFECT ON DYNAMIC RESPONSE OF S-FRP SANDWICH STRUCTURES

4.1 Introduction

Fiber-reinforced plastic (FRP) composites are advanced engineering materials with the combination of high-strength, high-stiffness fiber (e.g., E-glass and carbon) and low-cost, light weight, environmentally resistant matrix (e.g., polyester, polyurethane, vinylester, and epoxy resins). FRP composites have gain popularity in high-performance products which require being lightweight yet strong and taking harsh environmental condition. Wide applications of FRP composites have been found in civil, mechanical and aerospace engineering. Carbon Fiber-Reinforced Plastic (CFRP) is a key material in today's launch vehicles, spacecraft and solar panel substrates. First developed in the mid 1930's, Glass Fiber Reinforced Plastic (GFRP) has increasingly become popular in the building industry. Recently, GFRP composite sandwich beams/panels have also been used in highway bridge deck construction. However, the dynamic response of GFRP honeycomb sandwich beams/panels has not been thoroughly investigated, especially for applications in cold regions with extreme weather conditions. The temperature effect may substantially change the dynamic behavior of the GFRP materials and in turn cause potential failure of the GFRP sandwich beams/panels under working load, particularly in low temperature.

This chapter is concerned with the temperature effect on dynamic response of GFRP honeycomb sandwich beams/panels, particularly in low temperature. The main focus of this study is the development of reliable and effective scale-up techniques to predict the temperature effect based on Dynamic Mechanical Analysis (DMA). The rest of the chapter is organized as

follows. The DMA test of the small GFRP composite coupon samples from the sandwich beams are described in Section 4.2. A series of analytical analysis of GFRP sandwich beams under different temperature are conducted based on the DMA test data to predict the temperature effect on the modal frequency of the panels in Section 4.3. The frequency response tests of the sandwich panels under different temperatures are described in Section 4.4. An as-manufactured FRP sandwich deck panel is further investigated in Section 4.5.

4.2 DMA test of the polyester resin samples

DMA is a thermo-analytical technique used to test the mechanical properties of different materials. The DMA applies a small sinusoidal deformation in a cyclic manner to a rectangular sample to measure the stiffness and damping (such as dynamic modulus and tangent delta). In this study, the TA Instrument Q800 Dynamic Mechanical Analyzer (Q800 DMA) was adopted to investigate the thermal effect on the mechanical properties of the polyester resin samples cut from the resin-rich layer of sandwich beams. An overview of the installation is shown in Fig. 4.1. The DMA instrument uses a Gas Cooling Accessory (GCA) to perform sub-ambient DMA experiment, as shown in Fig. 4.1. The GCA utilizes liquid nitrogen, stored in a holding tank, to control the temperature of the testing chamber in the Q800 DMA. There is also an air filter regulator assembly to help remove any oil, water, and particulates from the air.

In this experiment, two samples cut from the resin-rich layer of the composite sandwich face sheets were used, as shown in Fig. 4.2. The dimensions of the samples are 52 mm in length, 12 mm in width, and 3.2 mm in thickness. These samples were tested at a temperature range from 80°C to -80°C. The result of this experiment is the dynamic modulus variation under temperature effect. The DMA test results are shown in Fig. 4.3. It is shown that the dynamic modulus of polyester resin obtained in DMA test at room temperature is consistent with the

Young's modulus (5.06 GPa at 25 ºC). In this study, it is assumed that the Young's modulus used in vibration analysis is the same as the dynamic modulus obtained from the DMA test.

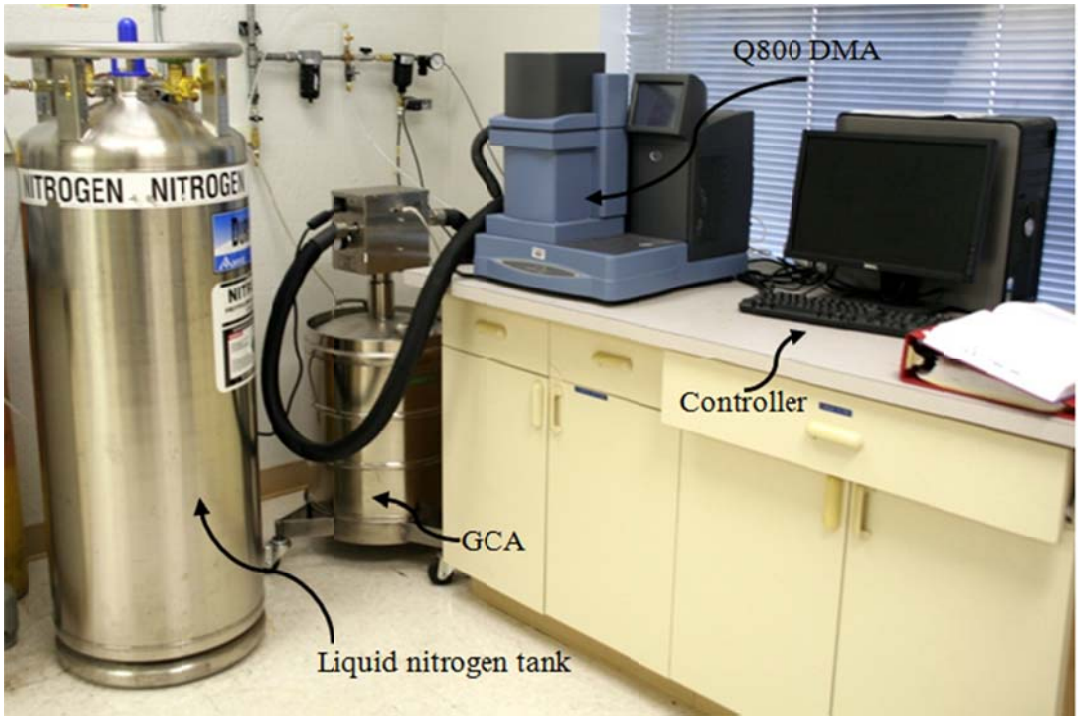

Figure 4.1 DMA test set-up.

Figure 4.2 Two DMA samples cut from sandwich beams.

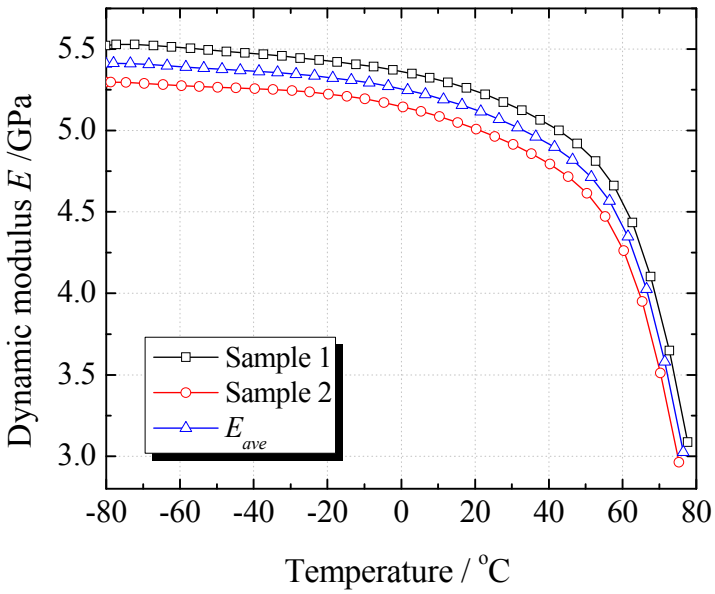

Figure 4.3 Temperature effect on dynamic modulus of polyester resin

4.3 Prediction of modal frequencies of FRP sandwich beams

4.3.1 Finite element analysis based on DMA test data

The commercial Finite Element Analysis package ABAQUS is used to conduct an eigenvalue analysis to extract the natural frequencies and the mode shapes of the sandwich beam with free-free boundary condition. The sandwich beam is modeled as two face sheets and a detailed sinusoidal core. The face sheets and the sinusoidal core walls are modeled as 4-node first-order plate elements S4 and 3-node first-order plate elements S3. The lay-ups and corresponding material properties at room temperature (25ºC) of face sheets and core walls are the same as presented in Section 3.2 (see Chapter 3). The equivalent stiffness properties of face sheets and honeycomb core at room temperature are also presented in Section 3.2. The beams at different temperatures are considered in the modeling. The temperature effect is considered significant for polyester resin and negligible for glass fiber. The corresponding equivalent

stiffness properties of face sheets and honeycomb core can be derived from the resin modulus at different temperatures obtained in DMA test, as described in Section 4.2.

Fig. 4.4 gives the first three global mode shapes of the sandwich beam with longitudinal core. The natural frequencies obtained by FEM of the sandwich beams with transverse core and longitudinal core at different temperature are shown in Fig. 4.5.

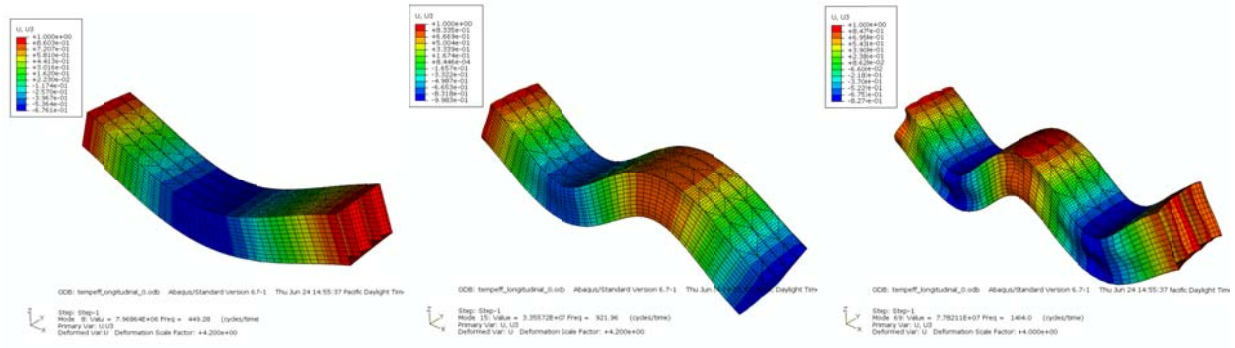

Figure 4.4 First three global mode shapes of the free-free sandwich beam with longitudinal core at 0 ºC from FEM

4.3.2 Analytical solution based on high-order sandwich beam theory

The analytical solution of free vibration based on high-order sandwich beam theory (HSBT) is presented in detail in Chapter 3. The beams at different temperatures are analyzed following this approach. As in the finite element analysis, the corresponding equivalent stiffness properties of face sheets and honeycomb core can be derived from the resin modulus at different temperatures obtained in DMA test. The natural frequencies obtained by HSBT of the sandwich beams with the transverse and longitudinal cores at different temperature are also shown in Fig. 4.5.

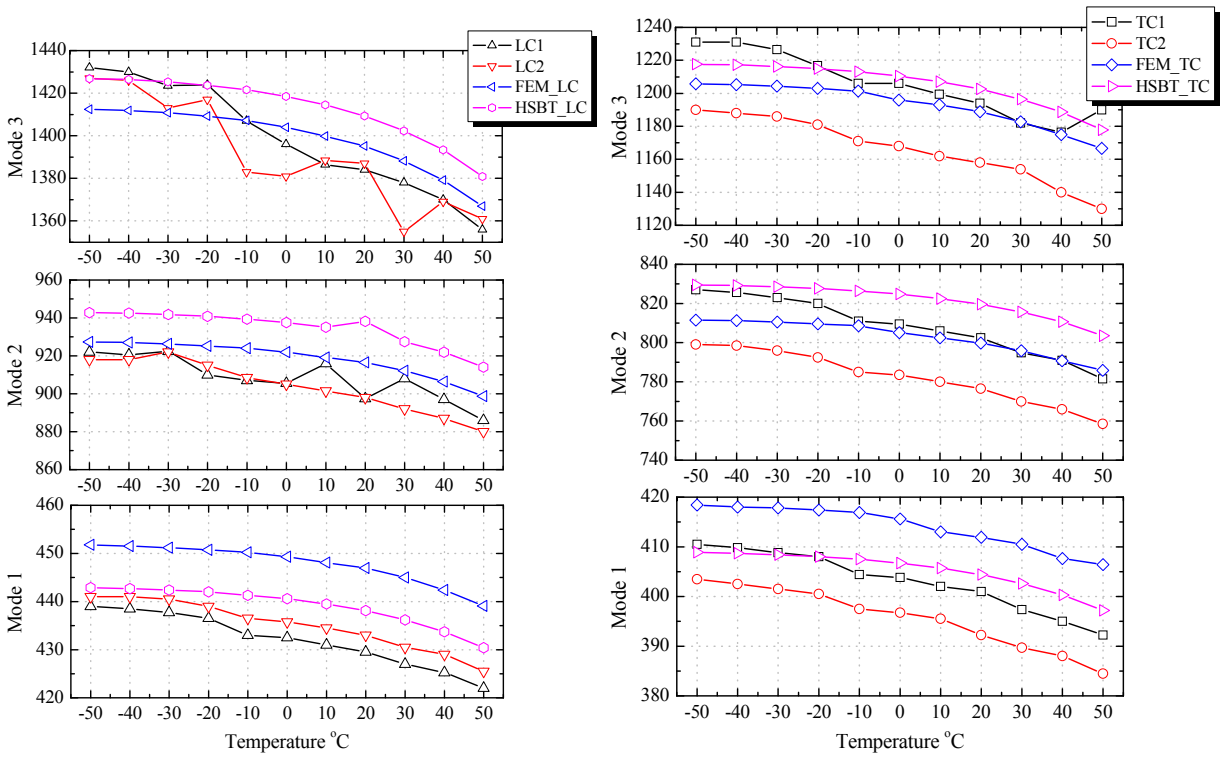

(a) Longitudinal core **(b) Transverse core**

Figure 4.5 Temperature effect on modal frequencies of composite sandwich beams (experimental data, FEM and high-order sandwich beam theory)

4.4 Experimental modal testing of sandwich beams

4.4.1 Experimental set-up

To verify the prediction of temperature effect on the modal frequency, two sandwich beams with the longitudinal core and two with the transverse core were experimentally tested in an environmental chamber. The four beams were put on soft foams to permit a free vibration at free boundary conditions, as shown in Fig. 4.6.

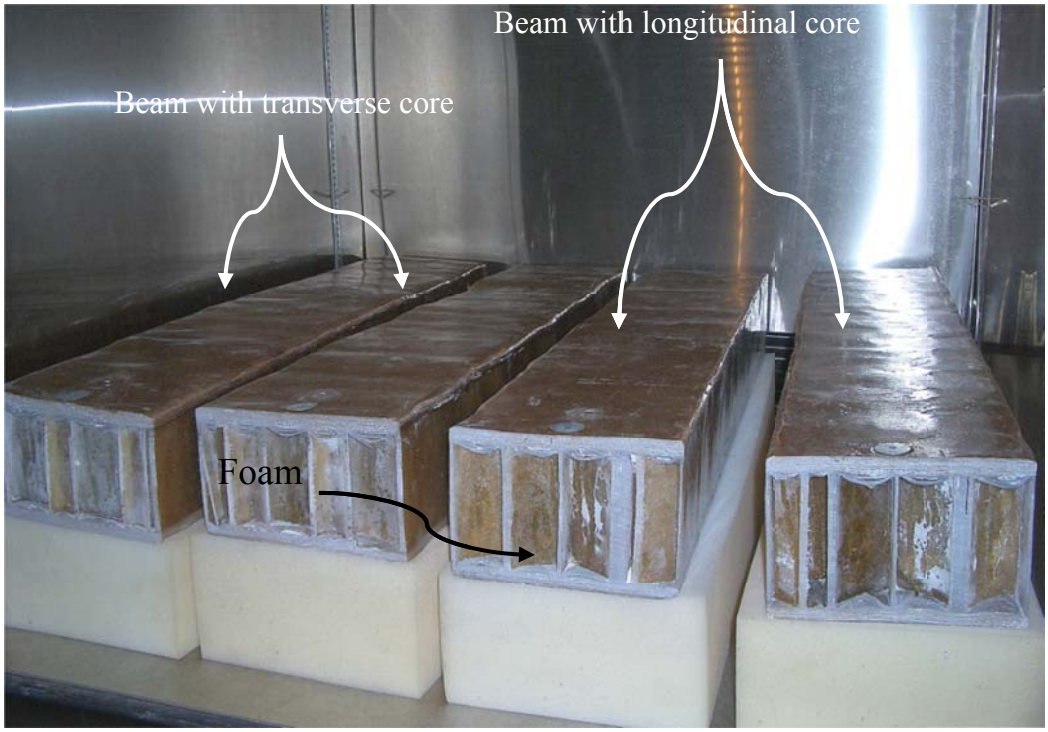

Figure 4.6 FRP sandwich beams on soft foams in the conditioning chamber.

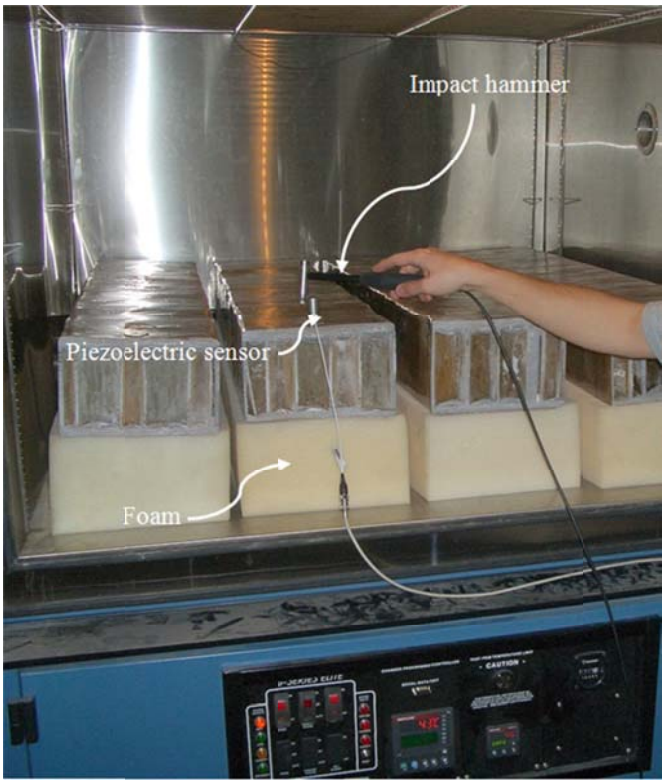

Figure 4.7 FRP sandwich beams under modal testing.

This experiment was conducted in a conditioning chamber between -50°C and 50°C at every 10°C. The modal testing in the conditioning chamber follows the procedure:

(1) The temperature ramps from room temperature to -50°C in 3.5 hours;

(2) The temperature stays at -50°C for half an hour; the modal tests of all beams are conducted in the last 10 minutes of the half hour;

(3) The temperature ramps from -50°C to -40°C in 1.5 hours;

(4) The temperature stays at -40°C for half an hour; the modal tests of all beams are conducted in the last 10 minutes of the half hour;

(5) Repeat step 3~4 to increase the temperature and conduct a modal testing at every 10°C interval until the temperature reaches 50°C.

The modal testing of the sandwich beams was conducted using a piezoelectric sensor and a modally tuned impact hammer as shown in Fig. 4.7. The beams were subjected to a dynamic pulse load using the modally tuned hammer (PCB 652B10). The response measurements were made using the accelerometer (PCB 352C68) to record the response of the structure. The analog excitation/response signals then pass a low-pass anti-aliasing filter to prevent the aliasing problem. A Krohn-Hite 3382 8-pole dual channel filter was employed to filter out the high frequency signals above the cut-off frequency of 2,000 Hz. The filtered signals were then digitized and collected by the data acquisition system dSPACE CP1103 at the sampling frequency of 4000Hz. The measurements for each beam were repeated 6 times, and the synchronized time histories from the excitation and response measurements were averaged to enhance the signal-to-noise ratio (SNR).

4.4.2 Experimental results

After collecting the excitation and response time-histories from each beam, the frequency-response functions (FRFs) of the tested beams are calculated from these excitation and response time-histories. Then, the modal frequencies of each beam are identified from the peaks of the FRF curves and listed in Fig. 4.5, where the abbreviation "tc" and "lc" denotes beams with the transverse and longitudinal cores, respectively. In Fig. 4.5, both the FEM and HSBT predictions show close agreement with the experimental data in all three modes. It is shown that the proposed DMA test-based approach can accurately predict the trend of modal frequencies change under the temperature effect and can effectively approximate the modal frequencies at different temperature. It should also be noted that both the FEM and HSBT slightly under-predict the temperature effect on the modal frequencies of higher mode because the temperature effect on glass fiber is completely neglected.

4.5 Temperature effect on FRP sandwich deck panel

In order to further investigate the temperature effect on the FRP sandwich deck panel, the modal analysis of FRP sandwich beams based on the DMA test data is scaled-up to analyze an as-manufactured FRP sandwich deck panel. FRP bridge decks are commonly placed transversely to the supporting structure such as the longitudinal girders, cross beams, and stringers. FRP decks are connected to the underlying supports by using the bolted connections. These connections are considered to act as the simply supported boundary condition. The FRP sandwich deck panel is exactly the same panel as experimentally investigated in Chapter 8, with the same boundary condition.

4.5.1 Finite element analysis of FRP sandwich deck panel

The commercial Finite Element Analysis package ABAQUS is used to conduct an eigenvalue analysis to extract the natural frequencies and the mode shapes of the sandwich deck panel with simply supported-simply supported (SS-SS) boundary condition at both the longitudinal ends. The lay-ups and corresponding material properties of face sheets and core walls are the same as the sandwich beams with the longitudinal core studied in Section 4.2. Hence, the corresponding equivalent stiffness properties of face sheets and sinusoidal core can be directly applied to sandwich deck panel. The only difference is that the sandwich deck panel is a plate-type structure with a length of 1.9812 m and a width of 1.4945 m .

Fig. 4.8 gives the first five global mode shapes of the sandwich panel. The modal frequencies obtained by FEM of the sandwich panel at different temperature are shown in Fig. 4.9.

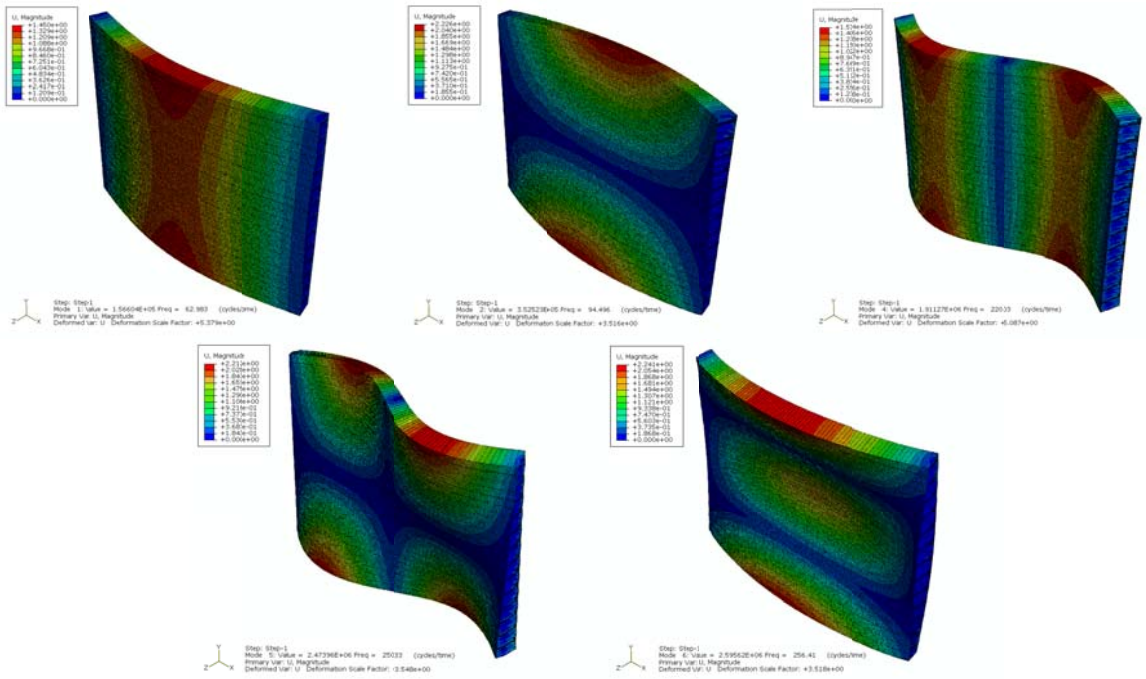

Figure 4.8 First five global mode shapes of the SS-SS sandwich panel from FEM.

4.5.2 Experimental modal testing of FRP sandwich deck panel

To verify the prediction of modal frequency, an as-manufactured FRP sandwich deck panel was experimentally tested. The FRP sandwich panel was placed transversely to the supporting concrete beams. The sandwich panel was connected to two underlying concrete supports using steel studs, which are considered to provide a simply supported boundary condition.

The same modal testing technique was applied to test the FRP sandwich deck panel as shown in Section 4.4. However, due to the large size of the panel, it is impossible to test the panel under the controlled temperature within a conditioning chamber. Therefore, only the modal data at room temperature (25°C) is available for comparison with the scale-up results using the DMA data, and they are shown in Fig. 4.9.

The comparison between the FEM results and modal testing data shows that the proposed DMA test-based approach can also be effectively applied to approximate the modal frequencies at different temperature. The FEM results also suggest that the temperature effect may introduce a 2%-3% modal frequency shift of the FRP sandwich panel over a 100°C temperature change, which is consistent with the FRP sandwich beam case.

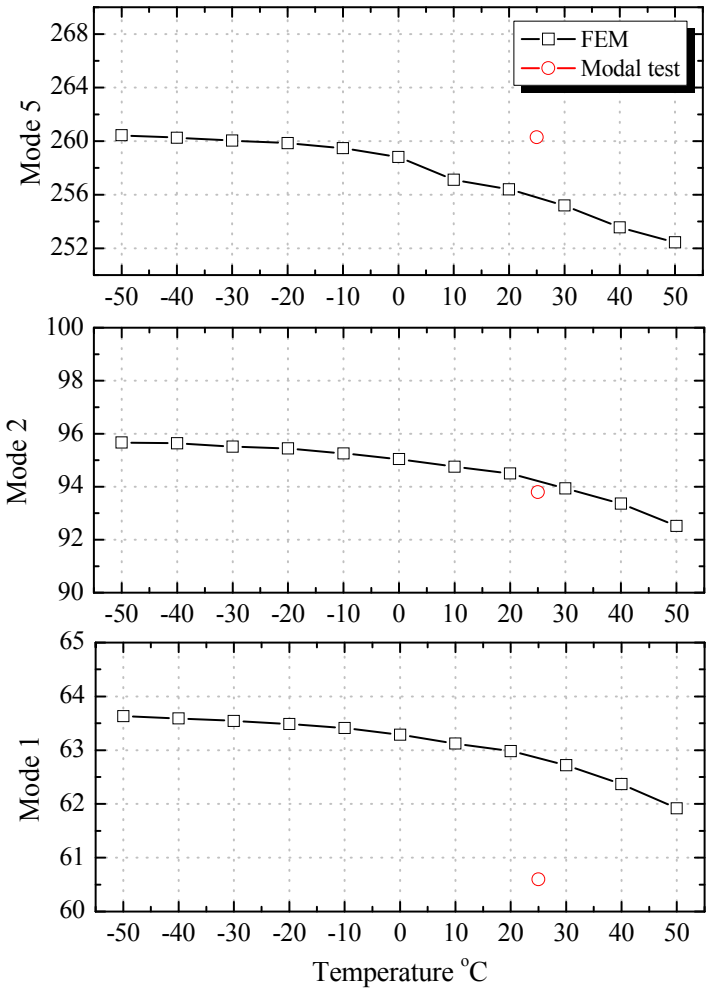

Figure 4.9 Comparison of temperature effect on modal frequencies of FRP sandwich panel (FEM, experimental data)

4.6 Summary

In this Chapter, a detailed study of temperature effect on the dynamic response of FRP sandwich beams/panels is presented. A series of FRP sandwich beams with the longitudinal and transverse cores and an as-manufactured FRP sandwich panel were investigated for dynamic response change under temperature effect.

It is shown that the proposed modal analysis approach based on the DMA test data and FE analysis or HSBT analysis can accurately predict the trend of modal frequencies change under

the temperature effect and can effectively approximate the modal frequencies at different temperature. The study suggests that the proposed DMA-based approach is a reliable and effective technique to predict the temperature effect on dynamic response of FRP sandwich beams/panels. It is also suggested in this study that the temperature effect may only introduce a 2%-3% modal frequency shift to the FRP sandwich beam/panel over a 100°C temperature change. Hence, using the modal frequency shift alone for the damage identification and condition assessment of FRP sandwich structures may not be reliable, especially in cold region, since the temperature effect may introduce some other considerable properties changes to FRP sandwich structures.

CHAPTER 5

2-D WAVELET-BASED DAMAGE IDENTIFICATION METHOD FOR PLATE-TYPE STRUCTURES

5.1 Introduction

A reliable and effective non-destructive damage detection method is crucial to maintain the safety and integrity of structures. Most non-destructive damage identification methods can be categorized as either local or global damage detection techniques (Doebling et al. 1996). Local damage detection techniques, such as ultrasonic methods and X-ray methods, have their limitations in that the vicinity of damage must be known *a priori* and readily accessible for testing. Hence, the vibration response-based global damage identification method has been developed to overcome these difficulties. The fundamental idea for dyanmic response-based damage detection is that the damage-induced changes in the physical properties (mass, damping, stiffness, etc.) will cause detectable changes in modal properties (natural frequencies, modal damping, mode shapes, etc.).

To detect damage using the natural frequency shift is the earliest global vibration response method. Salawu (1997) presented a comprehensive review on damage detection methods using the natural frequency shift. Compared to using the natural frequencies, the advantages of using the mode shapes and their derivatives as a basic feature for damage detection are obvious. First, the mode shapes contain local information, which makes them more sensitive to local damages and enables them to be used directly in multiple damage localization. Second, the mode shapes are less sensitive to environmental effects, such as temperature, than natural frequencies (Farrar and James 1997). Significant work has been done in localizing damage in beam-type structures using the mode shapes and their derivatives (Hadjileontiadis et al. 2005; Pandey et al. 1991;

Ratcliffe 1997; Stubbs and Kim 1996; Wang and Qiao 2008). Many viable damage detection methods for beams have been also successfully extended from one-dimensional (1-D) to two-dimensional (2-D) algorithms for damage detection of plates. Yoon et al. (Yoon et al. 2005) generalized the 1-D gapped smoothing method (GSM) by Ratcliffe (1997) to 2-D plate-like structural applications. Cornwell et al. (1999) generalized the strain energy-based damage index (DI) method for 1-D beam-type structure by Stubbs and Kim (1996) into 2-D plate-type structures. Hadjileontiadis and Douka (2007) extended the fractal dimension-based crack detection algorithm (Hadjileontiadis et al. 2005) to 2-D for detecting cracks in plate structures.

The application of 1-D wavelet transform to displacement mode shape for damage detection of beam-type structures has been extensively investigated (Douka et al. 2003; Gentile and Messina 2003; Liew and Wang 1998; Quek et al. 2001). Some researchers also extended the application of 1-D wavelet transform to damage detection of plate. Chang and Chen (2004) applied the 1-D wavelet transform on the mode shape data in x- and y-direction separately to detect stiffness loss in plate. Douka et al. (2004) applied a 1-D continuous wavelet analysis on mode shape to localize an all-over part-through crack parallel to one edge of the plate. However, these damage detection techniques are still 1-D in nature because the mode shape data along different linear lines are treated separately. Recently, the 2-D version of the wavelet transform approach has also become a promising technique for damage detection of plates. Loutridis et al. (2005) applied a 2-D discrete wavelet transform (DWT) of the flexural mode shape to detect cracks in plate. The wavelet coefficients of the detail of the first level decomposition were used to determine the location, length and depth of the crack. Kim et al. (2006a) introduced a damage detection technique based on the 2-D multi-resolution analysis of the flexural DI equation by the Haar wavelet. Numerical experiments showed that the wavelet transformation approach could

be successfully applied to localize and quantify small damage in the plate using only a few lower mode shapes. Rucka and Wilde (2006) employed the 2-D wavelet transform of the fundamental mode shape of plate using the reverse biorthogonal wavelet to locate damage in plate. The wavelet was constructed using the formulation of 2-D discrete wavelet. Both the horizontal and vertical wavelets were taken as tensor products of a 1-D scaling function and a 1-D wavelets function. Then, the transform in two directions were implemented separately. A modulus and angle of the wavelet transform were defined to combine the information of two transforms and adopted as the indicator of damage.

It should be noted that there are two different versions of the wavelet transform, i.e., the continuous wavelet transform (CWT) and the discrete wavelet transform (DWT). The CWT provides precise resolution of wavelet coefficients for damage detection, and it is hence mostly used for feature detection and analysis in signals; whereas the DWT offers a fast algorithm of evaluating wavelet coefficients in discrete resolutions, and it is thus more appropriate for data compression and signal reconstruction (Antoine et al. 2004). Although both the versions have been adopted in aforementioned works, the CWT is obviously more suitable for damage detection problems, due to its excellent performance as a singularity scanner.

The apparent limitation of wavelet transform method is that the rational evaluation of the wavelet transform requires the mode shape measurement with a relatively high spatial resolution. With the traditional sensors such as accelerometers, a large number of modal tests are required to achieve such measurement with sufficient spatial resolution and reasonable accuracy. However, with advanced measurement instrument, such as scanning laser vibrometer (SLV) (Qiao et al. 2007a; Qiao et al. 2007b), this difficulty can be overcome by its capability of scanning a large

number of measurement points synchronously. In addition, the spatial resolution can be further enhanced by the interpolation technique (Rucka and Wilde 2006).

In this chapter, a 2-D continuous wavelet transform (CWT)-based method is proposed for damage detection in plate-type structures. In particular, the 2-D CWT of the vibration mode shapes of plates is applied and evaluated to identify the location and shape of damage in the plates. The rest of the chapter is organized as follows. The 2-D CWT formulated by Antoine et al. (2004) is briefly introduced in Section 5.2. The application of the 2-D CWT in damage detection is thoroughly examined using a numerical plate model using finite element analysis in Section 5.3. The effectiveness and applicability of the 2-D CWT-based damage detection method is validated in Section 5.4 via an experimental program using smart piezoelectric sensors.

5.2 2-D CWT in damage detection

The 2-D continuous wavelet transform (CWT) considered in this study is based on the formulation by Antoine et al. (2004). Some of its basic concepts are briefly introduced here. For more information, interested readers are recommended to refer to the literature (Antoine et al. 2004).

5.2.1 2-D continuous wavelet transform

As in the 1-D case, a 2-D wavelet is an oscillatory, real or complex-valued function $\psi(\vec{x}) \in L^2(\mathbb{R}^2, d^2\vec{x})$ satisfying the admissibility condition on real plane $\vec{x} \in \mathbb{R}^2$. $L^2(\mathbb{R}^2, d^2\vec{x})$ denotes the Hilbert space of measurable, square integrable 2-D functions. If ψ is regular enough as in most cases, the admissibility condition can be expressed as:

$$\hat{\psi}(\vec{0}) = 0 \Leftrightarrow \int_{\mathbb{R}^2} \psi(\vec{x}) d^2\vec{x} = 0 \tag{5-1}$$

where $\hat{\psi}(\vec{k})$ is the Fourier transform of $\psi(\vec{x})$, and $\vec{k} \in \mathbb{R}^2$ is the spatial frequency.

Function $\psi(\vec{x})$ is called a mother wavelet and usually localized in both the position and frequency domains. The mother wavelet ψ can be transformed in the plane to generate a family of wavelet $\psi_{\vec{b},a,\theta}$. A transformed wavelet $\psi_{\vec{b},a,\theta}$ under translation by a vector $\vec{b}$, dilation by a scaling factor a, and rotation by an angel θ can be derived as

$$\psi_{\vec{b},a,\theta}(\vec{x}) = a^{-1}\psi(a^{-1}r_{-\theta}(\vec{x}-\vec{b})) \tag{5-2}$$

Given a 2-D signal $s(\vec{x}) \in L^2(\mathbb{R}^2, d^2\vec{x})$, its 2-D CWT (with respect to the wavelet ψ) $S(\vec{b},a,\theta) \equiv T_\psi s$ is the scalar product of s with the transformed wavelet $\psi_{\vec{b},a,\theta}$ and considered as a function of $(\vec{b},a,\theta)$ as:

$$\begin{aligned} S(\vec{b},a,\theta) &\equiv \left\langle \psi_{\vec{b},a,\theta}, s \right\rangle \\ &= a^{-1}\int_{\mathbb{R}^2} \overline{\psi(a^{-1}r_{-\theta}(\vec{x}-\vec{b}))} s(\vec{x}) d^2\vec{x} \\ &= a\int_{\mathbb{R}^2} \overline{\hat{\psi}(ar_{-\theta}(\vec{k}))} e^{i\vec{b}\cdot\vec{k}} \hat{s}(\vec{k}) d^2\vec{k} \end{aligned} \tag{5-3}$$

Because equation (5-3) is essentially a convolution of a 2-D signal s with a function $\psi_{\vec{b},a,\theta}$ of zero mean, the transform $S(\vec{b},a,\theta)$ is appreciable only in regions of parameter space $(\vec{b},a,\theta)$ where $\psi_{\vec{b},a,\theta}$ matches the features of signal s. When ψ is well localized in the spatial frequency domain and position domain, the 2-D CWT acts as a local filter in parameter space.

In the 1-D wavelet analysis, due to its intrinsic characteristic of keeping constant relative bandwidth, the wavelet analysis is more advantageous in detecting singularities at high frequency or small scale than, e.g., the windowed Fourier transform. The same argument applies to the 2-D wavelet analysis. When appropriately designed, the 2-D wavelet transform is also an

effective singularity scanner for 2-D signals. As in the 1-D case, the vanishing moments of the wavelet play an important role in detection of singularities. A wavelet ψ usually has vanishing moments $N \geq 1$:

$$\int x^{\alpha} y^{\beta} \psi(\vec{x}) d^2 \vec{x} = 0, \vec{x} = (x, y), 0 \leq \alpha + \beta \leq N \tag{5-4}$$

This property improves its efficiency at detecting singularities. A wavelet with vanishing moments N will not see the smooth part of the signal but only detects singularities in the $(N+1)$th derivatives of the signal.

One typical example of 2-D wavelets is the 2-D Mexican hat wavelet (Antoine et al. 2004), which is simply the Laplacian of a 2-D Gaussian. Another example is the 2-D morlet wavelet, which is the product of a plane wave and a Gaussian window. Both the wavelets can find their well-known counterpart in the 1-D wavelet analysis. Their expressions in the position domain are given as follows:

The 2-D Mexican hat wavelet: $$\psi(\vec{x}) = (2 - |\vec{x}|^2) \exp(-\frac{1}{2} |\vec{x}|^2) \tag{5-5}$$

The 2-D Morlet wavelet: $$\psi(\vec{x}) = \exp(i\overrightarrow{k_0} \cdot \vec{x}) \exp(-\frac{1}{2} |\vec{x}|^2) + \textit{correction term} \tag{5-6}$$

5.2.2 2-D CWT-based differentiation and filtering

Many researchers have shown that the displacement mode shape itself is not very sensitive to small damage either in beams or plates, even with the high density mode shape measurement (Huth et al. 2005; Khan et al. 1999). As an effort to enhance the sensitivity of mode shape data to the damage, the derivatives of mode shape are investigated for damage detection (Yoon et al. 2005). In practical damage detection situations, the mode shape derivatives cannot be obtained directly, often requiring the numerical differentiation methods, such as Laplace operator (Cao

and Qiao 2009). An important feature of these numerical differentiation methods is that this process tends to enhance the high frequency noise, therefore requiring a filtering process to compensate for such an effect. Gaussian filtering is one of the most widely used approaches to filter out these high frequency noises. In this case, the desired signal can be obtained by convolving the differentiated mode shape $s(x,y)$ with a Gaussian $g(x,y)$ as:

$$\tilde{s} = g(x,y) * \left(\frac{\partial}{\partial x}\right)^m \left(\frac{\partial}{\partial y}\right)^n s(x,y) \tag{5-7}$$

where (*) denotes the convolution operator. The 2-D Gaussian is defined as

$$g(x,y) = \exp(-\frac{|\vec{x}|^2}{2\sigma^2}) = \exp(-\frac{x^2+y^2}{2\sigma^2}),\ \ \vec{x} = (x,y) \tag{5-8}$$

Using the well-known property of convolution, we obtain

$$\begin{aligned} \tilde{s} &= g(x,y) * \left(\frac{\partial}{\partial x}\right)^m \left(\frac{\partial}{\partial y}\right)^n s(x,y) \\ &= \left(\frac{\partial}{\partial x}\right)^m \left(\frac{\partial}{\partial y}\right)^n g(x,y) * s(x,y) \end{aligned} \tag{5-9}$$

If we adopt the derivative of 2-D Gaussian as the mother wavelet and rewrite equation (5-3) as a convolution, we can see

$$S(\vec{b},a,\theta) = \left(\psi_{a,\theta} * s\right)(\vec{b}) = \left(\left(\frac{\partial}{\partial x}\right)^m \left(\frac{\partial}{\partial y}\right)^n g_{a,\theta} * s\right)(\vec{b}) = \tilde{s}_{a,\theta}(\vec{b}) \tag{5-10}$$

Hence, the desired differentiated and filtered signal can be obtained by a 2-D wavelet transform of the original mode shape with the derivative of 2-D Gaussian (Dergauss2d) as the wavelet. An example of the derivative of 2-D Gaussian is shown in the position and spatial frequency domains, respectively, in Fig. 5.1.

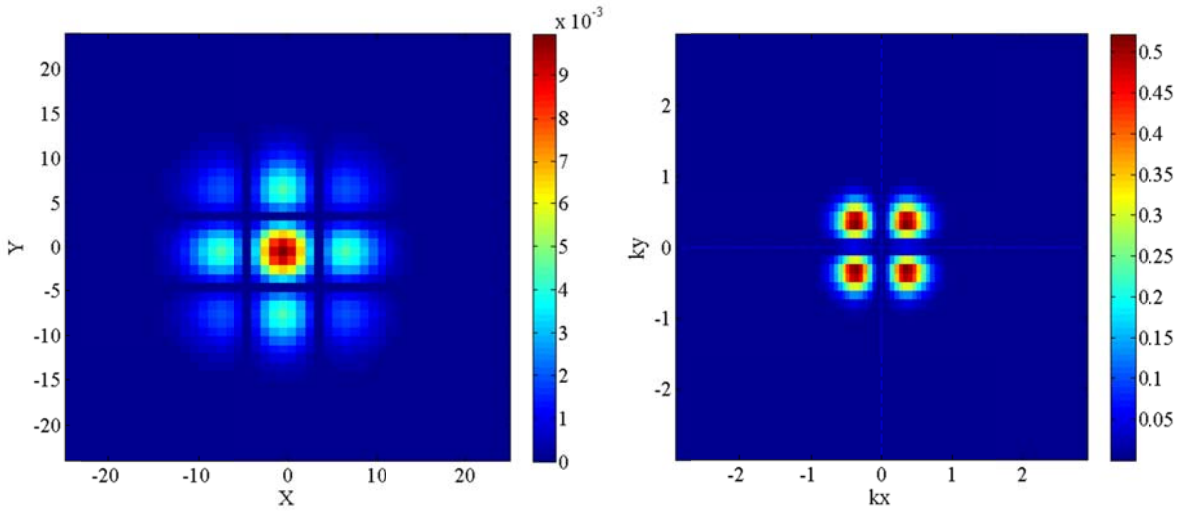

(a) (b)

Figure 5.1 A Dergauss2d wavelet in (a) position domain and (b) spatial frequency domain

$((\partial / \partial x)^m (\partial / \partial y)^n g_{a,\theta}$ *with* $n = 2, m = 2, a = 4, \theta = 0)$

5.2.3 Choice of 2-D wavelet for damage detection in plates

Due to its differentiation and filtering effect, the "Dergauss2d" wavelet becomes an ideal candidate for 2-D CWT-based damage detection in mode shapes of plates. However, which wavelet in the family of Dergauss2d is the most appropriate one for damage detection in plate structures is still a question to be addressed, i.e., the determination of the parameters m, n in the Dergauss2d wavelet $(\partial / \partial x)^m (\partial / \partial y)^n g_{a,\theta}$ is crucial to the success of the algorithm.

One guideline for choosing m and n is that both x and y should be equally weighted to avoid potential false indication of damage area and shape. Therefore, the parameters should be chosen as $m = n$. Another guideline is that the wavelet coefficients of the mode shape from an intact plate should be trivial so that the singularities induced by small damage will be easier to detect. Therefore, the wavelet should have enough vanishing moments (i.e., large enough m and n) so that it is blind to the "healthy" mode shape which appears in the low frequency region. In

addition, m and n should also be as small as possible so that it will not significantly magnify the high frequency noises during differentiation.

To determine the appropriate parameters m and n, the Dergauss2d wavelets with different parameters ($m = n = 1, 2, 3$) are tested on the numerically simulated fundamental mode shape of a healthy rectangular steel plate which is clamped on one side. The results are shown in Fig. 5.2. It can be seen that for $m = n \geq 2$, the Dergauss2d wavelets are blind to the "healthy" mode shape except the singularity at four corners caused by the boundary conditions. Furthermore, the parameters $m = n = 2$ are better than $m = n = 3$ because $m = n = 3$ gives a rougher surface and causes sharper peaks at boundaries due to its higher order differentiation. Therefore, when the first mode shape is used, the Dergauss2d wavelet with $m = n = 2$ is most appropriate for damage detection in plates.

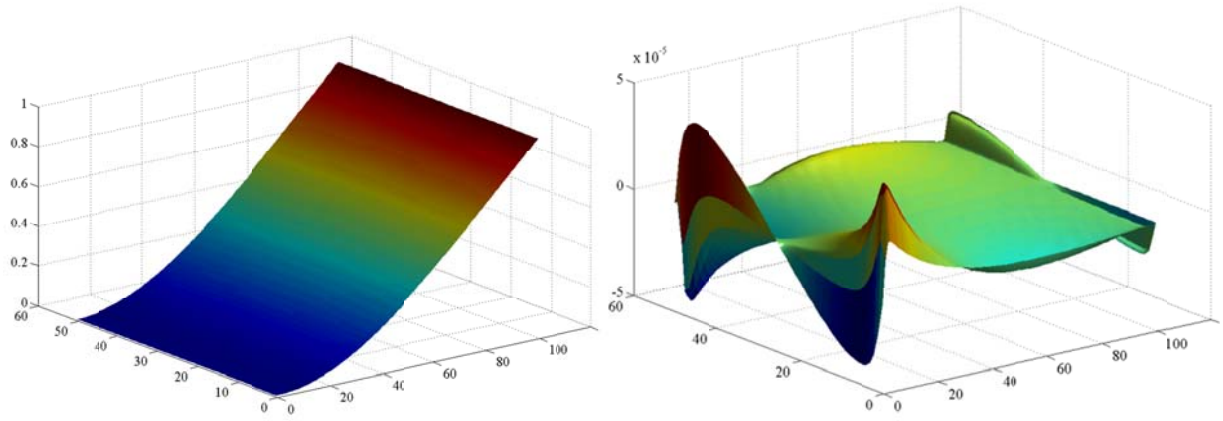

(a) (b)

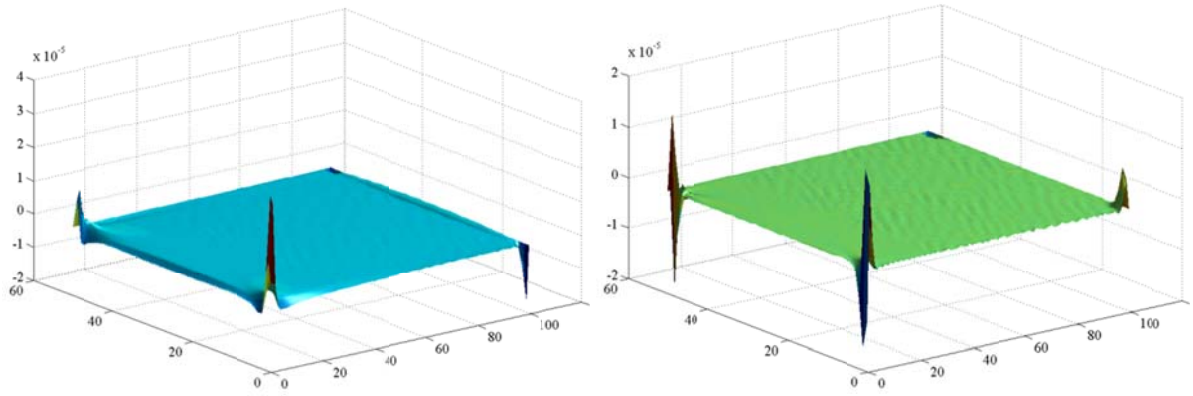

(c) (d)

Figure 5.2 The 2-D CWT of mode shape of a healthy plate using different Dergauss2d wavelets

(a) mode shape of the healthy plate clamped on one side; (b) Wavelet coefficients using Dergauss2d with *m,n=1*; (c) Wavelet coefficients using Dergauss2d with *m,n=2*; (d) Wavelet coefficients using Dergauss2d with *m,n=3*.

5.3 Numerical investigation of damage detection using 2-D CWT

5.3.1 Description of numerical model

The commercial Finite Element Analysis package ABAQUS is used to conduct an eigenvalue analysis to generate the mode shapes of the damaged plate. For simplicity, the structure is assumed to be a cantilevered steel plate of 1 m width × 0.125 m depth × 2 m length with damage. The material is assumed to be steel with Young's modulus E = 200 GPa, Poisson's ratio ν = 0.2 and density ρ = 7,850 kg/m^3. The plate is uniformly divided into approximately 5,000 4-node first-order plate elements S4 of size 0.02 m × 0.02 m and a few 3-node first-order plate elements S3. The mode shape data are extracted from all the 101 × 51 nodes in the model. Three different damage cases are independently induced in the finite element models: (A) a 0.17 m × 0.17 m rectangular damaged area centered at x = 0.52 m, y = 0.4 m with an angle 45º to x-axis; (B) a 0.06 m × 0.06 m rectangular damaged area centered at x = 0.45 m, y = 0.25 m; and (C) a 0.1 m length through-thickness crack centered at x = 0.46 m, y = 0.35 m. For cases (A) and (B), the Young's modulus of the elements in the damaged area is reduced by 30% to simulate the damage-induced stiffness loss. The finite element models with three types of damage scenarios are shown in Fig. 5.3. The displacement-normalized fundamental mode shapes of the plate with damage A (i.e., Case (A)) are shown in Fig. 5.4. Comparison between the damaged and healthy plate shows that the displacement mode shape reveals no local features capable of directly indicating the location or shape (area) of the damage.

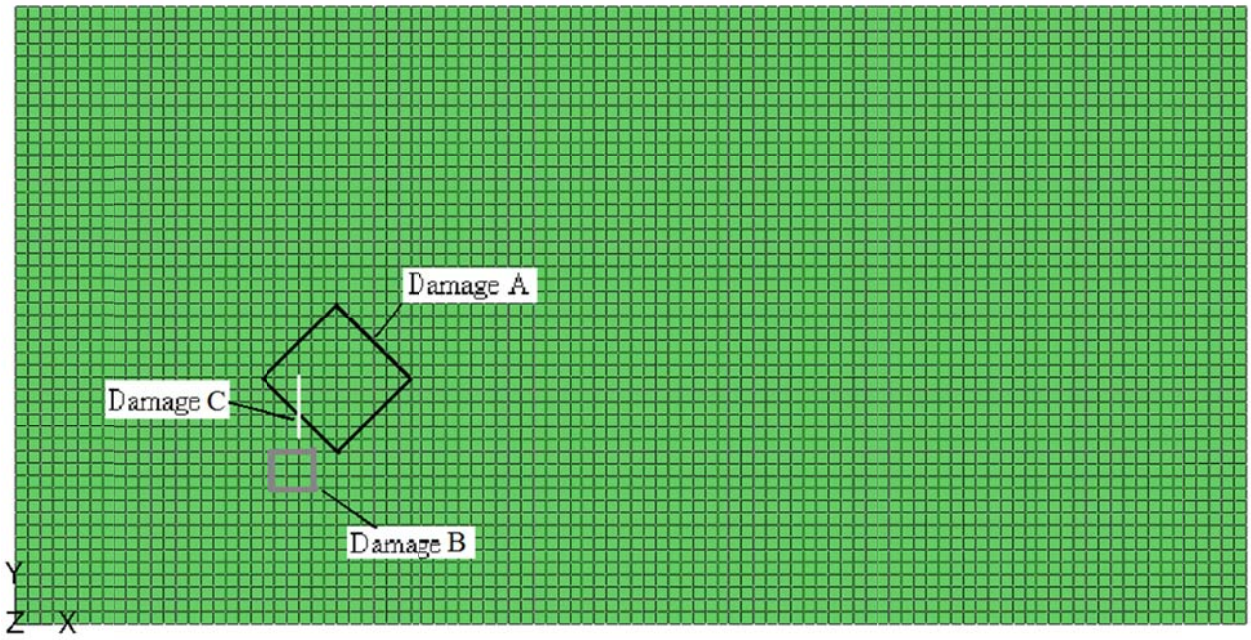

Figure 5.3 Finite Element models of the plate with three types of damage.

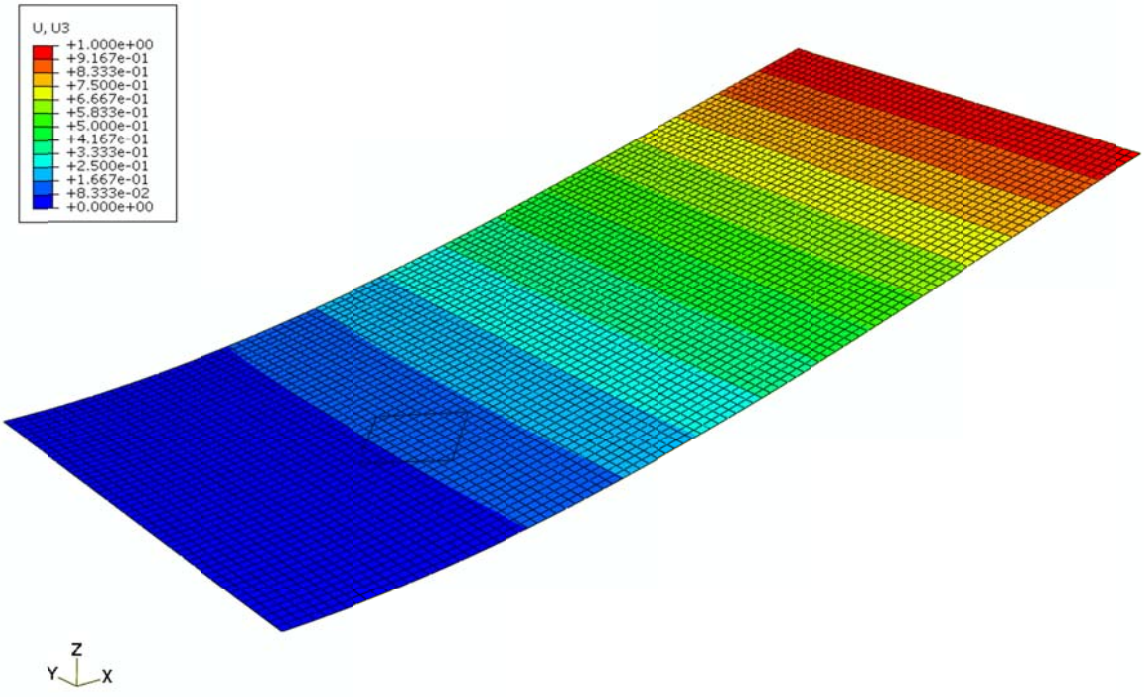

Figure 5.4 The fundamental mode shape of the plate with damage A.

5.3.2 Damage detection using the Dergauss2d wavelet

The 2-D CWT is applied to the fundamental mode shape with a Dergauss2d wavelet $(m = n = 2)$,

$$\begin{aligned} S(\vec{b}, a, \theta) &= = \int_{\mathbb{R}^2} s(\vec{x}) \left(\frac{\partial}{\partial x} \right)^2 \left(\frac{\partial}{\partial y} \right)^2 g_{a,\theta} d^2 \vec{x} \\ &= \left(\left(\frac{\partial}{\partial x} \right)^2 \left(\frac{\partial}{\partial y} \right)^2 g_{a,\theta} * s \right) (\vec{b}) \end{aligned} \tag{5-11}$$

The fundamental mode shape is treated as a 2-D spatially-distributed signal, in the form of a matrix with 101 rows and 51 columns, corresponding to the displacement at the element nodes along the plate length and width directions, respectively. The spatial resolution of the mode shape is further enhanced by a bivariate cubic spline interpolation. The bivariate cubic spline is constructed as the tensor product of two univariate cubic splines. It can be expressed as the weighted sum of products of two cubic spline functions:

$$f(x, y) = = \sum_i \sum_j a(i, j) g_i(x) h_j(y) \tag{5-12}$$

where $g_i(x)$ and $h_j(y)$ are the cubic spline function in *x* and *y* direction, respectively. By using the bivariate cubic spline interpolation, the mode shape is oversampled to 1001 rows and 501 columns. The spatial resolution of the data is thus enhanced from 0.02 m to 0.002 m accordingly.

The 2D-CWT is implemented in Matlab® using the YAW (Yet Another Wavelet) toolbox (Antoine et al. 2004; Jacques et al. 2007) developed by Jacques et al. Once the 2-D CWT is computed, we face a problem of visualization of wavelet coefficients because $S(\vec{b}, a, \theta)$ is a function of four variables: its position (*x*, *y*), scale *a*, and angle θ. Since the plate in this study is a rectangular oriented in *x* and *y* direction, the most effective angle θ for our damage detection

algorithm should align with *x*- or *y*-axis, i.e., $\theta = 0$ or $\pi / 2$. Hence, for simplicity, the variable θ is fixed at $\theta = 0$ in this study. The influence of choice of θ will not be our focus in this research. Then, the function $S(\vec{b}, a, \theta)$ becomes a function $S(\vec{b}, a)$ of the rest three variables.

If both of variables a and θ are fixed, the wavelet coefficients obtained from the CWT can also be viewed as a 2-D spatially distributed signal. The wavelet coefficients of the mode shape in the three given damage cases with $a = 10, \theta = 0$ are shown in Fig. 5.5. As shown in Fig. 5.5, all three types of damage can be correctly detected and located using the chosen variables of $a = 10, \theta = 0$. However, the effectiveness of the singularity detection can only be guaranteed by a carefully chosen scale a. When the scale a is not appropriate, the singularity caused by damage can be buried by the numerical errors, measurement noise or boundary distortion. Fig. 5.6(a) shows the wavelet coefficients in which the singularity induced by damage B is overshadowed by the peaks at corners as $a = 1$. When a = 40, the bump in damaged area can barely be noticed as shown in Fig. 5.6(b). Therefore, simply choosing one single scale a can lead to false indication of damage. A more effective algorithm is thus needed to make full use of the wavelet coefficients with the continuous scale resolution from the 2-D CWT for damage detection and localization.

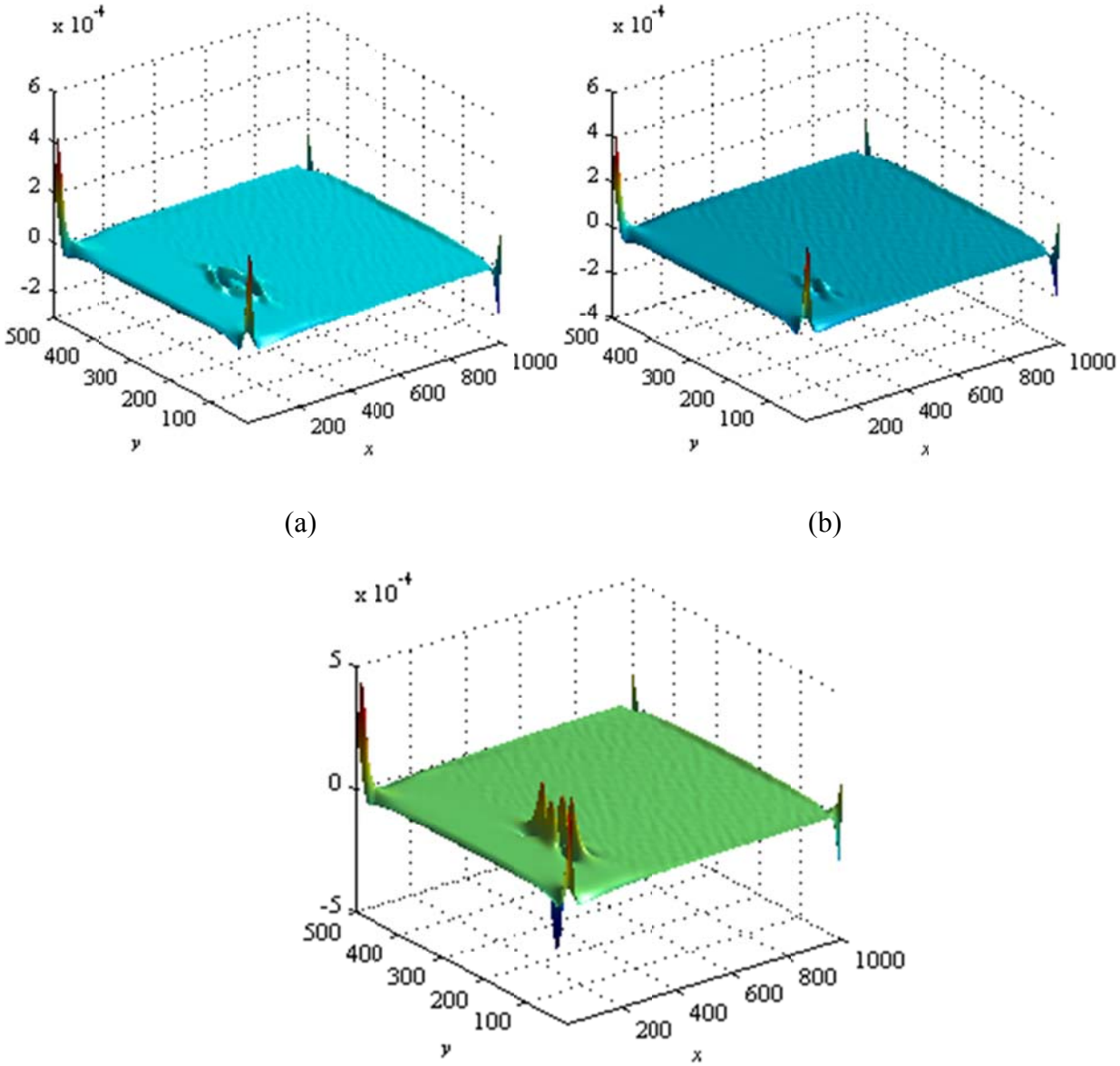

Figure 5.5 Wavelet coefficient of fundamental mode shape in three damage cases (a) damage A, (b) damage B, and (c) damage C (with Dergauss2d wavelet, $a = 10, \theta = 0$)

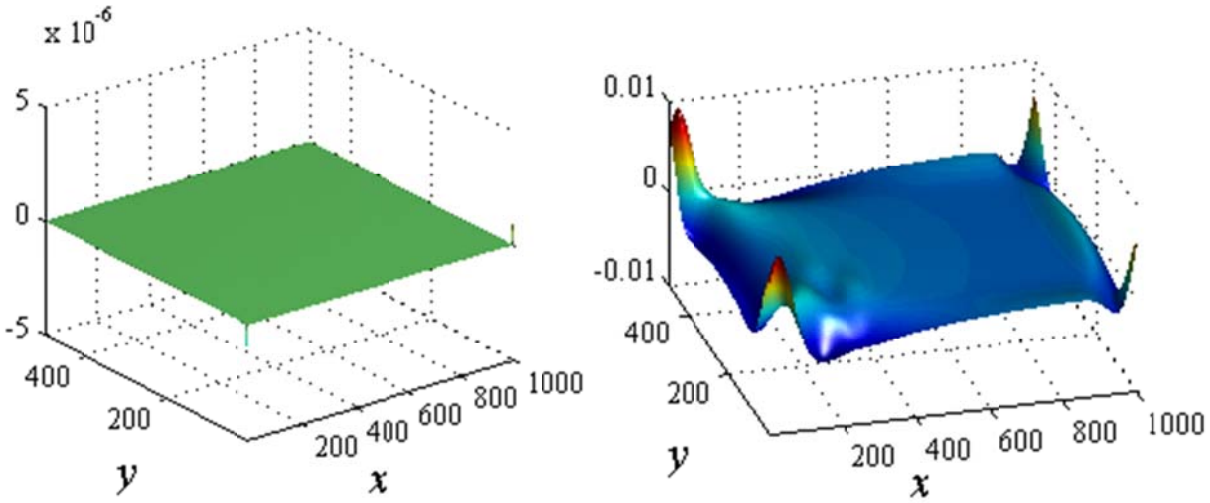

(a) (b)

Figure 5.6 Wavelet coefficients of the fundamental mode shape in damage B (a) a = 1; and (b) a = 40

To develop a viable algorithm, there are two main problems to be addressed. One is to alleviate the distortion of coefficients caused by the boundary condition. Since the CWT is in fact a convolution of a wavelet and a signal of finite length, the wavelet coefficients will be inevitably distorted by the discontinuity of mode shapes at their ends. The wavelet coefficients could reach an extremely high/low value near the boundaries, although no damage appears in those regions. Those extreme values can even overshadow the singularity caused by damage and make small damage difficult to be detected as shown in Fig. 5.6(a). This boundary distortion problem has been investigated in the 1-D CWT cases by many researchers (Gentile and Messina 2003; Poudel et al. 2007; Rucka and Wilde 2006). There are commonly two methods to reduce the boundary effect. One method is to extend the mode shape data beyond its original boundary by the cubic spline extrapolation based on the points near the boundaries. It should be noted that the cubic spline extrapolation is merely a way to treat the boundary distortions. Another method is simply to ignore those wavelet coefficients near the boundaries. From the definition of the

convolution, it is clear that the boundary distortion can affect the coefficients as far as a half-width of the wavelet away from the boundary. To prevent the extremely distorted value from overshadowing the damage-induced singularity, all the wavelet coefficients in these "boundary effect regions" are cut off or set to zeros. For simplicity, the second method was adopted in this study to treat the boundary distortion problem. The effect of this boundary distortion treatment, i.e., the cut-off of the boundary effect regions, is demonstrated in Fig. 5.7. As we can see, the elimination of coefficients near boundaries greatly helps the detection of damage in the plate. It should be noted that both the extrapolation method and the "set-to-zero" method will not be capable of detecting the damages close to the boundaries, since both of them smooth out the coefficients information near the boundaries.

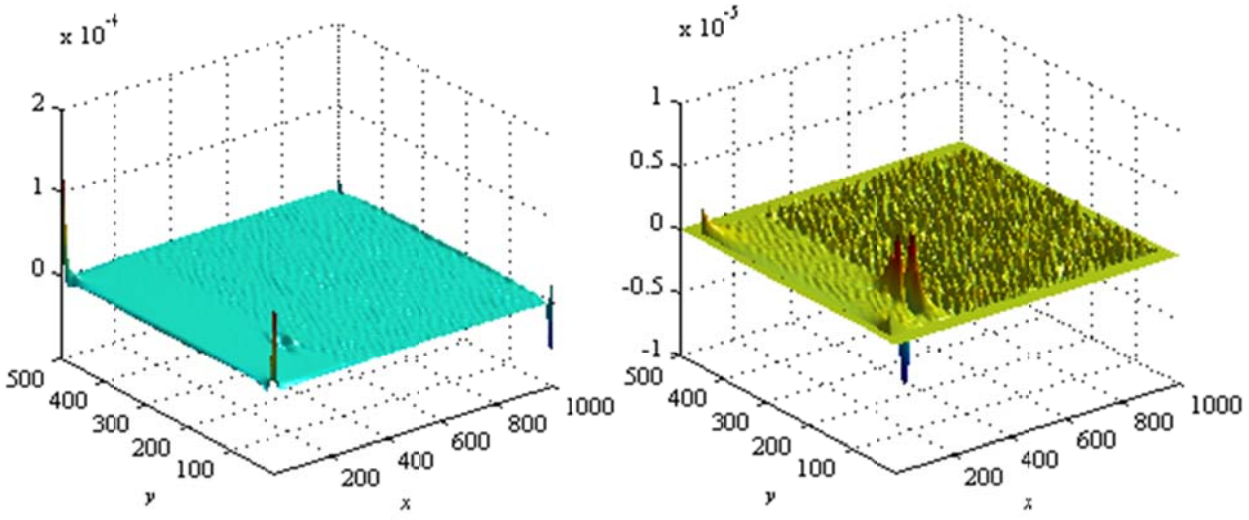

(a) **(b)**

Figure 5.7 Wavelet coefficients of the fundamental mode shape in damage B (a = 6) before and after boundary distortion treatment
(a) original wavelet coefficients; (b) wavelet coefficients after the boundary distortion treatment.

Another problem for detecting damage using the wavelet coefficients with the continuous scale resolution is how to visualize a function $S(\vec{b},a)$ with three independent variables. To solve this problem, an algorithm is proposed to visualize only the singular part of the coefficients instead of visualizing all of the coefficients. The algorithm can be divided into the following four steps:

(1) Step 1: 2-D CWT. The 2-D CWT of the plate mode shape is computed using MATLAB in continuous scale variation.

(2) Step 2: Boundary distortion treatment. All the wavelet coefficients in the "boundary effect regions" are set to zeros.

(3) Step 3: Threshold value calculation. The maximum and minimum values of the updated wavelet coefficients are calculated. The one with the larger absolute value is multiplied with a threshold ratio between 0 and 1 to generate a threshold value.

(4) Step 4: Isosurface generation. The points $(\vec{b},a)$ with the threshold value are connected to form an "isosurface" as the way of contour lines connecting points of equal elevation. The isosurface can be directly used to indicate the location and area of the damage.

A MATLAB® code is written to realize this algorithm. For damage detection in all three damage cases, the isosurfaces are generated using this algorithm as shown in Fig. 5.8. Because the singularity part of the signal lies in the high spatial frequency range, only the wavelet coefficients of low scales are of interest. In this case, the range of the scales in this study is chosen as from $a=1$ to 10. The threshold ratio is adjusted to 0.3 based on a few trial analyses to obtain a clear isosurface, although another threshold ratio t in range from 0.1 to 0.4 will also work for the damage detection. It can be seen that in all three damage cases the damage can be

correctly located. The isosurface marks the edges of the damaged area, demonstrating that this algorithm is capable of not only locating the damage but also indicating the area and shape of the damage, which is crucial to identify the size and type of the damage.

This algorithm is more advantageous than the one simply using wavelet coefficients from one scale, and the reason is two-fold: first, it avoids the false indication of damage caused by an inappropriate choice of a single scale because only the singularities shared by most of the scales can be identified as a damage; second, its noise immunity is more robust because some randomly distributed singular points caused by noise cannot form an clear isosurface. Furthermore, even if an isosurface is formed by noise, a damage-induced isosurface can be easily distinguished from a noise-induced isosurface by its consistency in most of the scales.

Further investigation shows that this algorithm can not only be applied on the fundamental bending mode shape but also works on the other mode shapes of the cantilevered plate including the torsional mode shape. Fig. 5.9 shows the isosurface generated in damage B using the first torsional mode shape. In the torsional mode case, Steps 3 and 4 in the algorithm are slightly adjusted, i.e., the isosurfaces defined by the threshold values from both the maximum and minimum values are overlaid to reflect the complete shape damage; otherwise, only half of the damaged area is shown.

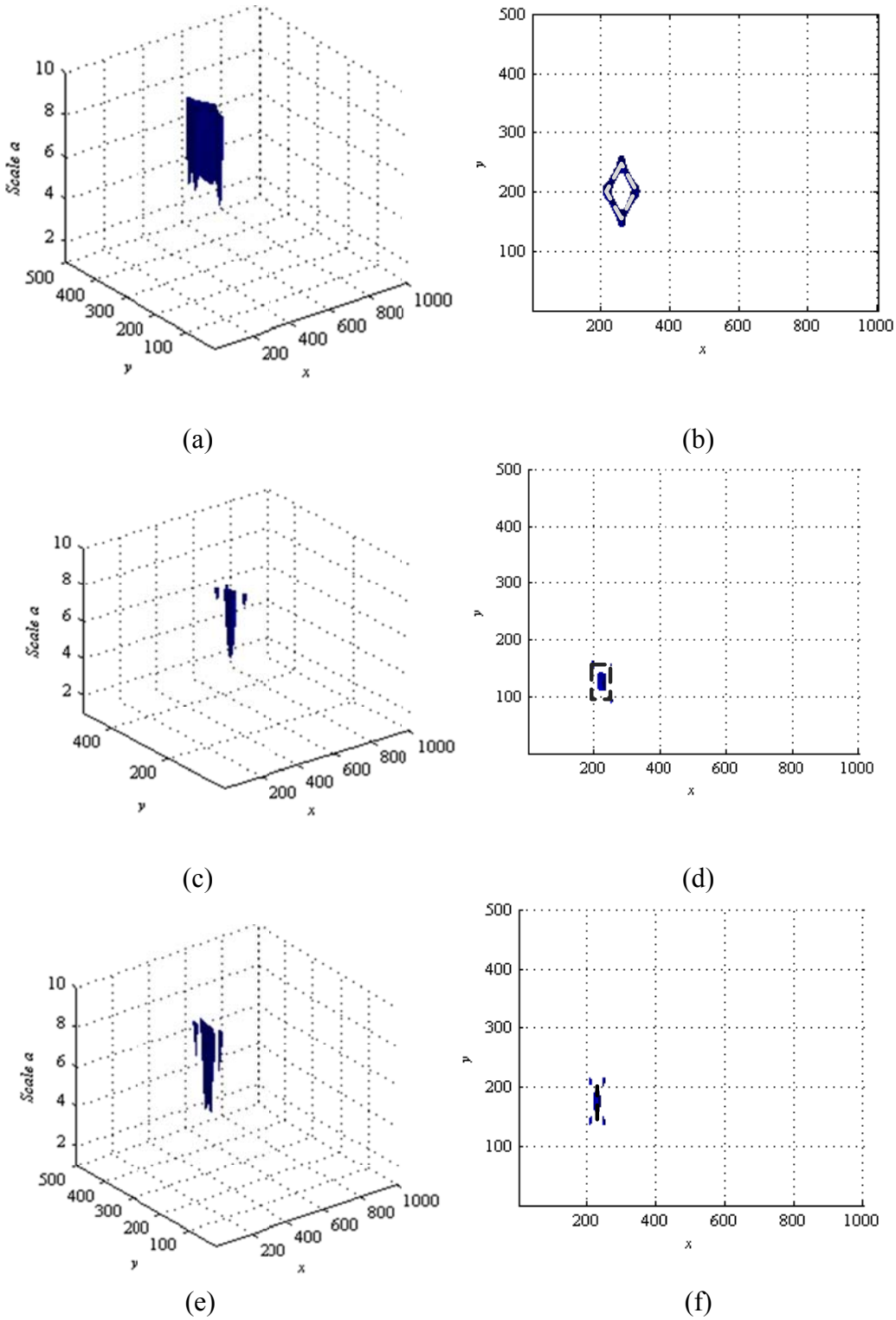

Figure 5.8 Isosurfaces generated by the proposed damage detection algorithm (the actual damages are marked in dash lines): (a) 3-D view and (b) top view of isosurface for damage A; (c) 3-D view and (d) top view of isosurface for damage B; (e) 3-D view and (f) top view of isosurface for damage C.

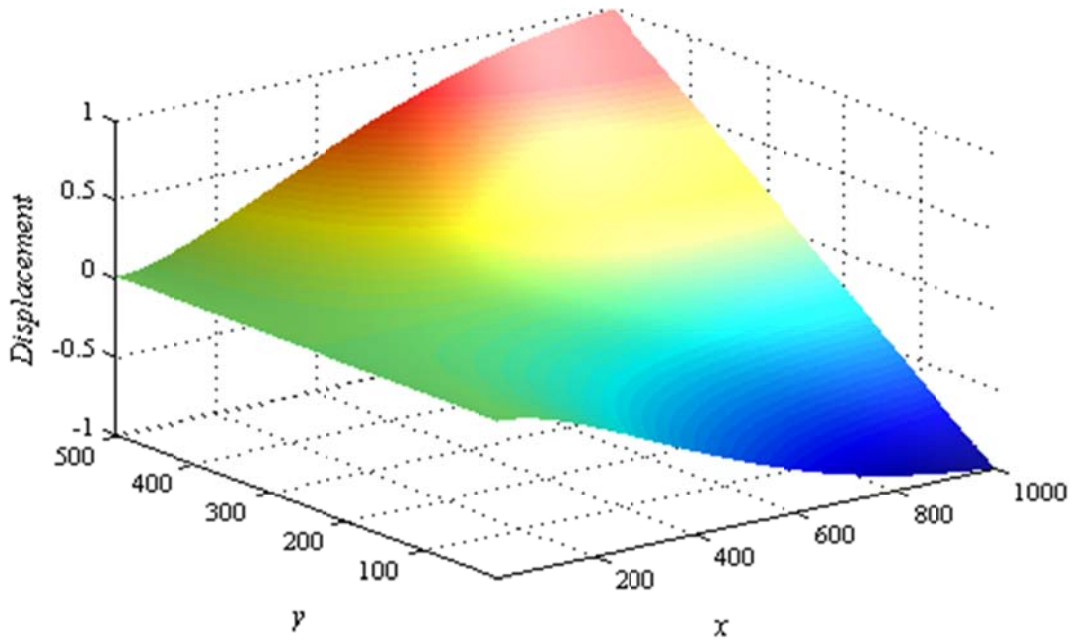

(a)

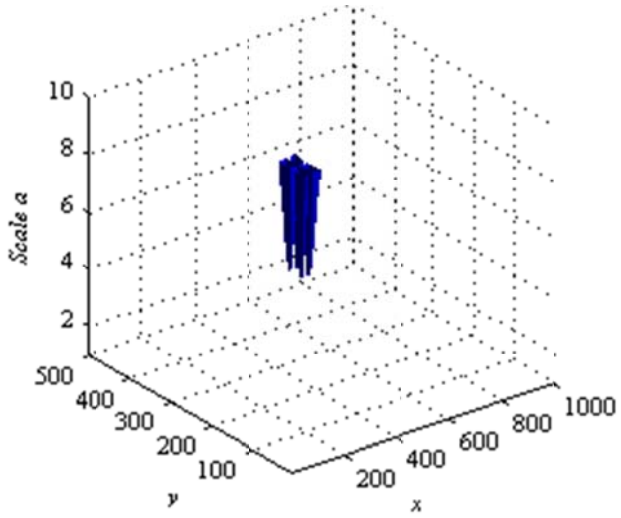

(b)

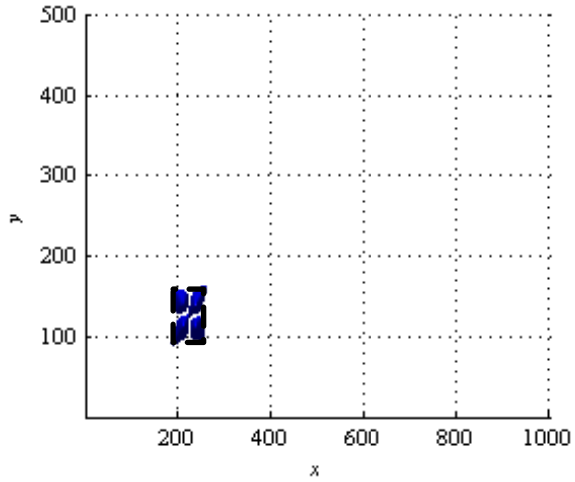

(c)

Figure 5.9 Isosurface in damage B using the first torsional mode shape

(a) The first torsional mode shape; (b) 3-D view of the isosurface; (c) top view of the isosurface.

5.4 Experimental verification

5.4.1 Experimental set-up and modal analysis

To demonstrate the 2-D CWT-based damage detection algorithm, a 0.508 × 0.254 × 0.00318 m (20 × 10 × 0.125 in.) FRP composite plate was experimentally tested. The plate is clamped at one end by a steel anchor beam. An artificially-induced and visible impact damage with an approximate diameter of 20.3 mm (0.8 in.) was induced in the plate before the modal testing.

The modal testing of the damaged plate was conducted with a roving excitation test. The plate is uniformly divided into 20×10 elements by the grid lines as shown in Fig. 5.10. The plate is subjected to a dynamic pulse load applied at each grid point using modally tuned hammer (PCB 652B10). A total of 20×9 grid points were tested corresponding to an actual spatial sampling distance of 25.4 mm (1.0 in.). The response measurements were made using one accelerometer (PCB 352C68) to record the response of the structure. The analog signals then pass a low-pass anti-aliasing filter to prevent the aliasing problem. A Krohn-Hite 3382 8-pole dual channel filter is employed to filter out the high frequency signals above the cut-off frequency of 250 Hz. The filtered signals are then digitized and collected by the data acquisition system dSPACE CP1103 at the sampling frequency of 500 Hz. The measurements at each point are repeated 16 times, and the synchronized time histories from the excitation and response measurements are averaged to enhance the signal-to-noise ratio (SNR). The complete experimental set-up is shown in Fig. 5.11. Then, the frequency-response functions (FRFs) of these tested points are calculated from these excitation and response time-histories. A typical FRF curve and its coherence curve from the test are illustrated in Fig. 5.12. Then, these FRF curves are imported to the modal analysis program ME'Scope for curve fitting and modal

extraction. Fig. 5.13 shows the 5th mode shape of the composite plate, which is used for the damage detection.

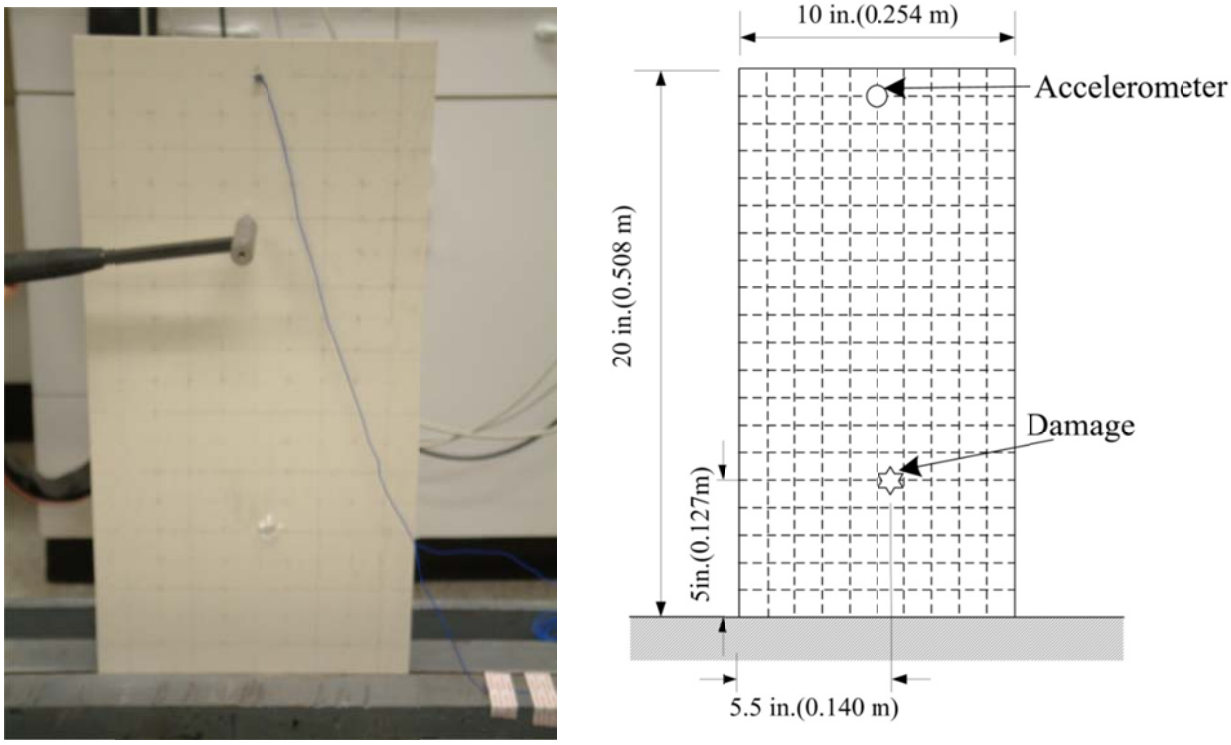

(a) (b)

Figure 5.10 A cantilevered FRP composite plate with artificially-induced impact damage for model testing

(a) test specimen and (b) grid for response measurement using accelerometer.

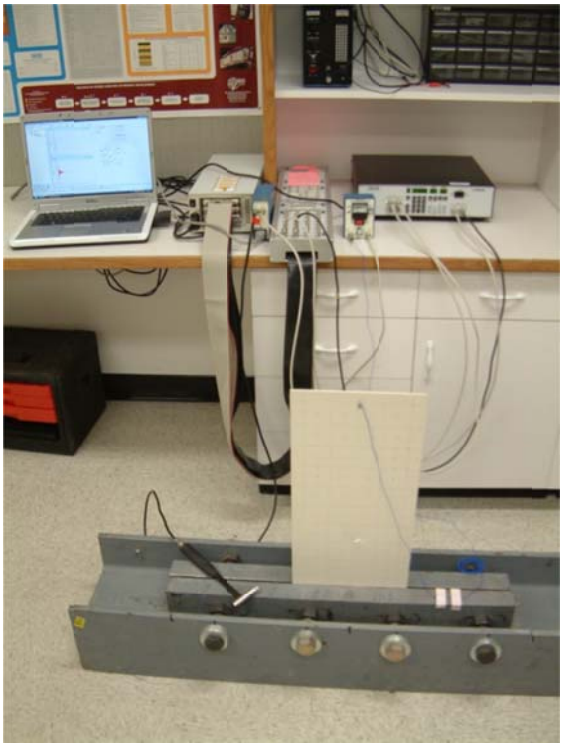

Figure 5.11 Experimental set-up and data acquisition system for modal analysis.

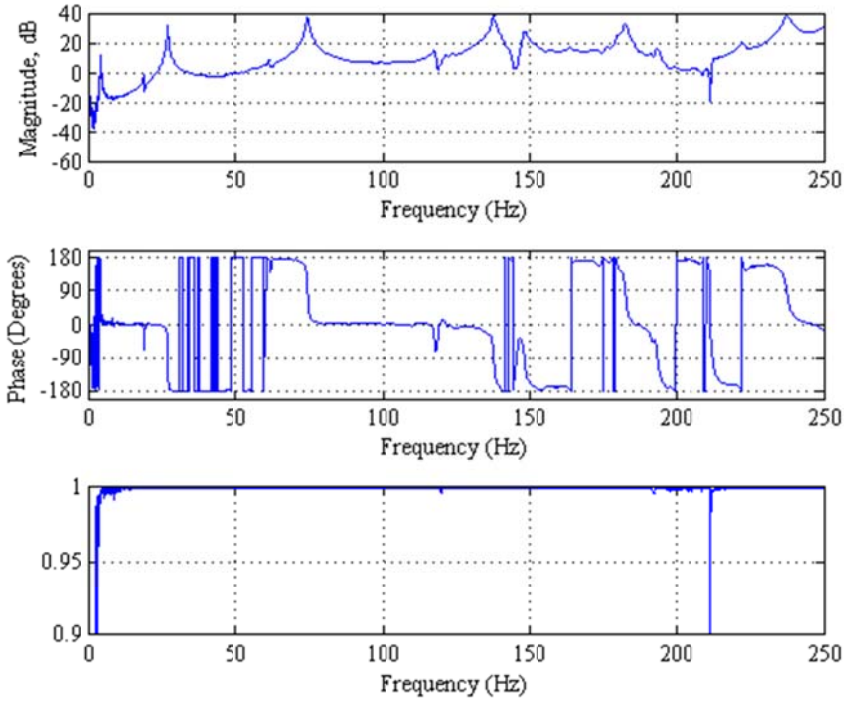

Figure 5.12 FRF and coherence curves for acceleration measurement at a typical point.

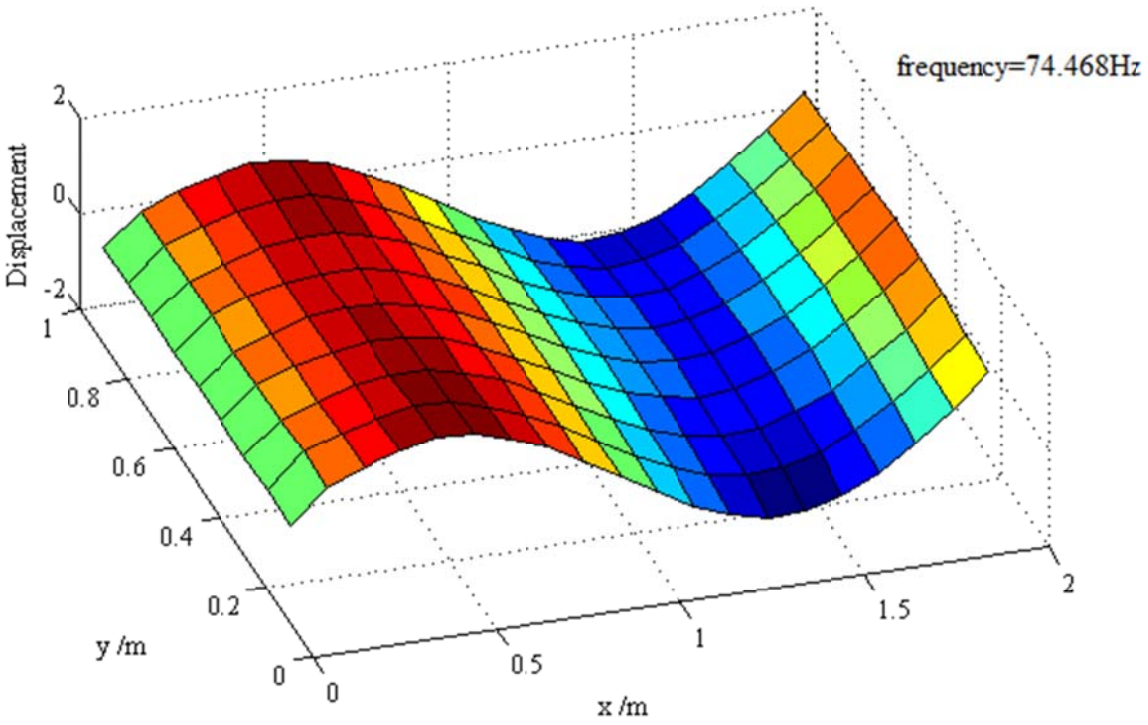

Figure 5.13 The 5th mode shape of the composite plate from the experimental modal analysis.

5.4.2 Damage identification using 2-D CWT-based algorithm

The proposed 2-D CWT-based algorithm is applied to the experimentally obtained 5th mode shape of the composite plate (see Fig. 5.13) for damage detection. First, the mode shape data is oversampled by 10 using the bivariate cubic spline interpolation to enhance the spatial sampling distance from 25.4 mm (1.0 in.) to 2.54 mm (0.10 in.). Then, the 2-D CWT-based damage detection algorithm is applied to the oversampled data. The investigation shows that in this case a scale from 1 to 10 is sufficient for damage detection. The threshold value is set to 0.4 in this case, although any threshold value between 0.3 and 0.5 can give a relatively clear isosurface indicating the damage. The results from the algorithm are shown in Fig. 5.14. The isosurface in Fig. 5.14 accurately indicate the location of the damage and illustrate the approximate shape of the damage. Although there is a small piece of noise-induced isosurface in

Fig. 5.14, it can be easily distinguished from the "real" damage-induced isosurface by its pattern as mentioned in Section 5.5.2. In conclusion, the results of this experiment demonstrate the validity and effectiveness of the 2-D CWT-based damage detection algorithm being applied to the experimental mode shape data.

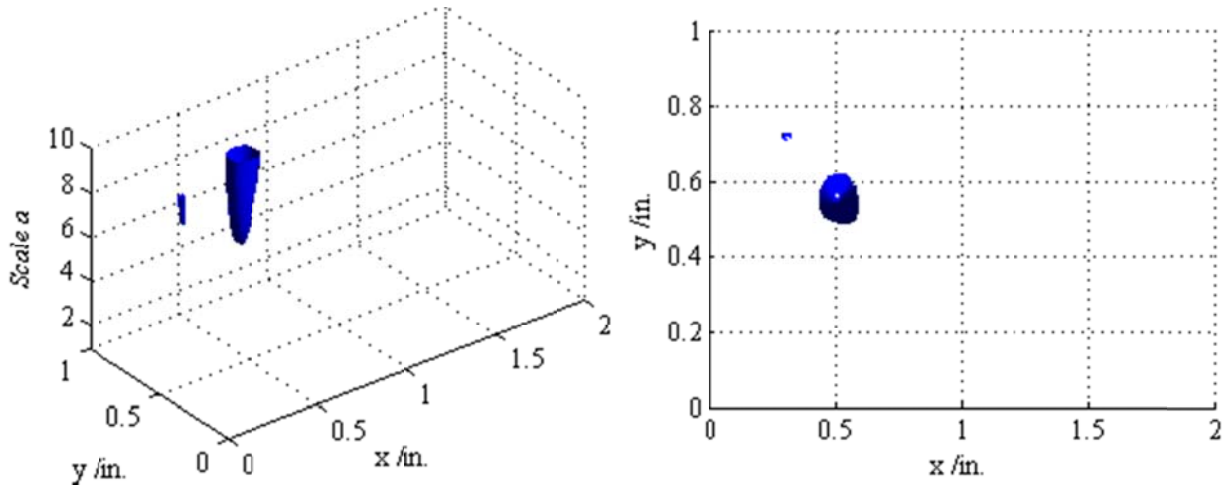

(a) 3D view **(b) top view**

Figure 5.14 Isosurface of 2-D CWT using the 5th mode shape data from experimental modal analysis.

5.5 Summary

In this Chapter, a 2-D CWT-based damage identification algorithm using "Dergauss2d" wavelet for plate-type structures is presented. An isosurface of 2-D wavelet coefficients at continuous scales is generated to indicate the location and approximate shape (or area) of the damage. The proposed algorithm is a dynamic response-based damage detection technique which only requires the mode shapes of the plate after damage. The viability of this method is demonstrated by analyzing the numerical and experimental mode shapes of a cantilevered plate.

This chapter paves some foundation for the application of 2-D CWT-based damage detection algorithm for plate- or shell-type structures (as demonstrated later in the experimental

evaluation of a full-scale deck panel in Chapter 8). However, more experiments are needed to demonstrate the practicality of this method for full-scale structures and *in-situ* damage detection application.

CHAPTER 6

COMPARATIVE STUDY OF DAMAGE DETECTION ALGORITHMS

6.1 Introduction

As reviewed in Chapter 2, extensive research has been conducted in the vibration or dynamic response-based 1-D damage detection algorithms for beam-type structures, and a broad range of algorithms and methods have been developed in this highlighted area. However, the research on the vibration-based 2-D damage identification algorithms for plate-type structures is relatively limited. In particular, for bridge deck type application, the damage identification algorithms for 2-D plate-type structures are in need.

In order to better understand the characteristics and advantages of different damage detection algorithms, comparative studies were conducted on the algorithms for the beam-type structures and plate-type structures. The study was based on the finite element simulation to evaluate the damage detection algorithms for beam-type and plate-type structures. First, a comparative study on the five extensively used damage detection algorithms for beam-type structure is presented in Section 6.2. Then, a comparative study of the proposed 2-D CWT based algorithm with two other 2-D damage detection algorithms, i.e., 2-D GSM and 2-D SEM, is presented in Section 6.3.

6.2 Comparative study of damage detection algorithm for beams

In this section, a comparative study based on the finite element model was conducted to evaluate the five extensively used damage detection algorithms for the beam-type structures. The five damage detection algorithms considered are (1) frequency-based Single Damage Indicator (SDI) method, (2) mode shape-based Generalized Fractal Dimension (GFD) method, (3)

curvature-based Mode Shape Curvature (MSC) method, (4) Gapped Smoothing Method (GSM), and (5) strain energy-based Damage Index Method (DIM). Although some of these methods are eligible for both damage localization and identification, only its damage localization ability was investigated here. For the SDI, MSC and DIM methods, the modal parameters from the first five modes are adopted. For the GFD and GSM methods, only the fundamental mode shape data are used. The characteristics of these five methods are summarized in Table 6.1.

The commercial FE analysis package ABAQUS is used to perform an eigenvalue analysis to generate the natural frequencies and mode shapes of the healthy and damaged beam. For simplicity, the structure is assumed to be a cantilevered beam of 0.01 m width × 0.01 m depth × 1 m length. The material is assumed to be isotropic with Young's modulus E = 1 GPa and Poisson's ratio v = 0.25. The beam is evenly divided into 50 3-node quadratic beam elements B32. The mode shape data are extracted from the 101 nodes along the beam length. At the damage location, the Young's modulus of the element(s) is reduced to simulate the damage-induced stiffness loss. The different damage severities are simulated by different bending stiffness reductions in the damaged element, i.e., when the damage severity is a, the Young's modulus of the damaged element E' is set to $(1-a)\,E$.

Table 6.1 Characteristics of five damage detection algorithms

Algorithms	Type	Modal parameters requirement	Basic assumption	Damage index
SDI	Model-based	Measured natural frequencies in healthy and damaged beam, or theoretical mode shape in healthy beam model	Single damage	Defined at element/sub-region
GFD	Response-based, damaged state response only	Measured fundamental mode shape in damaged beam	-	Defined at node/sensor
MSC	Response-based	Measured mode shape curvatures in healthy and damaged beam	-	Defined at node/sensor
GSM	Response-based, damaged state response only	Measured fundamental mode shape curvature in damaged beam	-	Defined at node/sensor
DIM	Model-based	Measured mode shape curvatures in damaged beam, or theoretical mode shape in healthy beam model	Single damage	Defined at element/sub-region

6.2.1 Single damage detection

First, a single damage with three different severities is considered. The damage is assumed to be at the 20th element which locates 0.38~0.40 m away from the cantilever clamped end (x = 0). The simulated natural frequency change ratio and damage severity relationship in the first five modes is given in Table 6.2. The natural frequency change ratio suggests that mode 5 should be the most sensitive mode to this specific damage.

Since the damage index/indicator from each algorithm has its unique physical meaning, it is meaningless to compare them directly. For comparison, assuming that the damage index at a different location is a normally distributed random variable, a Normalized Damage Index (NDI) can be obtained using Eq. (2-11). A threshold value NDI = 2 is usually used to detect damage, i.e., a NDI larger than the threshold value indicates the location of potential damage.

Table 6.2 Natural frequency change ratio in three damage severities

Damage severity, *a*	Bending stiffness ratio, *E'I/EI*	Natural frequency change ratio = $(f_h - f_d)/f_h$				
		Mode 1	Mode 2	Mode 3	Mode 4	Mode 5
0.1	*0.9*	0.001	0.0014	0.0011	0.0004	0.0022
0.2	*0.8*	0.0023	0.0032	0.0026	0.0007	0.0049
0.3	*0.7*	0.0038	0.0054	0.0043	0.0012	0.0083
0.5	*0.5*	0.0089	0.0125	0.0098	0.0027	0.0183
0.7	*0.3*	0.0204	0.0279	0.0214	0.0059	0.0385
0.9	*0.1*	0.0726	0.0888	0.0617	0.0175	0.0980

It should also be noted that for the GFD method (Wang and Qiao 2007), the damage index is subjected to the choice of scale parameter *S* (see Eq. (2-8)). In this study, the investigation showed that an *S* value larger than 100 should be adopted in order to detect the damage and the normalized damage index varies little when *S* is chosen between 10^3 and 10^6. Hence, a constant scale parameter *S* = 1,000 is chosen for all cases when the GFD algorithm is implemented.

A comparison of NDI for all the five algorithms in the case of a single damage with severity $a = 0.1$ are shown in Fig. 6.1. For the SDI and DIM method with element-wise damage indices other than node-wise indices, their indices are placed at the midpoint of the corresponding element. It can be seen that all the five algorithms can detect and locate the damage correctly. Further results show that these algorithms can successfully locate the damage in all three damage severity cases. It is interesting to note that there is a small bump in the SDI curve around $x = 0.6$ m, since due to the frequency-based nature of SDI method, this bump will become an equally sharp peak as the one at $x = 0.4$ m if the boundary condition is symmetric. The peak values of NDI in three different cases of damage severities are collected in Fig. 6.2. It shows that all the methods give satisfactory damage indices, except the GFD. The GFD method gives relatively low NDI and drops below zero when $a = 0.3$, which indicates that this method is not so sensitive to small damage and may lead to a false negative indication of damage in some cases of damage severity. The MSC method always gives the largest peak values, and its peak values are insensitive to damage severity. The SDI method gives peak values decreasing with the damage severity, which indicates that this method may gradually lose its effectiveness when damage severity increase. It is also not surprising to see that the GSM gives oscillating peak values since the NDI from the GSM should not be expected to correlate with damage severities when only the damaged state data are used.

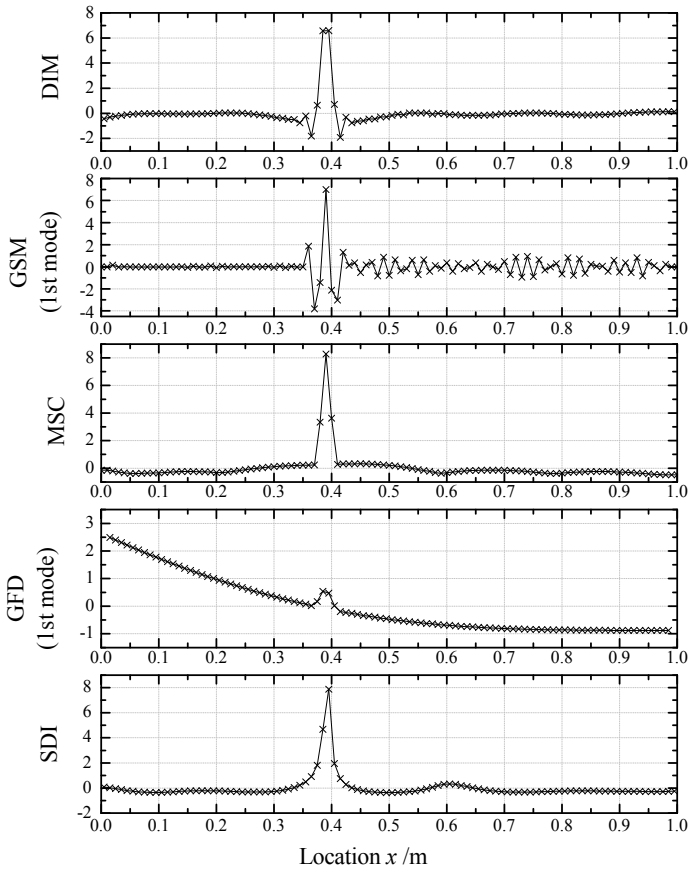

Figure 6.1 NDI along beam length for five algorithms in the case of single damage (damage location x = 0.38~0.40 m, damage severity *a* = 0.1).

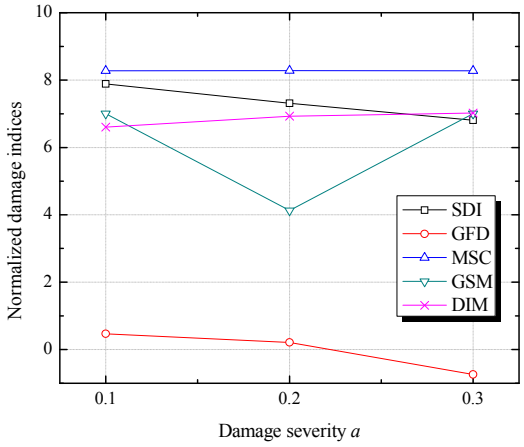

Figure 6.2 Peak values of NDI for five algorithms at different severities (*a* = 0.1, 0.2 and 0.3).

6.2.2 Multiple damage detection

Second, two multiple damage cases with two separate damage elements are considered. For the first case, the multiple damages with the same severity $a = 0.1$ are assumed to be at the 3rd and 20th elements which locate 0.04~0.06 m and 0.38~0.40 m, respectively, away from the cantilever clamped end ($x = 0$). For the second case, the multiple damages are assumed to be at the 20th and 30th elements, which locate 0.38~0.40 m and 0.58~0.60 m, respectively, away from the cantilever clamped end ($x = 0$).The comparison of NDI in two multiple damage cases are shown in Fig. 6.3. It shows that MSC, GSM and DIM can locate the multiple damages successfully. It is interesting to note that the DIM methods can correctly locate the multiple damages even though it is originally derived from the single damage assumption. Our first attempt in using the GSM to detect the multiple damages shows that the GSM cannot locate the multiple damages if the fundamental mode is adopted as suggested in the literature (Ratcliffe 1997). However, further investigation shows that the higher modes actually work better than the fundamental modes in this case. Therefore, the NDI curve of the GSM shown in Fig. 6.3 is evaluated from the fifth mode shape curvature. However, using the fifth mode expands the irregular bump area, which leads to inaccuracy in damage localization. For different modes, there is a trade-off between the sensitivity and the damage localization accuracy in the GSM method. The GFD method, on the other hand, can locate damages in the first case, but it can only locate one of the two damages in the second case. It can be seen from the NDI curve that the sensitivity of the GFD to damage highly depends on the location of damage. The bump in the NDI curve is more obvious in the 3rd element than in the 20th element; while the bump in 30th element can barely be noticed. Hence, it is more effective for the GFD to detect the damage near the cantilever end than that near the free end. Although the frequency-based SDI method is

derived from a single damage assumption and designed mainly for single damage detection, surprisingly it can still approximately locate both damages in the second case with both the peaks shift toward each other a little. But it is obviously not a reliable algorithm for multiple damage detection, e.g., it cannot detect the damage at 20^{th} element in the first case. The reason of the failure in the first case for the frequency-based SDI method is that in a cantilevered beam the natural frequency change is more sensitive to damage near the cantilevered end than that near the free end if their damage severities are similar. Due to its single damage assumption and frequency-based nature, the SDI method tends to predict the damage location at the primary damage which dominates the damage-induced frequency change. To support this conclusion, it can also be noticed in the second case that the peak values at the 20^{th} element are higher than the 30^{th} element. In summary, MSC and GSM work well for localizing multiple damages if the mode is carefully chosen. DIM also works well in the separated multiple damage case even though using it for multiple damage detection violates its single damage assumption, while GFD and SDI are not suitable for multiple damage localization.

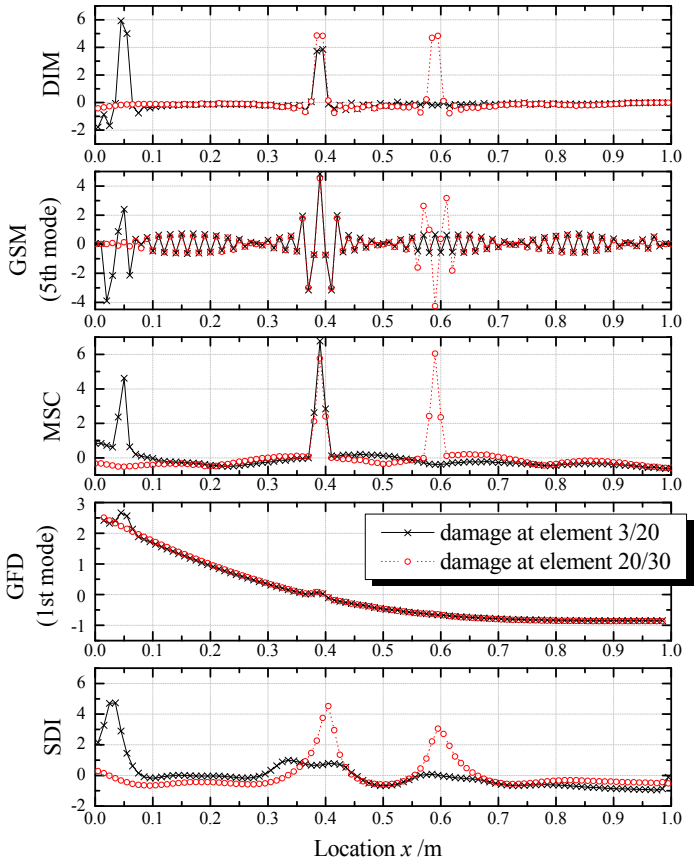

Figure 6.3 NDI along beam length for five algorithms in two multiple-damage cases (Damage case 1: located at 3rd (0.04~0.06 m) and 20th (0.38~0.40 m) elements, and damage case 2: 20th (0.38~0.40 m) and 30th (0.58~0.60 m) elements).

6.2.3 Large-area damage detection

After the single damage and multiple damage cases, a large-area damage case is considered. Large-area damage can be caused by impact damage or delamination in composite laminates. In this study, the damage is assumed to be at the region from the 20th element to 23rd element which locates 0.38~0.46 m away from the cantilevered end (x = 0). The damage severity of each damaged element is assumed to be a = 0.1.

A comparison of NDI for the five considered algorithms in the large-area damage case is shown in Fig. 6.4. It shows that both the MSC and DIM can locate the large-area damage

successfully; the GFD method is not very sensitive to the large-area damage although the slight irregularity in its NDI curve around the damaged region can still be noticed; the GSM and SDI methods show only one major peak in their curves which indicates the approximate location of damage, but they fail to identify the exact location and the length of the damage.

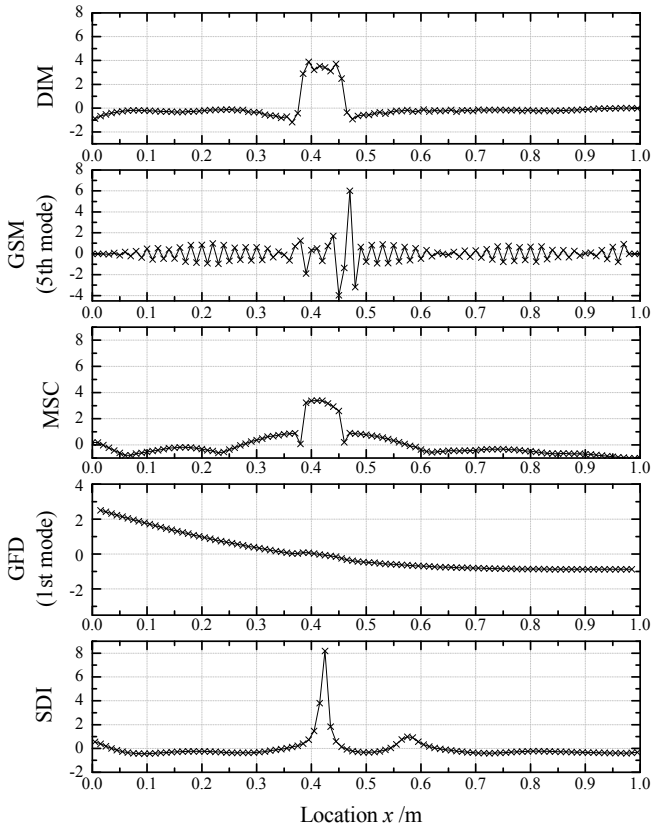

Figure 6.4 NDI along beam length for five algorithms in large-area damage case (damage located from the 20th to 23rd elements (0.38~0.46 m)).

6.2.4 Evaluation of measurement noise effect

In experimental modal analysis, measurement noises are inevitable. To evaluate the robustness of damage detection algorithms under measurement noise, the simulated mode shape data are contaminated with certain level of artificial random noise to generate "measured" mode shapes. The original simulated mode shapes are extracted from a single-damage case with a

damage severity a = 0.5 at the 20th element. Only the mode shape-based and curvature-based methods are studied here for comparison. The frequency-based SDI method is excluded because it is difficult to find a common ground to compare the level of noise from the frequency and mode shape measurement. The mode shape curvatures are obtained from two methods: derived from the displacement mode shape data or directly measured from the strain mode shape.

The contaminated mode shapes are represented as

$$\varphi'_{ij} = \varphi_{ij} + r_{ij}\rho\varphi_{rms,j} \tag{6-1}$$

where φ'_{ij} and φ_{ij} are the displacement mode shape or strain mode shape components of the jth mode at the ith DOF with noise and without noise, respectively; r is the normally distributed random variables with a mean equal to zero and a variance equal to 1; ρ is the random noise level; and $\varphi_{rms,j}$ is the root-mean-square of the jth displacement mode shape or strain mode shape.

When the mode shape curvatures are derived from the displacement mode shape, the comparison of damage detection resulted from the different algorithms are shown in Fig. 6.5. It should be noted that for the GSM and GFD methods, it is difficult to detect damage using the fundamental mode in this case. Since the most sensitive mode to this damage location is the 5th mode as suggested by the frequency change ratio in Table 6.2, the 5th mode shape instead of the first mode shape is used. When ρ = 0.0001, all four methods can locate the damage correctly. When ρ = 0.001, only the GFD method is capable of locating the damage; while both the GSM and DIM methods give the false indication of damage location; the MSC method indicates the correct damage location but also gives a false indication with the small peak at x = 0.18 m. When ρ = 0.01, all the methods fail to correctly locate damage. Although the GFD shows a peak at the damage location, it also gives a false positive indication of damage at x = 0.62 m. This

result shows that the GFD method is more robust than the MSC method; while the MSC method is better than the other two remaining methods (i.e., GSM and DIM) under measurement noise. The main reason is that the mode shape curvatures used in the MSC method are derived from the displacement mode shape by the central difference approximation (see equation (2-9)), while the damaged state curvatures used in the DIM are derived by cubic spline interpolation. For the GSM method, the damaged state curvatures are derived by the central difference approximation, while the baseline curvature derivation involves the cubic polynomial interpolation. This derivation process, no matter by the central difference approximation or the cubic interpolation, will greatly magnify the measurement error. This processing error weakens the robustness of the curvature-based algorithms under measurement noise. The results also show that the cubic interpolation will introduce larger processing error than the finite difference approximation, which makes the GSM and DIM methods very sensitive to measurement noise.

To manifest this conclusion, a similar damage detection case is studied, in which the mode shape curvatures are directly obtained from the simulated strain mode shape and then contaminated by artificial measurement noise to generate the "measured" strain mode shape. Again, the original simulated mode shape are extracted from a single-damage case with a damage severity $a = 0.5$ at the 20^{th} element (0.38~0.40 m from the cantilever clamped end of $x = 0$). The comparison of curvature-based damage detection algorithms are shown in Fig. 6.6. The result shows that when the directly measured curvature mode shape is used, the GSM method can correctly locate damage even under level of noise $\rho = 0.1$; the MSC method can correctly locate damage under level of noise $\rho = 0.2$; while the DIM method can even locate damage under level of noise $\rho = 0.4$. All the three methods perform much better than the mode shape-based GFD method when the processing-induced error is eliminated. Therefore, for the curvature-

based methods, if at the similar noise level, the directly measured curvature has a great advantage over the derived curvatures in laboratory or *in-situ* experiments.

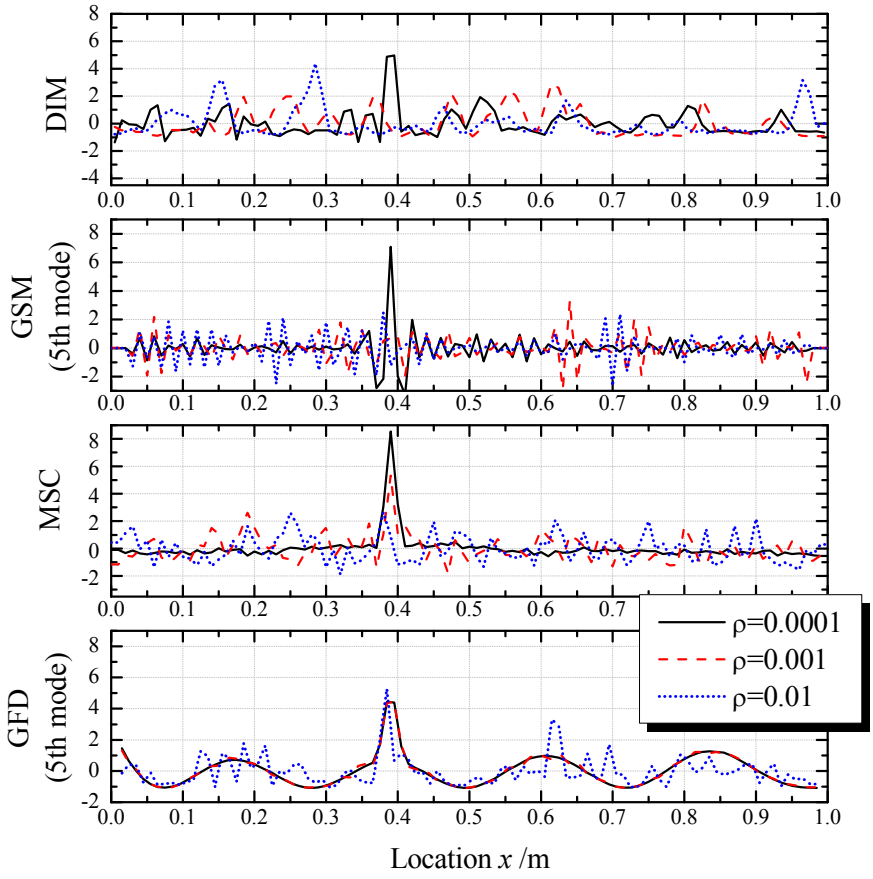

Figure 6.5 Measurement noise effect on damage detection algorithms case 1 (Curvature derived from the displacement mode shape; single damage at 0.38~0.40 m and *a* = 0.5).

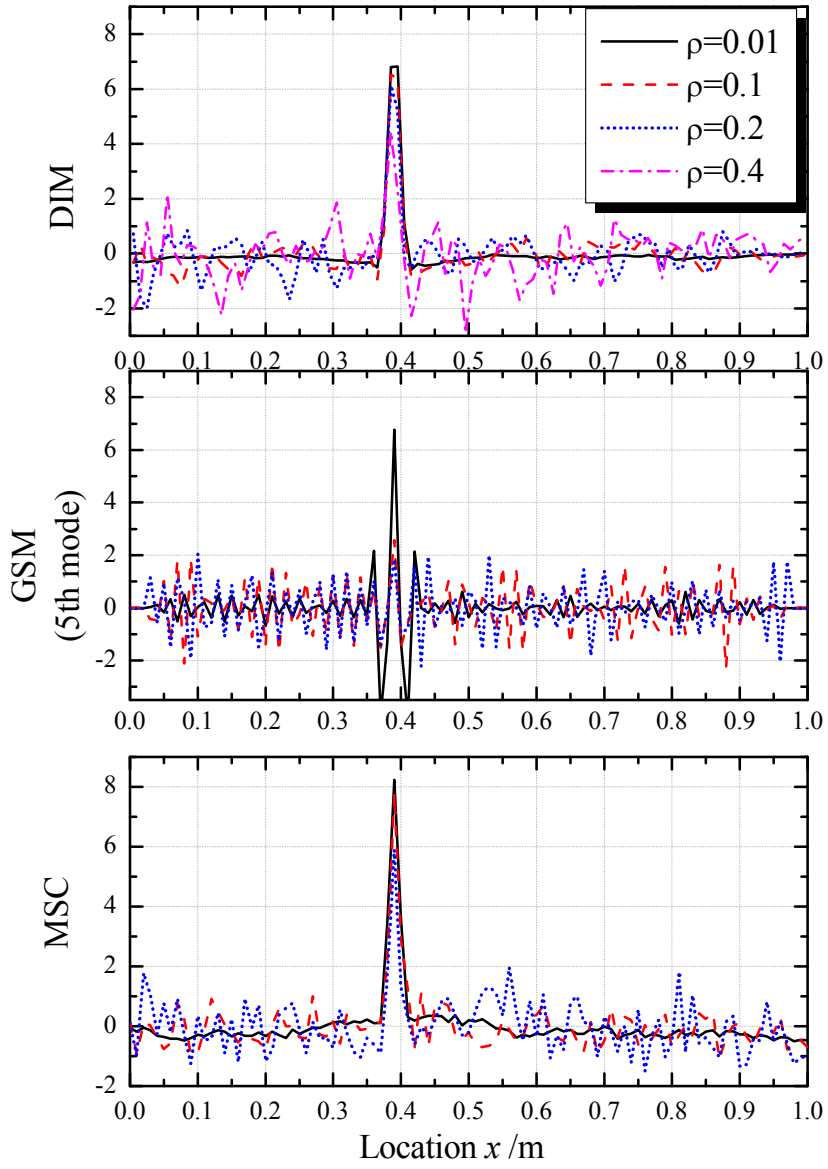

Figure 6.6 Measurement noise effect on damage detection algorithms case 2 (Curvature directly measured from the strain mode shape; single damage at 0.38~0.40 m, *a* = 0.5).

6.2.5 Evaluation of sensor spacing effect

In experimental modal analysis, the mode shapes usually can only be measured at a relatively small number of locations, especially for *in-situ* experiments. The sparse distribution of sensors will often pose difficulties for damage detection algorithms to detect and locate the

damage. Even though novel measurement systems, such as scanning laser vibrometer (SLV), can be employed to obtain high-density mode shape data in laboratory-scale experiments, the robustness of damage detection algorithms under limited measured data points is still of interest for their practicality for *in-situ* experiment.

To simulate the data acquisition process, the "measured" mode shape data are extracted from the FE-generated mode shapes at uniformly spaced locations. The effect of sensor spacing on the algorithms was studied. The mode shape curvatures are again obtained from two methods: derived from the displacement mode shape data or directly measured from the strain mode shape. Three cases with sensor spacing of $s = 0.02$, $s = 0.05$ and $s = 0.10$ were studied.

When the derived curvatures are used, the results are illustrated in Fig. 6.7. The GFD cannot detect the damage when the sensor spacing reaches $s = 0.05$. When $s = 0.10$, the DIM method gives a false indication of damage at the cantilevered end of beam, and it tends to give the periodical false indication along the beam; the MSC and GSM can barely detect the damage, and the GSM also tends to give the ambiguous prediction at $x = 0.6$ m. Another feature can also be noticed as pointed out by Zhou et al. (2007), that the GSM and MSC tends to predict damage location at the sensor location due to the piecewise nature of derived curvatures and can only predict the damage location with the accuracy of half of the sensor spacing.

When the directly measured curvatures are used, the results are illustrated in Fig. 6.8. The results show that all three curvature-based methods (i.e., the GSM, MSC and DIM) can correctly locate the damage without any false indication. For the GSM method, all the five modes can be used independently to locate the damage. Therefore, for the curvature-based methods, the directly measured curvature has its advantage over the derived curvatures in the case of large

sensor spacing. With the increase of sensor spacing, the predicted damage zone tends to spread, and the accuracy of damage location prediction will decrease accordingly.

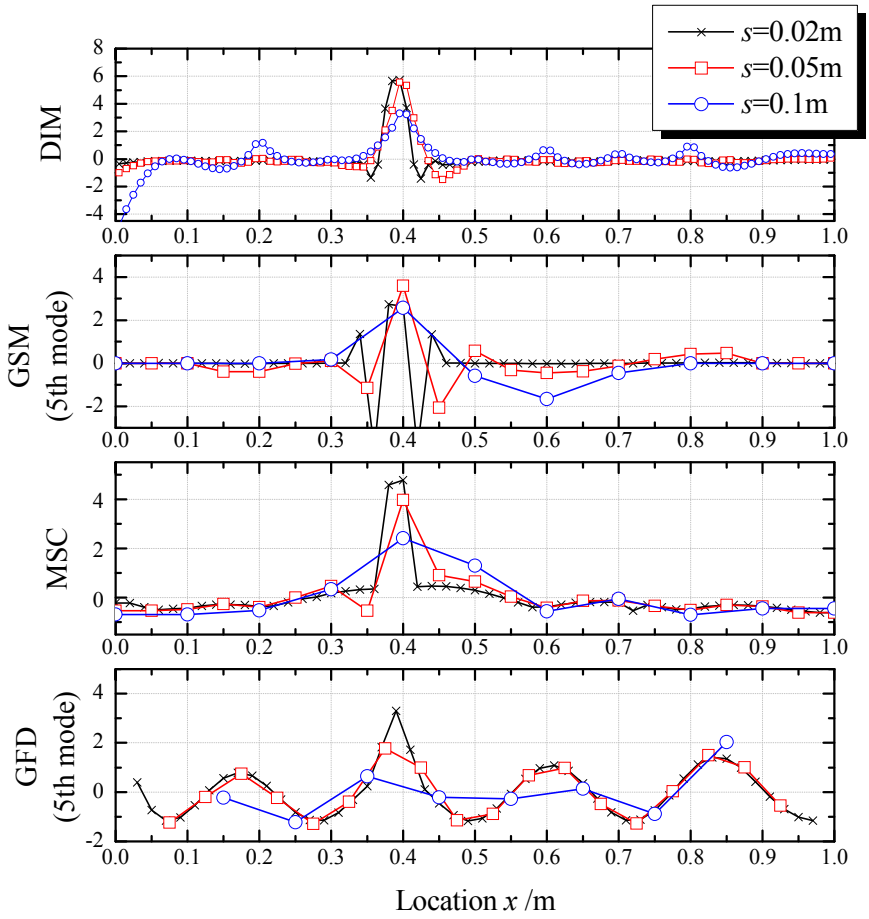

Figure 6.7 Sensor spacing effect on damage detection algorithms case 1 (Curvature derived from displacement mode shape; single damage at 0.38~0.40 m, *a* = 0.5).

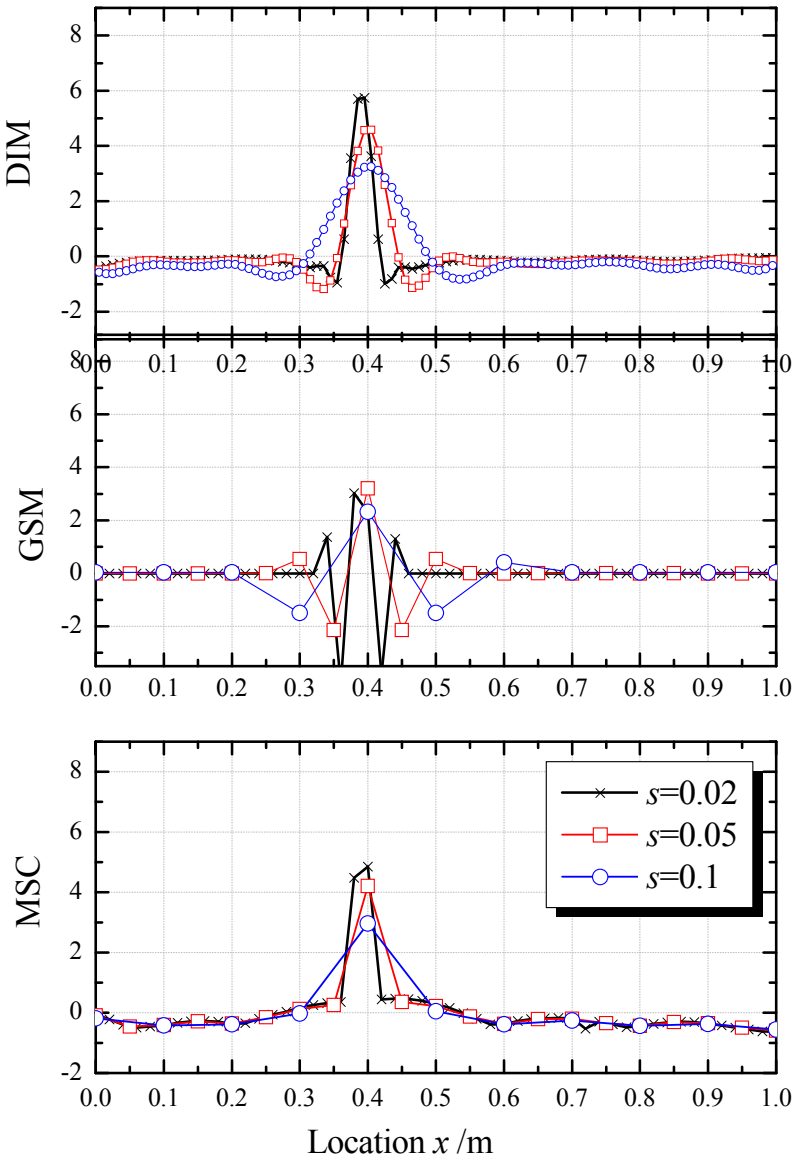

Figure 6.8 Sensor spacing effect on damage detection algorithms case 2 (curvature directly measured from the strain mode shape; single damage at 0.38~0.40 m, *a* = 0.5).

6.2.6 Summary on comparative study

Based on the above case illustrations and discussions, the capabilities of the aforementioned five damage detection algorithms in terms of their single and multiple damage identification, large-area damage identification, degree of noise immunity, and tolerance for sensor spacing are summarized in Table 6.3. The following conclusions are drawn from the

comparisons among the five damage detection algorithms in terms of single vs. multiple damages, damage area, methods of acquiring mode shape curvatures, noise, and sensor spacing:

(1) In noise-free and small sensor spacing condition, all five methods are capable of locating single damage; while only the MSC, GSM and DIM methods can locate the multiple damages, and only the MSC and DIM can locate the large-area damage.

(2) The fundamental mode may not always be the most effective mode for damage detection in the GFD and GSM methods, as suggested by others. A higher mode may be more sensitive to damage detection in some cases. The natural frequency change ratio can be a good indicator of sensitivity of certain modes to the damage.

(3) When the mode shape curvatures are derived from the displacement mode shape, the mode shape-based GFD method is more robust under the measurement noise than the curvature-based methods due to their processing-induced errors. However, when curvatures are directly measured from the strain mode shape, the curvature-based methods are much more robust and promising than the mode shape-based GFD method.

(4) When the mode shape curvatures are derived from the displacement mode shape, the MSC and GSM methods are more robust than others in the large sensor spacing case. For the curvature-based methods, the directly measured curvature has great advantage over derived curvatures in the case of large sensor spacing. If at the same noise level, the directly measure curvatures are preferred than the derived curvatures for damage detection in all studied cases.

(5) In general, the GFD method is not a very sensitive damage detection method, and it requires high density mode shape measurement and low-noise level. The MSC and

DIM methods are relatively robust in high measurement noise and large sensor spacing condition. Although the GSM is not as robust as the MSC and DIM methods, it is still a good choice for damage detection algorithm when only the damaged state structures are available for test as in most *in-situ* experiment.

Table 6.3 Capabilities of five damage detection algorithms

Algorithm	Single damage detection	Multiple damage detection	Large-area damage detection	Noise immunity	Sensor spacing tolerance
SDI	Yes	No	No	N/A	N/A
GFD	Yes	No	No	Excellent	Fair
MSC	Yes	Yes	Yes	Good (Good*)	Good (Good*)
GSM	Yes	Yes	No	Fair (Good*)	Good (Good*)
DIM	Yes	Yes	Yes	Fair (Excellent*)	Fair (Excellent*)

*Note: The results from directly measured curvature mode shape are shown in parentheses.

6.3 Comparative study of damage detection algorithms for plates

To further evaluate performance of the proposed 2-D CWT-based damage detection algorithm as introduced in Chapter 5, a comparative study of this algorithm with other two established damage detection methods for a plate was conducted. The two other damage detection methods considered are: (1) the two-dimensional Gapped Smoothing Method (2-D GSM) by Yoon et al. (Yoon et al. 2005), and (2) the two-dimensional Strain Energy Method (2-D SEM) by Cornwell et al. (Cornwell et al. 1999). The comparative study is based on the numerically simulated fifth mode shape of a damaged plate (i.e., damage B in Section 5.3.1). The choice of this mode is based on its natural frequency change ratio which is a good indicator of the mode sensitivity to the damage event. The natural frequency change ratio in the fifth

mode is the largest in the first five modes, and it is hence considered as the most sensitive mode to this specifically given damage (i.e., damage B in this study).

6.3.1 2-D GSM and 2-D SEM

The 2-D gapped smoothing method (GSM) adopts the one-dimensional GSM by Ratcliffe to two dimensional plate-like structural applications. The curvature mode shape $\nabla^2 w_{ij}$ is first calculated from the displacement mode shape w_{ij} by the central difference approximation at grid point (i, j) as:

$$\nabla^2 w_{ij} = (w_{i+1,j} + w_{i-1,j} - 2w_{i,j}) / h_x^2 + (w_{i,j+1} + w_{i,j-1} - 2w_{i,j}) / h_y^2 \tag{6-2}$$

where h_x and h_y are the horizontal and vertical grid increments, respectively.

Then, a smoothed surface is generated based on the curvature values at its neighboring grid points using the bivariate curve fitting. The smoothed curvature shape is evaluated at grid point (i, j) on the smoothed surface. The damage index β at point (i, j) can be then obtained by

$$\beta_{ij} = \left| \nabla^2 w_{ij} - C_{ij} \right| \tag{6-3}$$

where C_{ij} is the smoothed curvature at point (i, j).

While the 2-D strain energy method (SEM) subdivides the plate into N_x subdivisions in the x direction and N_y subdivisions in the y direction. It assumes that if the damage is primarily located at a single sub-region, then the fractional strain energy will remain relatively constant in undamaged sub-regions. For plates, the Young's modulus and the Poisson's ratio are assumed to be essentially constant over the whole plate for both the undamaged and damaged modes. The fractional strain energy f_{ijk} in sub-region (i, j) for the kth mode is given by classic plate theory as:

$$f_{ijk} = \frac{\int_{b_j}^{b_{j+1}} \int_{a_i}^{a_{i+1}} \left(\frac{\partial^2 w_i}{\partial x^2}\right)^2 + \left(\frac{\partial^2 w_i}{\partial y^2}\right)^2 + 2v\left(\frac{\partial^2 w_i}{\partial x^2}\right)\left(\frac{\partial^2 w_i}{\partial y^2}\right) + 2(1-v)\left(\frac{\partial^2 w_i}{\partial x \partial y}\right)^2 dxdy}{\int_0^b \int_0^a \left(\frac{\partial^2 w_i}{\partial x^2}\right)^2 + \left(\frac{\partial^2 w_i}{\partial y^2}\right)^2 + 2v\left(\frac{\partial^2 w_i}{\partial x^2}\right)\left(\frac{\partial^2 w_i}{\partial y^2}\right) + 2(1-v)\left(\frac{\partial^2 w_i}{\partial x \partial y}\right)^2 dxdy} \tag{6-4}$$

where w_k is the kth bending mode shape of the plate; a and b are the dimensions of the plate in x and y directions, respectively; the sub-region (i, j) is the rectangular region enclosed by $x = a_i$, $x = a_{i+1}$, $y = b_j$ and $y = b_{j+1}$.

The damage index β at sub-region (i, j) can be obtained by

$$\beta_{ij} = \frac{\sum_{k=1}^{m} f_{ijk}^*}{\sum_{k=1}^{m} f_{ijk}} \tag{6-5}$$

where f_{ijk} and f_{ijk}^* are the fractional strain energy from the healthy and damaged plate, respectively.

For the sake of comparison, both the damage index in the 2-D GSM and 2-D SEM are normalized. A normalized damage index Z at point (for the 2-D GSM) or sub-region (i, j) (for the 2-D SEM) can be obtained using

$$Z_{ij} = \frac{\beta_{ij} - \overline{\beta}}{\sigma_\beta} \tag{6-6}$$

where $\overline{\beta}$ and σ_β represent the mean and standard deviation of the damage indices, respectively. Usually, a damage detection criterion can be set when the normalized damage index Z_{ij} is larger than 2. The main characteristics of three damage detection algorithms are summarized in Table 6.4.

Table 6.4 Characteristics of three damage detection algorithms

Algorithms	Type	Modal parameter requirement	Damage index
2-D CWT	Response-based, only damaged state response required	Mode shape data in damaged beam	Defined at node/sensor
2-D GSM	Response-based, only damaged state response required	Mode shape data in damaged beam	Defined at node/sensor
2-D SEM	Model-based	Measured mode shape data in damaged beam and experimental/theoretical/numerical mode shape data in healthy plate model	Defined at element/sub-region

The 2-D GSM and 2-D SEM are directly applied to the numerical finite element mode shape of the damaged plate to verify their ability to detect the damage. The normalized damage indices are shown in Fig. 6.9. The results show that both the methods are able to detect the location of damage B in the ideal situation. Like the 2-D CWT, the 2-D GSM also works in sizing the damage area, although without special treatment, a similar boundary distortion problem occurs at the clamped end of the plate.

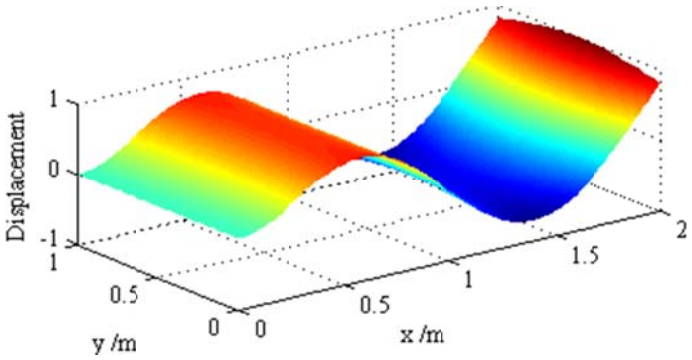

(a)

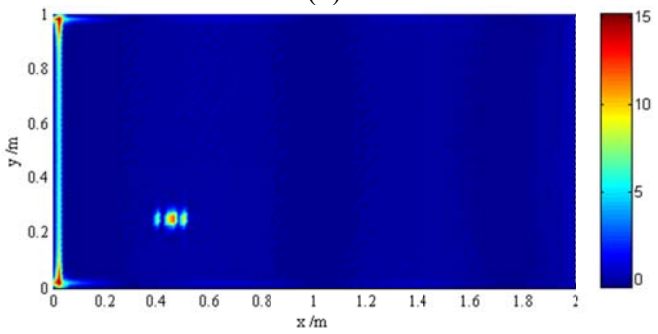

(b)

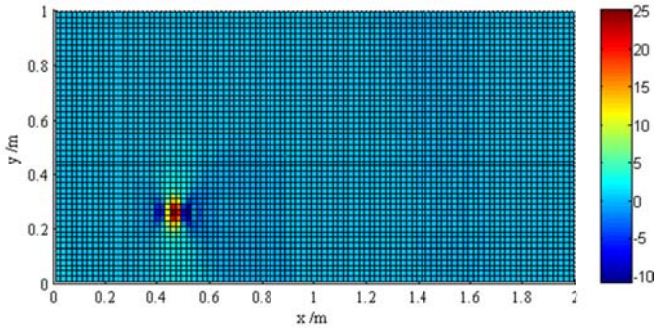

(c)

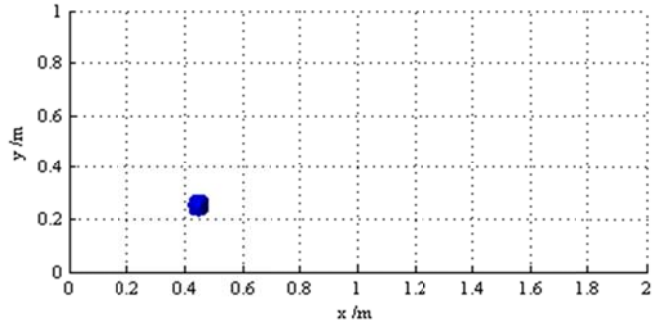

(d)

Figure 6.9 Damage detection for damage B using the 5th mode shape (a) the 5th displacement mode shape; (b) normalized damage indices by 2-D GSM; (c) normalized damage indices by 2-D SEM; and (d) isosurface by 2-D CWT.

6.3.2 Effect of measurement noise

In experimental modal testing, measurement noises are inevitable. To evaluate the robustness of a damage detection method, it is essential to investigate its noise immunity performance. In order to simulate the effect of measurement noise, a series of normally distributed random numbers are added to the numerical mode shapes to generate the noise-contaminated mode shapes. The original numerical mode shape data are extracted from all the 101×51 nodes in the finite element model. The new mode shape data can be expressed as:

$$w'(x,y) = w(x,y) + \rho \cdot r \cdot w_{rms} \tag{6-7}$$

where w' and w are the displacement mode shapes with and without noise, respectively; r is the normally distributed random variables with a mean equal to zero and a variance equal to 1; ρ is the random noise level; and w_{rms} is the root-mean-square of the displacement mode shape.

Based on the noisy mode shape data established by equation (6-1), the effect of measurement noise at different levels is illustrated in Figs. 4.10 to 4.12. As shown in Fig. 6.10, the 2-D GSM can only correctly detect the damage when $\rho = 1\times10^{-5}$, with a large boundary distortion at the clamped end. After the noise level reaches $\rho = 5\times10^{-5}$, the 2-D GSM cannot detect the damage anymore. Fig. 6.11 indicates that the 2-D SEM offers a better noise immunity than the 2-D GSM. The damage can be correctly localized when $\rho = 5\times10^{-5}$, if the boundary distortion is neglected. But in the case of $\rho = 1\times10^{-4}$, the damage can barely be noticed. Compared to both the 2-D GSM and 2-D SEM, the 2-D CWT clearly exhibits its superior noise immunity. As shown in Fig. 6.12, the damage location can be successfully identified when $\rho = 1\times10^{-4}$. Further investigation shows that the 2-D CWT is effective in detecting the given damage with noise level as high as $\rho = 2.5\times10^{-4}$. Although in the case of $\rho = 2.5\times10^{-4}$, some

pieces of isosurface caused by noise begin to appear, it is not difficult to distinguish these isosurfaces from the one caused by real damage by its pattern. Since these isosurfaces are caused by random noise, their existence and shapes are not as consistent from the low scale to high scale as the real one.

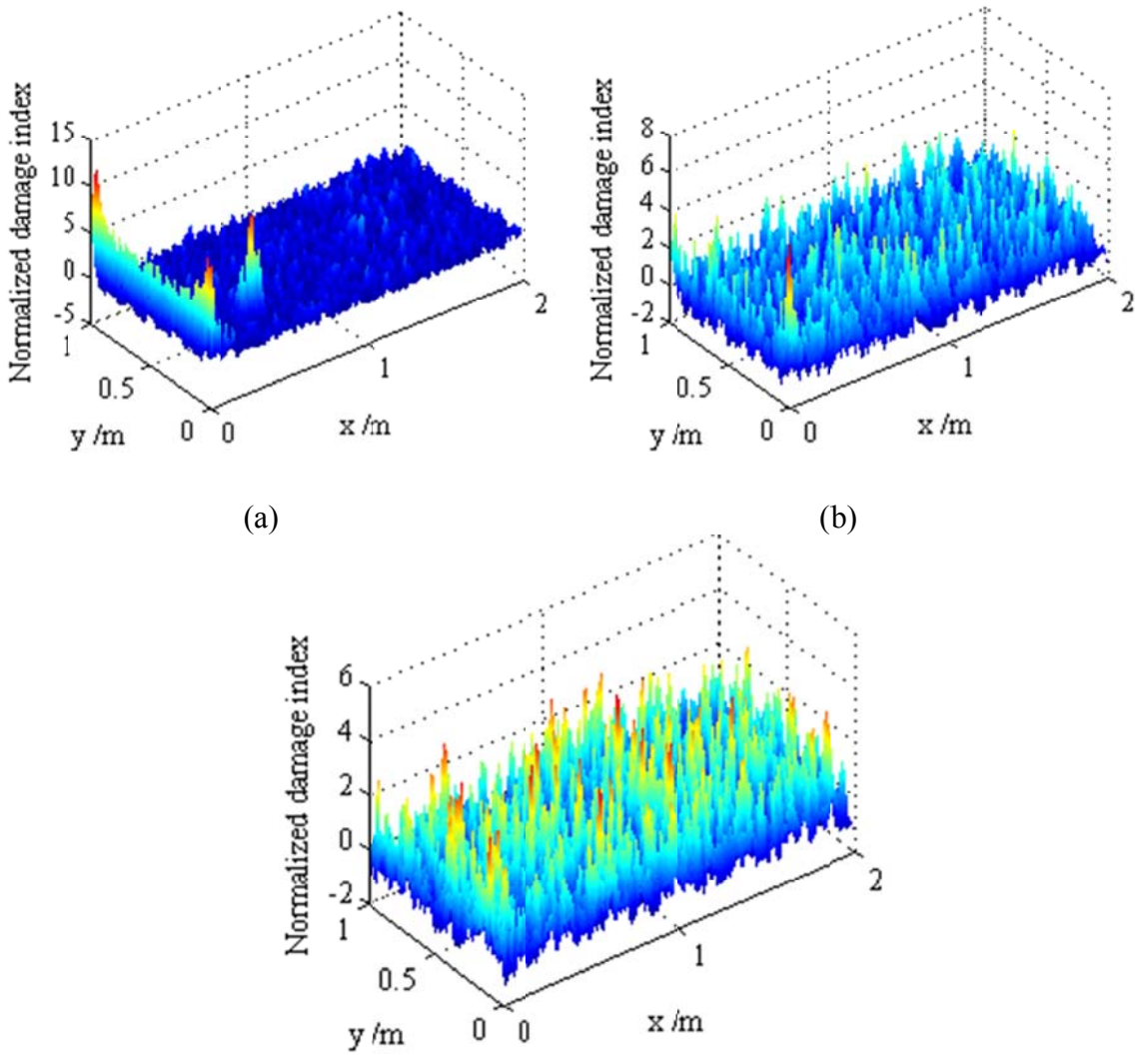

Figure 6.10 Normalized damage indices of 2-D GSM using the 5th mode shape data with different noise levels

(a) $\rho = 1\times10^{-5}$**; (b)** $\rho = 5\times10^{-5}$**; and (c)** $\rho = 1\times10^{-4}$**.**

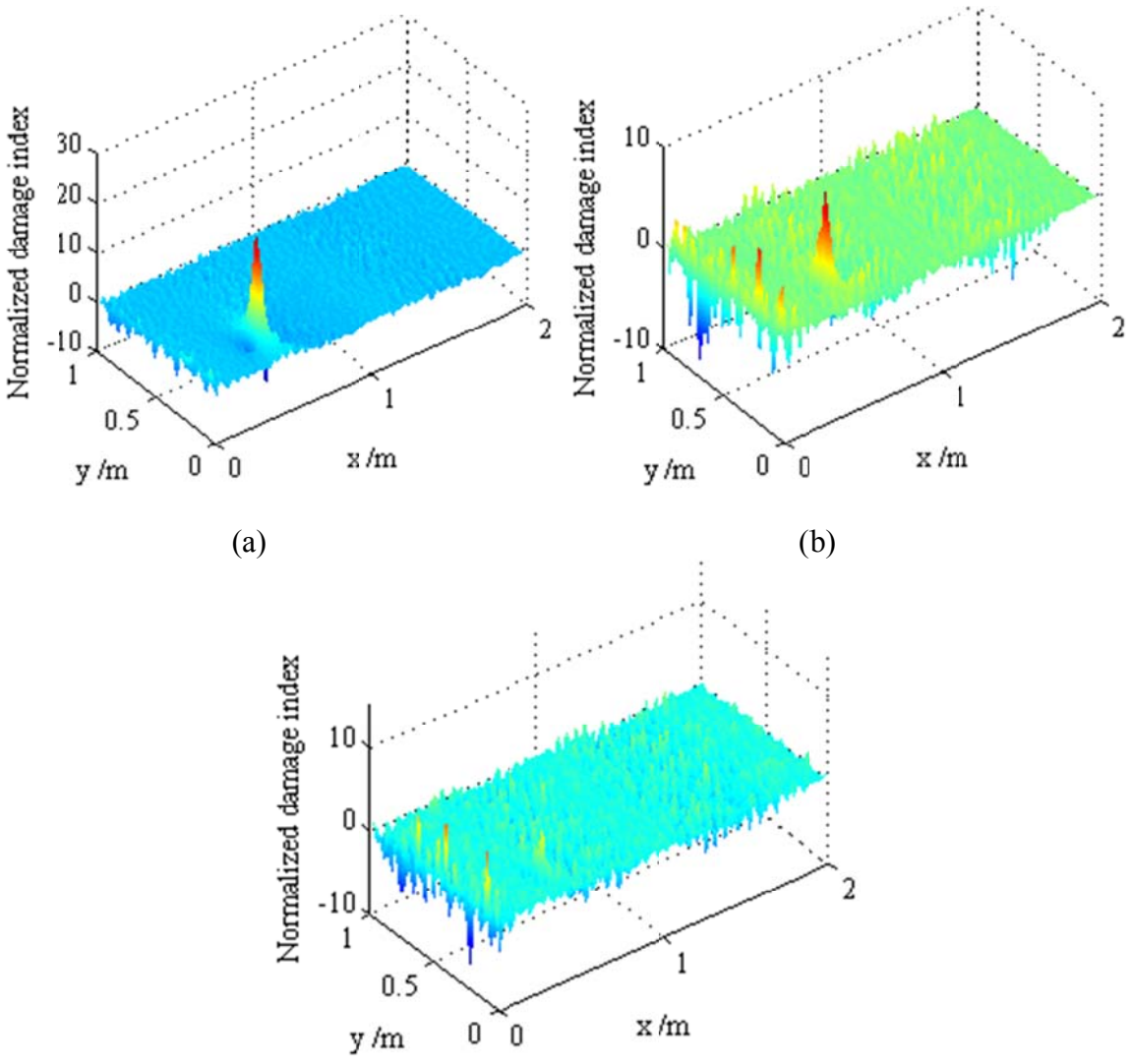

Figure 6.11 Normalized damage indices of 2-D SEM using the 5th mode shape data with different noise levels

(a) $\rho = 1\times10^{-5}$**; (b)** $\rho = 5\times10^{-5}$**; and (c)** $\rho = 1\times10^{-4}$**.**

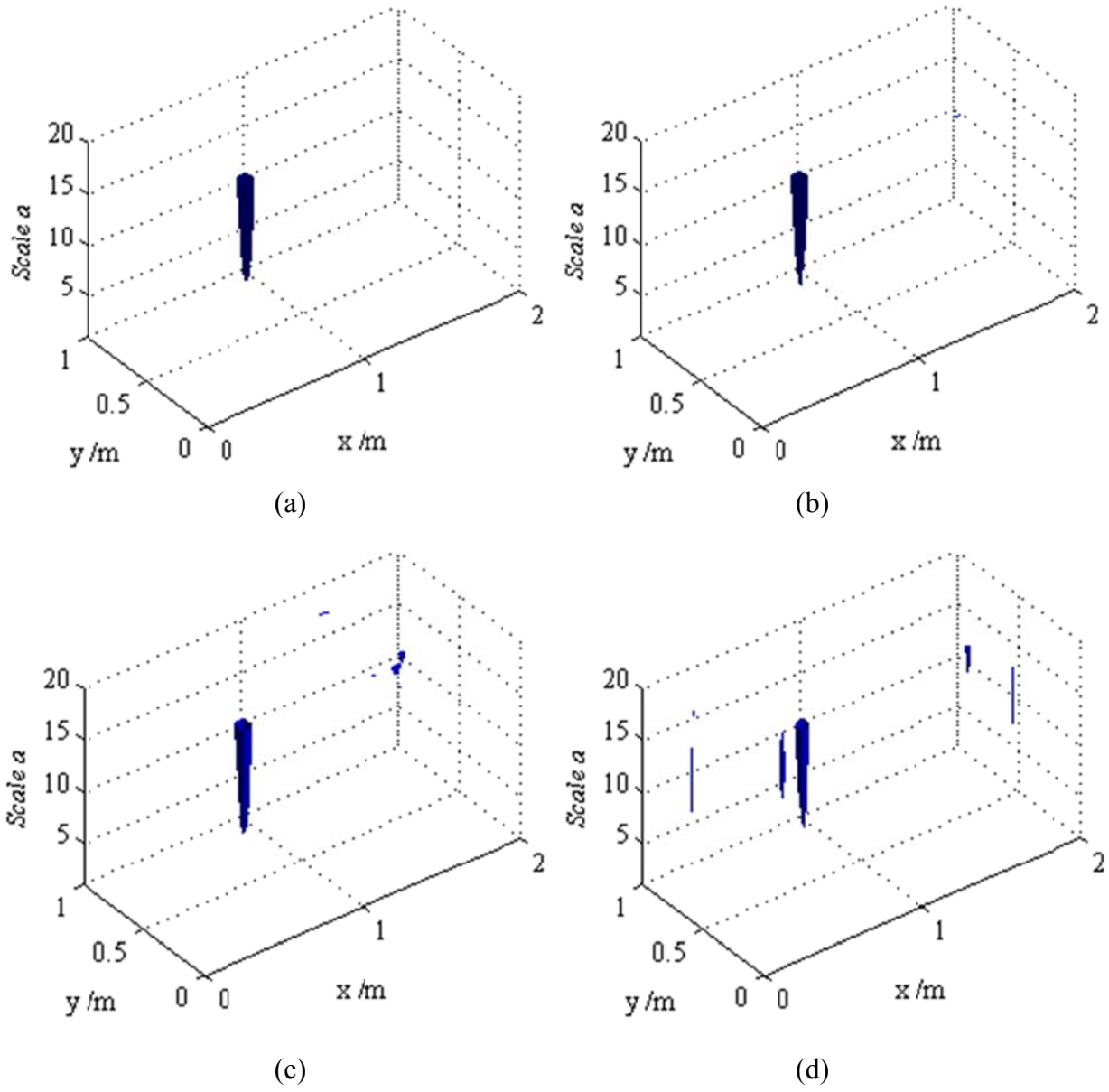

Figure 6.12 Isosurfaces of 2-D CWT using the 5th mode shape data with different noise levels

(a) $\rho = 1\times10^{-5}$**; (b)** $\rho = 5\times10^{-5}$**; (c)** $\rho = 1\times10^{-4}$**; and (d)** $\rho = 2.5\times10^{-4}$**.**

6.3.3 Effect of sensor spacing

In experimental modal analysis, the mode shapes can be only measured at a relatively small number of locations, especially for *in-situ* experiments. The sparse distribution of sensors will often pose difficulties for damage detection algorithms to effectively detect and localize the

damage. Even though the novel measurement systems, such as scanning laser vibrometer (SLV), can be adopted to obtain high-density mode shape data in laboratory-scale experiments, the robustness of the damage detection algorithms under the limited measured data points is still of interest for their practicality for *in-situ* experiment.

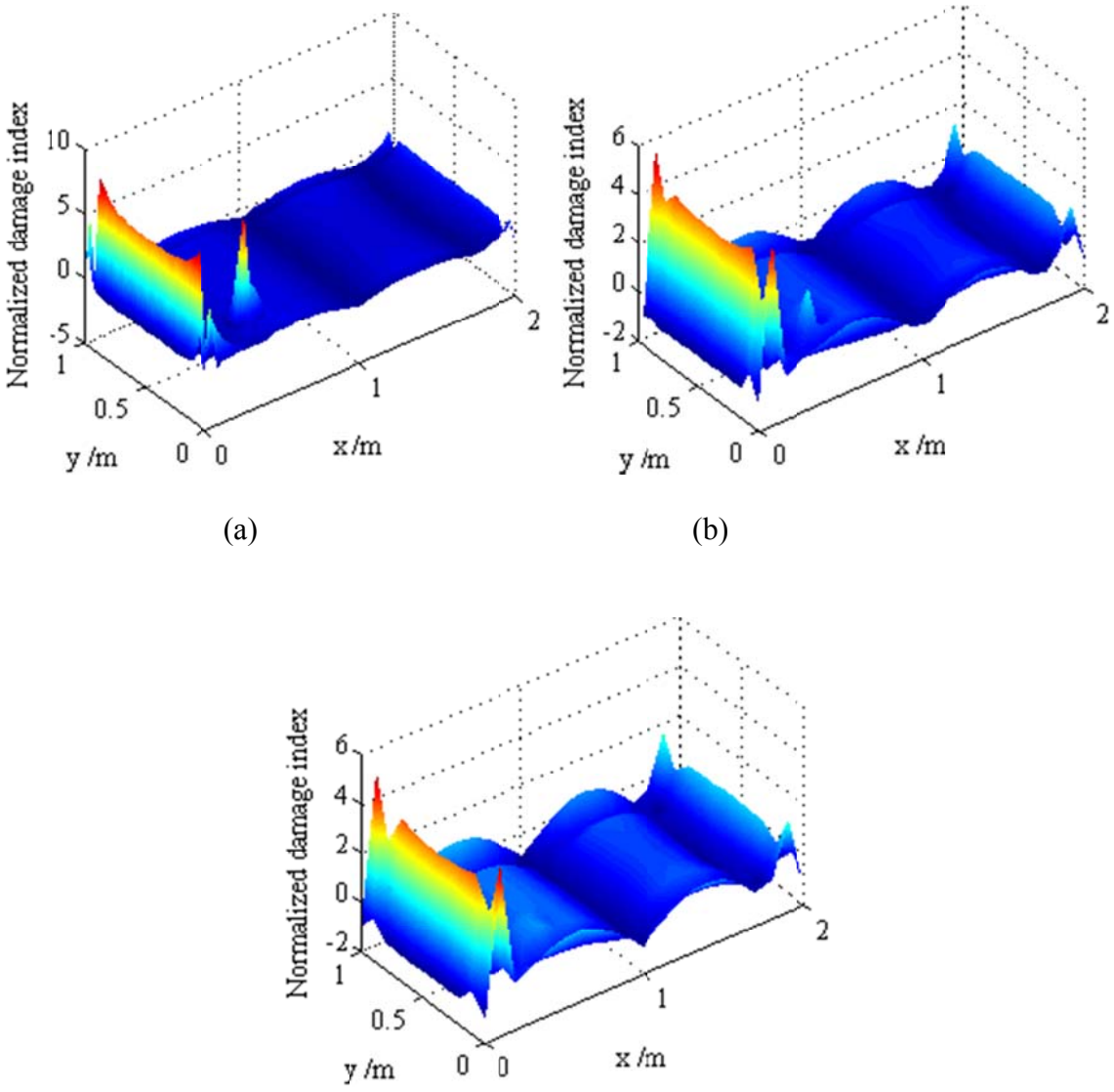

Figure 6.13 Normalized damage indices of 2-D GSM using the 5th mode shape data with different sensor spacing

(a) $s = 0.04m$ **; (b)** $s = 0.08m$ **; and (c)** $s = 0.1m$ **.**

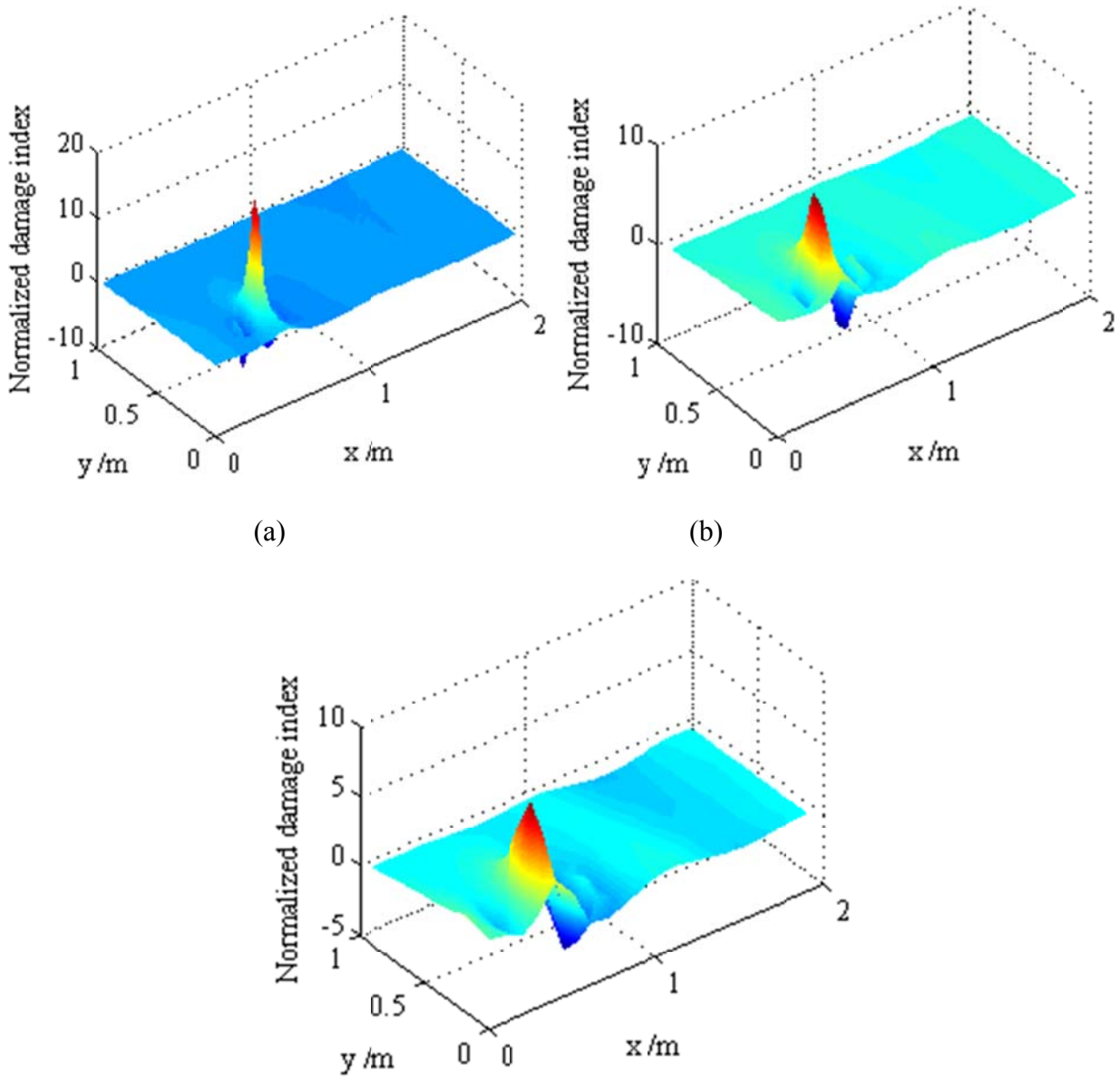

Figure 6.14 Normalized damage indices of 2-D SEM using the 5th mode shape data with different sensor spacing

(a) $s = 0.04m$ **; (b)** $s = 0.08m$ **; and (c)** $s = 0.1m$ **.**

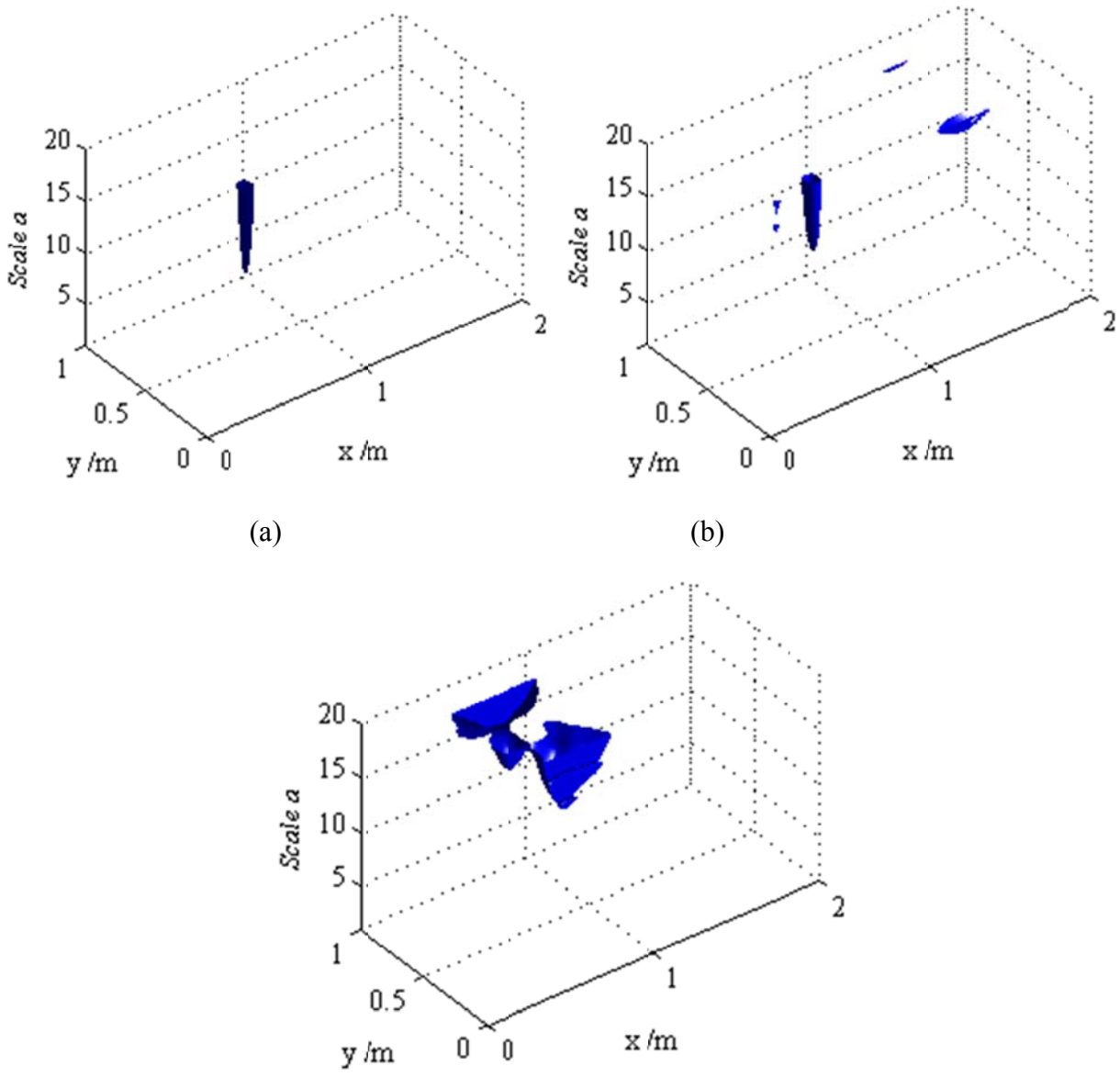

Figure 6.15 Isosurfaces of 2-D CWT using the 5th mode shape data with different sensor spacing

(a) $s = 0.04m$ **; (b)** $s = 0.08m$ **; and (c)** $s = 0.1m$ **.**

In order to evaluate the effect of different sensor spacing, the mode shape data are extracted from in the finite element model with three different intervals (s = 0.04 m, 0.08 m and 0.10 m) for the numerically simulated plate with in-plane dimensions of 1 m × 2 m. In these

three cases, the extracted mode shape data form a matrix of 51×26, 26×13, and 21×11, respectively, for s = 0.04 m, 0.08 m, and 0.10 m. Figs. 6.13~6.15 illustrate the effect of different sensor spacing. As shown in Fig. 6.13, the 2-D GSM can only correctly detect the damage when s = 0.08 m if the large boundary distortion at the clamped end is neglected. But the damage-induced singularity can barely be noticed after the noise level reaches $s = 0.10$ m. In Fig. 6.14, the 2-D SEM can correctly indicate the damage in all three sensor spacing cases. However, its ability to localize the damage gradually decreases when the sensor spacing increases. As shown in Fig. 6.15, the 2-D CWT shows its ability to detect and localize the damage before the sensor spacing reaches s = 0.08 m. But it fails to detect the damage when s = 0.10 m, similar to the case of the 2-D GSM. The results show that the robustness of the 2-D CWT damage detection algorithms under the limited measured data points is as good as the 2-D GSM, but not as good as the 2-D SEM. However, it should be noted that both the 2-D GSM and 2-D CWT are the response-based algorithms; while the 2-D SEM is a model-based algorithm, requiring a relatively accurate numerical/analytical model of the healthy structure, which is not feasible for almost all the *in-situ* structural tests.

6.4 Summary

In this chapter, a comparative study of damage detection algorithms for beam-type structures is first presented. The study is based on the finite element model to evaluate the five extensively-used 1-D damage detection algorithms. The MSC and DIM methods are more robust than the GFD method in high measurement noise and large sensor spacing condition. Although the GSM is not as robust as the MSC and DIM methods, it is still a good choice for damage detection algorithm when only the damaged state structures are available for test as in most *in-situ* experiment.

Then, a comparative study of the proposed 2-D CWT based algorithm with two other 2-D damage detection algorithms, i.e., 2-D GSM and 2-D SEM, shows that the proposed 2-D CWT-based algorithm as introduced in Chapter 5 is superior in noise immunity and robust under limited sensor data. The proposed algorithm is a response-based damage detection technique which only requires the mode shapes of the plate after damage. Therefore, the proposed 2-D CWT-based algorithm is more advantageous in laboratory or *in-situ* damage detection experiment, and it can be used in damage identification of bridge deck structures.

CHAPTER 7

DAMAGE SEVERITY CORRECTION FACTOR-BASED DAMAGE IDENTIFICATION METHOD FOR PLATE-TYPE STRUCTURES

7.1 Introduction

A reliable and effective non-destructive damage identification method is crucial to maintain the safety and integrity of structures. The most common non-destructive damage identification techniques are visual inspection and conventional nondestructive testing (NDT). However, the visual inspection techniques are unable to detect damage which is embedded in a structure or invisible to human eyes; while the conventional nondestructive testing (NDT) have their limitations in which the vicinity of damage must be known *a priori* and readily accessible for testing. Hence, worldwide research efforts have been focused on vibration response-based damage identification method to overcome these difficulties. The basic idea for vibration response-based damage detection is that the damage-induced changes in the physical properties (mass, damping, stiffness, etc.) will cause detectable changes in modal properties (natural frequencies, modal damping, mode shapes, etc.) (Doebling et al. 1996). Therefore, it is intuitive that damage can be identified by analyzing the changes in vibration features of the structure.

In order to find effective and accurate damage identification methods, extensive research effort has focused on damage identification methods utilizing mode shapes, frequencies or modal parameters derived from mode shapes and frequencies, such as modal strain energy, modal flexibility and uniform load surface. As discussed in the literature review (see Chapter 2), most of the popular damage identification methods are initially developed in the context of one-dimensional (1-D) beam-type structures, such as the modal curvature-based Mode Shape Curvature method (Pandey et al. 1991), Gapped Smoothing Method (Ratcliffe 1997), modal

strain energy-based Damage Index Method (Stubbs et al. 1995) and modal compliance-based Modal Compliance Method (Choi et al. 2005). Even though many methods have been developed, no single method is completely effective in all situations. A comparative study by Farrar and Jauregui (1996) based on experimental data showed that the strain energy-based damage index performed best among some popular existing damage identification methods.

Modal strain energy-based method is a widely used category of damage identification methods. These methods use the fractional modal strain energy change for damage detection. For beam-type or plate-type structures, the modal strain energy can be directly related to (and are usually derived from) the strain mode shape. Stubbs et al. (Stubbs and Kim 1996; Stubbs et al. 1995) developed a damage index (DI) method based on the modal strain energy. This method assumes that if the damage is primarily located at a single sub-region, then the fractional strain energy will remain relatively constant in sub-regions. For beam-type structures, the bending stiffness EI is assumed to be essentially constant over the length of the beam for both the undamaged and damaged modes. Shi and Law (Shi and Law 1998; Shi et al. 2000b) presented a damage localization method for beam, truss or frame type structures based on the modal strain energy change. The Modal Strain Energy Change (MSEC) at the element level is suggested as an indicator for damage localization. Law et al. (1998) applied this strain energy method to detect the damage location in a structure with incomplete and noisy measured modal data. The method consists of three stages: expansion of the measured mode shapes, localization of the damage domain using the elemental energy quotient difference, and damage quantification based on sensitivity of the modal frequency.

There have been very limited theoretical studies on the damage identification method for two-dimensional (2-D) plate-type structures, suitable for bridge deck type applications. Also,

most of the damage identification methods for plates mainly focus on detecting damage location. Either they cannot quantify damage severity or rely heavily on numerical model for quantification. Cawley and Adams (1979) were probably the first to locate the defects within a rectangular plate using the natural frequency changes only. Dos Santos et al. (2000) used the natural frequencies and mode shapes to locate and quantify the damage within a laminated rectangular plate. Ge and Lui (2005) recently proposed a damage identification method capable of identifying the location and computing the severity of the damage. The method made use of the stiffness and mass properties of undamaged structures and the eigenvalues and eigenvectors of damaged structures to locate and quantify the damage. It should be noted that the above mentioned methods (Cawley and Adams 1979; dos Santos et al. 2000; Ge and Lui 2005) are all the numerical FEM model-based.

Some viable damage identification methods for beams have been also successfully extended from 1-D to 2-D algorithms for damage detection of plates, but these methods are not able to quantify damage. Yoon et al. (2005) generalized the 1-D GSM by Ratcliffe (1997) to 2-D plate-like structural applications. Hadjileontiadis and Douka (2007) extended the fractal dimension-based crack detection algorithm (Hadjileontiadis et al. 2005) to 2-D for detecting cracks in plate structures. Cornwell et al. (1999) generalized the strain energy-based damage index (DI) method for 1-D beam-type structure by Stubbs (1995) into 2-D plate-type structures.

The objective of this chapter is to propose a modal strain energy-based damage severity correction factor method for damage identification of plate-type of structures. The proposed method can be easily implemented in experimental testing and used to locate and quantify damage. The method is a response-based one; thus, it does not require a numerical model of the structure. This method requires that the modal frequencies and curvature mode shapes before

and after damage be known, but the normalized mode shape are not required. The rest of this chpateris organized as follows. The theoretical background of the proposed damage correction factor method is presented in Section 7.2. The application of the proposed method is thoroughly examined and discussed based on a numerical plate model in Section 7.3. The effectiveness and applicability of the damage detection method is validated in Section 7.4 via an experimental program on an FRP sandwich bridge panel using a smart piezoelectric sensor network. Finally, the concluding remarks are given in Section 7.5.

7.2 Theory

7.2.1 Free vibration of healthy and damaged structure

The equation of motion for free vibration of an undamped structural dynamic system leads to the following eigenvalue problem:

$$(K - \lambda_i M)\phi_i = 0 \tag{7-1}$$

where K is the stiffness matrix; M is the mass matrix; λ_i is the eigenvalue of the ith mode, $\lambda_i = (2\pi f_i)^2$; f_i is the modal frequency of the system; and ϕ_i is the vibration mode shape vector of the ith mode. Note that both K and M are symmetric matrices.

Structural damage, such as cracks, delamination and barely visible impact damage (BVID), usually cause a loss in stiffness but not a loss in mass. The change of structural stiffness matrix ΔK introduced by structural damage can be modeled by a proportional damage model, i.e., ΔK can be expressed as a function of the undamaged element stiffness by the equation

$$\Delta K = -\sum_{j=1}^{n} \alpha_j K_j \tag{7-2}$$

where n is the total element number; K_j is the stiffness matrix of the jth element; α_j is the damage severity of the jth element. The damage severity is defined as the fractional change in elemental stiffness ($\alpha_j = 0$ for healthy element).

Assuming the mass loss is negligible, the eigenvalue problem of a damaged structure can be expressed as

$$[(K + \Delta K) - (\lambda_i + \Delta\lambda_i)M](\phi_i + \Delta\phi_i) = 0 \tag{7-3}$$

Expanding equation (7-3) and premultiplying ϕ_i^T leads to

$$\phi_i^T (K - \lambda_i M + \Delta K - \Delta\lambda_i M)(\phi_i + \Delta\phi_i) = 0 \tag{7-4}$$

Note that $\phi_i^T (K - \lambda_i M)$ equals to zero by taking transpose of euation (7-1). Equation (7-4) can be simplified to

$$\phi^T (\Delta K - \Delta\lambda M)(\phi + \Delta\phi) = 0 \tag{7-5}$$

Expanding equation (7-5) and using equation (7-1), we have

$$\phi_i^T \Delta K \phi_i - \frac{\Delta\lambda_i}{\lambda_i}\phi_i^T K \phi_i + \phi_i^T \Delta K \Delta\phi_i - \frac{\Delta\lambda_i}{\lambda_i}\phi_i^T K \Delta\phi_i = 0 \tag{7-6}$$

7.2.2 Modal strain energy

For a plate-type structure, the elemental modal potential energy can be expressed by the elemental modal strain energy. The potential energy of jth element in the ith mode of the healthy plate can be expressed as

$$\phi_i^T K_j \phi_i = U_{ij} = \frac{1}{2}\int\int_{A_j} k_j[(\kappa_{xx,i}{}^2 + \kappa_{yy,i}{}^2 + 2\nu\kappa_{xx,i}\kappa_{yy,i} + 2(1-\nu)\kappa_{xy,i}{}^2)]dxdy = k_j\gamma_{ij} = k\gamma_{ij} \tag{7-7}$$

where $k_j = (EI)_j$ is the bending stiffness of the jth element in the healthy plate, which is a constant k over the plate; and γ_{ij} is defined as

$$\gamma_{ij} = \int\int_{A_j} [(\kappa_{xxi}{}^2 + \kappa_{yyi}{}^2 + 2\nu\kappa_{xxi}\kappa_{yyi} + 2(1-\nu)\kappa_{xyi}{}^2)]dxdy \tag{7-8}$$

where the curvature mode shape $\kappa_{xx}, \kappa_{yy}, \kappa_{xy}$ can be derived from the displacement mode shape data using the finite difference approximation, or they can be directly measured as the strain mode shape using piezoelectric sensors such as PZT and PVDF. Deriving the curvature mode shape from the displacement mode shape data using the finite difference approximation may introduce considerable processing error. Therefore, using the directly measured strain mode shape data is advantageous (Fan and Qiao 2011).

Combining equations (7-2) and (7-7), we have

$$\phi_i^T \Delta K \phi_i = -\sum_{j=1}^{n} \alpha_j \phi_i^T K_j \phi_i = -k\sum_{j=1}^{n} \alpha_j \gamma_{ij} \tag{7-9}$$

Similarly, the total potential energy of all elements in the *i*th mode of healthy plate is

$$\phi_i^T K \phi_i = U_i = \frac{1}{2}\int\int_{A} k[(\kappa_{xxi}{}^2 + \kappa_{yyi}{}^2 + 2\nu\kappa_{xxi}\kappa_{yyi} + 2(1-\nu)\kappa_{xyi}{}^2)]dxdy = k\gamma_i \tag{7-10}$$

where γ_i is defined as

$$\gamma_i = \sum_{j=1}^{n} \gamma_{ij} = \int\int_{A} [(\kappa_{xxi}{}^2 + \kappa_{yyi}{}^2 + 2\nu\kappa_{xxi}\kappa_{yyi} + 2(1-\nu)\kappa_{xyi}{}^2)]dxdy \tag{7-11}$$

The potential energy of *j*th element in the *i*th mode of the damaged plate can be expressed as

$$(\phi_i^T + \Delta\phi_i^T)(K_j + \Delta K_j)(\phi_i + \Delta\phi_i) = k_j{}^* \gamma_{ij}{}^* = (1-\alpha_j)k\gamma_{ij}{}^* \tag{7-12}$$

where the superscript * denotes the damaged state.

Neglecting the high-order terms of $\Delta\phi_i$ in equation (7-12) and using equations (7-2), (7-7) and (7-9), we have

$$(1-\alpha_j)k\gamma_{ij}^{*} = \phi_i^T K_j \phi_i + 2\phi_i^T K_j \Delta\phi_i + \phi_i^T \Delta K_j \phi_i + 2\phi_i^T \Delta K_j \Delta\phi_i$$
$$= (1-\alpha_j)k\gamma_{ij} + 2(1-\alpha_j)\phi_i^T K_j \Delta\phi_i \tag{7-13}$$

So we can derive

$$\phi_i^T K_j \Delta\phi_i = k(\gamma_{ij}^{*} - \gamma_{ij})/2 \tag{7-14}$$

It can be further derived from equation (7-14) that

$$\phi_i^T \Delta K \Delta\phi_i = -k\sum_{j=1}^{n} \alpha_j (\gamma_{ij}^{*} - \gamma_{ij})/2 \tag{7-15}$$

$$\phi_i^T K \Delta\phi_i = \frac{k}{2}(\gamma_i^{*} - \gamma_i) \tag{7-16}$$

7.2.3 Damage severity correction factor

Consider a plate with a small damage severity, in which all the high order terms in equation (7-6) are negligible. In this case, equation (7-6) can be rewritten as

$$\phi_i^T \Delta K \phi_i - \frac{\Delta\lambda_i}{\lambda_i}\phi_i^T K \phi_i = 0 \tag{7-17}$$

Substituting equations (7-9) and (7-10) into equation (7-17), we obtain

$$\sum_{j=1}^{n} \frac{\gamma_{ij}}{\gamma_i}\alpha_j = -\frac{\Delta\lambda_i}{\lambda_i} \tag{7-18}$$

In equation (7-18), $\frac{\Delta\lambda_i}{\lambda_i}$ is the *i*th modal eigenvalue change ratio, which reflects the global effect of damage on the *i*th mode. $\frac{\gamma_{ij}}{\gamma_i}$ is defined as the damage location factor (DLF), which reflects the sensitivity of the *i*th vibration mode to the damage at the *j*th element. DLF is an important factor for damage localization and damage quantification. In the case of a small damage severity,

it can be seen from equation (7-18) that the modal eigenvalue change ratio is a linear function of damage severity α_j for a given mode and damage location.

Consider a plate with a moderate/large damage severity, in which the high order terms in equation (7-6) are not negligible. Substituting equations (7-9), (7-10), (7-15), (7-16) into equation (7-6) and simplifying the equation, we obtain

$$\sum_{j=1}^{n} \left(\frac{\gamma_{ij}^{*} / \gamma_{ij} + 1}{\gamma_i^{*} / \gamma_i + 1} \right) \frac{\gamma_{ij}}{\gamma_i} \alpha_j = -\frac{\Delta \lambda_i}{\lambda_i} \tag{7-19}$$

In the case of a moderate damage severity, it can be seen from equation (7-19) that the modal eigenvalue change ratio is a nonlinear function of damage severity α_j for a given damage location. Here, a Damage Severity Correction Factor (DSCF) is defined as

$$DSCF_{ij} = \frac{\gamma_{ij}^{*} / \gamma_{ij} + 1}{\gamma_i^{*} / \gamma_i + 1} \tag{7-20}$$

DSCF given in equation (7-20) represents the nonlinear effect of damage severity α_j at the *j*th element on the *i*th modal eigenvalue change ratio. It is a function of damage location and severity and can be easily calculated from the modal strain energy. In the case of a small damage, the nonlinear model equation (7-19) can be reduced to linear model as given in equation (7-18) by approximately setting $DSCF \approx 1$.

It should be noted that DSCF is related to the curvature mode shape normalization. If the curvature mode shape data from healthy and damaged state are not normalized on the same basis (e.g., mass-normalized), the value of DSCF may differ depending on the normalization. In this case, in order to keep DSCF consistent, the total modal strain energies from the healthy and damaged state are assumed to be the same. Then, the curvature mode shapes can be normalized

so that the total modal strain energy from healthy and damaged state are the same. Based on this assumption, DSCF can be approximated from the unnormalized curvature mode shape by

$$DSCF_{ij} = (\frac{\gamma_{ij}^{*}\gamma_i}{\gamma_i^{*}\gamma_{ij}} + 1)/2 \tag{7-21}$$

DSCF can be shown as a good damage location indicator and an important factor in damage quantification. In this study, a damage identification method based on DSCF was proposed for damage localization and quantification.

7.2.4 Damage identification method

The DSCF-based damage identification method consists of three steps: modes selection, damage localization, and damage quantification.

Step 1: Sensitive modes selection: selecting vibration modes for damage identification using the modal eigenvalue change ratio $\frac{\Delta\lambda_i}{\lambda_i}$.

Before applying any damage identification algorithm to modal parameters obtained in modal testing, the sensitivity of the vibration modes to the existing damage should be evaluated to ensure the effectiveness and accuracy of damage localization and damage quantification. The modal eigenvalue change ratio $\frac{\Delta\lambda_i}{\lambda_i}$ is widely adopted as a mode sensitivity indicator.

Step 2: Damage localization: locating damage using DSCF and DLF.

The strain energy-based DSCF is proposed as a good indicator for damage location. A damage index β_{ij}^{*} at the *j*th element in the *i*th mode can be defined as:

$$\beta_{ij}^{*} = \begin{cases} DSCF_{ij} & if\ DLF_{ij} > \dfrac{5}{n}\% \\ \\ 1 & if\ DLF_{ij} \le \dfrac{5}{n}\% \end{cases} \tag{7-22}$$

where n is the total element number. Since DLF_{ij} is the damage location factor which reflects the sensitivity of the ith vibration mode to the damage at the jth element, a vibration mode is insensitive to damage at an element with extremely low damage location factor in this mode. Therefore, this mode is inadequate to detect damage at this element even if the damage exists. The damage index with extremely low DLF_{ij} is directly set to 1 correspondingly to avoid the potential numerical error. In this study, the criterion for extremely low DLF_{ij} is set as 5% of the average DLF_{ij} in the ith mode.

Then, assuming that the damage indices β^{*} at different elements is a normally distributed random variable, the damage index β_{ij}^{*} can be normalized as

$$Z_{ij}^{*} = \frac{\beta_{ij}^{*} - \overline{\beta_{i}^{*}}}{\sigma_{\beta i}^{*}} \tag{7-23}$$

where $\overline{\beta}_i$ and $\sigma_{\beta i}$ represent the mean and standard deviation of the damage indices in the ith mode, respectively. A damage detection criterion can be set as the normalized damage index Z_{ij}^{*} larger than 2, to filter out small damage indices induced by measurement noise.

$$Z_{ij}^{*} = 0 \text{ if } \left| Z_{ij}^{*} \right| < 2 \tag{7-24}$$

Furthermore, in order to eliminate the false positive indication of damaged element induced by measurement error and numerical error at those elements with low strain energy. A modified damage indices β_j at the jth element can be derived from DLF_{ij} and Z_{ij}^{*}.

$$\beta_j = \sum_{i=1}^{m} Z_{ij}^{*} \times DLF_{ij} \tag{7-25}$$

Finally, a normalized damage index Z_j can be generated from β_j,

$$Z_j = \left| \frac{\beta_j - \overline{\beta}}{\sigma_\beta} \right| \tag{7-26}$$

and the same damage detection criterion can be set as in equation (7-26).

$$Z_j = 0 \text{ if } Z_j < 2 \tag{7-27}$$

Step 3: Damage quantification: quantifying damage severity using modal eigenvalue change ratio, DLF and DSCF.

Once the damaged element is detected in Step 2, DSCF can be further used to calculate damage severity. If multiple modes are available, equation (7-19) can be written in the matrix form as

$$RA = F \tag{7-28}$$

$$R = \begin{bmatrix} DLF_{11} \times DSCF_{11} & DLF_{12} \times DSCF_{12} & \ldots & DLF_{1n} \times DSCF_{1n} \\ DLF_{21} \times DSCF_{21} & DLF_{22} \times DSCF_{22} & \ldots & DLF_{2n} \times DSCF_{2n} \\ \ldots & \ldots & \ldots & \ldots \\ DLF_{m1} \times DSCF_{m1} & DLF_{m2} \times DSCF_{m2} & \ldots & DLF_{mn} \times DSCF_{mn} \end{bmatrix}, A = \begin{Bmatrix} \alpha_1 \\ \alpha_2 \\ \ldots \\ \alpha_n \end{Bmatrix}, F = \begin{Bmatrix} -\frac{\Delta\lambda_1}{\lambda_1} \\ -\frac{\Delta\lambda_2}{\lambda_2} \\ \ldots \\ -\frac{\Delta\lambda_m}{\lambda_m} \end{Bmatrix}$$

where *m* is the total number of vibration modes; *n* is the total damaged element number; DLF is the damage location factor γ_{ij} / γ_i.

For a unique solution, the number of the used vibration modes should equal to the total number of unknown parameters (elemental damage severities). However, for laboratory test or *in-situ* application, the number of accessible vibration modes which is suitable for damage

identification is very limited (typically the first few modes), usually much less than the number of unknown parameters required. Furthermore, due to the existence of measurement errors, more measured modes than unknown parameters are required to construct a system of over-determined equations to improve the accuracy of damage severities estimation. Therefore, to avoid non-uniqueness, appropriate assumptions on damage location or damage severity distribution have to be made to reduce the number of unknown parameters. For example, in damage identification with large sensor spacing, it is usually assumed that the damage only happens in a single element; in delamination identification case, it is reasonable to assume that the damage severity is the same for one delaminated area if the delamination propagates between the same layers inside a composite plate.

When the number of measured modes is larger than the total number of unknown parameters, the least square fitting method is used to obtain the best solution.

$$A = (R^T R)^{-1} R^T F \tag{7-29}$$

It should be noted that the three steps in the DSCF method are independent of each other. Each single step can be used in combination with other damage detection/quantification method for damage identification. For example, the third step of damage quantification can be used independently to estimate the damage severity based on the damage localization results from other damage detection algorithm. But it is still advantageous to follow the three steps as a whole set since the modal eigenvalue change ratio and DSCF generated in the first two steps can be directly used in Step 3.

7.3 Numerical study

7.3.1 Finite element model

An eigenvalue analysis of a rectangular plate with 600 mm in length × 288 mm in width ×0.001 mm in thickness was conducted using the commercial finite element code ABAQUS, and the model is shown in Fig. 7.1. The material is assumed to be isotropic with Young's modulus E = 20 GPa, Poisson's ratio v = 0.25 and density ρ = 2,400 kg/m3. The plate is uniformly discretized into 1,200 4-node first-order plate elements S4 of size 12 mm × 12 mm. The plate is with simply-supported boundary conditions at two edges $y = \pm 300$ mm. The damage is simulated by reducing stiffness of 16 elements in the region $48 < x < 96$ and $84 < y < 132$ with the center of the damage at $x = 72, y = 108$. Six different cases with damage severity α = 0~0.5 are simulated in the finite element analysis. The curvature mode shape data are extracted from all the 51 × 25 nodes in the model. The first five displacement mode shapes of the healthy plate are shown in Fig. 7.2. Comparison between the damaged and healthy plate shows that the displacement mode shape reveals no local features capable of directly indicating the location or area of the damage.

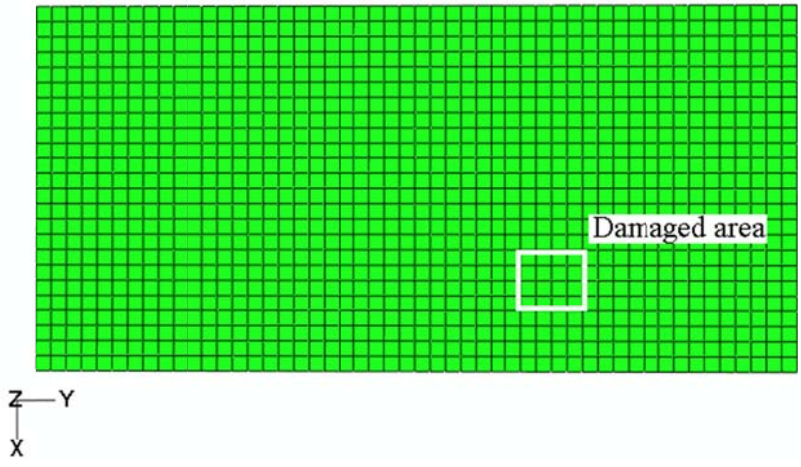

Figure 7.1 Finite element modeling of a plate with damage.

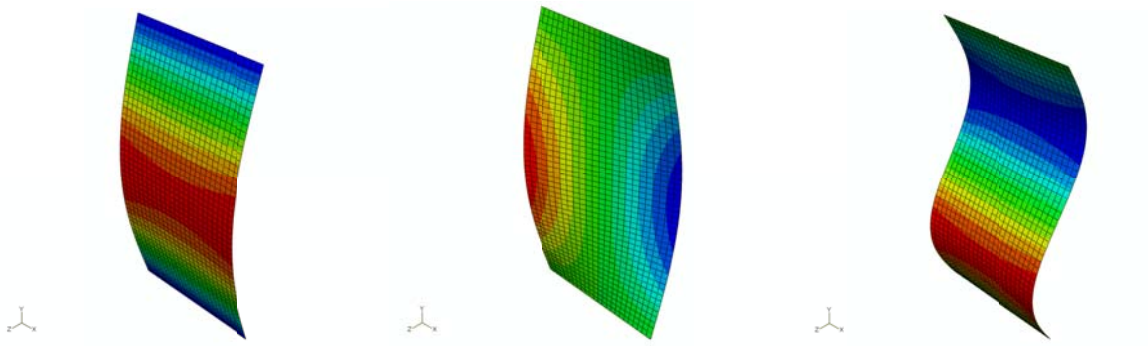

Mode 1 Mode 2 Mode 3

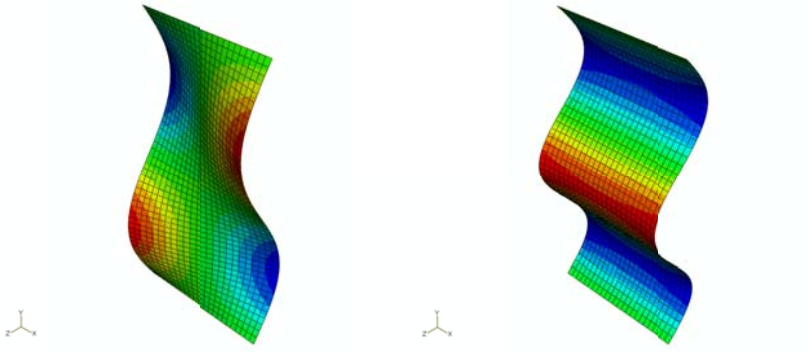

Mode 4 Mode 5

Figure 7.2 The first five mode shapes of the healthy plate.

7.3.2 Damage identification

The DSCF method is applied to the curvature mode shape generated in FEA for damage identification. The aforementioned three steps of the damage identification method are discussed based on the numerical simulation results.

In order to apply the method, the damage location factor (DLF) and damage severity correction factor (DSCF) should be derived from the curvature mode shape generated from the healthy and damaged plate. First, a bivariate cubic spline interpolation function is constructed for the curvature mode shape. The bivariate cubic spline is constructed as the tensor product of

two univariate cubic splines. It can be expressed as the weighted sum of products of two cubic spline functions:

$$f(x,y) == \sum_i \sum_j a(i,j) g_i(x) h_j(y) \tag{7-30}$$

where $g_i(x)$ and $h_j(y)$ are the cubic spline function in x and y direction, respectively. Then, using the bivariate cubic spline function, γ_{ij} and γ_{ij}^* can be calculated from equation (7-8). Finally, DLF and DSCF can be calculated from γ_{ij} and γ_{ij}^*. It should be noted that DLF can be calculated from the damage curvature mode shape data only, and it is constant for a given element and vibration mode; while DSCF requires both the healthy and damaged curvature mode shape data, and it is a nonlinear function of damage severity for a given element and vibration mode.

Mode sensitivity

First, the forward problem is investigated. Assuming the damage severity is constant over all the 16 damaged elements, the modal eigenvalue change ratio at different damage severity can be calculated using DLF and DSCF, as shown in Fig. 7.3. The linear model and the nonlinear model are used to predict the modal eigenvalue change ratio using equations (7-18) and (7-19), respectively. It can be seen from Fig. 7.3 that the linear model gives accurate prediction of all modal eigenvalue change ratios at low severity (< 10%) but has high error at moderate/high severity (> 10%). The error of the linear model increases with the increase of damage severity. The nonlinear model performs much better than the linear model in all damage severity and vibration modes, especially in the high damage severity and in the 1st and 3rd modes. It can be noticed that compared to other modes, modes 1 and 3 are more sensitive to the damage at this

specific location since they have higher modal eigenvalue change ratio at all damage severity level.

Then, the inverse problem is investigated. The modal eigenvalue change ratio, DLF and DSCF are calculated from the numerical data and then used to estimate the damage severity, assuming that the damage location is known and damage severity is constant over all the 16 damaged elements. When data from a single mode is used for damage quantification, the severity estimation results are shown in Fig. 7.4. It can be seen that the damage severity can be accurately estimated in the modes with the high eigenvalue change ratio. Significant error in damage severity estimation may be induced from the modes with the low eigenvalue change ratio. The nonlinear model performs better in damage quantification in all modes and damage severity than the linear model. Using the nonlinear model may improve the accuracy of severity estimation for those modes with the low eigenvalue change ratio.

As discussed above, using modes with the low modal eigenvalue change ratio may lead to high error in damage quantification. Therefore, it is necessary to use the modal eigenvalue change ratio as a mode sensitivity indicator to ensure the quality of damage quantification.

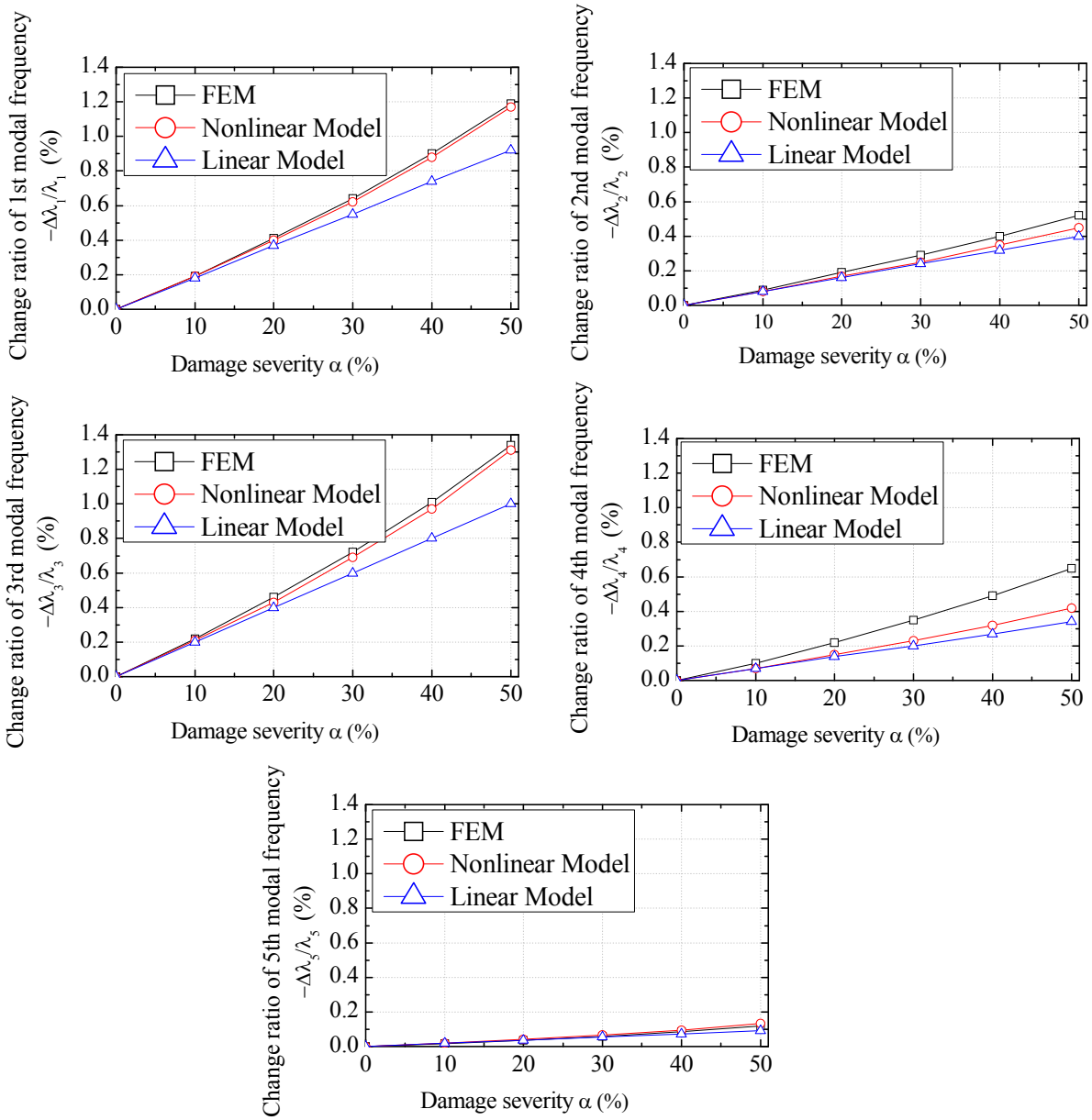

Figure 7.3 Modal eigenvalue change ratio at different damage severity.

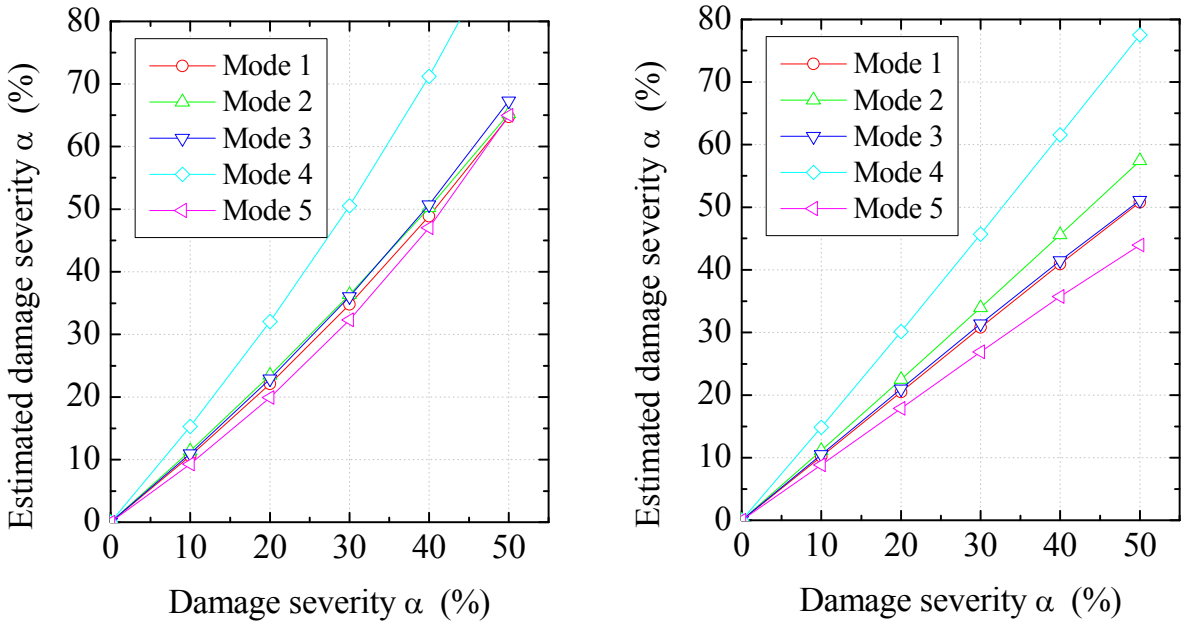

(a) Linear model (b) Nonlinear model

Figure 7.4 Estimation of damage severity with data from different vibration mode.

Damage localization

Based on the numerical simulation data, the DSCF-based damage index *Z* distribution over the plate was investigated as an attempt to locate damage. The strain energy-based Damage Index (DI) method (Cornwell et al. 1999) is also applied to the same set of data for comparison.

First, the curvature mode shape data from mode 1~5 are used for damage localization. The simulated data from plate with damage severity $\alpha = 0.5$ are adopted. The results are show in Fig. 7.5. Both the DI and DSCF methods can correctly approximate the location of the damage. The DI method gives three false positive and three false negative indications of elements, while the DSCF method gives three false positive and four false negative indications of elements.

Then, the curvature mode shape data from modes with the high eigenvalue change ratio, i.e., mode 1 and mode 3, are used. The simulated data from plate with damage severity $\alpha = 0.1$

are adopted. The results are shown in Fig. 7.6. It can be seen that both the results from the DI and DSCF methods are improved by using the sensitive mode only. Both the methods give two false positive and three false negative indications of elements. Therefore, it further manifests that the modal eigenvalue change ratio can be used as a mode sensitivity indicator to ensure the quality of damage localization.

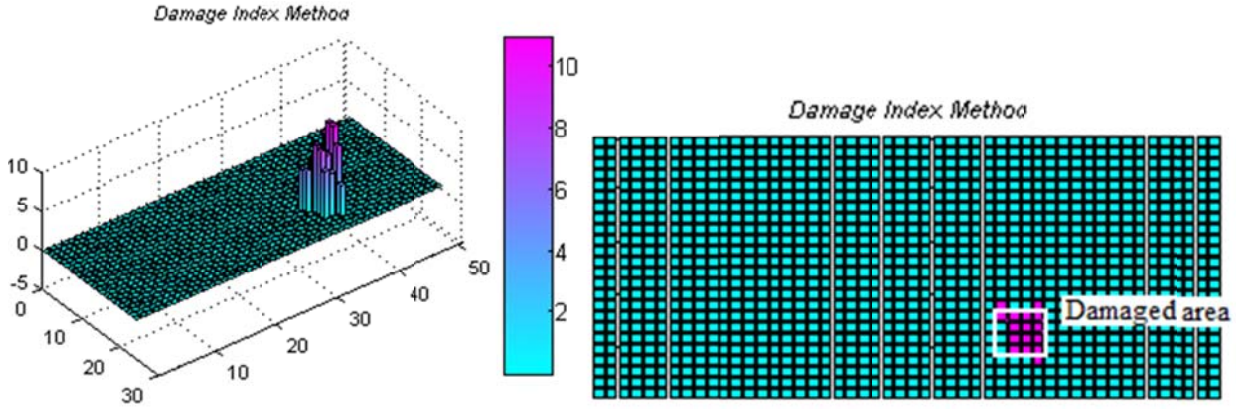

(a)

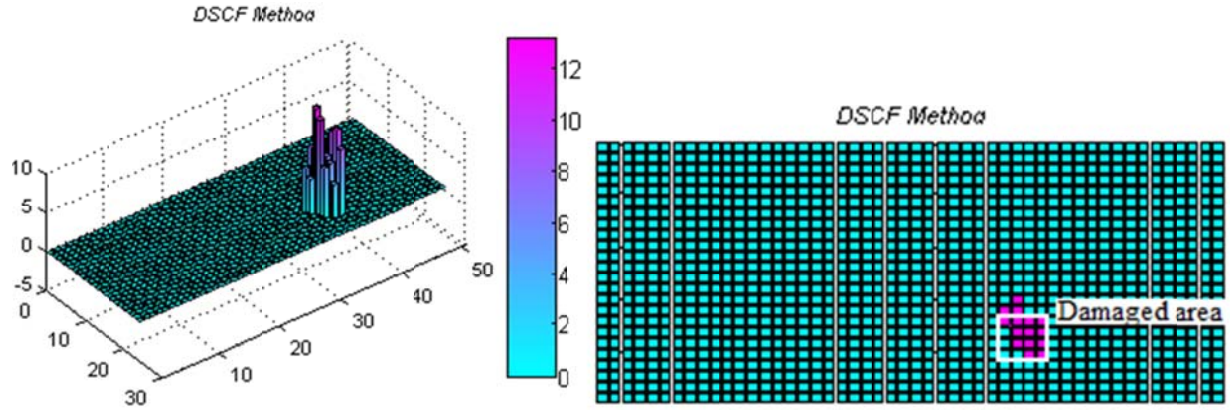

(b)

Figure 7.5 Normalized damage index using 1st~5th modes for (a) DI method and (b) DSCF method.

It can also be noticed that the normalized damage index from the DI and DSCF methods shows close agreement with each other. Further investigation shows that the normalized damage index from the DI method, DSCF method, and Modal Strain Energy Change (MSEC) method are the same when the data from only one mode are used. This is because they are all the strain

energy-based method. For a given plate, their damage indices are essentially a linear function of the elemental strain energy of the damaged plate.

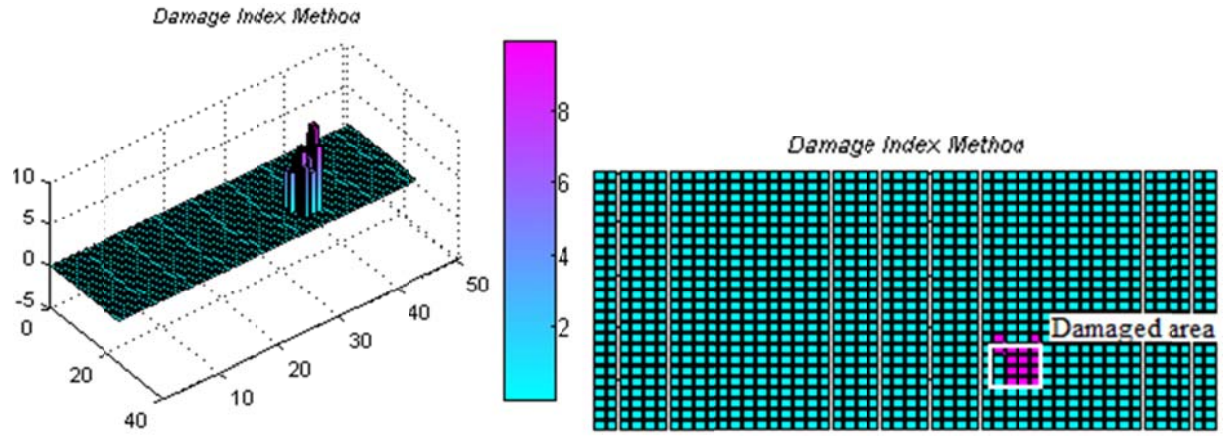

(a)

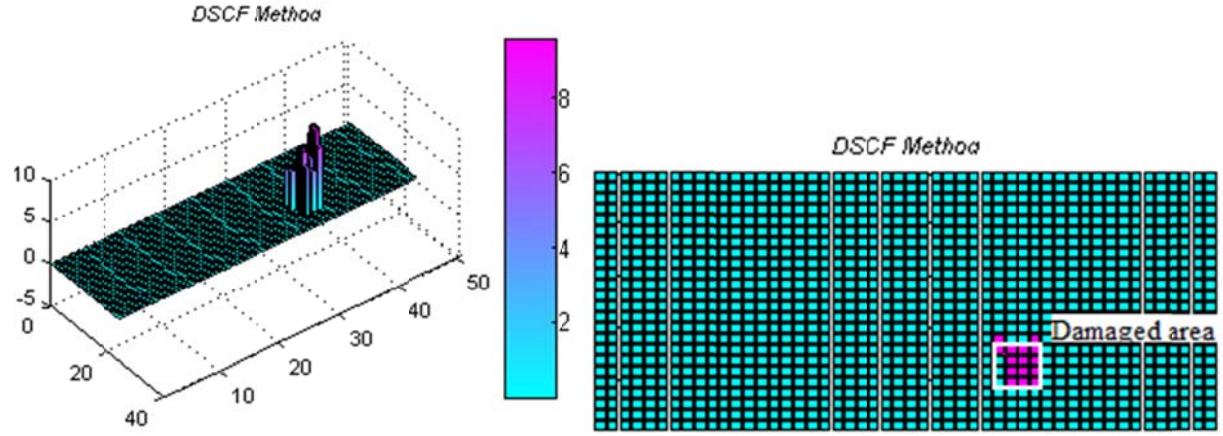

(b)

Figure 7.6 Normalized damage index using 1st and 3rd modes for (a) DI method and (b) DSCF method.

Damage quantification

After damage location is identified, the third step of the DSCF damage identification method can be applied to the numerical data for damage quantification. In order to examine the accuracy of the damage quantification, it is assumed that the damage localization step correctly identified all the 16 damaged elements and damage severity is constant for all damaged elements.

The damage quantification results of DSCF method are presented in Fig. 7.7. The results using 1^{st}~5^{th} mode based on the linear and nonlinear models are shown in Fig. 7.7 for comparison. It is obvious that the linear model gives acceptable damage severity estimation at low severity range (<10%) but has poor performance in higher severity range (>10%). While the nonlinear model performs better than the linear model and gives accurate estimation over all range. This is consistent with the results from the single mode.

The results based on all 1^{st}~5^{th} modes and the ones based on the sensitive modes only (1^{st} and 3^{rd} mode) are also compared in Fig. 7.7. It is shown that including the modes with the low eigenvalue change ratio may slightly deteriorate the quality of damage quantification. Therefore, using the sensitive modes only can further improve the accuracy of damage quantification.

In conclusion, the nonlinear model and sensitive modes should be used in the DSCF damage method to ensure the quality of damage quantification.

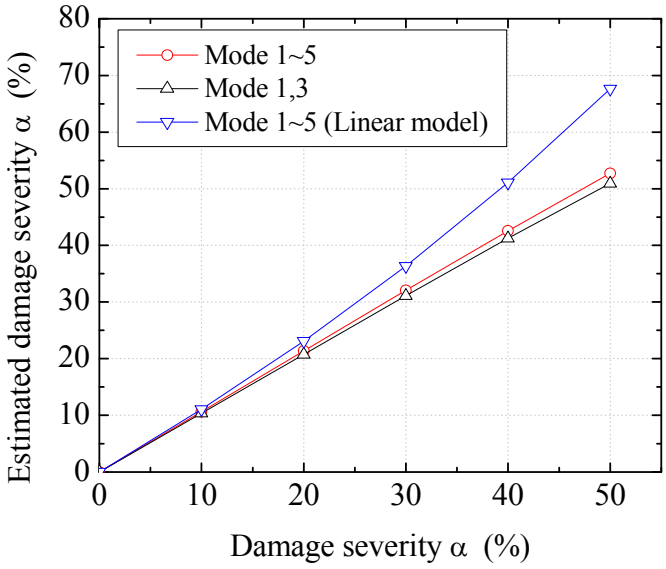

Figure 7.7 Damage quantification results comparison.

7.3.3 Effect of measurement noise

In experimental modal testing, measurement noises are inevitable. To evaluate the robustness of a damage identification method, it is essential to investigate its noise immunity performance. In order to simulate the effect of measurement noise, a series of normally distributed random numbers are added to the numerical mode shapes to generate the noise-contaminated mode shapes. The new curvature mode shape data can be expressed as:

$$\kappa'(x,y) = \kappa(x,y) + \rho \cdot r \cdot \kappa_{rms} \tag{7-31}$$

where κ' and κ are the curvature mode shapes with and without noise, respectively; r is the normally distributed random variables with a mean equal to zero and a variance equal to 1; ρ is the random noise level; and κ_{rms} is the root-mean-square of the curvature mode shape.

Based on the 1st and 3rd mode shape data with artificially-induced noise, the effect of measurement noise on damage localization and damage quantification was investigated separately.

An example of damage localization of plate with damage severity $\alpha = 0.3$ and noise level $\rho = 0.3$ is shown in Fig. 7.8. The damage localization results at various severity and noise levels are shown in Table 7.1. When $\alpha = 0.1$ and $\rho = 0.3$, the damage localization results are still able to detect the damage but fail to approximate the area of the damage. In all the other cases listed, the damage area can be approximated with some false positive/negative element indications.

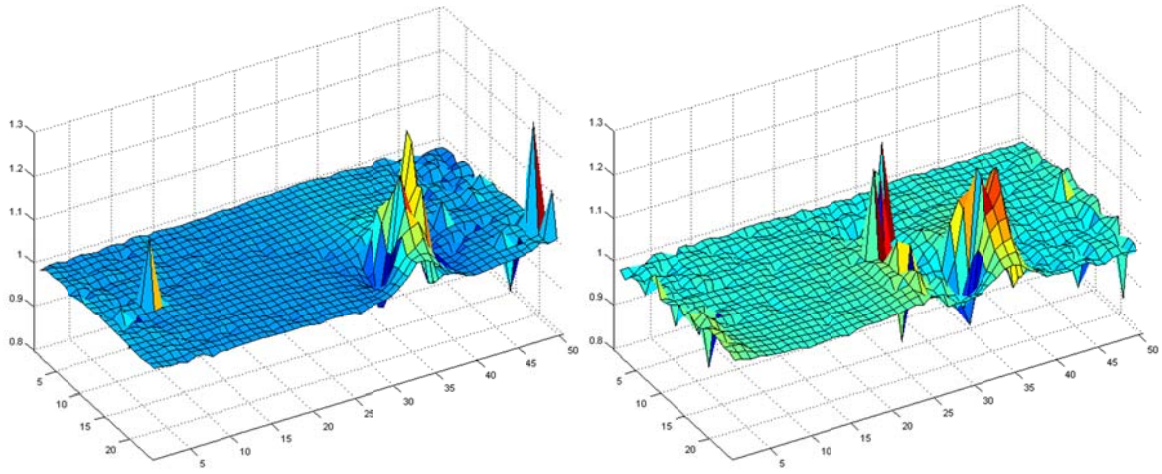

(a) DSCF in 1st Mode (b) DSCF in 3rd Mode

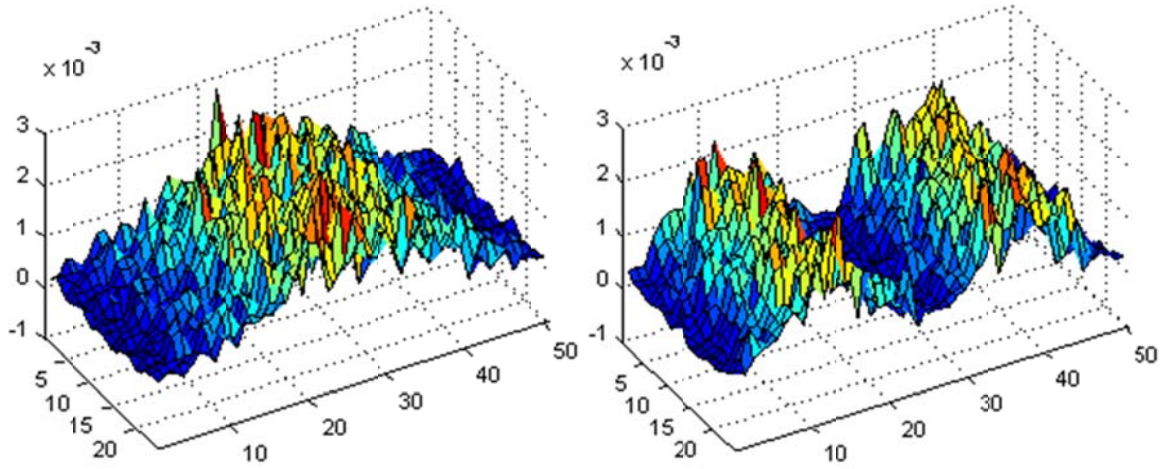

(c) DLF in 1st Mode (d) DLF in 3rd Mode

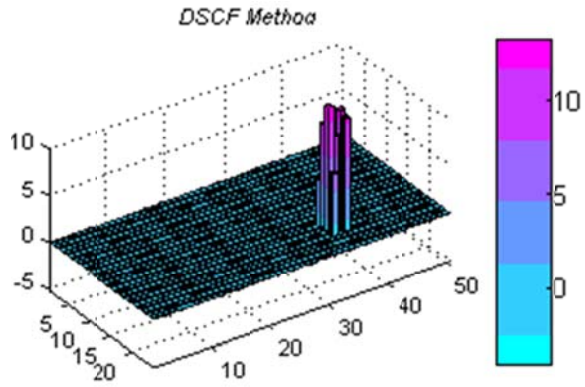

(e) Damage index Z_j from DSCF method

Figure 7.8 Damage localization under measurement noise (damage severity $\alpha = 0.3$, noise level $\rho = 0.3$).

Table 7.1 Damage localization results at different noise level

Damage severity	False indication	Noise level			
		$\rho = 0$	$\rho = 0.1$	$\rho = 0.2$	$\rho = 0.3$
$\alpha = 0.1$	False positive	2	8	0	0
	False negative	4	4	9	15
$\alpha = 0.2$	False positive	2	8	0	5
	False negative	4	4	8	4
$\alpha = 0.3$	False positive	3	2	2	2
	False negative	4	4	5	4
$\alpha = 0.4$	False positive	3	3	3	0
	False negative	3	5	5	5
$\alpha = 0.5$	False positive	2	3	2	1
	False negative	3	5	5	4

Then, assuming the damage location and area is correctly identified, the damage quantification was investigated based on the curvature mode shape data with different levels of noise. It is shown in Fig. 7.9 that the DSCF-based damage quantification algorithm gives error within 20% up to noise level $\rho = 0.3$.

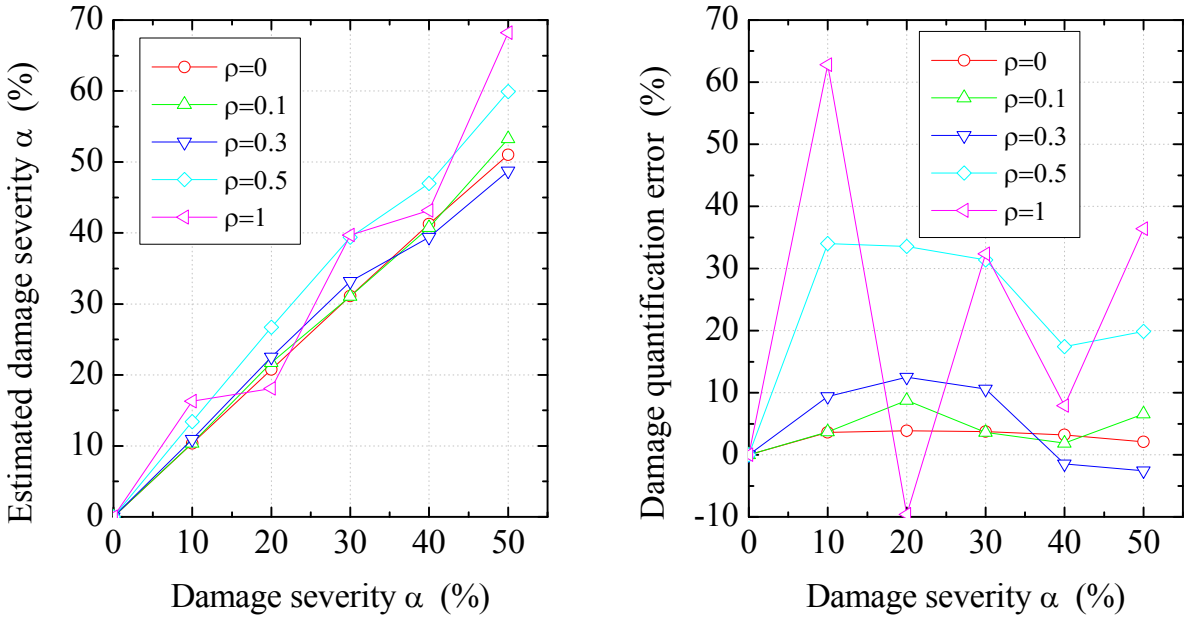

(a) (b)

Figure 7.9 Damage quantification at different noise levels.

7.3.4 DSCF using partial strain energy

The elemental modal strain energy of a plate can be derived from the curvature mode shape κ_{xx}, κ_{yy} and κ_{xy}. Obtaining the curvature mode shape from the directly measured strain mode shape using the piezoelectric sensors such as PZT and PVDF is more accurate than deriving it from the displacement mode shape data using the finite difference approximation, due to the potential high error of finite difference approximation induced by measurement error. However, one PVDF or PZT sensor can only be used to measure the strain response in one direction at a time. Therefore, a sensor array positioned in one direction can only capture the strain/curvature mode shape in that direction at a time. Hence, there is a need to explore the possibility of damage identification using the partial modal strain energy from the modal strain/curvature mode shape in one direction.

The partial modal strain energy in *y* direction can be derived from equation (7-8) by setting $\kappa_{xx} = \kappa_{xy} = 0$.

$$\gamma_{ij}^{y} = \int\int_{A_j} \kappa_{yyi}{}^2 dxdy \tag{7-32}$$

The DSCF-based damage localization results using the 1st and 3rd mode partial strain energy in the *y*-direction are listed in Table 7.2. The same set of curvature mode shape data with the artificially-induced noise as used in Section 5.3.3 is adopted here. The results from the full strain energy are listed in parentheses for comparison. It is shown that using the partial strain energy in the *y*-direction gives similar (sometimes even better) indications of damaged elements as using the full strain energy.

Table 7.2 Damage localization using partial strain energy at different noise level

Damage severity	False indication	Noise level			
		$\rho = 0$	$\rho = 0.1$	$\rho = 0.2$	$\rho = 0.3$
$\alpha = 0.1$	False positive	3 (2)	7 (8)	0 (0)	0 (0)
	False negative	4 (4)	4 (4)	10 (9)	15 (15)
$\alpha = 0.2$	False positive	3 (2)	7 (8)	0 (0)	3 (5)
	False negative	4 (4)	4 (4)	8 (8)	4 (4)
$\alpha = 0.3$	False positive	3 (3)	3 (2)	2 (2)	3 (2)
	False negative	4 (4)	5 (4)	4 (5)	5 (5)
$\alpha = 0.4$	False positive	3 (3)	3 (3)	3 (3)	0 (0)
	False negative	3 (3)	4 (5)	5 (5)	5 (5)
$\alpha = 0.5$	False positive	2 (2)	3 (3)	2 (2)	1 (1)
	False negative	3 (3)	5 (5)	5 (5)	4 (4)

The DSCF-based damage quantification using the partial modal strain energy in *y* direction and full strain energy are compared in Fig. 7.9. It is shown that if a single mode is used, the partial modal strain energy gives better estimation for mode 1, 3 and 5. But the partial modal strain energy is inadequate to give acceptable estimation for modes 2 and 4.

Further investigation shows that modes 1, 3 and 5 are pure bending modes in the *y*-direction, thus the *y*-direction curvature and corresponding strain energy dominate in this mode. Therefore, using the partial strain energy may perform as well as (or even better than) using the full strain energy. However, modes 2 and 4 are torsion mode, in which using the partial strain energy in *y* direction may deteriorate the results. Hence, using the partial strain energy in dominant direction of a pure bending mode not only makes the experimental testing easier but also may improve the quality of damage localization and quantification. However, it should also be noted that the damage quantification using the partial strain energy in dominant direction will only indicate the bending stiffness loss in this particular direction.

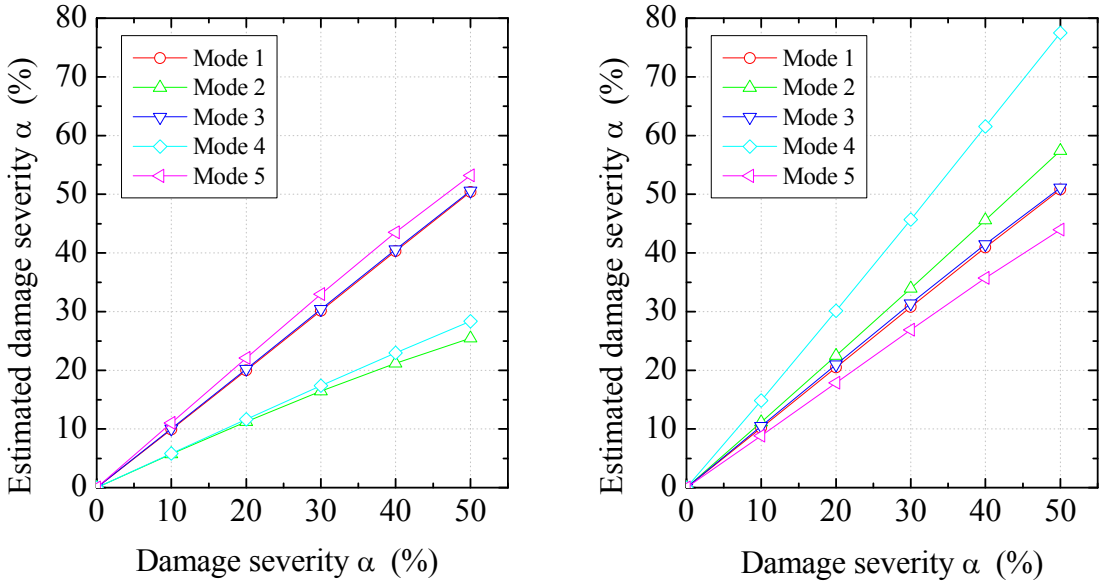

(a) Partial modal strain energy in y direction (b) Full modal strain energy

Figure 7.10 Estimation of damage severity with data from different vibration mode.

7.4 Summary

A DSCF-based damage identification method for plate-type structures is presented. The proposed damage location factor matrix DLF and damage severity correction factor matrix DSCF can be generated from the curvature mode shape of a plate. The damage identification method using DSCF and DLF are presented for damage localization and quantification. It consists of three steps: sensitive mode selection, damage localization, and damage quantification. The proposed method is a response-based damage identification technique which requires the modal frequencies and curvature mode shapes before and after damage.

The viability of this method is demonstrated by the numerical investigation. The numerical study shows that the method can correctly detect the damage, approximate the damage area and quantify the damage severity up to noise level $\rho = 0.2$ at low damage severity. It is also shown that using the partial strain energy in dominant direction of a pure bending mode may not only make experimental testing easier but also improve the quality of damage localization and quantification. This chapter paves some foundation for the application of DSCF-based damage identification algorithm for plate-type structures, as demonstrated in the next chapter for damage identification (both damage localization and quantification) of an as-manufactured FRP sandwich deck panel.

CHAPTER 8

DAMAGE IDENTIFICATION OF FRP SANDWICH DECK PANELS

8.1 Introduction

FRP composites have gained popularity in high-performance products which require being lightweight yet strong and taking harsh environmental condition. Wide applications of FRP composites have been found in civil, mechanical and aerospace engineering. Recently, GFRP composite sandwich beams/panels have also been used in highway bridge deck construction. However, FRP sandwich deck structures are susceptible to defects, such as manufacture imperfection, delamination, core crushing, debonding between face sheets and core, etc. These defects can be originated from imperfections in the manufacturing process or developed during service life. Damage resulting in system defects can occur during service life from impact of wheel loads to the structures (e.g., heavy service loads or fatigue), or due to environment-induced effects (e.g., temperature and moisture) in the FRP decks. These defects can significantly reduce structural strength and may grow to failure. Accordingly, reliable and accurate SHM techniques are an important proactive and cost effective way to prevent a catastrophic failure, which often leads to tragic consequences. As a core technique to SHM, an effective and reliable damage identification method is crucial to ensure safety and enhance structural life.

In this chapter, a structural health monitoring strategy using the proposed dynamic response-based damage identification methods introduced in the previous chapters (Chapters 5 and 7) is presented for damage identification of an as-manufactured honeycomb FRP sandwich deck panel. A preliminary investigation showed that (1) for the vibration-based damage identification method, the modal parameters such as modal frequencies and mode shapes can be

easily obtained using the modal testing technique; (2) for the wave-based damage identification method, the Lamb wave dissipates quickly on face sheet of sandwich panel due to the existence of the "soft" honeycomb (in this case, the core is in sinusoidal shape) core. In the sandwich structures, a large portion of Lamb wave energy inside the face sheets can be scattered or reflected by the vertical core, which makes the Lamb wave difficult to capture at relatively long distance. Therefore, the Lamb wave-based damage identification method is more suitable for thin plates than large-size sandwich structures. If the Lamb wave-based damage identification method is adopted for FRP sandwich panel, only a small area of the panel can be examined at each test. Hence, the vibration or dynamic response-based damage identification method was adopted in this study to examine the sandwich deck panel. A structural health monitoring strategy using the combination of experimental modal testing technique and proposed 2-D CWT-based/DSCF-based damage identification method is presented in this chapter.

The rest of the chapter is organized as follows. The modeling of the as-manufactured FRP honeycomb sandwich deck panel is given in Section 8.2. The finite element analysis of the FRP sandwich panel and the damage identification of the sandwich panel based on the FE simulation data and using the 2-D CWT-based method (see Chapter 5) and DSCF-based method (see Chapter 7) are described in Sections 8.3 and 8.6, respectively. The experimental modal testing of the sandwich panel and the damage identification of the sandwich panel based on experimental data and using 2-D CWT-based method and DSCF-based method are presented in Sections 8.4 and 8.5, respectively. The content of this chapter is concluded in Section 8.7.

8.2 Modeling of FRP honeycomb sandwich structure

Using a micro/macro mechanics approach for face laminate and a mechanics of material approach for honeycomb core, the modeling of equivalent elastic properties at room temperature for the face laminates and honeycomb core in the sandwich is presented in this section.

8.2.1 Geometry of FRP sandwich deck panels

The as-manufactured FRP sandwich deck panels studied in this chapter are a plate-type structure with a length of 1.981 m and a width of 1.495 m. The sandwich panel was connected to two underlying concrete supports using steel studs, which provides a means to connect the FRP deck to the underneath bridge girder and is considered to provide a simply supported boundary condition to the deck panel. The FRP sandwich panel consists of two face laminates and a sinusoidal honeycomb core, as shown in Fig. 8.1. The thickness of face laminates and honeycomb core are $t_f = 13.5mm$ and $t_c = 128mm$, respectively. The constituent materials used for the composite sandwich panel (both the face laminates and core) consist of E-glass fibers and polyester resin, and their mechanical properties at room temperature (25 ºC) are listed in Table 8.1.

The wave function of corrugated core wall can be defined as

$$y = \frac{b}{2}(1 - \cos\frac{\pi x}{a}) \tag{8-1}$$

The dimensions of the sinusoidal core are a = 50.8 mm (2.0 in.), b = 50.8 mm (2.0 in.), $t_1 = t_2$ = 3.34 mm (0.131 in.) (Qiao and Wang 2005) (as shown in Fig. 8.2).

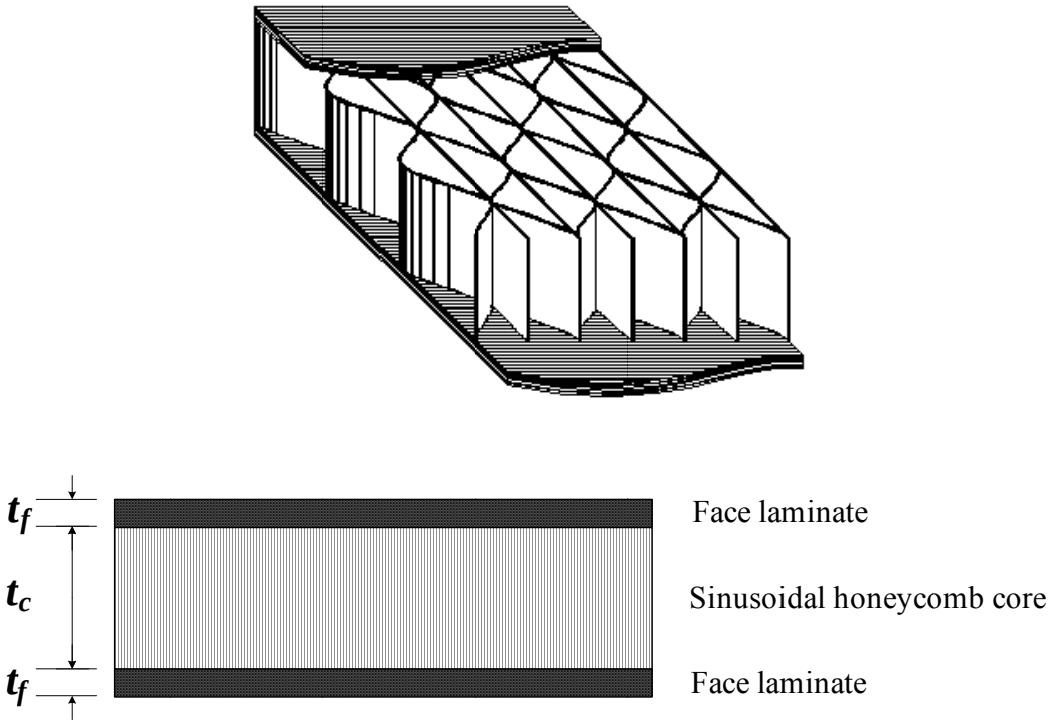

Figure 8.1 Configuration of FRP sandwich panel with longitudinal core

(t_f =13.5 mm, t_c =128 mm).

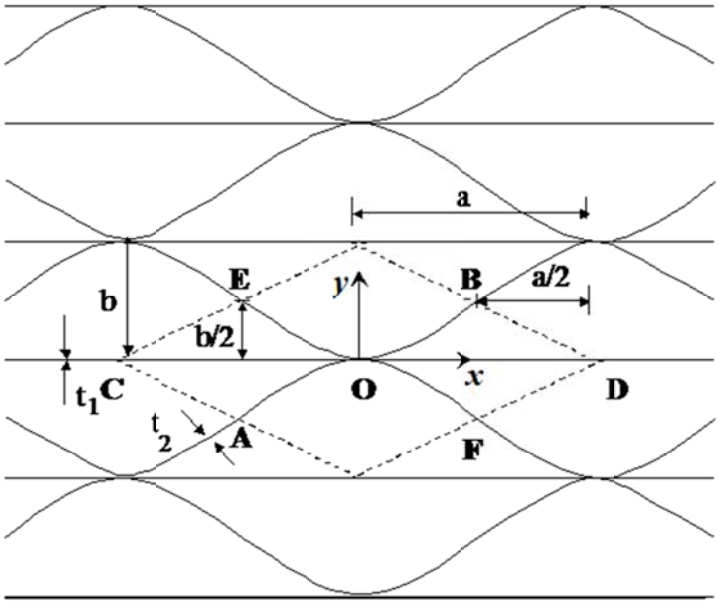

Figure 8.2 Geometry of sinusoidal core in honeycomb structures

(a = 50.8 mm (2.0 in.), b = 50.8 mm (2.0 in.), t_1 = t_2 = 3.34 mm (0.131 in.)).

Table 8.1 Mechanical properties of the constituent materials

Material	E, GPa ($\times 10^6$ psi)	G, GPa ($\times 10^6$ psi)	v	Density ρ, g/cm^3 (lb/in.^{3})
E-glass fiber	72.4 (10.5)	28.8 (4.18)	0.255	2.55 (0.092)
Polyester resin	5.06 (0.734)	1.63 (0.237)	0.300	1.14 (0.041)

8.2.2 Modeling of face laminates

To predict the equivalent properties of the face laminates from the fiber and matrix material properties, a micro-macro mechanics approach is adopted. First, the properties of each layer in the face sheet can be computed using the existing micromechanics approaches (Barbero 1999), such as rule of mixtures (ROM), periodic microstructure (PM), and composite cylinders (CC). In these micromechanics models, each ply is modeled as a homogeneous, linearly elastic and generally orthotropic material. Then, based on the ply properties and lay-up, the apparent stiffnesses of the face laminate can be predicted by classical lamination theory (macromechanics).

Face laminate lay-up

A typical face laminate may include the following four types of fiber layers: (1) Chopped Strand Mat (ChopSM), which is made of randomly oriented short discontinuous fibers resulting in nearly isotropic in-plane properties. This type of layer is commonly used as a bonding layer in lay-up. (2) Continuous Strand Mat (ContSM), which consists of randomly oriented continuous fibers and also can be modeled as an isotropic layer. This type of layer is commonly used as backing material for non-woven fabrics. (3) Bidirectional stitched fabrics (SF) with balanced off-angle fibers (e.g., 0º/90 º or ±45 º); and (4) unidirectional layer of fiber bundles or rovings.

In this study, the lay-up of face laminate in the as-manufactured honeycomb sandwich deck panel includes 5 ChopSM bonding layers (ChopSM308) and 4 bi-directional combination mat layers (CDM3208), as shown in Fig 8.3. Each CDM3208 combination layer consists of a 0º/90 º SF and a ContSM layer. The properties of face sheet layers, such as nominal weight w, thickness t, and fiber volume fraction V_f, are listed in Table 8.2.

Micromechanics

The stiffness of each layer can be predicted from micromechanics models. For directional layers, a micromechanics model for composites with Periodical Microstructure (PM) is adopted to obtain the elastic constants. While for the randomly oriented layers (ChopSM and ContSM), the elastic constants are evaluated by averaging the elastic constants over all possible orientations by integration. The well-known approximate expression by Tsai and Pagano is adopted in this study (Tsai and Pagano 1968).

$$\begin{aligned} E &= \frac{3}{8}E_1 + \frac{5}{8}E_2 \\ G &= \frac{1}{8}E_1 + \frac{1}{4}E_2 \\ \upsilon &= \frac{E}{2G} - 1. \end{aligned} \tag{8-2}$$

where E_1 and E_2 are the longitudinal and transverse moduli of a fictitious unidirectional layer having the same volume fraction as the CSM layer.

All the layer stiffness properties derived from micromechanics models are listed in Table 8.2.

Macromechanics

After the elastic properties of each layer are computed, the equivalent stiffness properties of the face laminate are predicted by classical lamination theory. A set of equivalent in-plane laminate stiffness properties can be derived for the laminates. These properties represent the stiffness of an equivalent, orthotropic plate that behaves like the actual laminate under in-plane loads. It should be noted that from lamination theory, both the bending and in-plane stiffness can be derived. For the face sheet laminates, only in-plane stiffness is derived in this study because when the sandwich panel is subjected to transverse loading, the face sheets mainly contribute to the overall stiffness of the sandwich panel through the in-plane (extension/compression) stiffness rather than bending stiffness. The equivalent in-plane stiffness properties of face laminates are listed in Table 8.3.

8.2.3 Modeling of honeycomb core

The microstructure of core walls consists of 2 layers of ChopSM (ChopSM308). The ChopSM can be modeled as an isotropic layer, and its stiffness properties are listed in Table 8.2. So the core wall can also be modeled as an isotropic layer with double thickness of the ChopSM and the same stiffness properties as the ChopSM.

Table 8.2 Layer material properties from micromechanics models

Ply name	Orientation	E_1, GPa	E_2, GPa	G_{12}, GPa	Nominal weight, w, kg/m^2	Thickness, t, mm	ρ_{ply}, g/cm^3	V_f
ChopSM 308	Random	10.67	10.67	3.86	0.915	1.668	1.37	0.164
CDM 3208	0 º	34.38	12.08	4.25	0.531	0.49	1.74	0.424
	90 º	34.45	12.10	4.26	0.601	0.55	1.74	0.425
	Random	19.59	19.59	7.04	0.256	0.25	1.70	0.396

Table 8.3 Equivalent in-plane stiffness properties of face laminates

	ρ_f, g/cm^3	E_x^f, GPa	E_y^f, GPa	G_{xy}^f, GPa	v_{xy}^f
Face laminate	1.506	15.06	15.30	4.21	0.30

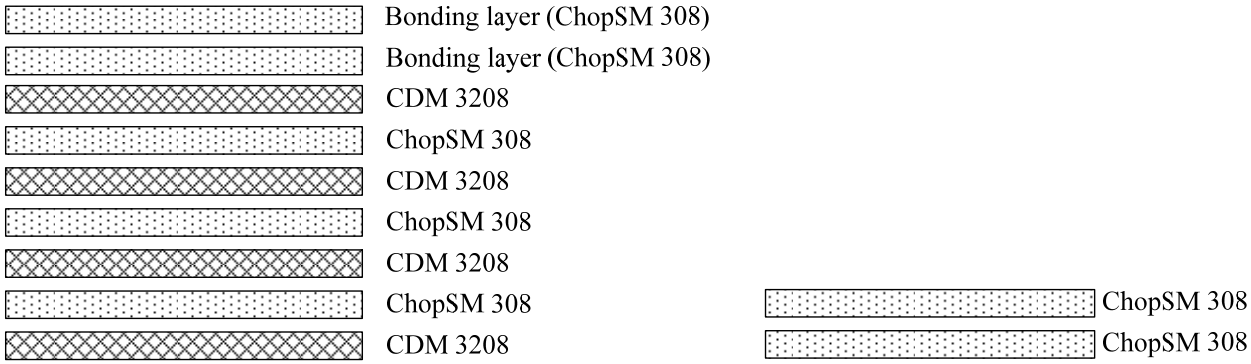

(a) face laminate lay-up (b) honeycomb core lay-up

Figure 8.3 Lay-up of face laminates and core.

8.3 Damage detection based on FEA using 2-D CWT-based algorithm

8.3.1 Finite element analysis of healthy and damaged sandwich panel

The sandwich deck panel is a plate-type structure with a length of 1.9812 m and a width of 1.4945 m. The Finite Element Analysis package ABAQUS is used to conduct an eigenvalue analysis to extract the natural frequencies and the mode shapes of the sandwich deck panel with simply supported (SS)-simply supported (SS) boundary condition. The sandwich panel is modeled as two face sheets and a detailed sinusoidal core. The face sheets and the sinusoidal core walls are modeled as 4-node first-order plate elements S4 and 3-node first-order plate elements S3. The lay-ups and corresponding material properties of face sheets and core walls are the same as shown in Fig. 8.3 and Table 8.2. The corresponding equivalent stiffness properties of face sheets and honeycomb core walls are derived as described in Section 6.2. The finite element analysis is conducted on both a healthy and a damaged sandwich panel. The damage is a debonding between the top face sheet and core at a corner of the sandwich panel, as shown in Fig. 8.4. It is simulated by detaching the node/element connection between the top face sheet and core elements. The simulated mode shapes of the FRP sandwich panel is shown in Fig. 8.5. It should be noted that the mode shapes of the healthy and damaged panel are very close to each other so only that from the damaged panel is shown in the figure.

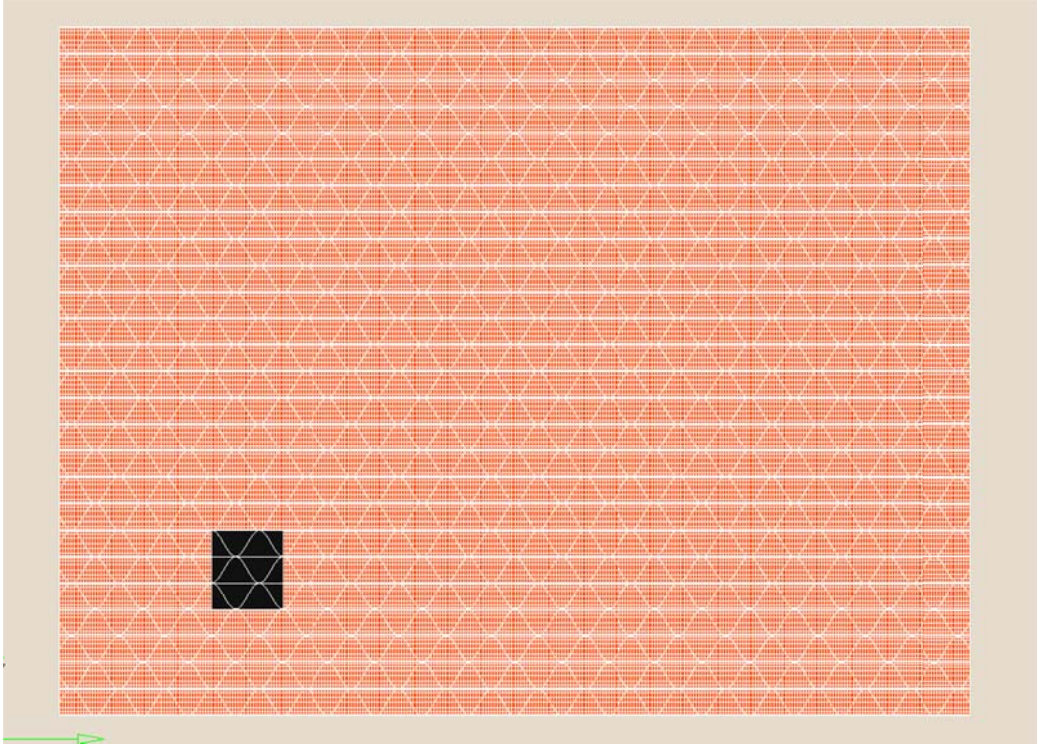

Figure 8.4 The area with the face sheet-core debonding in sandwich panel model.

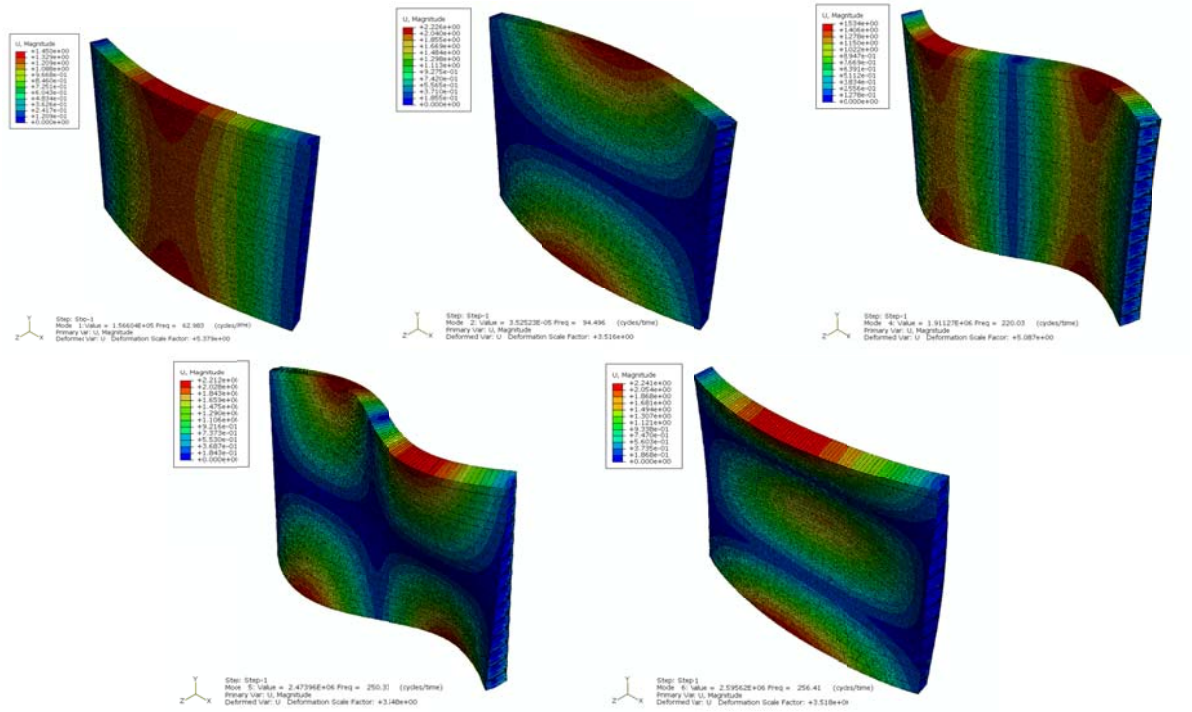

Figure 8.5 First five global mode shapes of the SS-SS sandwich panel from FEM.

8.3.2 Damage identification based on FE simulation data

Per discussion in Section 6.1, the 2-D CWT-based damage identification algorithm proposed in Chapter 3 is applied to the FE simulation data of the first mode shape for the sake of damage detection. From the mode shape data, a grid of data point is first extracted for analysis. The selected points include all the points every 0.1016 m in the *x*-direction and every 0.1150 m in *y*-direction from point (0.0254, -0.6898) to point (1.9558, 0.6898). The extracted data points from the fundamental mode shape are shown in Fig. 8.6.

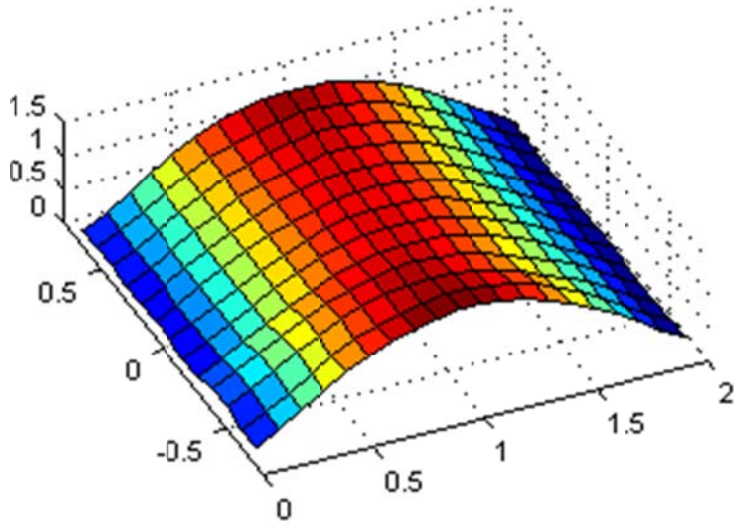

Figure 8.6 Extracted data points from the fundamental mode shape.

The 2-D CWT-based damage identification algorithm is then applied to the data extracted at these points from the damaged panel. First, the wavelet coefficients of the mode shape data are calculated using "Dergauss2d" wavelet. The coefficients with scale of $a = 2$ is shown in Fig. 8.7. It can be easily noticed that there are multiple peaks of coefficients around the debonded area for damaged panel. In contrast, the coefficients for healthy panel are flat with only a few variations at four corners. Then, the isosurface of the wavelet coefficients in continuous scale variation is shown in Fig. 8.8. The threshold ratio of $t = 0.3$ is adopted in this analysis. It can be

seen in the figure that the isosurface can correctly identify the location of the debonding and approximate the area of the debonding with some extent of shift. Some small isosurfaces can also be noticed in the figure. However, their existences and shapes are not as consistent from the low scale to high scale as the debonding one, and it is clear that these isofurfaces are caused by noise other than real damage.

For comparison, the 2-D CWT-based damage detection algorithm is applied to the healthy panel, and the result is shown in Fig. 8.9. It can be seen that there is no isosurface when scale $a < 12$ but a large isosurface when $a > 12$. So it is obvious that applying this method to the healthy panel will also generate an isosurface, since the wave of the vibration mode itself will be captured by the wavelet when its scale is high. Therefore, it is confirmed that only an isosurface evolving from the low scale to high scale indicates a localized damage to the panel.

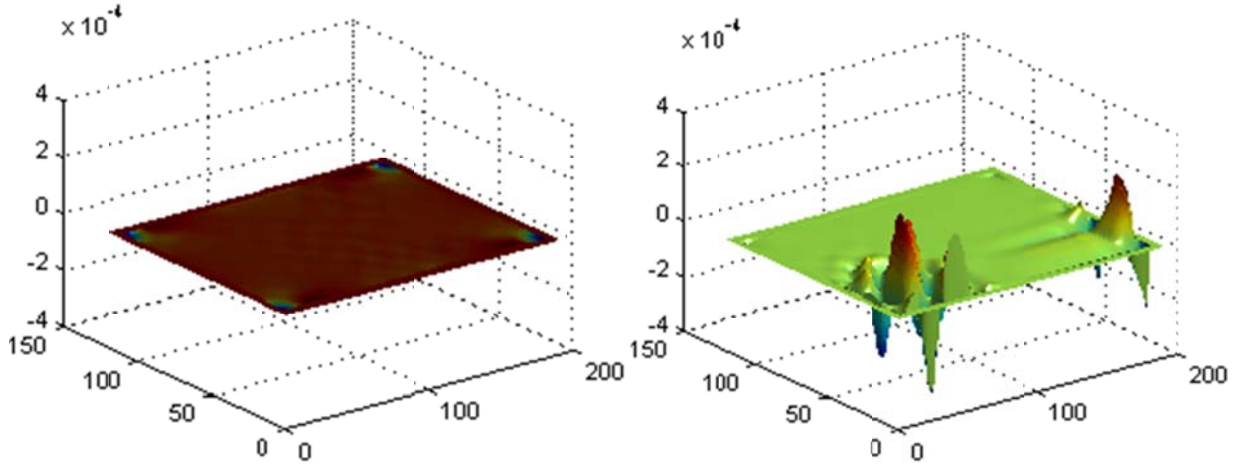

(a) healthy (b) damaged

Figure 8.7 Wavelet coefficients of the fundamental mode shape *a* = *2*.

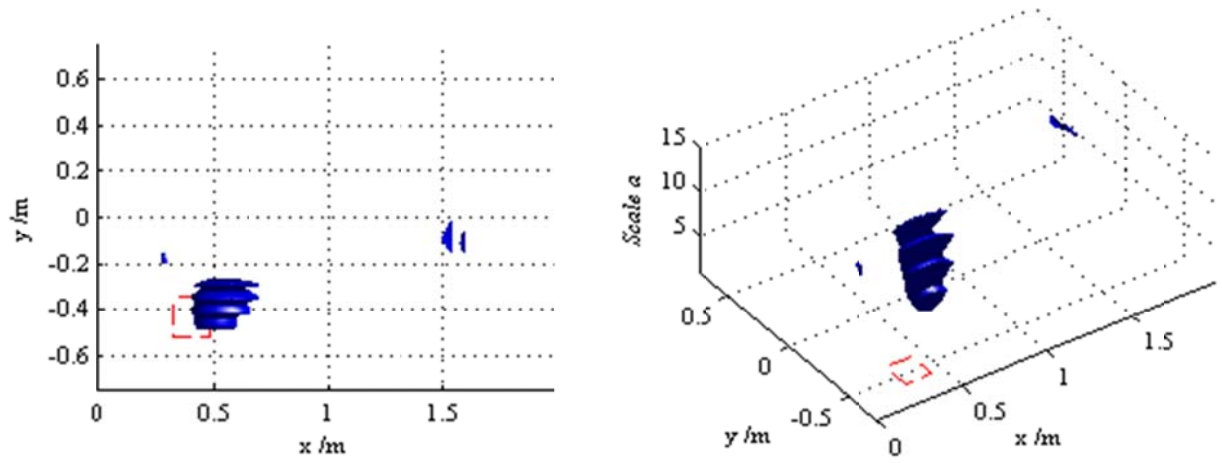

Figure 8.8 Isosurface of the damaged panel using the fundamental mode shape (Actual damaged area marked in red dash line).

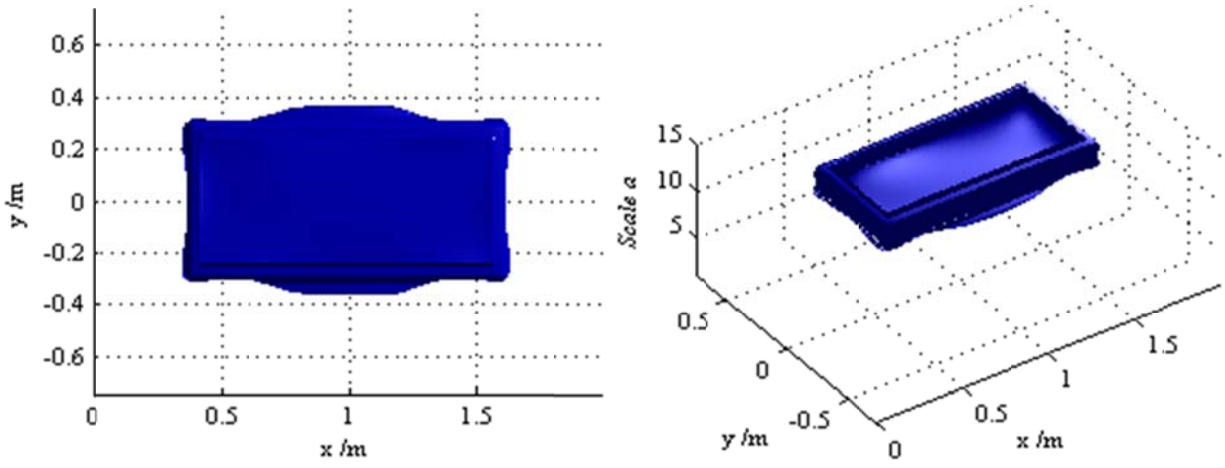

Figure 8.9 Isosurface of the healthy panel using the fundamental mode shape.

8.4 Damage detection based on modal testing using 2-D CWT-based algorithm

8.4.1 Experimental set-up and modal analysis

For damage identification, an as-manufactured FRP sandwich deck panel was experimentally tested. The geometry, lay-up and corresponding material properties of the FRP sandwich deck panel are presented in Section 8.2. The FRP sandwich panel is placed

transversely on the two supporting concrete beams. The sandwich panel is connected to the two underlying concrete supports using the steel studs, which is considered to provide a simply supported boundary condition. A 13.5 kg mass with a diameter of 101.6 mm (4 in.) is attached to the top face sheet as an artificially-induced "damage" or "abnormality" before the modal testing. The center of the mass is located at the central point (0.4318, -0.4572) of points 44, 45, 54 and 55.

The modal testing of the FRP sandwich panel was conducted with a roving excitation test. For simplicity, only a quarter of the panel with the artificially-induced damage was tested. The quarter of the panel is divided into 9×7 elements by the grid lines. The panel was subjected to a dynamic pulse load applied at each grid point using modally tuned hammer (PCB 086C20). A total of 10×8 grid points were tested corresponding to an actual spatial sampling distance of 101.6 mm (4.0 in.). The response measurements were made using one accelerometer (PCB 352C68) at point No. 20 to record the response of the structure. The analog signals then pass a low-pass anti-aliasing filter to prevent the aliasing problem. A Krohn-Hite 3382 8-pole dual channel filter was employed to filter out the high frequency signals above the cut-off frequency of 500 Hz. The filtered signals were then digitized and collected by the data acquisition system dSPACE CP1103 at the sampling frequency of 1000 Hz. The experimental set-up is shown in Fig. 8.10. The measurements at each point were repeated 8 times, and the synchronized time histories from the excitation and response measurements were averaged to enhance the signal-to-noise ratio (SNR). Then, the frequency-response functions (FRFs) of these tested points were calculated from these excitation and response time-histories. Finally, these FRF curves were imported to the modal analysis program ME'Scope for curve fitting and modal extraction.

Fig. 8.11 shows the user interface of ME'Scope while conducting the modal analysis and extracting the 3rd mode shape of the sandwich panel. The modes generated in the modal analysis are listed in Table 6.4. It should be noted that the "healthy panel" means that the panel is at as-manufactured state without artificially-induced damage or abnormality; while the "damaged panel" means the sandwich panel with a mass attached to the top face sheet to simulate a damaged state. There is no guarantee that there is no imperfection/delamination/debonding induced during manufacturing/transportation process.

From the modal analysis result, it can be seen that the existence of the mass slightly reduces the modal frequencies of the sandwich panel. It should also be noted that the 1st and 2nd modes from the modal testing and FEM are consistent with each other, while the 3rd identified mode from the modal testing of the healthy sandwich panel matches the 5th mode from FE and damaged panel. From the mode shapes generated in the FE analysis, it can be seen that both the modes have a nodal line at the midline of the panel length direction. In this test, the sensor is located at point 20 which exactly lies on the nodal line of the healthy panel. So no response signal were generated when the panel was vibrating under the 3rd and 4th mode. Therefore, it is reasonable to conclude that the present modal testing experiment is unable to capture the 3rd and 4th modes as indicated by FE. Actually, the modal testing set-up cannot be used to capture any modes with a nodal point at point 20. However, for the damaged panel, since the damage has deteriorated the symmetry of the sandwich panel, the midline in the length direction is no longer the nodal line for the 3rd and 4th vibration modes. Hence, these two modes can be identified in the case of the damaged panel. This problem discussed above should not affect the application of the proposed 2-D CWT damage identification algorithm, since there are still several other well-captured vibration modes available for analysis.

Figure 8.10 Experimental set-ups for modal testing of FRP sandwich panel.

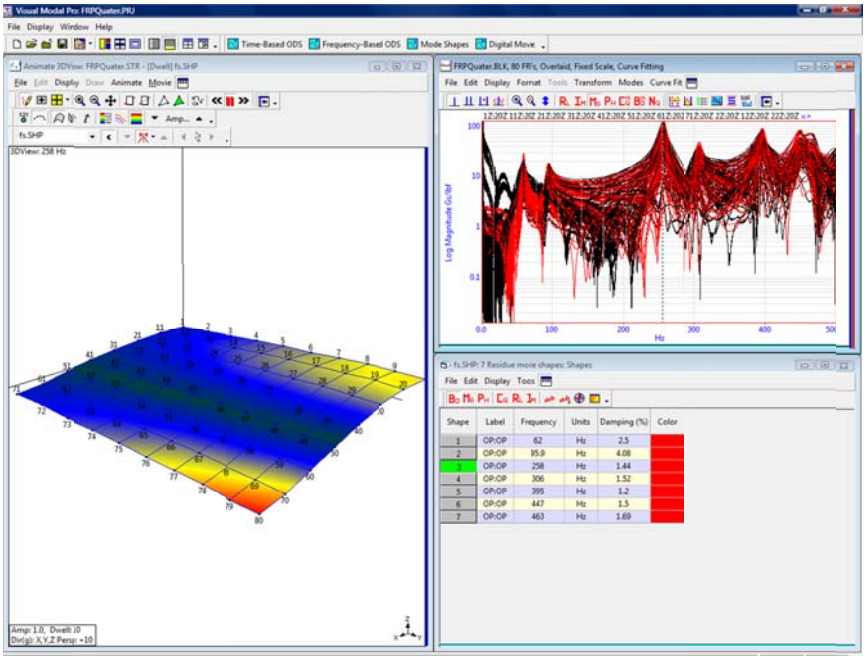

Figure 8.11 The 5th mode shape of healthy FRP sandwich panel from modal analysis package ME'Scope.

Table 8.4 Modal frequencies from experimental modal analysis

	Mode 1	*Mode 2*	*Mode 3*	*Mode 4*	*Mode 5*
Healthy Panel	61.95	95.94	-	-	258.00
Damaged Panel	60.63	93.60	175.02	207.24	256.45

8.4.2 Damage detection based on modal testing data

After obtaining the experimental modal analysis data of mode shapes, the 2-D CWT-based damage identification algorithm is applied to the mode shape data for damage detection. It should be noted that it is commonly noisy in the low frequency range (< 100 Hz) due to the room noise, electromagnetic interference. But it is also difficult to excite the large sandwich structure in the high frequency range (> 500Hz) using impact hammer. Therefore, the 5^{th} vibration mode in the middle range of frequencies (200~400 Hz) was selected for damage identification to ensure the best Signal to Noise Ratio (SNR).

The displacement-normalized mode shape used for damage identification is shown in Fig. 8.12. The mode shape from the damaged panel resembles that from the healthy panel, with minor difference in their general shape. Hence, it is difficult to find the damage location by directly comparing the two mode shapes. The 2-D CWT-based damage identification algorithm is applied to the mode shape of the healthy and damaged panel. First, the mode shape data is oversampled by 10 using the bivariate cubic spline interpolation to enhance the spatial sampling distance from 101.6 mm (4.0 in.) to 10.16 mm (0.40 in.). Then, the 2-D CWT-based algorithm is applied to the oversampled data. The investigation shows that in this case a scale from 1 to 10 is

sufficient for damage detection. The threshold value is set to 0.3 in this case. The results from the algorithm are shown in Fig. 8.13.

In the damaged panel case, the major isosurface span from scale of $a = 4$ to $a = 10$, which clearly indicate a localized damage. The isosurface covers an area slightly larger than the damaged area. For a more accurate estimation of the damaged area, a denser grid of measuring points is required. The other two isosurfaces only limited to a small scale range may be caused by measuring error or noise as discussed in Chapter 5.

In the healthy panel case, there are also two isosufaces in the high scale range ($a > 6$). One possible reason is that the isosurfaces may be caused by the already existed imperfection or delamination or debonding in those indicated areas induced during manufacturing/transportation process. It should be noted that in this algorithm the isosurface only indicates the location/area with the mode shape discontinuity, i.e., the most possible location of damage. Isosurface has no indication of the absolute value of the damage extent.

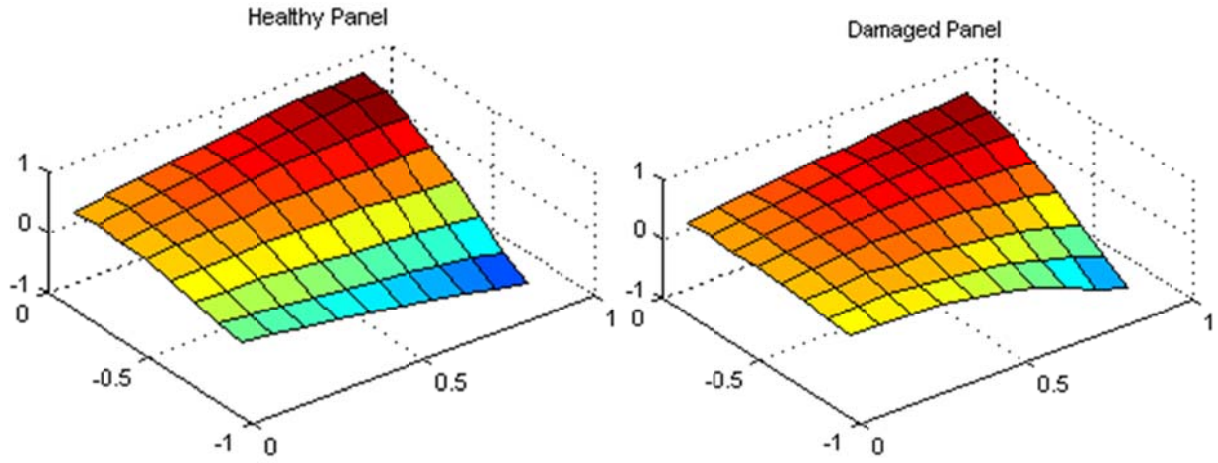

(a) Healthy panel (b) Damaged panel

Figure 8.12 The 5th mode shape for damage identification.

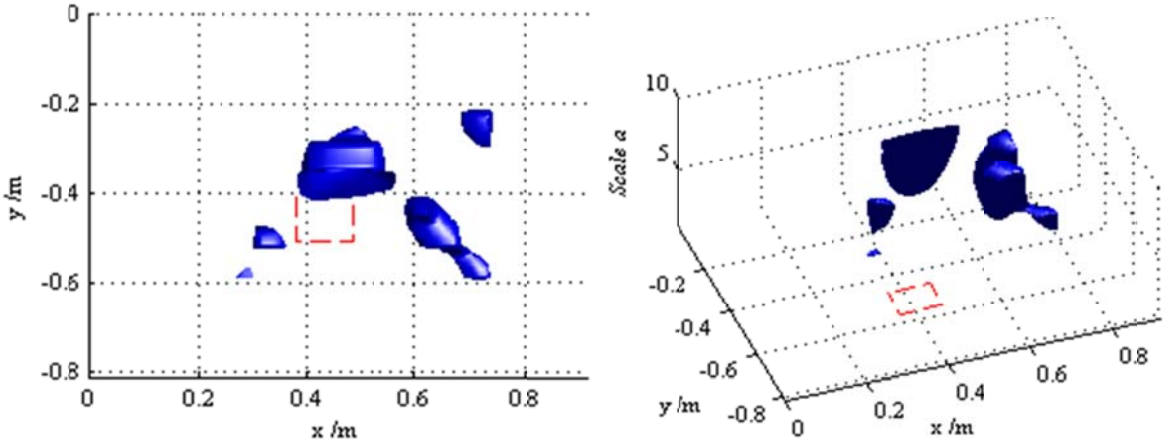

(a) Healthy panel

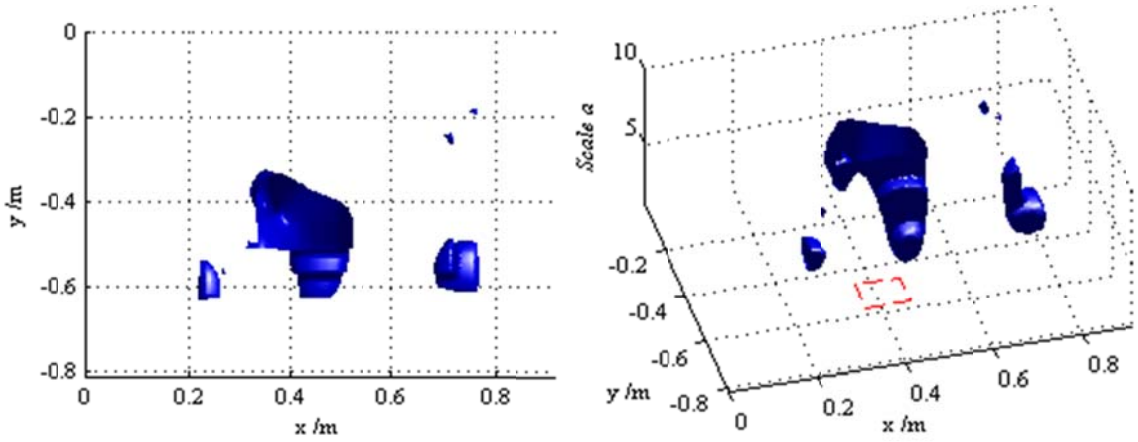

(b) Damaged panel

Figure 8.13 Isosurface of the sandwich panel

(Damage location marked in red dash line)

8.5 Damage identification based on modal testing using DSCF-based algorithm

8.5.1 Experimental setup

The modal testing of the FRP sandwich plate was conducted using a PVDF (Polyvinylidene Fluoride) sensor network bonded to the top surface in the longitudinal direction. The PVDF sensors used in the experiment are model DT1-028K/L from the Measurement Specialties company. A total of 285 nodes of PVDF sensors are uniformly distributed into 19

rows and 15 columns on the surface of the panel to build a sensor network. The plate is divided into 18×14 elements by the 19×15 sensors.

The panel was subjected to a dynamic pulse load applied at the central point using modally tuned hammer (PCB 086C20). The response measurements were captured by the sensor network to record the response of the structure subjected to the fixed point force excitation. A total of 19×15 node points were monitored corresponding to an actual spatial sampling distance of 101.6 mm. The coherent signals of the excitation and the response were digitized and collected by the data acquisition system dSPACE CP1103 at a sampling frequency of 4,000 Hz. Due to the fact that only 20 channels are available, only one column of nodes with 19 sensors were measured in each experiment. In this way, the 285 transfer functions between the hammer excitation and different PVDF sensors can still be measured for modal analysis in 15 experiments. The experimental set-up using the distributed PVDF sensor network is shown in Fig. 8.14.

After the healthy FRP sandwich panel was tested, three stages of damage with increasing severity were artificially induced into the sandwich panel. In the first stage of induced damage (Damage Stage 1), a saw cut was induced between the top face sheet and honeycomb core to simulate the debonding between the top face sheet and honeycomb core. A 203.2 mm ×203.2 mm area of face sheet-core debonding (cut) is shown in Fig. 8.15. In the second stage of increasing damage (Damage Stage 2), another saw cut was further induced between the bottom face sheet and honeycomb core in the same area of the top face sheet-core debonding to simulate the debonding between the bottom face sheet and honeycomb core. In the third stage of the largest damage in this study (Damage Stage 3), the two vertical sides of the core between the two face sheet-core debonding areas were cut to simulate the core crashing scenario, as also shown in Fig. 8.15.

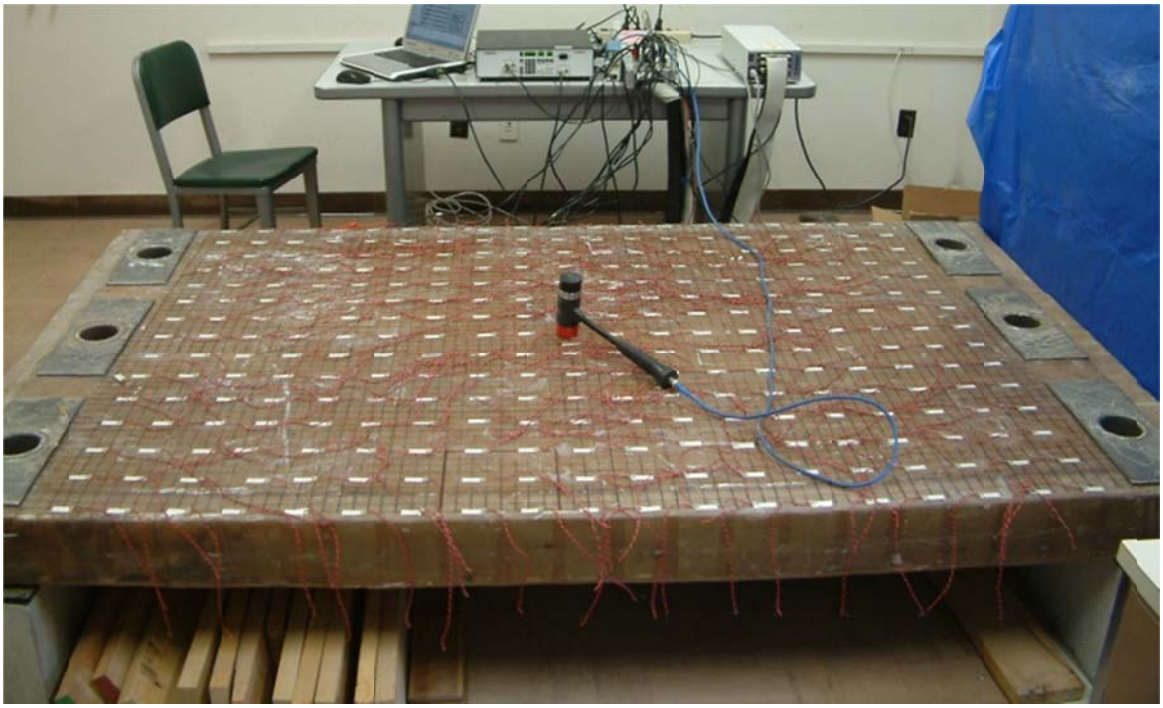

Figure 8.14 Experimental setup using the distributed PVDF sensor network

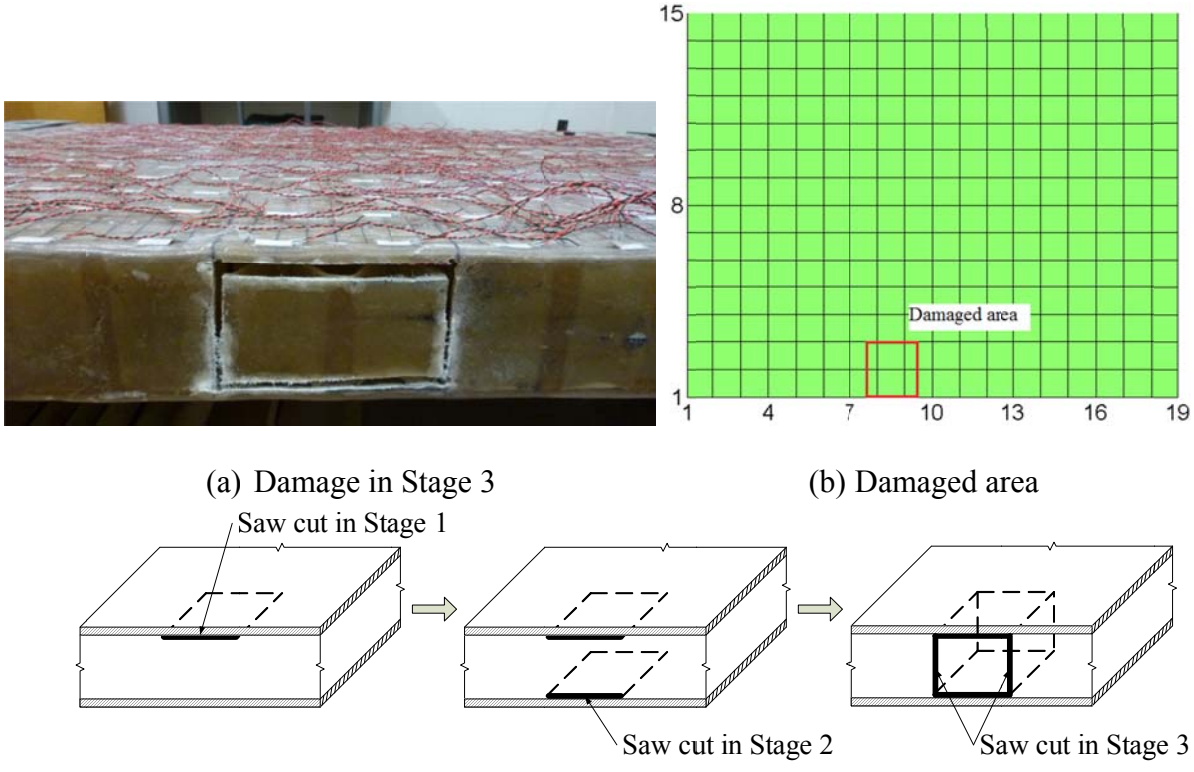

(a) Damage in Stage 3 (b) Damaged area

(c) Schematic sketch of the three damage stages

Figure 8.15 Artificially-induced damages in FRP sandwich plate

8.5.2 Modal testing results

The measurements for each experiment were repeated 16 times, and a pre-trigger of 0.05 seconds at the level of 0.01 volt is set to synchronize the time-domain signal. The synchronized time history data from the excitation and response measurements were averaged to enhance the signal-to-noise ratio (SNR), as shown in Fig. 8.15. Then, the frequency domain power spectral densities were generated from the excitation and response time domain data using Fast Fourier Transform (FFT), as shown in Fig. 8.16. The frequency-response functions (FRFs) of these tested points were calculated from the excitation and response frequency domain data. The FRF curve and its coherence curve, corresponding to the time-domain data in Fig. 8.16 and the frequency-domain data in Fig. 8.17, are illustrated in Fig. 8.18. Finally, these FRF curves were imported to the modal analysis program ME'Scope for curve fitting and modal extraction. The modal testing was conducted using a fixed point force excitation and a distributed PVDF sensor network, so the extracted mode shape should be the strain/curvature mode shape of the plate (Wang 1998).

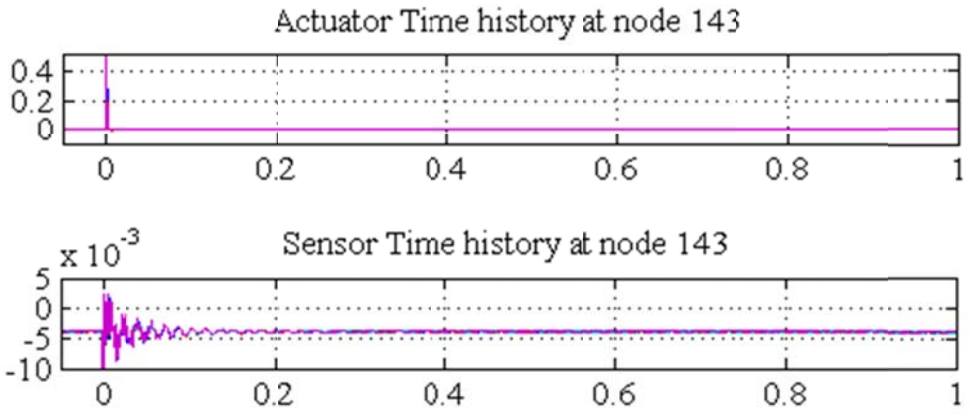

Figure 8.16 Time domain data from actuator and sensor (both at node143).

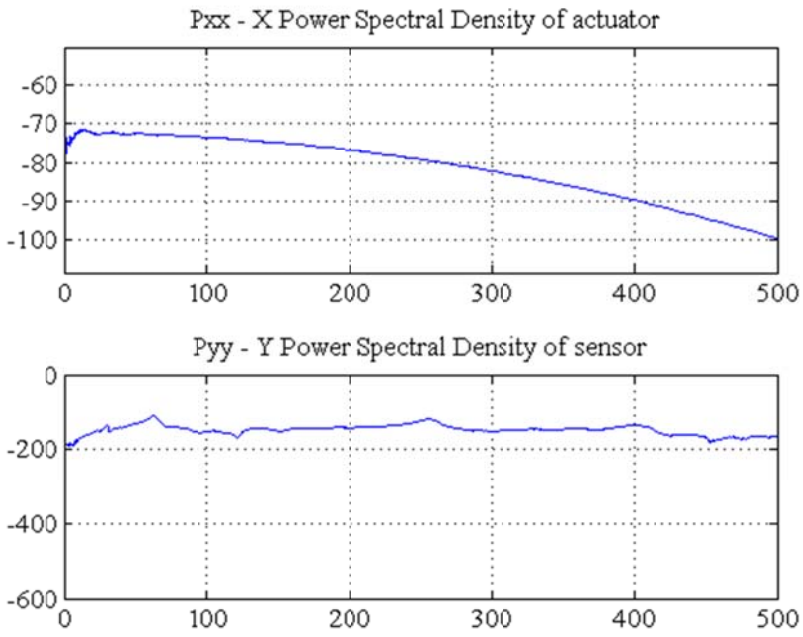

Figure 8.17 Frequency domain data from actuator and sensor (both at node143).

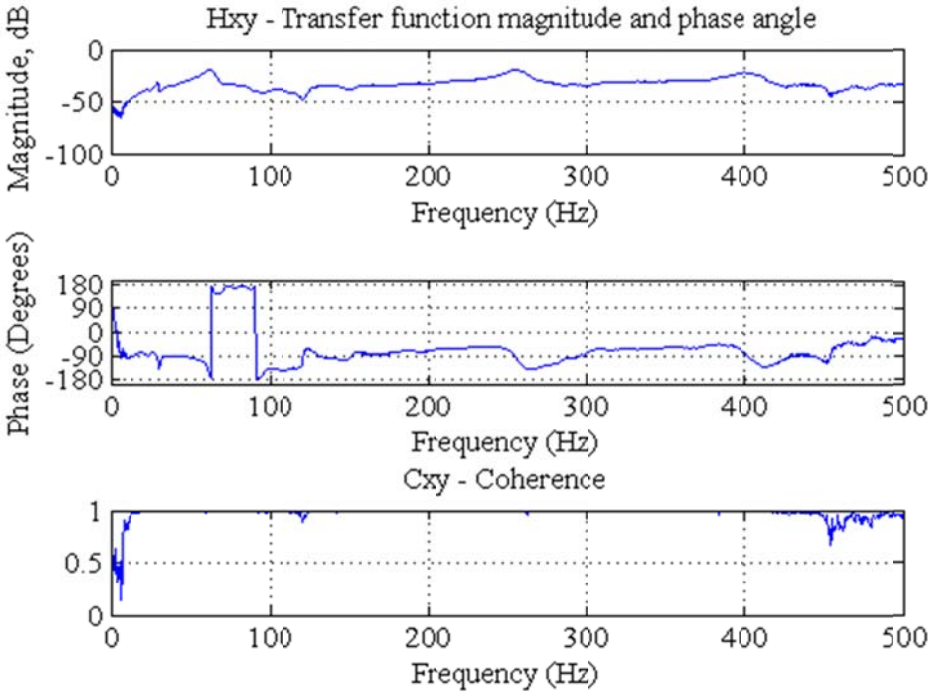

Figure 8.18 A frequency-response function and its coherence functions (both sensor and actuator are at node 143).

Since the plate was tested using a PVDF sensor network in the longitudinal direction (*y*-direction), only the curvature mode shape in the longitudinal direction (κ_{yy}) was captured. Therefore, only the longitudinal bending modes, in which κ_{yy} is dominant, are suitable for damage identification. In the excitation frequency range of the modally tuned hammer, the 1st and 3rd bending modes were captured. However, the second bending mode cannot be captured because the fixed point force excitation was applied at the central point of the plate, which is the nodal line of the second bending mode. Hence, the first and third bending modes in the longitudinal direction were investigated for damage identification. It should be noted that the modal frequency of the first bending mode lies closely around 60 Hz. Because the PVDF sensors are prone to electro-magnetic interference (EMI), their responses around 60 Hz could be noisy due to EMI from power system. In the healthy stage and three damage stages, the modal testing was conducted to extract the modal frequencies and curvature mode shapes of the plate. The curvature mode shapes and modal frequencies of the FRP sandwich panel are presented in Fig. 8.19.

8.5.3 Damage identification using experimental data

The DSCF-based damage identification method is applied to the as-manufactured FRP sandwich deck panel for damage identification.

Step 1: Mode sensitivity.

For the 1st longitudinal bending mode, the modal eigenvalue change ratios at three damage stages are 0.57%, 0.91% and 3.59%, respectively. For the 3rd longitudinal bending mode, the modal eigenvalue change ratios at three damage stages are 0.71%, 1.55%, and 4.07%,

respectively. It can be seen from the eigenvalue change ratios, both modes are sensitive to the damage, so both can be used for damage identification.

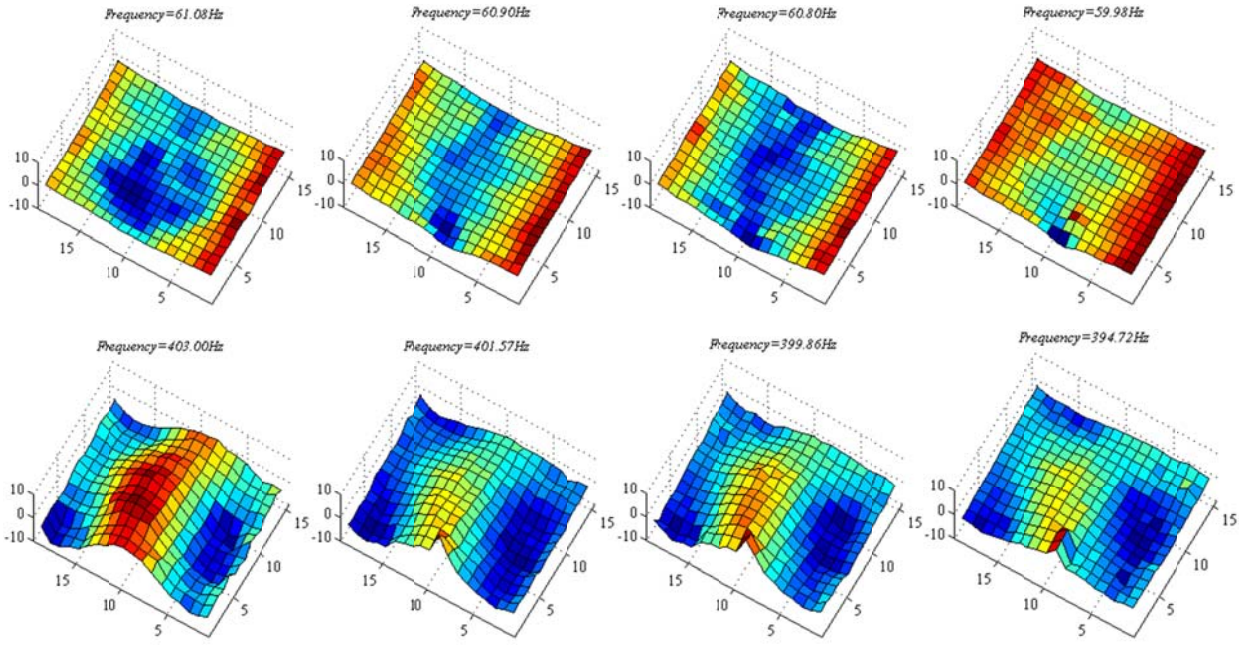

(a) Healthy (b) 1st stage (c) 2nd stage (d) 3rd stage

Figure 8.19 Longitudinal curvature mode shape (κ_{yy}) and modal frequency of 1st and 3rd longitudinal bending mode from experiment

Step 2: Damage localization.

The modal strain energy of a plate can be derived from the curvature mode shapes of κ_{xx}, κ_{yy} and κ_{xy}. However, one PVDF sensor can only be used to measure the strain response in one direction. Therefore, a sensor array positioned in one direction can only capture the strain/curvature mode shape in that direction at a time. Hence, for a longitudinal bending mode, the modal strain energy is approximated by its partial modal strain energy in the dominant direction. Assuming $\kappa_{xx} = \kappa_{xy} = 0$, the partial modal strain energy in the y direction can be derived as

$$\gamma_{ij}^{y} = \int\int_{A_j} \kappa_{yyi}^{2} dxdy \tag{8-3}$$

The DLF and DSCF matrices for damaged identification can be generated as follows. First, a bivariate cubic spline interpolation function is constructed for curvature mode shape. The bivariate cubic spline is constructed as the tensor product of two univariate cubic splines. It can be expressed as the weighted sum of products of two cubic spline functions:

$$f(x,y) == \sum_{i}\sum_{j} a(i,j) g_i(x) h_j(y) \tag{8-4}$$

where $g_i(x)$ and $h_j(y)$ are the cubic spline function in the *x* and *y* direction, respectively. Then, using the bivariate cubic spline function, γ_{ij} and γ_{ij}^{*} can be calculated from equation (8-3). Finally, the DLF and DSCF matrix can be calculated from γ_{ij} and γ_{ij}^{*}.

The DSCF-based damage indices using the modal strain energy from the 1st and 3rd longitudinal bending modes are shown in Fig. 8.20. Although the damaged area does not exactly match the sensor grids, the DSCF damage localization method correctly approximate the location and area of the damage. It can be noticed that in damage stage 3, a false positive indication is given near the damaged area. There might be two reasons: (a) the effect of damage might spread out to surrounding elements (Choi et al. 2006); and (b) When cutting the two sides of the damaged area, the saw cut might damage the sinusoidal core of the neighboring element.

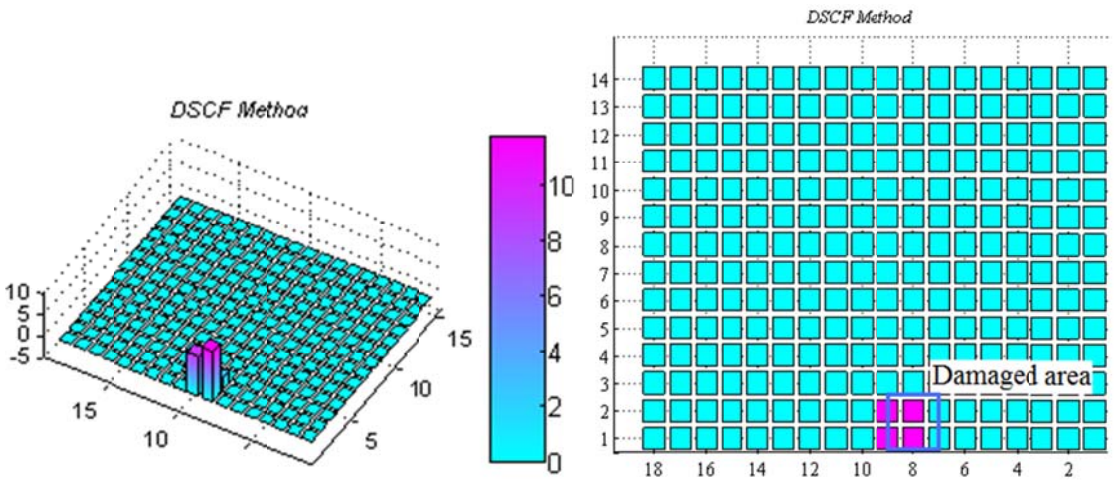

(a) Damage stage 1

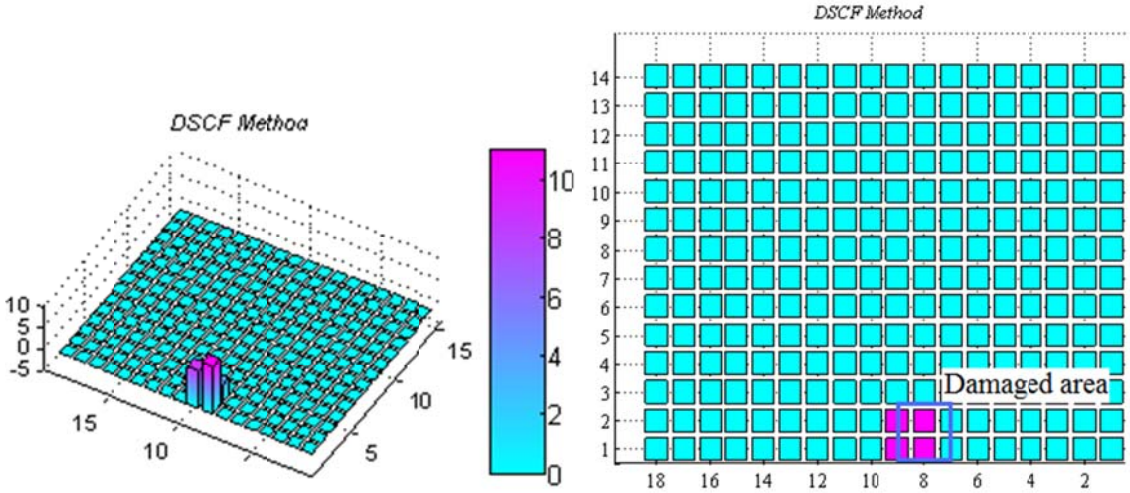

(b) Damage stage 2

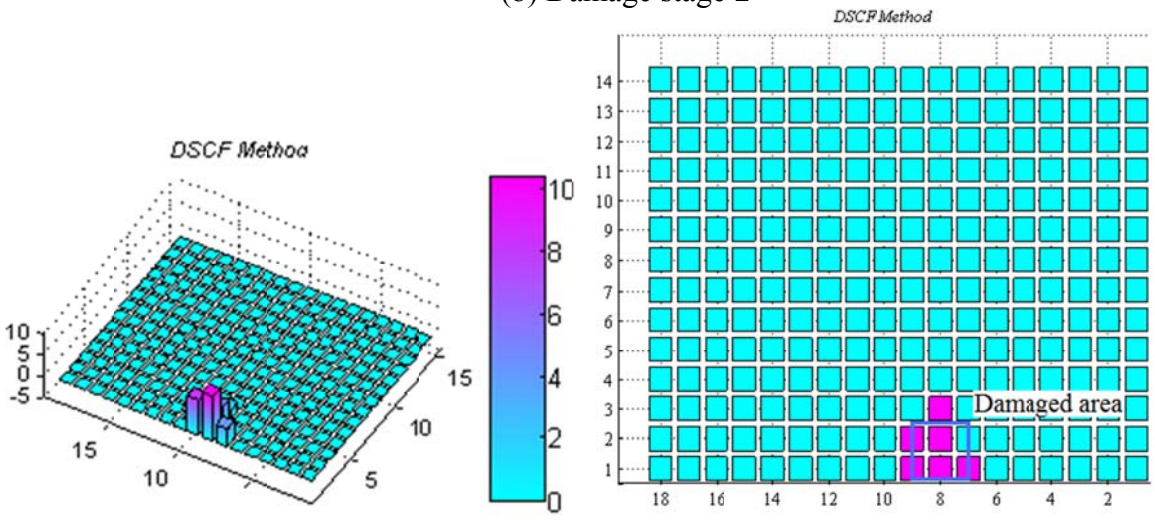

(c) Damage stage 3

Figure 8.20 Damage localization of FRP sandwich plate at three damage stages

Step 3: Damage quantification

Assuming that each damaged element has the same damage severity, the DSCF method can be further applied for damage quantification using DLF and DSCF derived in Step 2. The damage quantification results of DSCF method are presented in Fig. 8.21. The damage quantification results, based on the four damaged elements indicated in damage stages 1 and 2, are marked in black. The damage quantification result, based on the six damaged elements indicated in damage stage 3, is also shown in red for comparison. As shown in figure, the damage severity increases consistently with the damage stages.

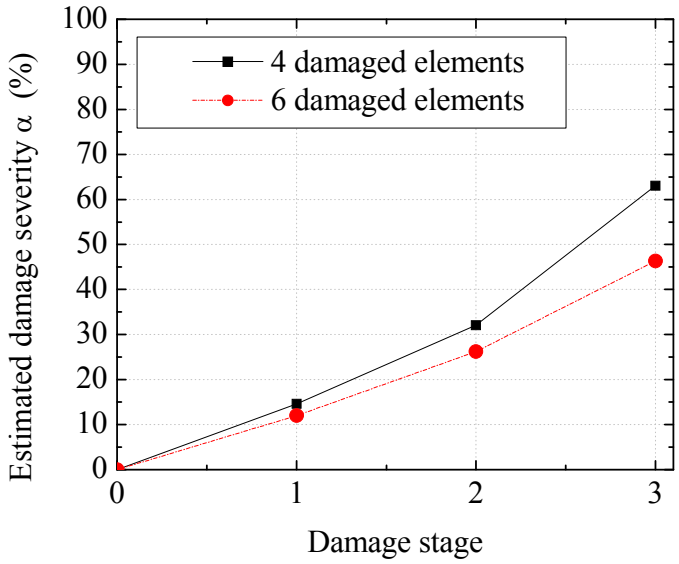

Figure 8.21 Damage quantification of FRP sandwich plate at three damage stages

8.6 Damage identification based on FEA using DSCF-based algorithm

After the experimental modal testing of the FRP sandwich panel, a numerical modal analysis of FRP sandwich panel was conducted to verify the experimental results. The DSCF-based method is also applied to the numerical data for damage identification.

8.6.1 Finite element modal analysis of FRP sandwich panel

The commercial Finite Element Analysis package ABAQUS is used to conduct an eigenvalue analysis of the FRP sandwich plate. A detailed model of the sandwich panel is constructed in ABAQUS, as shown in Fig. 8.22. The face sheets and the sinusoidal core walls are modeled as 4-node first-order plate elements S4 and 3-node first-order plate elements S3. The corresponding stiffness properties of face sheets and core walls are derived in Section 6.2. The boundary conditions are considered to be simply supported at two longitudinal edges.

The finite element analysis is conducted on both the healthy and damaged sandwich panel. Three damaged sandwich panel models are set up to simulate the sandwich panels with artificially induced damage in the three damage stages. The debonding between the face sheets and core is simulated by detaching the node/element connection between the face sheets and core elements. The cuts in the sinusoidal core are simulated similarly. The simulated mode shapes of the FRP sandwich panel are shown in Fig. 8.22. The displacement mode shapes of the healthy and damaged panel are very close to each other so only that from the healthy panel is shown in the figure. The strain mode shape can be then extracted from the 19×15 nodes corresponding to the 19×15 PVDF sensors in experimental test, as shown in Fig. 8.23.

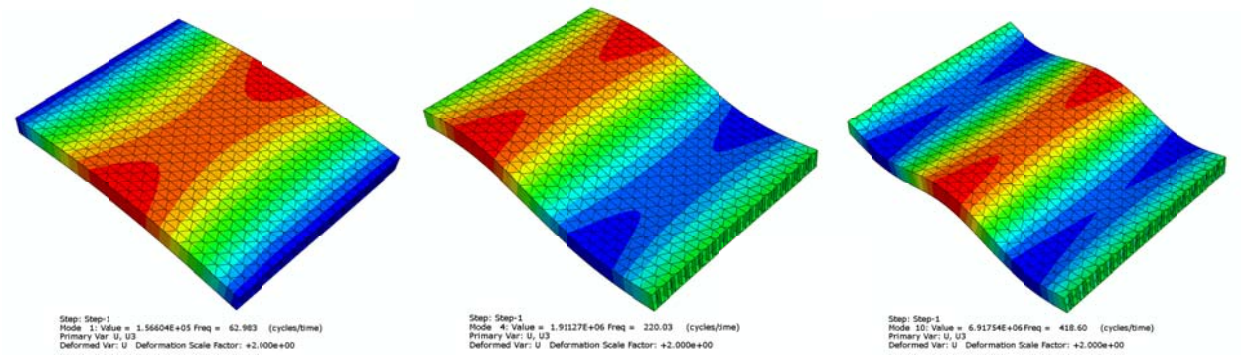

(a) 1st mode (b) 2nd mode (c) 3rd mode

Figure 8.22 First three longitudinal bending mode shapes of the SS-SS sandwich panel from FEM (contour of vertical displacement U3).

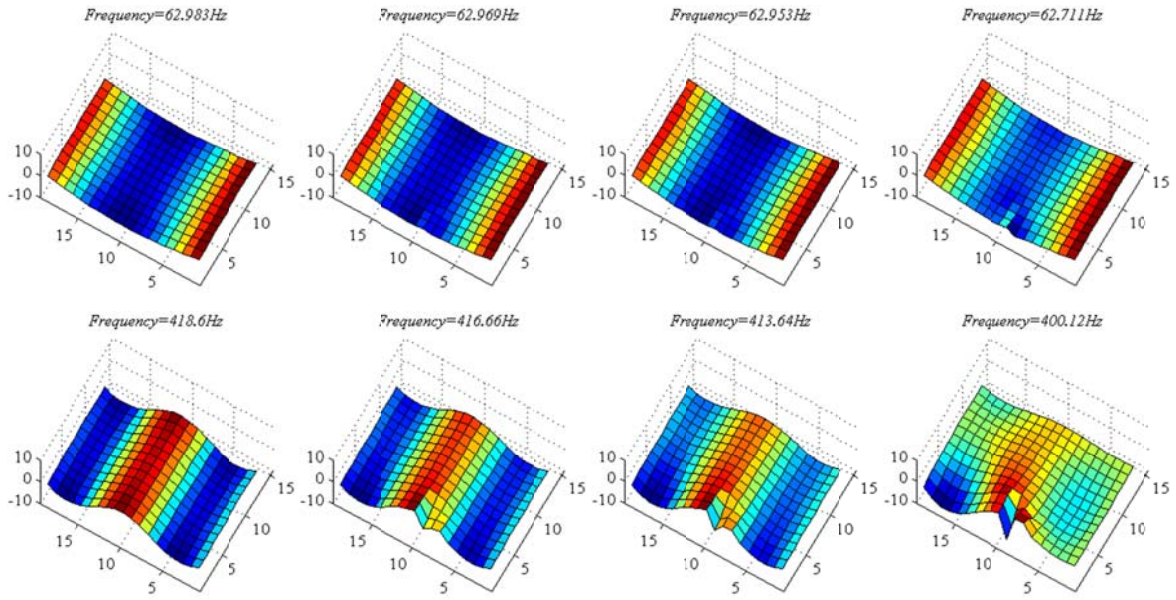

(a) Healthy (b) 1st stage (c) 2nd stage (d) 3rd stage

Figure 8.23 Longitudinal curvature mode shape (κ_{yy}) and modal frequency of the 1st and 3rd longitudinal bending modes from FEA.

8.6.2 Damage identification using FE simulation data

Step 1: Mode sensitivity.

The modal frequencies of the healthy sandwich panel from the finite element analysis are 62.983 Hz and 418.6 Hz, which shows close agreements with experimental test (i.e., 61.08Hz

and 403.00 Hz) for the 1st and 3rd modes, respectively. The result confirms that the boundary conditions at the two longitudinal ends should be modeled as simply supported, and the free vibration modes of the FRP sandwich panel can be accurately predicted by the detailed FE model. The modal eigenvalue change ratios at three damage stages from the FEA and experimental test are compared in Table 8.5. The FEA results show that both the modes are sensitive to the damage, so both can be used for damage identification. It can also be noticed that the FEA tends to underestimate the modal eigenvalue change ratios for the 1st mode but over-predict the ratios for the 3rd mode.

Table 8.5 Modal eigenvalue change ratios from FE and experiment

vibration mode		***1st stage (%)***	***2nd stage (%)***	***3rd stage (%)***
1st Mode	*FEA*	0.044	0.095	0.862
	Experiment	0.57	0.91	3.59
3rd Mode	*FEA*	0.925	2.356	8.635
	Experiment	0.71	1.55	4.07

Step 2: Damage localization.

The DSCF-based damage localization method is applied to the curvature mode shapes for damage localization. The damage indices using the modal strain energy from the 1st and 3rd longitudinal bending modes are shown in Fig. 8.24. The results show the same indication of damaged elements in the 1st and 2nd damage stages as the results from experimental test data. In the 3rd damage stage, the FE results indicate damaged elements at the two sides of the damaged core, which is corresponding to the sawcut in the 3rd damage stage.

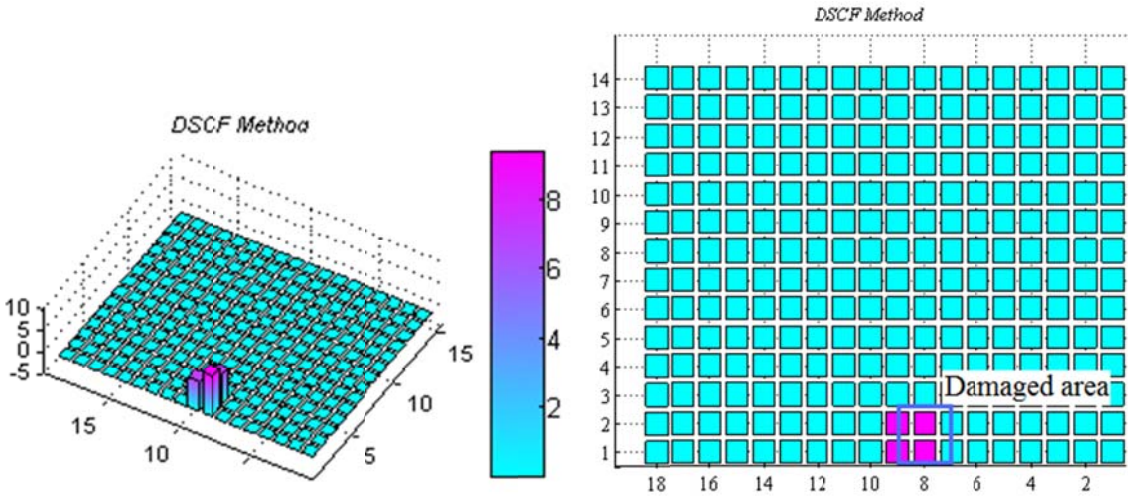

(a) Damage stage 1

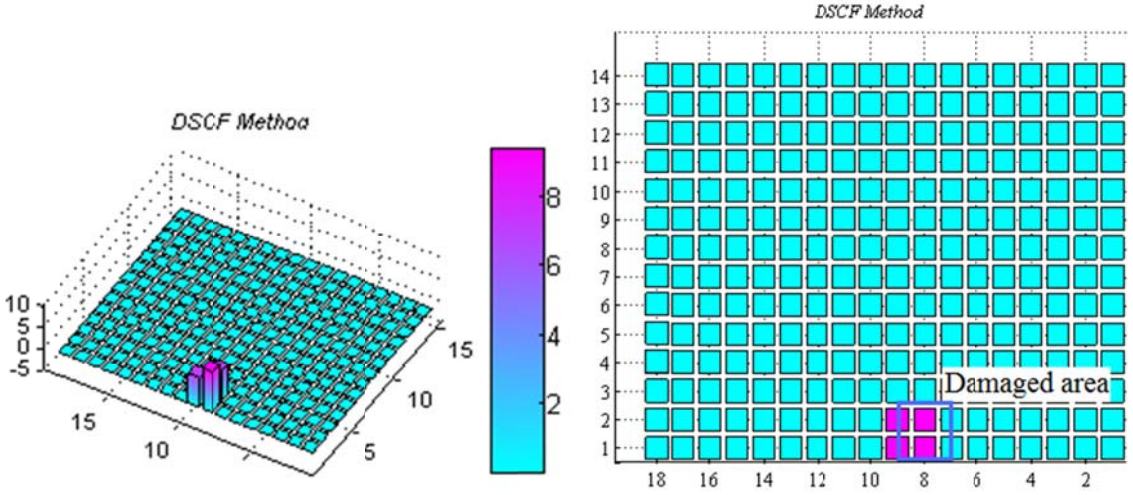

(b) Damage stage 2

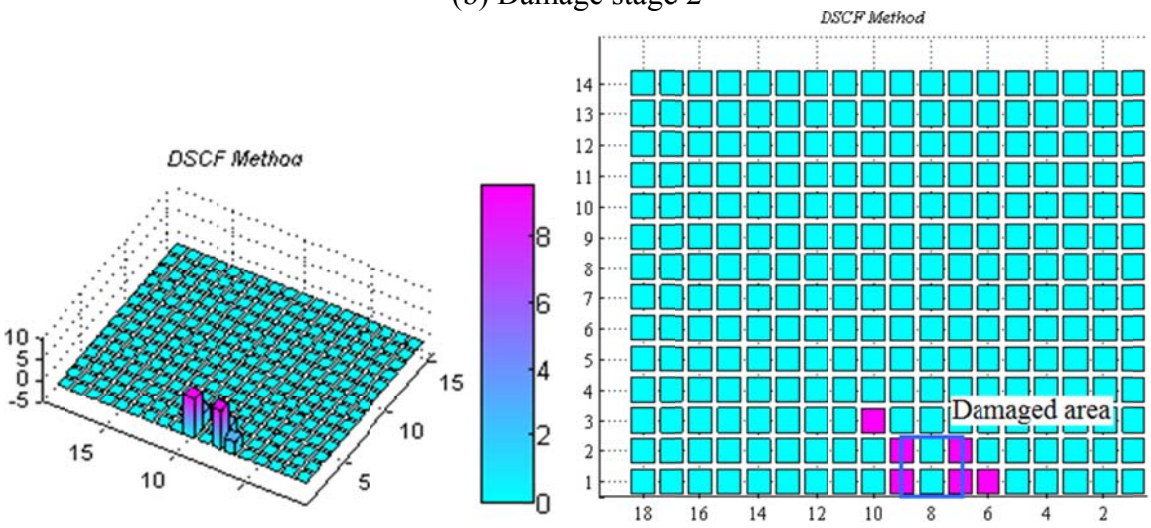

(c) Damage stage 3

Figure 8.24 Damage localization at three damage stages using FEA data.

Step 3: Damage quantification.

Assuming the each damaged element has the same damage severity, the DSCF method can be further applied for damage quantification using the FEA data. The damage quantification results, based on the damaged elements indicated in Step 2, is shown in Fig. 8.25. As shown in the figure, the damage quantification results from both the FEA and experimental data show the same trend, i.e., the damage severity increases consistently with the damage stages. The damage quantification results based on the experimental data are also shown for comparison. It can be seen that in Damage stages 1 and 2, two damage quantification results show close agreement with each other, while in Damge stage 3 the results show considerable discrepancy due to their difference in damaged element indication and modal eigenvalue change ratios. Based on the FEA data, the core crashing can induce over 90% of stiffness reduction in the damaged elements.

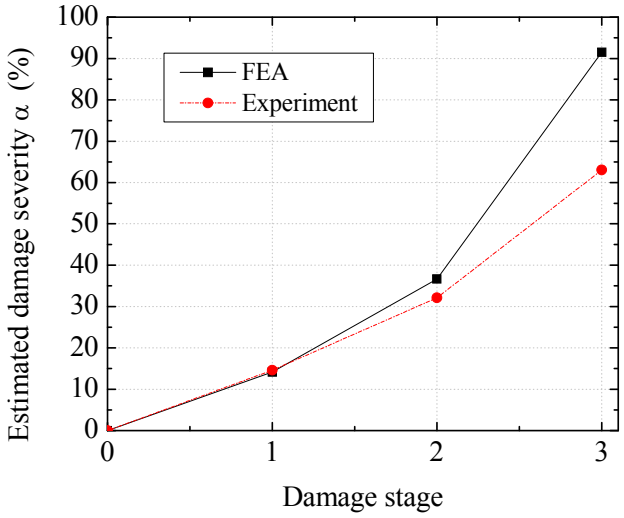

Figure 8.25 Damage quantification of FRP sandwich plate.

8.7 Summary

In this chapter, the two dynamic response-based damage identification methods proposed in this study (in Chapters 5 and 7) were applied for damage localization and quantification of an

as-manufactured FRP sandwich deck panel with distributed sensor points. Both the finite element simulation and experimental modal analysis were performed to examine the dynamic vibration modes of the FRP sandwich deck panel.

The numerical and experimental results show that the experimental modal testing can accurately capture the out-of-plane bending/twisting displacement mode shapes of the sandwich panel in a frequency range of less than 500 Hz. The 2-D CWT-based damage identification algorithm can be directly applied to the displacement mode shape data generated by the FE modal analysis technique to indicate the location of damage and approximate the damage area. The study presented in this Chapter shows that this technique is robust and effective for real-size composite sandwich beam/plate-type structures in laboratory. The proposed structural health monitoring strategy using a combination of experimental modal testing technique and 2-D CWT-based damage identification method can be effectively used for damage detection of composite sandwich plate-type structure or deck panel. However, in this algorithm the isosurface only indicates the location/area with the mode shape discontinuity, i.e., the most possible location of damage. Isosurface has no indication of the absolute value of the damage extent.

It is also demonstrated that a surface-bonded PVDF sensor network and impact hammer system can be effectively used to capture the curvature mode shape in the dominant direction of a single bending mode. The experimental results verified that the DSCF method can be used with the partial strain energy to effectively locate and quantify damage. However, in damage quantification step, to avoid non-uniqueness, the assumption of uniform distribution of damage severity on damaged elements is made to reduce the number of unknown parameters. Further study is needed for the damage severity distribution pattern.

The proposed structural health monitoring strategy using the combination of a distributed PVDF sensor network and the DSCF-based damage identification method can be effectively used for damage localization and quantification of composite sandwich plate-type structures in general and FRP sandwich bridge deck panels in particular. This strategy has shown its great potential to be further developed into a reliable real-time structural health monitoring system in the S-FRP sandwich materials. Studies towards the development of a real-time structural health monitoring/damage identification system using the DSCF-based method and piezoelectric sensor network for *in-situ* application should be the subject of future research.

CHAPTER 9

POTENTIAL INTEGRATION OF WIRELESS COMMUNICATION TECHNOLOGIES FOR STRUCTURAL HEALTH MONITORING

9.1 Introduction

In the last few years, the development of wireless sensor networks (WSN) has received increasing attention in their potential applications in structural health monitoring. The response of structure can be studied and material fatigue and/or progressive damage of structure can be monitored closely and continuously.

Wireless sensors are not sensors, but rather autonomous nodes to which traditional structural sensors (e.g., strain gauges, accelerometers, LVDT, etc.) can be attached, i.e., they do not convert mechanical force or movement into an electrical signal themselves but rely on traditional sensors to convert mechanical energy to electric energy.

The basic features of wireless sensor networks include:

(1) Short-range broadcast communication and multi-hop routing;

(2) Distributed deployment and cooperative effort of sensor nodes;

(3) Frequently changing topology due to fading and node failures;

(4) Ability to collect, process and transmit response data from structures.

Lynch and Loh (2006) categorized the functional parts of wireless sensors into three or four subsystems: Sensing interface, Computational core, Wireless transceiver and, for some, Actuation interface.

The sensing interface includes mainly analog-to-digital converter (ADC) channel(s) to convert analog sensor signal into digital signal. Function of the conversion resolution can be sample rate, and the number of channels available on its ADC.

The computational core includes a microcontroller that can store measurement data in random access memory (RAM) and data identification algorithms (such as damage detection routines) in read only memory (ROM). A major classifier for microcontrollers is the size (in bits) of their internal data bus with most microcontrollers classified as 8-, 16-, or 32-bits.

A wireless transceiver is an electrical radio component that can be used for both the transmission and reception of data. If a wireless radio operates on the Industrial, Scientific, and Medical (ISM) frequencies, the Federal Communications Commission (FCC) mandates the maximum power an antenna can output is 1W, which effectively limits the transmission range.

Some wireless sensors have an (optional) actuation interface. The actuation interface provides the capability to command actuators to make wireless sensor an active sensor, thus making a wireless smart structure. The core element of the actuation interface is DAC channel(s) to convert digital signal from microcontroller into continuous analog signal.

In addition to these four functional subsystems, a power source unit is required to be the energy source of all these subsystems; two optional off-board units can be attached for signal conditioning and power amplification. The subsystems and optional off-board units are illustrated in Fig. 9.1.

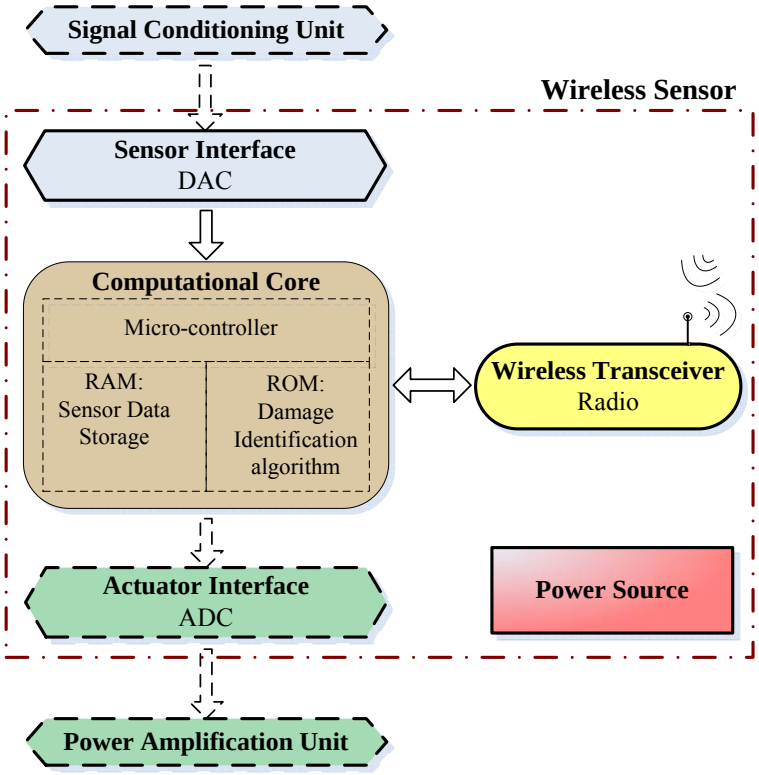

Figure 9.1 Schematic diagram of the subsystems and optional off-board units for wireless sensor

A wireless sensor network consists of hundreds to thousands of organized sensor nodes. The simplest topology for wireless sensor network architecture is a star topology, as shown in Fig. 9.2(a). Mitchell et al. (2001;2002) have proposed a two-tier wireless sensor network architecture using wireless sensors, as shown in Fig. 9.2(b). The architecture emphasizes the partitioning of the monitoring system functionality between wireless sensors and wireless data servers (called wireless cluster nodes). The wireless sensor nodes are designed to collect sensor data and transferred data wirelessly to nearby wireless data servers (cluster nodes). The wireless data servers have both a short-range radio (for communication with wireless sensors in its cluster) as well as a long-range radio (for communication with other remote cluster nodes). The wireless

data server nodes are designed to both store and process the vast amounts of data collected from the wireless sensors in the cluster and they are accessible from internet.

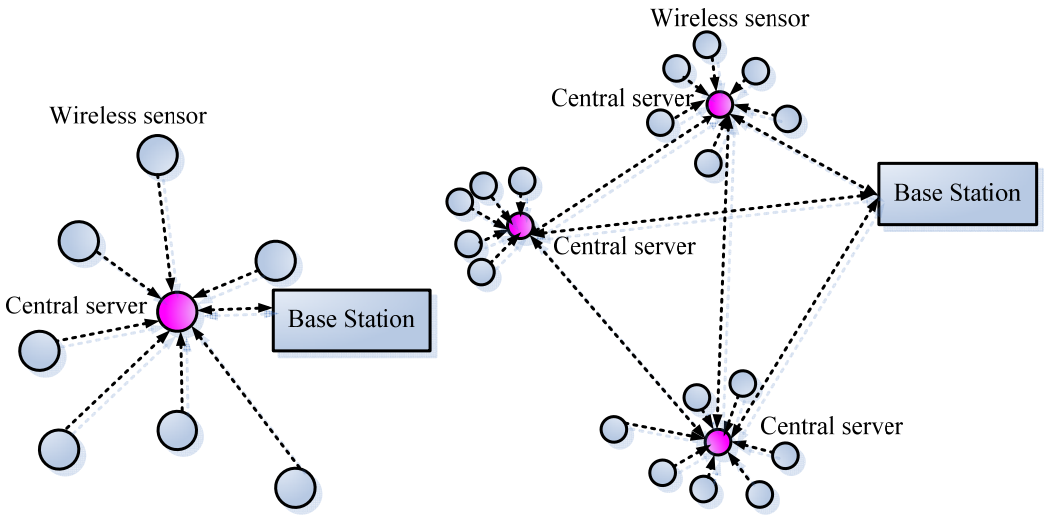

(a) Star topology (b) Two tier topology

Figure 9.2 Wireless sensor network topologies

9.2 Advantages of wireless sensors

Compared to traditional wired sensors, wireless sensors have advantages in the following aspects: low cost, easy installation, dense deployment, local computation capability.

Interest in wireless sensors was initially motivated by their lower cost than traditional sensors. Traditional structural monitoring systems employ coaxial wires for communication between sensors and the repository. While coaxial wires provide a very reliable communication link, their installation in structures can be expensive and labor-intensive. For example, structural monitoring systems installed in tall buildings have been reported in the literature to cost in excess of $5,000 (USD) per sensing channel (Celebi 2002). The cost of installing over 350 sensing channels upon the Tsing Ma suspension bridge in Hong Kong was estimated to have exceeded $8 million (Farra 2001).

Wireless sensor nodes can reduce cabling costs and increase the flexibility of instrumentation placement. One of the earliest field validations of wireless sensors for monitoring the performance of highway bridges was described by Maser et al (1996). The total cost of the system is roughly $1,000 per sensor node and $2,000 for the data repository. Companies, such as Crossbow, Ember, Sensoria, and Millenial, are building small sensor nodes with wireless capabilities. However, a per-node cost of $100 to $200 (not including sophisticated sensors) is prohibitive for large networks. Nodes must become an order of magnitude cheaper in order to render applications with a large number of nodes affordable. The advances in wireless communications and electronics are continuously driving the development of wireless sensors in this direction.

Due to easy installation and reduced or no wiring, wireless sensor network shows its potential in dense deployment of large number of sensors. Compared to the use of a few expensive (but highly accurate) sensors, the strategy of deploying a large number of inexpensive sensors has significant advantages, at smaller or comparable total system cost: much higher spatial resolution; higher robustness against failures through distributed operation; uniform coverage; small obtrusiveness; ease of deployment; reduced energy consumption; and, consequently, increased system lifetime. The main point is to position sensors close to the source of a potential problem phenomenon, where the acquired data are likely to have the greatest benefit or impact.

Another attractive feature of wireless sensors for SHM is the local computational resources. In order to minimize power consumption for wireless sensors, it becomes particularly important to minimize the amount of data to be transmitted, especially when multi-hops from the data source to the central data server is involved. One feasible approach to achieve this goal is to

process the collected measurements locally in the sensor nodes and then transmit only significant results to the central server. In order to do this, the exploited processing algorithm must consider the hardware limitations of the MCU of the sensor nodes. The distributed signal processing and local-based damage detection/identification may significantly reduce the amount of data to be transmitted to central server, which is more efficient in energy consumption. Therefore, it would considerably extend the life time of the network and reduce the total time required by the system to complete a structural test of the monitored structure, i.e., the latency. Bocca et al. (2011) developed a WSN in which the nodes, equipped with a 3-axis accelerometer, process the collected vibration measurements locally by the Goertzel algorithm in real-time. The proposed distributed approach reduces the latency by 80% and increases the system life time by 52%, when compared to traditional centralized architectures.

The above mentioned advantages make wireless sensor network ideal for structural health monitoring application. A schematic of potential integration of the proposed Smart Fiber-Reinforced Polymer (S-FRP) sandwich panel with wireless sensor network is shown in Fig. 9.3.

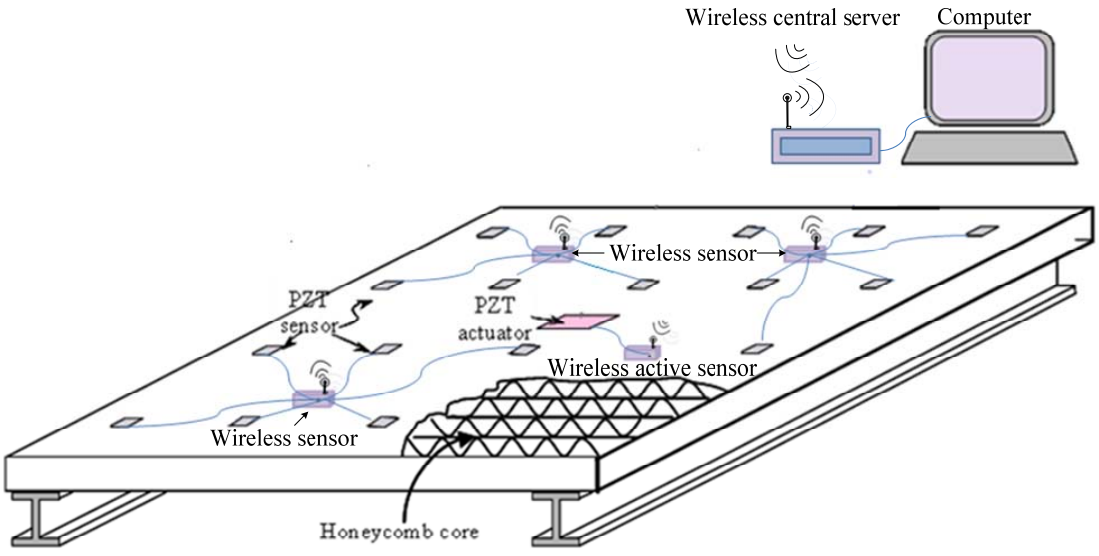

Figure 9.3 Smart Fiber-Reinforced Polymer (S-FRP) sandwich panel with wireless sensor network for bridge decks

9.3 Limitations of wireless sensors

The limitations and challenging issues on wireless sensors are in the following aspects: power consumption, data reliability, time synchronization, sampling rate, local data processing, multi-scale network topologies, and formulation of power-efficient data driven usage strategies. The current research in wireless sensors network mainly focuses on how to tackle these challenging issues.

First, power consumption is considered as the major limitation and most difficult constraints of wireless sensors network. Since the integration of wireless communication removes the need for transmitting data from one point to another with cables, the lack of cables requires remote power generation or portable power supplies to be coupled with wireless sensors. Currently, batteries represent the most common portable power source for wireless sensors. However, batteries only contain a finite amount of power; when batteries are exhausted, replacement can be a difficult task, especially when sensors are in locations where human access (such as extremely cold regions and chemical inaccessible areas) is limited. In addition, there are environmental issues regarding the disposal of batteries. Therefore, in order to extend the lifetime of the network, the design of wireless sensors requires energy efficient strategies and a rational analysis to determine the trade-off between functionality and power consumption.

The researchers tried to solve the power consumption problems with two approaches. One is to enhance the energy efficiency of the wireless sensor to extend its lifetime under finite power supplies. Another is to explore sustainable power source such as radio-frequency identification (RFID), energy harvesting (Park et al. 2008), and solar energy.

Optimal power efficiency can be approached by the exploitation of suitable transmission routing protocols, signal processing algorithms, damage identification algorithms and sleep

modes of wireless sensors. When subjected to finite power supplies, the trade-off between the sensor operations (i.e., sampling, processing, transmission, receptions and, possibly, actuation) also plays an important role in power usage. Balancing these parameters will be the focus of the design process of WSNs. It should be noted that in WSNs, among all these operations, transmissions and receptions of packets have by far the heaviest impact on power consumption. Current RF transmission techniques (e.g., Bluetooth) consume about 100 nJ per bit for a distance of 10 to 100 m, making communication very expensive compared to sampling and processing.

One popular method to enhance power efficiency is to adopt multi-hopping data transmission protocol. Multi-hopping is more energy efficient than having longer-range radios which offer direct connectivity between sensor nodes and central data server. In a multi-hopping network, the wireless sensor nodes can communicate with each other for sending or receiving information from central data server either directly or through intermediate nodes, so each node in a sensor network acts as a router inside the network. When the communication range of two wireless sensors is shorter than their physical separation, connectivity can still be established by multi-hopping. Bhattacharyya et al. (2010) presented a comparative study of eight *ad hoc* network routing protocols for WSNs, including LEACH, TEEN, APTEEN, PEGASIS, SPIN, DD, RR and GEAR. Since the sensor networks are application specific, it is difficult to simply conclude that any particular protocol is better than other.

In exploration of sustainable power source, the development of power-free wireless sensors known as radio-frequency identification (RFID) sensors makes them promising sensors for data transmission (Lynch and Loh 2006). RFID sensors are a passive radio technology, which capture radio energy emanated from a remote reader so that it can communicate its measurement

back. RFID sensors explicitly developed for structural health monitoring (SHM) are also included as part of their paper's scope.

Another feasible solution to energy source is energy harvesting systems, such as piezoelectric energy harvesters. This technology is particularly suitable for SHM applications, since vibrations are always present across structures. However, the production of energy by these systems is usually low, and it is optimal only at specific frequencies of vibrations.

Research groups also investigated the use of solar battery technology (e.g., rechargeable thin-film lithium battery and super charge ion battery) to charge capacitors with photocurrents from the ambient light sources (Bogue 2010).

In summary, power consumption is the key issue in development of wireless sensors, and it is a critical problem needed to be solved by comprehensive approaches via the exploitation of all aspects of wireless sensors, such as energy efficient transmission and reception protocols, energy harvesting, and energy efficient local algorithms for structural health monitoring.

Second, the quality of wireless transmission has been another important concern that has restricted the application of WSNs. Quality refers to the capability of a wireless sensor network (WSN) to deliver data reliably and timely.

Data transmission reliability in a wireless sensor network is inherently lower than that in cable-based systems, particularly when long distance node-to-node communication is involved. The limited wireless bandwidth can also impede real-time data transmission as required by feedback structural control systems.

Time synchronization in wireless sensor networks can also be a problem for some centralized structural health monitoring system. Each wireless sensor in the network has its own hardware oscillator-based clock providing timing signals to the sensor. Due to varying oscillator

frequencies, the clocks on the sensors drift with respect to each other and have to be continuously synchronized with each other in order to maintain a constant operation time signal. The time synchronization is required by some centralized off-line processing methods such as modal analysis, but is not required by some local-based damage identification algorithms. The theoretical analysis (Krishnamurthy et al. 2008) showed that time asynchronicity in sensor data leads to the errors in reconstructed mode shape proportional to $e^{\omega i t_0}$, and therefore, it is dependent on both the time delay and modal frequency. Time synchronization algorithms developed in the past for wired sensor systems achieve very high accuracy of <1 μs, but the same level of accuracy is a challenging task for wireless sensor networks. A number of methods have been developed and tested in this direction. Computer clocks on the internet are synchronized using the network time protocol (NTP). Another approach is to install a Global Positioning System (GPS) on every wireless sensor to keep track of the real time. There are also methods which have been developed specifically for wireless sensor networks, such as reference broadcast scheme (RBS), timing-sync protocol sensor network (TPSN), lightweight tree based synchronization (LTS) and global beacon synchronization methods.

Since power consumption and time synchronization impede the centralized off-line modal analysis technique for SHM, some modal identification techniques are specifically developed for wireless sensors. Cho et al. (2008) proposed a distributed modal identification scheme for using a WiMMS wireless sensor. Caicedo and Marulanda (2011) developed a fast mode identification technique to identify operational mode shapes for online structural health monitoring, which shows a potential to be used on WSNs.

Sampling rate of the sensing interface may be another concern for some applications. Ordinarily, low sampling rates (e.g., less than 500 Hz) are adequate for global vibration-based

structural monitoring. However, wireless sensors are increasingly explored for use in acoustic and ultrasonic NDE; as a result, there has been a growing need for higher sampling rates in excess of 500 kHz (Grisso et al. 2005; Lynch 2005).

9.4 Wireless sensors

Some available laboratory and commercial wireless sensors are listed and compared in Table 9.1. It can be seen from the table that batteries are the most common portable power source for wireless sensors. Technologies such as energy harvesting and solar batteries are still in their infancy for application in SHM. Energy efficient microcontroller is often adopted for local signal processing and local damage identification. Therefore a local-based damage identification algorithm with low computational cost should be of future research interest. Although active sensor is a promising concept for wireless sensor, most of active sensors still only exist in laboratory. For the time being, the sampling rate of sensing interface of wireless sensor is enough for vibration-based damage identification application, but too low (< 100 kHz) to be used for general acoustic wave-based damage detection application.

Table 9.1 Comparison of wireless sensors

	Lynch et al. (2004)	Wang et al. (2003) Gu et al. (2005)	UC Berkeley-Crossbow MICA2	Intel iMote	Microstrain	Rockwell Science Center	Lynch et al. (2004)	Wang et al. (2006)
General Information								
Commercial availability	No	No	Yes	Yes	Yes	Yes	No	No
Dimensions (cm)	12×10×2		6×3×1			7.3×7.3×8.9		10.2×6.5×4.0
Power Source	Battery (9V)	Battery	Coin Cell	Battery	Battery (3.6V)	Battery (two 9V)		Battery (two 9V)
Features		PVDF sensors are attached and tested	Open-source Motes; Last 30h on two AA batteries			Ability to self-organize in the field	Wireless active sensor	Wireless active sensor
Sensing Interface								
A/D Channels	1	8	8		8	4	32	4
Sampling Rate	100kHz	>50 Hz	1kHz		1.7 kHz	400 Hz	40 kHz	100 kHz
A/D Resolution	16-bit	12-bit	10-bit		12-bit	20-bit	10-bit	16-bit
Computation Core								
Processor	Ateml AT90S8515 AVR /MPC555PowerPC	Analog Devices ADuC832	Atmel ATmega 128L	Zeevo ARM7TDMI	MicroChip PIC16F877	Intel Stron-gARM 1100		ATmega128
Bus Size	8-bit/32-bit	8-bit	8-bit	32-bit	8-bit	32-bit		8-bit
Clock Speed	4 MHz / 20 MHz		7.383 MHz	12 MHz		133 Mhz		8 MHz
ROM for algorithm storage	8 kB / 26 kB	62kB	128 kB	64 kB		1 MB		128 kB
RAM for data storage	512 kB / 448 kB	2kB	4 kB	512 kB	2 MB	128 kB		4 kB / 128kB
Wireless Transceiver								
Radio	Proxim RangeLan2	Linx Technologies	Chipcon CC1000	Wireless BT Zeevo	RF Monolithics DR-3000-1	Conexant RDSSS9M		24XStream
Frequency Band	2.4 GHz	916 MHz	900 MHz	2.4 GHz	916.5 MHz	916 MHz		2.4835 GHz
Spread Spectrum	Yes	No	Yes (Software)	Yes		Yes		
Enclosed Range	150 m	61 m				100 m		180 m
Data Rate	1.6 Mbps	33.6 kbps	38.4 kbps	600 kbps	75 kbps	100 kbps		19.2 kbps
Actuation Interface								
D/A Channels		2					1	1
D/A Resolution		12-bit					12-bit	16-bit

CHAPTER 10

CONCLUSIONS AND RECOMMENDATIONS

10.1 Summary and concluding remarks

Viable and effective structural health monitoring and damage identification methods for composite beams and plate-type structures were studied in this project, with the aim to develop integrated smart honeycomb fiber reinforced polymer (S-FRP) composite sandwich bridge decks, especially for the cold region transportation applications. A thorough literature review on the topic showed that the research on the 2-D damage identification method for plate-type structures is relatively limited, though the 1-D damage identification methods are extensively studied and well developed. There are also very limited studies on the effect of cold temperature on the performance of FRP composite sandwich structures.

A detailed study on free vibration of the honeycomb FRP sandwich beams with sinusoidal core was conducted. The free vibration analysis is based on a high-order sandwich beam theory (HSBT) for improved accuracy. The results are compared with Timoshenko's beam theory, numerical simulation and experimental test results to illustrate the effectiveness of the high-order approach. The results demonstrated the validity of the high order beam theories, which improve the accuracy of sandwich beam analysis without high cost of evaluation. HSBT shows its potential in application for structural health monitoring and usage assessment of composite sandwich structures. The study also suggested that in general the dynamic response of sinusoidal core sandwich beam is sensitive to the variation of core transverse shear modulus but insensitive to the variation of compression stiffness through the thickness.

The temperature effect on dynamic response of FRP sandwich beams/panels was investigated, and the scale-up of test results from dynamic mechanical analysis (DMA) to predict

the large structural response was studied. A series of FRP sandwich beams with the core oriented in both the longitudinal and transverse directions and an as-manufactured FRP sandwich panel were investigated for dynamic response change under temperature effect. The study suggested that the proposed DMA-based approach is a reliable, efficient and effective technique to predict the temperature effect on dynamic response of FRP sandwich beams/panels. It was also suggested in this study that the temperature effect may introduce a moderate 2%-3% modal frequency shift to the FRP sandwich beam/panel over a 100°C temperature change. Therefore, using the modal frequency shift alone for FRP sandwich structural damage identification may not be reliable because temperature effect cannot introduce considerable modal frequencies shift. It indicated that the material data obtained in the DMA test using small coupon samples can be scaled up to predict the macro-level structural behavior.

To make smart structures (such as the proposed S-FRP sandwich materials) a viable technology for transportation infrastructure application, effective damage identification techniques are needed. As concluded from the extensive literature survey in this study, the damage identification techniques for 1-D beams structures are well developed, while the availability of the methods for 2-D plate-type structures (such as bridge deck panels) are relatively limited. To meet this immediate need, a new 2-D CWT-based method was proposed for damage detection of plate-type of structures. The 2-D CWT-based damage detection algorithm is a response-based damage detection technique for plate-type structures using "Dergauss2d" wavelet. The isosurfaces of 2-D wavelet coefficients of mode shape is generated to indicate the location and approximate shape (or area) of the damage. The viability of this method was demonstrated by analysis of the numerical and experimental mode shapes of a cantilevered composite plate. A comparative study with two other 2-D damage detection

algorithms, i.e., 2-D GSM and 2-D SEM, showed that the proposed 2-D CWT-based algorithm is superior in noise immunity and robust under limited sensor data.

Though many damage detection methods are capable of locating the damage area, there is still a need to assess the severity of the defects or damages in the structures. In this study, a DSCF-based damage identification method was also developed for damage identification of plate-type structures. A damage location factor matrix DLF and a damage severity correction factor matrix DSCF are generated from the curvature mode shape of a plate. The damage identification method using DSCF and DLF are presented for both damage localization and quantification. The proposed method is also a response-based damage identification technique which requires the modal frequencies and curvature mode shapes before and after damage. The viability of this method is demonstrated by both the numerical and experimental investigations.

The two proposed vibration-based methods were then applied to an as-manufactured FRP sandwich deck panel for damage identification. Application of the 2-D CWT-based damage detection method on the mode shape data from the numerical FE and experimental modal analysis showed that it can effectively indicate the location of damage and approximate the damage area in a FRP sandwich plate-type structure. Application of the DSCF-based damage identification method on the curvature mode shape data from the numerical FE and experimental modal analysis illustrated that it is not only capable of effectively indicating the location of damage but also approximating the damage severity in an FRP sandwich plate-type structure.

To make the proposed S-FRP sandwich materials as bridge deck panels more practical in remote and/or cold regions, the integration of the response-based SHM and distributed smart piezoelectric sensor array on the FRP sandwich decks with wireless sensor networks (WSNs) is needed. Though many commercial wireless sensors are available nowadays, their reliable and

extensive application in the structural health monitoring of bridge structures is still limited. The potential integration and application of WSNs with the proposed S-FRP deck panels were considered, and the obstacles of applying WSNs were discussed.

In summary, the developed structural health monitoring strategy using the combination of experimental modal testing technique and 2-D CWT-based damage identification method is effective for damage detection of composite sandwich plate-type structures and does not require high-cost modal testing system. While the other developed structural health monitoring strategy using combination of distributed PVDF sensor array and DSCF-based damage identification method can be effectively used for damage localization and quantification of composite sandwich plate-type structures. The latter strategy shows great potential to be further developed into an *in-situ* real-time structural health monitoring system for plate-type structures. The extensive experimental and analytical study on the development of S-FRP sandwich materials for highway bridge decks conducted in this project paves the foundation for smart infrastructure development, particularly suitable and practicable for remote and/or cold regions. Outcomes of this study deliver a viable technology using integrated advanced polymer sandwich materials and smart piezoelectric sensors/actuators along with the developed response-based damage identification and structural health monitoring strategies to address transportation safety, security, and innovation in cold regions.

10.2 Recommendations for future studies

The research on structural health monitoring and damage identification of plate-type composite structures suitable for highway bridge deck application is still a novel field of study. There are still many related topics subjected to future research. Based on the research in this study, the following topics are recommended for future study:

(1) Development of an effective damage identification method for non-flat complex structures with irregular shapes, such as sandwich shell structures;

(2) Development of a reliable *in-situ* real-time structural health monitoring system for plate-type structures;

(3) Studies towards the application of statistical pattern recognition techniques for identification of damage severity and types;

(4) Integration and testing of wireless sensor networks (WSNs) with the developed dynamic response-based damage identification and structural health monitoring strategies and development of viable wireless S-FRP composite structural technology suitable for transportation applications.

(5) Implementation of the proposed S-FRP composite sandwich decks in highway bridges, particularly in the cold regions, to test their field applicability, reliability, and effectiveness. .

REFERENCES

Abdel Wahab, M. M., and De Roeck, G. (1999). "Damage detection in bridges using modal curvatures: Application to a real damage scenario." *Journal of Sound and Vibration*, 226(2), 217-235.

Abdo, M. A. B., and Hori, M. (2002). "A numerical study of structural damage detection using changes in the rotation of mode shapes." *Journal of Sound and Vibration*, 251(2), 227-239.

Adams, R. D., Cawley, P., Pye, C. J., and Stone, B. J. (1978). "A vibration technique for non-destructively assessing the integrity of structures." *Journal of Mechanical Engineering Science*, 20(2), 93-100.

Amaravadi, V., Rao, V., Koval, L. R., and Derriso, M. (2001). "Structural health monitoring using wavelet transforms." *Smart structures and integrated systems. Proc SPIE*, 4327, 258-69.

Antoine, J. P., Murenzi, R., Vandergheynst, P., and Ali, S. T. (2004). *Two-dimensional wavelets and their relatives*, Cambridge university press, Cambridge.

Au, F. T. K., Cheng, Y. S., Tham, L. G., and Bai, Z. Z. (2003). "Structural damage detection based on a micro-genetic algorithm using incomplete and noisy modal test data." *Journal of Sound and Vibration*, 259(5), 1081-1094.

Barbero, E. J. (1999). *Introduction to composite materials design*, Taylor & Francis.

Bocca, M., Toivola, J., Eriksson, L. M., Hollmé andn, J., and Koivo, H. (2011). "Structural Health Monitoring in Wireless Sensor Networks by the Embedded Goertzel Algorithm." *Cyber-Physical Systems (ICCPS), 2011 IEEE/ACM International Conference on*, 206 -214.

Bogue, R. (2010). "Wireless sensors: a review of technologies, products and applications." *Sensor Review*, 30(4), 285.

Caicedo, J. M., and Marulanda, J. (2011). "Fast mode identification technique for online monitoring." *Structural Control and Health Monitoring*, 18(4), 416–429.

Cao, M., and Qiao, P. (2008). "Integrated wavelet transform and its application to vibration mode shapes for the damage detection of beam-type structures." *Smart materials and structures*, 17(5), 055014.

Cao, M. S., and Qiao, P. Z. (2009). "Novel Laplacian scheme and multiresolution modal curvatures for structural damage identification." *Mechanical Systems and Signal Processing*, 23(4), 1223-1242.

Carden, E. P., and Fanning, P. (2004). "Vibration based condition monitoring: A review." *Structural Health Monitoring*, 3(4), 355-377.

Cawley, P., and Adams, R. D. (1979). "The location of defects in structures from measurements of natural frequencies." *Journal of Strain Analysis*, 49-57.

Celebi, M. (2002). *Seismic Instrumentation of Buildings (With Emphasis on Federal Buildings)*. United States Geological Survey, Menlo Park, CA.

Chang, C. C., and Chen, L. W. (2004). "Damage detection of a rectangular plate by spatial wavelet based approach." *Applied Acoustics*, 65(8), 819-832.

Chang, C. C., and Chen, L. W. (2005). "Detection of the location and size of cracks in the multiple cracked beam by spatial wavelet based approach." *Mechanical Systems and Signal Processing*, 19(1), 139-155.

Chaudhari, T. D., and Maiti, S. K. (2000). "A study of vibration of geometrically segmented beams with and without crack." *International Journal of Solids and Structures*, 37(5), 761-779.

Chinchalkar, S. (2001). "Determination of crack location in beams using natural frequencies." *Journal of Sound and Vibration*, 247(3), 417-429.

Cho, S. (2008). "Smart wireless sensor technology for structural health monitoring of civil structures." *International Journal of Steel Structures*, 8(4), 267.

Choi, S., Park, S., Park, N. H., and Stubbs, N. (2006). "Improved fault quantification for a plate structure." *Journal of Sound and Vibration*, 297(3-5), 865-879.

Choi, S., Park, S., Yoon, S., and Stubbs, N. (2005). "Nondestructive damage identification in plate structures using changes in modal compliance." *Ndt & E International*, 38(7), 529-540.

Cornwell, P., Doebling, S. W., and Farrar, C. R. (1999). "Application of the strain energy damage detection method to platelike structures." *Journal of Sound and Vibration*, 224(2), 359-374.

Davalos, J. F., Kim, Y. C., and Barbero, E. J. (1994). "Analysis of Laminated Beams with a Layer-Wise Constant Shear Theory." *Composite Structures*, 28(3), 241-253.

Davalos, J. F., Qiao, P. Z., Xu, X. F., Robinson, J., and Barth, K. E. (2001). "Modeling and characterization of fiber-reinforced plastic honeycomb sandwich panels for highway bridge applications." *Composite Structures*, 52(3-4), 441-452.

Dilena, M., and Morassi, A. (2004). "The use of antiresonances for crack detection in beams." *Journal of Sound and Vibration*, 276(1-2), 195-214.

Doebling, S. W., Farrar, C. R., Prime, M. B., and Shevitz, D. W. (1996). "Damage Identification and Health Monitoring of Structural and Mechanical Systems from Changes in their Vibration Characteristics: A Literature Review." *Los Alamos National Laboratory report*(LA-13070-MS).

dos Santos, J. V. A., Soares, C. M. M., Soares, C. A. M., and Pina, H. L. G. (2000). "Development of a numerical model for the damage identification on composite plate structures." *Composite Structures*, 48(1-3), 59-65.

Douka, E., Loutridis, S., and Trochidis, A. (2003). "Crack identification in beams using wavelet analysis." *International Journal of Solids and Structures*, 40(13-14), 3557-3569.

Douka, E., Loutridis, S., and Trochidis, A. (2004). "Crack identification in plates using wavelet analysis." *Journal of Sound and Vibration*, 270(1-2), 279-295.

Fan, W., and Qiao, P. Z. (2011). "Vibration-based Damage Identification Methods: A Review and Comparative Study." *Structural Health Monitoring-an International Journal*, 10(1), 83-111.

Farrar, C. R., and James, G. H. (1997). "System identification from ambient vibration measurements on a bridge." *Journal of Sound and Vibration*, 205(1), 1-18.

Farrar, C. R., and Jauregui, D. (1996). "Damage detection algorithms applied to experimental and numerical modal data from the I-40 bridge." Los Alamos National Laboratory, LA.

Farrar, C. R., and Jauregui, D. A. (1998a). "Comparative study of damage identification algorithms applied to a bridge: I. Experiment." *Smart Materials & Structures*, 7(5), 704-719.

Farrar, C. R., and Jauregui, D. A. (1998b). "Comparative study of damage identification algorithms applied to a bridge: II. Numerical study." *Smart Materials & Structures*, 7(5), 720-731.

Farra, C. R. (2001). *Historical Overview of Structural Health Monitoring*. Lecture Notes on Structural Health Monitoring Using Statistical Pattern Recognition, Los Alamos Dynamics, Los Alamos, NM.

Frostig, Y., Baruch, M., Vilnay, O., and Sheinman, I. (1992). "High-Order Theory for Sandwich-Beam Behavior with Transversely Flexible Core." *Journal of Engineering Mechanics-Asce*, 118(5), 1026-1043.

Frostig, Y., and Thomsen, O. T. (2004). "High-order free vibration of sandwich panels with a flexible core." *International Journal of Solids and Structures*, 41(5-6), 1697-1724.

Ge, M., and Lui, E. M. (2005). "Structural damage identification using system dynamic properties." *Computers & Structures*, 83(27), 2185-2196.

Gentile, A., and Messina, A. (2003). "On the continuous wavelet transforms applied to discrete vibrational data for detecting open cracks in damaged beams." *International Journal of Solids and Structures*, 40(2), 295-315.

Gordaninejad, F., and Bert, C. W. (1989). "A New Theory for Bending of Thick Sandwich Beams." *International Journal of Mechanical Sciences*, 31(11-12), 925-934.

Grisso, B. L., Martin, L. A., and Inman, D. J. (2005). "A Wireless Active Sensing System for Impedance-based Structural Health Monitoring." *Proceedings of the 23rd International Modal Analysis Conference*, Orlando, FL.

Gu, Hua, Zhao, Yang, and Wang, Ming L. (2005). "A wireless smart PVDF sensor for structural health monitoring." *Structural Control and Health Monitoring*, 12(3-4), 329-343.

Gudmundson, P. (1982). "Eigenfrequency Changes of Structures Due to Cracks, Notches or Other Geometrical Changes." *Journal of the Mechanics and Physics of Solids*, 30(5), 339-353.

Hadjileontiadis, L. J., and Douka, E. (2007). "Crack detection in plates using fractal dimension." *Engineering Structures*, 29(7), 1612-1625.

Hadjileontiadis, L. J., Douka, E., and Trochidis, A. (2005). "Fractal dimension analysis for crack identification in beam structures." *Mechanical Systems and Signal Processing*, 19(3), 659-674.

Hamey, C. S., Lestari, W., Qiao, P. Z., and Song, G. B. (2004). "Experimental damage identification of carbon/epoxy composite beams using curvature mode shapes." *Structural Health Monitoring*, 3(4), 333-353.

Hao, H., and Xia, Y. (2002). "Vibration-based damage detection of structures by genetic algorithm." *Journal of Computing in Civil Engineering*, 16(3), 222-229.

Hemez, F. M. (2004). "Uncertainty Quantification and the Verification and Validation of Computational Models." *Damage Prognosis for Aerospace, Civil and Mechanical Systems*.

Hong, J. C., Kim, Y. Y., Lee, H. C., and Lee, Y. W. (2002). "Damage detection using the Lipschitz exponent estimated by the wavelet transform: applications to vibration modes of a beam." *International Journal of Solids and Structures*, 39(7), 1803-1816.

Hu, C. S., and Afzal, M. T. (2006). "A statistical algorithm for comparing mode shapes of vibration testing before and after damage in timbers." *Journal of Wood Science*, 52(4), 348-352.

Huth, O., Feltrin, G., Maeck, J., Kilic, N., and Motavalli, M. (2005). "Damage identification using modal data: Experiences on a prestressed concrete bridge." *Journal of Structural Engineering-Asce*, 131(12), 1898-1910.

Ibekwe, S. I., Mensah, P. F., Li, G. Q., Pang, S. S., and Stubblefield, M. A. (2007). "Impact and post impact response of laminated beams at low temperatures." *Composite Structures*, 79(1), 12-17.

Icten, B. M., Atas, C., Aktas, M., and Karakuzu, R. (2009). "Low temperature effect on impact response of quasi-isotropic glass/epoxy laminated plates." *Composite Structures*, 91(3), 318-323.

Jacques, L., Coron, A., Vandergheynst, P., and Demanet, L. (2007). "Yet Another Wavelet Toolbox. ." http://rhea.tele.ucl.ac.be/yawtb/.

Jiang, L. J., Tang, J., and Wang, K. W. (2006). "An enhanced frequency-shift-based damage identification method using tunable piezoelectric transducer circuitry." *Smart Materials & Structures*, 15(3), 799-808.

Just-Agosto, F., Shafiq, B., and Serrano, D. (2007). "Development of a damage detection scheme applicable to sandwich composites." *Journal of Sandwich Structures & Materials*, 9(4), 343-363.

Kasper, D. G., Swanson, D. C., and Reichard, K. M. (2008). "Higher-frequency wavenumber shift and frequency shift in a cracked, vibrating beam." *Journal of Sound and Vibration*, 312(1-2), 1-18.

Khan, A. Z., Stanbridge, A. B., and Ewins, D. J. (1999). "Detecting damage in vibrating structures with a scanning LDV." *Optics and Lasers in Engineering*, 32(6), 583-592.

Kim, B. H., Kim, H., and Park, T. (2006a). "Nondestructive damage evaluation of plates using the multi-resolution analysis of two-dimensional Haar wavelet." *Journal of Sound and Vibration*, 292(1-2), 82-104.

Kim, B. H., Park, T., and Voyiadjis, G. Z. (2006b). "Damage estimation on beam-like structures using the multi-resolution analysis." *International Journal of Solids and Structures*, 43(14-15), 4238-4257.

Kim, J. T., Park, J. H., and Lee, B. J. (2007). "Vibration-based damage monitoring in model plate-girder bridges under uncertain temperature conditions." *Engineering Structures*, 29(7), 1354-1365.

Kim, J. T., Ryu, Y. S., Cho, H. M., and Stubbs, N. (2003). "Damage identification in beam-type structures: frequency-based method vs mode-shape-based method." *Engineering Structures*, 25(1), 57-67.

Kim, J. T., and Stubbs, N. (2003). "Crack detection in beam-type structures using frequency data." *Journal of Sound and Vibration*, 259(1), 145-160.

Krishnamurthy, V., Fowler, K., and Sazonov, E. (2008). "The effect of time synchronization of wireless sensors on the modal analysis of structures." *Smart Materials and Structures*, 17(5), 055018.

Law, S. S., Shi, Z. Y., and Zhang, L. M. (1998). "Structural damage detection from incomplete and noisy modal test data." *Journal of Engineering Mechanics-Asce*, 124(11), 1280-1288.

Lee, J. J., Lee, J. W., Yi, J. H., Yun, C. B., and Jung, H. Y. (2005). "Neural networks-based damage detection for bridges considering errors in baseline finite element models." *Journal of Sound and Vibration*, 280(3-5), 555-578.

Lele, S. P., and Maiti, S. K. (2002). "Modelling of transverse vibration of short beams for crack detection and measurement of crack extension." *Journal of Sound and Vibration*, 257(3), 559-583.

Lestari, W., and Qiao, P. Z. (2005). "Damage detection of fiber-reinforced polymer honeycomb sandwich beams." *Composite Structures*, 67(3), 365-373.

Lestari, W., and Qiao, P. Z. (2006). "Dynamic characteristics and effective stiffness properties of honeycomb composite sandwich structures for highway bridge applications." *Journal of Composites for Construction*, 10(2), 148-160.

Lestari, W., Qiao, P. Z., and Hanagud, S. (2007). "Curvature mode shape-based damage assessment of carbon/epoxy composite beams." *Journal of Intelligent Material Systems and Structures*, 18(3), 189-208.

Li, H. J., He, C. J., Ji, J. L., Wang, H., and Hao, C. Z. (2005). "Crack damage detection in beam-like structures using RBF neural networks with experimental validation." *International Journal of Innovative Computing Information and Control*, 1(4), 625-634.

Liang, R. Y., Choy, F. K., and Hu, J. L. (1991). "Detection of Cracks in Beam Structures Using Measurements of Natural Frequencies." *Journal of the Franklin Institute-Engineering and Applied Mathematics*, 328(4), 505-518.

Liang, R. Y., Hu, J. L., and Choy, F. (1992). "Theoretical-Study of Crack-Induced Eigenfrequency Changes on Beam Structures." *Journal of Engineering Mechanics-Asce*, 118(2), 384-396.

Liew, K. M., and Wang, Q. (1998). "Application of wavelet theory for crack identification in structures." *Journal of Engineering Mechanics-Asce*, 124(2), 152-157.

Loutridis, S., Douka, E., Hadjileontiadis, L. J., and Trochidis, A. (2005). "A two-dimensional wavelet transform for detection of cracks in plates." *Engineering Structures*, 27(9), 1327-1338.

Lu, X. Q., and Liu, D. S. (1992). "An Interlaminar Shear-Stress Continuity Theory for Both Thin and Thick Composite Laminates." *Journal of Applied Mechanics-Transactions of the Asme*, 59(3), 502-509.

Lynch, J. P. (2005). "Design of a wireless active sensing unit for localized structural health monitoring." *Structural Control & Health Monitoring*, 12(3-4), 405–423.

Lynch, J. P., and Loh, K. J. (2006). "A Summary Review of Wireless Sensors and Sensor Networks for Structural Health Monitoring." *The Shock and Vibration Digest*, 38(2), 91–128.

Lynch, J. P., Law, K. H., Kiremidjian, A. S., and Carryer, E. (2004). "Design and Performance Validation of a Wireless Sensing Unit for Structural Monitoring Applications." *Structural Engineering and Mechanics*, 17, 3–4.

Maity, D., and Tripathy, R. R. (2005). "Damage assessment of structures from changes in natural frequencies using genetic algorithm." *Structural Engineering and Mechanics*, 19(1), 21-42.

Maser, K., Egri, R., Lichtenstein, A., and Chase, S. (1996). “Field evaluation of a wireless global bridge evaluation and monitoring system.” *Proceeding of 11th conf. on engineering mechanics*, Fort Lauderdale. (Fla), 955-958.

Messina, A., Williams, E. J., and Contursi, T. (1998). "Structural damage detection by a sensitivity and statistical-based method." *Journal of Sound and Vibration*, 216(5), 791-808.

Mitchell, K., Dang, N., Liu, P., Rao, V. S, and Pottinger, H. J. (2001). “Web-controlled wireless network sensors for structural health monitoring.” *Society of Photo-Optical Instrumentation Engineers (SPIE) Conference Series*, Society of Photo-Optical Instrumentation Engineers (SPIE) Conference Series, V. K. Varadan, ed., 234-243.

Mitchell, Kyle, Rao, Vittal S, and Pottinger, Hardy J. (2002). “Lessons learned about wireless technologies for data acquisition.” SPIE proceedings series, Society of Photo-Optical Instrumentation Engineers, Bellingham, WA, International.

Morassi, A. (1993). "Crack-Induced Changes in Eigenparameters of Beam Structures." *Journal of Engineering Mechanics-Asce*, 119(9), 1798-1803.

Morassi, A. (2001). "Identification of a crack in a rod based on changes in a pair of natural frequencies." *Journal of Sound and Vibration*, 242(4), 577-596.

Morassi, A., and Rollo, M. (2001). "Identification of two cracks in a simply supported beam from minimal frequency measurements." *Journal of Vibration and Control*, 7(5), 729-739.

Murigendrappa, S. M., Maiti, S. K., and Srirangarajan, H. R. (2004a). "Experimental and theoretical study on crack detection in pipes filled with fluid." *Journal of Sound and Vibration*, 270(4-5), 1013-1032.

Murigendrappa, S. M., Maiti, S. K., and Srirangarajan, H. R. (2004b). "Frequency-based experimental and theoretical identification of multiple cracks in straight pipes filled with fluid." *Ndt & E International*, 37(6), 431-438.

Murty, A. V. K. (1985). "On the Shear Deformation-Theory for Dynamic Analysis of Beams." *Journal of Sound and Vibration*, 101(1), 1-12.

Nandwana, B. P., and Maiti, S. K. (1997). "Detection of the location and size of a crack in stepped cantilever beams based on measurements of natural frequencies." *Journal of Sound and Vibration*, 203(3), 435-446.

Ndambi, J. M., Vantomme, J., and Harri, K. (2002). "Damage assessment in reinforced concrete beams using eigenfrequencies and mode shape derivatives." *Engineering Structures*, 24(4), 501-515.

Ni, Y. Q., Hua, X. G., Fan, K. Q., and Ko, J. M. (2005). "Correlating modal properties with temperature using long-term monitoring data and support vector machine technique." *Engineering Structures*, 27(12), 1762-1773.

Ojalvo, I. U. (1977). "Departures from classical beam theory in laminated, sandwich and short beams." *AIAA Journal* 15(10), 1518-1521.

Pandey, A. K., and Biswas, M. (1994). "Damage Detection in Structures Using Changes in Flexibility." *Journal of Sound and Vibration*, 169(1), 3-17.

Pandey, A. K., Biswas, M., and Samman, M. M. (1991). "Damage Detection from Changes in Curvature Mode Shapes." *Journal of Sound and Vibration*, 145(2), 321-332.

Park, G., Rosing, T., Todd, M. D., Farrar, C. R., and Hodgkiss, W. (2008). "Energy Harvesting for Structural Health Monitoring Sensor Networks." *Journal of Infrastructure Systems*, 14(1).

Patil, D. P., and Maiti, S. K. (2003). "Detection of multiple cracks using frequency measurements." *Engineering Fracture Mechanics*, 70(12), 1553-1572.

Pawar, P. M., and Ganguli, R. (2005). "Matrix crack detection in thin-walled composite beam using genetic fuzzy system." *Journal of Intelligent Material Systems and Structures*, 16(5), 395-409.

Pawar, P. M., Reddy, K. V., and Ganguli, R. (2007). "Damage detection in beams using spatial Fourier analysis and neural networks." *Journal of Intelligent Material Systems and Structures*, 18(4), 347-359.

Plunkett, J. D. (1997). "Fiber-reinforcement polymer honeycomb short span bridge for rapid installation."

Poudel, U. P., Fu, G. K., and Ye, H. (2007). "Wavelet transformation of mode shape difference function for structural damage location identification." *Earthquake Engineering & Structural Dynamics*, 36(8), 1089-1107.

Qiao, P., and Cao, M. (2008). "Waveform fractal dimension for mode shape-based damage identification of beam-type structures." *International Journal of Solids and Structures*, 45(23), 5946-5961.

Qiao, P. H., Lu, K., Lestari, W., and Wang, J. L. (2007a). "Curvature mode shape-based damage detection in composite laminated plates." *Composite Structures*, 80(3), 409-428.

Qiao, P. Z., Lestari, W., Shah, M. G., and Wang, J. L. (2007b). "Dynamics-based damage detection of composite laminated beams using contact and noncontact measurement systems." *Journal of Composite Materials*, 41(10), 1217-1252.

Qiao, P. Z., and Wang, J. L. (2005). "Mechanics of composite sinusoidal honeycomb cores." *Journal of Aerospace Engineering*, 18(1), 42-50.

Quek, S. T., Wang, Q., Zhang, L., and Ang, K. K. (2001). "Sensitivity analysis of crack detection in beams by wavelet technique." *International Journal of Mechanical Sciences*, 43(12), 2899-2910.

Rahai, A., Bakhtiari-Nejad, F., and Esfandiari, A. (2007). "Damage assessment of structure using incomplete measured mode shapes." *Structural Control & Health Monitoring*, 14(5), 808-829.

Ratcliffe, C. P. (1997). "Damage detection using a modified laplacian operator on mode shape data." *Journal of Sound and Vibration*, 204(3), 505-517.

Ratcliffe, C. P. (2000). "A frequency and curvature based experimental method for locating damage in structures." *Journal of Vibration and Acoustics-Transactions of the Asme*, 122(3), 324-329.

Ratcliffe, C. P., and Bagaria, W. J. (1998). "Vibration technique for locating delamination in a composite beam." *Aiaa Journal*, 36(6), 1074-1077.

Reddy, J. N. (1987). "A Generalization of Two-Dimensional Theories of Laminated Composite Plates." *Communications in Applied Numerical Methods*, 3(3), 173-180.

Ren, W. X., and De Roeck, G. (2002a). "Structural damage identification using modal data. I: Simulation verification." *Journal of Structural Engineering-Asce*, 128(1), 87-95.

Ren, W. X., and De Roeck, G. (2002b). "Structural damage identification using modal data. II: Test verification." *Journal of Structural Engineering-Asce*, 128(1), 96-104.

Rucka, M., and Wilde, K. (2006). "Application of continuous wavelet transform in vibration based damage detection method for beams and plates." *Journal of Sound and Vibration*, 297(3-5), 536-550.

Ruotolo, R., and Surace, C. (1997). "Damage assessment of multiple cracked beams: Numerical results and experimental validation." *Journal of Sound and Vibration*, 206(4), 567-588.

Salawu, O. S. (1997). "Detection of structural damage through changes in frequency: A review." *Engineering Structures*, 19(9), 718-723.

Salawu, O. S., and Williams, C. (1994). "Damage location using vibration mode shapes." *International Modal Analysis Conference*, 933-9.

Shi, Z. Y., and Law, S. S. (1998). "Structural damage localization from modal strain energy change." *Journal of Sound and Vibration*, 218(5), 825-844.

Shi, Z. Y., Law, S. S., and Zhang, L. M. (2000a). "Damage localization by directly using incomplete mode shapes." *Journal of Engineering Mechanics-Asce*, 126(6), 656-660.

Shi, Z. Y., Law, S. S., and Zhang, L. M. (2000b). "Structural damage detection from modal strain energy change." *Journal of Engineering Mechanics-Asce*, 126(12), 1216-1223.

Sohn, H., Farrar, C. R., Hemez, F. M., Shunk, D. D., Stinemates, D. W., and Nadler, B. R. (2003). "A Review of Structural Health Monitoring Literature: 1996-2001." *Los Alamos National Laboratory report*(LA-13976-MS).

Stubbs, N., and Kim, J. T. (1996). "Damage localization in structures without baseline modal parameters." *Aiaa Journal*, 34(8), 1644-1649.

Stubbs, N., Kim, J. T., and Farrar, C. R. (1995). "Field verification of a nondestructive damage localization and severity estimation algorithm." *Proceedings of 13th International Modal Analysis Conference*, 1, 210-8.

Swamidas, A. S. J., and Chen, Y. (1995). "Monitoring Crack-Growth through Change of Modal Parameters." *Journal of Sound and Vibration*, 186(2), 325-343.

Tauchert, T. R. (1975). "On the validity of elementary bending theory for anisotropic elastic slabs." *Journal of Composite Materials*, 9, 207-214.

Topole, K. G., and Stubbs, N. (1995). "Nondestructive Damage Evaluation in Complex Structures from a Minimum of Modal Parameters." *Modal Analysis-the International Journal of Analytical and Experimental Modal Analysis*, 10(2), 95-103.

Tsai, S. W., and Pagano, N. J. "Invariant properties of composite materials." *Composite Materials WorkShop*, Lancaster,PA, 233-252.

Wang, B. T. (1998). "Structural modal testing with various actuators and sensors." *Mechanical Systems and Signal Processing*, 12(5), 627-639.

Wang, H., and Qiao, P. (2008). "On irregularity-based damage detection method for cracked beams." *International Journal of Solids and Structures*, 45(2), 688-704.

Wang, J., and Qiao, P. Z. (2007). "Improved damage detection for beam-type structures using a uniform load surface." *Structural Health Monitoring-an International Journal*, 6(2), 99-110.

Wang, M. L., Gu, H., Lloyd, G. M., and Zhao, Y. (2003). "A Multichannel Wireless PVDF Displacement Sensor for Structural Monitoring." *Proceedings of the International Workshop on Advanced Sensors, Structural Health Monitoring and Smart Structures*, Tokyo, Japan.

Wang, Q., and Deng, X. M. (1999). "Damage detection with spatial wavelets." *International Journal of Solids and Structures*, 36(23), 3443-3468.

WANG, Y., P, L. J., and H, L. K. (2006). *Wireless sensing, actuation and control : With applications to civil structures*. Lecture notes in computer science, Springer, Berlin, ALLEMAGNE.

Wu, D., and Law, S. S. (2004). "Damage localization in plate structures from uniform load surface curvature." *Journal of Sound and Vibration*, 276(1-2), 227-244.

Wu, D., and Law, S. S. (2005). "Sensitivity of uniform load surface curvature for damage identification in plate structures." *Journal of Vibration and Acoustics-Transactions of the Asme*, 127(1), 84-92.

Wu, H. C., Fu, G., Gibson, R. F., Yan, A., Warnemuende, K., and Anumandla, V. (2006). "Durability of FRP composite bridge deck materials under freeze-thaw and low temperature conditions." *Journal of Bridge Engineering*, 11(4), 443-451.

Xu, X. F., Qiao, P. Z., and Davalos, J. F. (2001). "Transverse shear stiffness of composite honeycomb core with general configuration." *Journal of Engineering Mechanics-Asce*, 127(11), 1144-1151.

Yang, M. J., and Qiao, P. Z. (2005). "Higher-order impact modeling of sandwich structures with flexible core." *International Journal of Solids and Structures*, 42(20), 5460-5490.

Yoon, M. K., Heider, D., Gillespie, J. W., Ratcliffe, C. P., and Crane, R. M. (2005). "Local damage detection using the two-dimensional gapped smoothing method." *Journal of Sound and Vibration*, 279(1-2), 119-139.

Yoon, M. K., Heider, D. J., Gillespie Jr., W., Ratcliffe, C. P., and Crane, R. M. (2001). "Local damage detection using a global fitting method on mode shape data." *Proceedings of SPIE, the International Society for Optical Engineering*, 4359(1), 231–237.

Zhang, Z., and Aktan, A. E. (1998). "Application of modal flexibility and its derivatives in structural identification." *Research in Nondestructive Evaluation*, 10(1), 43-61.

Zhong, S., Yadiji, S. O., and Ding, K. (2008). "Response-only method for damage detection of beam-like structures using high accuracy frequencies with auxiliary mass spatial probing." *Journal of Sound and Vibration*, 311(3-5), 1075-1099.

Zhong, S. C., and Oyadiji, S. O. (2007). "Crack detection in simply supported beams without baseline modal parameters by stationary wavelet transform." *Mechanical Systems and Signal Processing*, 21(4), 1853-1884.

Zhou, Z. G., Wegner, L. D., and Sparling, B. F. (2007). "Vibration-based detection of small-scale damage on a bridge deck." *Journal of Structural Engineering-Asce*, 133(9), 1257-1267.